The Development of Mononuclear Platinum Hybrid Biomaterials for Antigene Therapeutic Application

Joseph Hennessy B.Sc.

Ph.D. Thesis

Assoc. Prof. Andrew Kellett

School of Chemical Sciences

Faculty of Science and Health

Dublin City University

Ireland

January 2022

Declaration

I hereby certify that this material, which I now submit for assessment on the programme of study leading to the award of Doctor of Philosophy is entirely my own work, and that I have exercised reasonable care to ensure that the work is original, and does not to the best of my knowledge breach any law of copyright, and has not been taken from the work of others save and to the extent that such work has been cited and acknowledged within the text of my work.

Signed: ID No.: 11357506 Date: 10/01/2022

Acknowledgement

Foremost, I would like to express my sincere gratitude to my supervisor Assoc. Prof. Andrew Kellett for his continuous support, encouragement and guidance from the beginning of my PhD studies. Without his motivation and wisdom, the project would not be where it is today. It is a great privilege to have been granted the opportunity to work within the group under his guidance.

I would like to thank Dr. Zara Molphy for her years of hard work, guidance, kindness and her endless supply of patience while being a mentor to me. To my friends and colleagues in the PPtBio lab, Sinéad and Bríonna, I'd like to thank you greatly for making everyday fun and enjoyable and to always keeping our spirits up throughout both the good and bad science days. Finally, I'd like to thank Dr. Creina Slator for her continuous help and guidance. To my fellow Kellett Research Group colleagues, past and present, thank you for the help and teamwork along the way.

I would like to acknowledge the technical staff in the School of Chemistry, NRF and NICB for their help and assistance throughout my PhD.

Lastly, I would like to thank my family for their constant support and encouragement, I am incredibly grateful for all they do and without them following this path in my life would not have been possible.

Scientific Output

Awards:

2016 Irish Research Council Government of Ireland Postgraduate Scholarship GOIPG/2016/117.

Publications:

- **J. Hennessy**, B. McGorman, Z. Molphy, N. P. Farrell, D. Singleton T. Brown and A. Kellett. A Click Chemistry Approach to Targeted DNA Crosslinking with *cis*-Platinum(II) Modified Triplex Forming Oligonucleotides. Angewandte Chemie, **2021**, Accepted: DOI: anie.202110455.

Patents:

- Patent application filed for "A cis-platinum(II)-oligomer hybrid". Application number GB2113541.3. (Date filed: 22/09/2021)

Posters:

- Hennessy J., O'Carroll S., Farrell N., and Kellett A. 2019. Development of Polynuclear Pt(II) Biomaterials for Antisense Therapeutic Application and the Detection of Human Genetic Diseases. DCU Annual Chemistry Research Day. Dublin City University, 10th May 2019.
- Hennessy J., Singleton D., Mnich K., Samali A., Slator C., Farrell N., Brown T., and Kellett A. 2019. The Development of Platinum(II) Hybrid Biomaterials for Antigene Therapeutic Application. Centre for Synthesis & Chemical Biology (CSBC) 18th Annual Symposium. Trinity Biomedical Sciences Institute, TCD. 6th December 2019.
- Hennessy J., McGorman B., Singleton D., Brown T., Molphy Z., and Kellett A. 2021. Platinum(II) Hybrid Biomaterials for Antigene Therapeutic Application. Inorganic Ireland Symposium, 14th May 2021. NUIG.

Scientific Talks:

Hennessy J., and Kellett A. 2020. The Development of Platinum(II)-Hybrid Biomaterials for Antisense Therapeutic Application. DCU Annual Chemistry Research Day. Dublin City University. Dublin City University, 5th June 2020

Manuscript under review / in preparation:

1. **J. Hennessy**, M. Coche, D. Singleton, T. Brown and A. Kellett. Thiazole Orange Modified Triplex Forming Oligonucleotides Enhance Molecular Recognition at the DNA interface. (Manuscript in preparation, 2021).
2. **J. Hennessy** and A. Kellett. Platinum(II)-DNA Hybrids: A Modern Approach to the Development of Targeted Platinum(II) Agents – A Review. (Review manuscript in preparation, 2021).

Table of Contents

Declaration iii

Acknowledgement v

Scientific Output vi

Table of Contents ..... *viii*

Table of Figures xi

Table of Schemes xxii

Table of Tables xxiii

List of Abbreviations xxv

Abstract xxix

Chapter I *1*

I. 1. DNA structure and function 2
I. 1. 1. Canonical DNA structures 2

I. 2. Platinum Therapeutics 6
I. 2. 1. Platinum Metallodrug Chemistry 6
I. 2. 2. Cisplatin – Discovery to Application 8
I. 2. 3. Second Generation Platinum(II) Agents 12
I. 2. 4. *Trans*-platinum Derivatives 14
I. 2. 5. Platinum(IV) Prodrugs 15
I. 2. 6. Polynuclear Platinum(II) Complexes 17
I. 2. 7. Drug Targeting and Delivery 19

I. 3. Click Chemistry 22
I. 3. 1. Nucleic Acid Click Chemistry 24
I. 3. 2. Platinum(II) Click Chemistry 27

I. 4. Gene-Editing 29
I. 4. 1. Antisense Technology 30
I. 4. 2. Therapeutic Oligonucleotides 31
I. 4. 3. Triplex Forming Oligonucleotides 33
I. 4. 4. DNA-Crosslinking Hybrids 35
I. 4. 4. 1. Psoralen Hybrids 35
I. 4. 4. 2. Platinum-DNA Hybrids 39

I. 5. Conclusion 43

I. 6. References 44

Chapter II *62*

II. 1. Rationale 63

II. 2. References 67

Chapter III *68*

III. 1. Abstract 69

III. 2. Organic and Inorganic Synthesis 70
III. 2. 1. Chapter Aims 70
III. 2. 2. Rationale 70
III. 2. 3. General Information and Methods 70
III. 2. 4. Synthesis 73
III. 2. 5. Development of Synthetic Routes 89

III. 3. References **104**

Chapter IV ***106***

IV. 1. Abstract **107**

IV. 2. Oligonucleotide Generation **108**
IV. 2. 1. Chapter Aims 108
IV. 2. 2. Rationale 108
IV. 2. 3. General Information 109
IV. 2. 4. Oligonucleotide Development 114
IV. 2. 4. 1. Alkyne-Modified TFOs 114
IV. 2. 4. 2. TOTFOs and AA-TOTFOs 115
IV. 2. 4. 3. Click chemistry using CuAAC and SPAAC strategies 119

IV. 3. Conclusion **123**

IV. 4. References **124**

Chapter V ***125***

V. 1. Abstract **126**
V. 1. 1. Chapter Aims 127
V. 1. 2. Rationale 127

V. 2. Introduction **129**
V. 2. 1. Preparation of Azide-Modified *cis*-Platinum(II) Complexes 131
V. 2. 2. DNA Binding Ability of N_3-Pt(II) Complexes 134
V. 2. 3. *In-vitro* cytotoxicity analysis 136
V. 2. 4. Triplex Formation by Pt(II)-TFO hybrids 138
V. 2. 5. PAGE analysis of Pt(II)-hybrids 140
V. 2. 5. 1. Alkyne TFO triplex formation 141

V. 3. Conclusion **148**

V. 4. References **150**

Chapter VI ***156***

VI. 1. Abstract **157**
VI. 1. 1. Chapter Aims 158
VI. 1. 2. Rationale 158

VI. 2. Generation of *cis*-Pt(II)-AA-TOTFOs **159**
VI. 2. 1. General Information 159
VI. 2. 2. *cis*-Pt(II)-AA-TOTFO design and development 159
VI. 2. 2. 1. PAGE analysis of AA-TOTFO Carbo Hybrids 161

VI. 3. Conclusion **169**

Chapter VII ***171***

VII. 1. Abstract **172**
VII. 1. 1. Chapter Aims 173
VII. 1. 2. Rationale 173

VII. 2. Introduction **173**

VII. 3. Generation of Cu(II)-Phen analogues **176**
VII. 3. 1. Development of synthetic routes 176
VII. 3. 2. Materials and Methods 177
VII. 3. 2. 1. Organic Synthesis 177
VII. 3. 2. 2. Oligonucleotide Development and General Information 180
VII. 3. 3. Thermal melting analysis of TFO2-AMN hybrids 181
VII. 3. 4. PAGE Analysis and Chemical Nuclease Activity of TFO2 Hybrids 183

VII. 3. 4. 1. Summary 187
VII. 3. 4. 2. Future Work 188

VII. 4. Conclusion 190

VII. 5. References 191

Thesis Conclusions and Future Work 194

Chapter VIII 196

VIII. 1. Appendix A 197
VIII. 1. 1. NMR, IR and ESI-MS analysis 197

VIII. 2. Appendix B 229
VIII. 2. 1. Alkyne-Modified TFOs, Pt(II)-TFO Hybrids and Cu(II)-AMN-TFOs 229
VIII. 2. 2. Pt(II)-TOTFO sequences and Hybrids 232
VIII. 2. 3. ESI-MS and HPLC of Oligonucleotides 234
VIII. 2. 3. 1. Alkyne-TFOs 234
VIII. 2. 3. 2. Pt(II)-TFO Hybrids 237
VIII. 2. 3. 3. TOTFOs and Pt(II)-TOTFOs 245
VIII. 2. 3. 4. AA-TOTFOs and Pt(II)-AA-TOTFOs 251

VIII. 3. Appendix C 258
VIII. 3. 1. UV Thermal Melting Analysis for N_3-Platinum(II) Complexes 258
VIII. 3. 2. UV Thermal Melting Analysis *cis*-Pt(II)-TFO Hybrids 262

VIII. 4. Appendix D 266
VIII. 4. 1. Cell Line Characteristics and Cell Viability Experimental Parameters 266

VIII. 5. Appendix E 267
VIII. 5. 1. Supplementary PAGE analysis 267

VIII. 6. Appendix F 272
VIII. 6. 1. NMR analysis 272
VIII. 6. 2. ESI-MS and HPLC for TFO2 Hybrids 275

Table of Figures

Figure I-1. A. Structural configuration of DNA nucleotides and nucleobases. **B.** Specific base-pair recognition between complimentary strands – Adenine:Thymine and Guanine:Cytosine **C**. Conformational twist geometries of the deoxyribose ring structure within DNA. 3
Figure I-2. Three conformational forms dsDNA helix: A-DNA (PDB: 1VJ4), B-DNA (PDB: 1BNA) and Z-DNA (PDB: 2DCG).[6] 4
Figure I-3. Molecular orbital diagram for Pt(II) d_8 square planar and d_6 octahedral geometries. 6
Figure I-4. Demonstration of the trans-effect. **A.** Synthesis of cisplatin. **B.** Synthesis of transplatin. 8
Figure I-5. Timeline of the discovery of cisplatin to the current state of the art regarding platinum(II) therapeutic agents today. 9
Figure I-6. A. Watson and Crick base pairing between thymine-adenine and cytosine-guanine. Orientation of major and minor groove of the duplex sequence. **B.** N7 position of purine bases deoxyadenosine and deoxyguanosine. N7 is implicated in the majority of platinum(II) lesions. 10
Figure I-7. A. Aquation of cis chemotype platinum(II) molecules – initially monosubstituted complex are formed prior to complete conversion under cellular conditions to the final di-aqua cation. **B.** Ratio of dsDNA by cis-platinum(II) species. 11
Figure I-8. First, second and regionally approved generations of cisplatin analogues. From **top left** to **bottom right**: cisplatin, carboplatin, oxaliplatin, nedaplatin (Japan), heptaplatin (Korea) and lobaplatin (China). Date shown indicates year of first approval.[42] 13
Figure I-9. A. Mono- and bifunctional trans-platinum(II) species with L and L' representing a variety of heteroaromatic ligands such as pyridine, quinoline and benzothiazole. **B.** Examples of trans-platinum(II) complexes with substituted asymmetric aliphatic ligands dimethylamine, isopropylamine and propylamine. **C.** An iminoether-substituted trans-platinum(II) complex. 15
Figure I-10. Nature of Pt(II) and Pt(IV) constituent ligands and the properties that are controlled. Pt(IV) complexes possess axial ligands (R) that can undergo extensive modification to provide a wide range of characteristics. 16
Figure I-11. Prominent Pt(IV) complexes that have participated in clinical trials. 17
Figure I-12. Polynuclear platinum complexes synthesised by the Farrell group. Note the terminal amines on TriplatinNC-A and amine chains on TriplatinNC-A that interact in a non-covalent fashion. 18
Figure I-13. Left – Examples of Active-DTD platinum-hybrids. (Est-en)$PtCl_2$, a platinum(II)-hybrid which possess affinity for ER. D-glucose-$PtCl_2$, developed by Keppler and co-workers, showcases similar activity to oxaliplatin analogues. Pt-CTX is a peptide conjugated hybrid exploits unregulated peptide receptor proliferation in tumour vasculature. **Right** – Passive-DTD platinum-hybrids. Bi(PEG-PLA)-Pt(IV) polymer hybrid which showcases excellent drug release kinetics and enhanced activity

in comparison to cisplatin. Pt-PLGA-PEG nanoparticles developed by Lippard et. al.[83] that greatly improve the therapeutic index of cisplatin for prostate cancer. 21
Figure I-14. A. Schematic of copper catalysed alkyne-azide cycloaddition reaction. **B.** Strain promoted alkyne-azide cycloaddition reaction. **C.** Cycloalkynes utilised as strain promoting click reagents: DIFO, DIBO and BCN. 23
Figure I-15. Schematic of solid-phase phosphoramidite synthesis cycle. In general, azide substituents are not well received in the synthesis as reaction with phosphorus have been documented – thus alkyne moieties are the preferred reactive handle to introduce onto the oligo. Solid-phase phosphoramidite synthesis with platinum constituents is also poorly accepted with the inactivation of the metal core observed in some instances. 25
Figure I-16. Click reaction of an azide and alkyne modified nucleobase to form unnatural clicked PCR template. Recognition by polymerases produce amplified product. 26
Figure I-17. Interstrand cross-linking achieved between duplex sequences through click chemistry of modified azide and alkyne uracil nucleobases. Note the azide was incorporated post-synthetically through alteration of an amino intermediate. 27
Figure I-18. A. Schematical representation of sequence-targeted Zinc Finger Nucelases (ZFNs) and Transcription Activator-like Effector Nucleases (TALENs). **B.** Clustered Regularly Interspaced Short Palindromic Repeats (CRISPRs). Scheme is derived from ref[115] and created using BioRender.com. 29
Figure I-19. Therapeutic oligonucleotide modifications within the clinic and under development. Phosphorothioate linkages (**PS**) improves the nuclease stability of ASOs and are generally found combined with 2-MOE modifications, as the 2' position is most commonly used in nuclease degradation processes.[135] **PMO** ASOs represent a class of ASOs that retain the nuclease stability of typical PS ASOs without any of the consequential loss of affinity for target substrates.[136] **PS-RNA** modifications represent the most widely used clinical SiRNA constructs.[137] **PNA** significantly changes the application of oligos at physiological pHs due to the inherent neutral backbone. **LNA**s are a growing class of modified nucleic acids that prevent degradation through the 2' position similar to 2-MOE modifications. Miraversen is an innovative hepatitis treatment representative of this class.[138] 32
Figure I-20. A. Structure of a parallel DNA triplex. **Top.** Triplets generated by parallel triplex formation (T-AT, C^+-GC and G-GC). **Bottom.** Antiparallel triplets (T-AT, A-AT and G-GC). Note that both T-AT and G-GC triplets are possible in either configuration. **B.** Illustration of parallel and antiparallel triplex formation. 34
Figure I-21. Psoralen and significant derivatives. Isopsoralen, 8-methoxypsoralen (8-MOP), 4,5',8-trimethylpsoralen (TMP), 4'-hydroxymethyl-4,5',8-trimethylpsoralen (HMT) and 4'-aminomethyl-4,5',8-trimethylpsoralen (AMT).[158] 36
Figure I-22. A. Platinated building block developed by Reedijk and co-workers for implementation in solid-phase synthesis.[170] **B.** Cis-platinum(II)

derived TFO hybrid designed by Sharma and DNA McLaughlin.[176] **C.** Example of a mono-and bis-functionalised trans-platinum(II) TFO hybrid developed by Miller and colleagues,[168] where (**Pt-G**) denotes a guanine nucleobase coupled at the N7 position to a trans-platinum(II) reagent. **D.** Internally modified N^4-(aminoalkyl) cytosine TFO with a trans-platinum(II) derived reagent coupled.[180] 41
Figure II-1. Project Overview – Generation of Platinum(II)-TFO Hybrid Biomaterials with specific triplex formation and crosslinking to intended duplex targets. 66
Figure III-1. Azide-functionalised cis-platinum(II) complexes designed and developed in Chapter III. 69
Figure III-2. A. Azide-modified N,N chelating ligands generated. **B.** cis-platinum(II) complexes with azide handles for future click chemistry applications. 90
Figure IV-1. Representation of triplex formation and crosslinking afforded by the click chemistry generated cis-platinum(II) TFO hybrids. 107
Figure IV-2. A. Library of alkyne-modified TFO1-6 with associated sequence length, base modification, location and target duplex sequence. **B.** Alkyne-modified nucleobases where C = Octadinyl-dC, U= Octadinyl-dU and X = 5'-BCN-dC. 115
Figure IV-3. A. Alkyne-modified TOTFOs with octadinyl-dC and 5-(1-propargylamino)-dU nucleobase incorporations **B.** Octadinyl-dC modified nucleobase, 5-(1-propargylamino)-dU and schematic depicting TO coupled pdU nucleobase. 116
Figure IV-4. A. AA-TOTFO series where X = AP-C3 monomer and U = pdU nucleobase modification. **B.** AP-C3 alkyne-amine monomer and schematic of the nucleobase once conjugated with both TO and N_3-Pt-Carbo. 118
Figure IV-5. Schematic representation of the CuAAC and SPAAC click strategies. 119
Figure V-1. Representation of the triplex-mediated crosslinking of the GFP gene by cis-platinum(II) TFO hybrids. 126
Figure V-2. Overview of cis-Pt(II)-TFO hybrid design and application. Development of azide bearing platinum(II) complex prior to click chemistry generation of Pt(II)-TFO hybrids. Triplex formation is obtained through parallel Hoogsteen binding to the target dsDNA. Crosslink formation with the duplex target is facilitated by the triplex formation. 128
Figure V-3. Recent crosslinking constructs introduced into nucleic acid systems. Psoralen-derivatised constructs (1991),[9] tethered cis-platinum(II) units (2002)[18, 19] and mono-functional trans-platinum(II) TFO adducts (2012).[20] 129
Figure V-4. A. Alkyne-modified nucleobases. Click combination with each of the azide-functionalised platinum(II) complexes. **B**. TFO sequences with nucleobases modifications denoted and specific recognition sites indicated within the respective duplex target. 133
Figure V-5. A. dsDNA sequences of the GFP gene with triplex recognition site in red. **B.** ΔT_M of target dsDNA sequences treated with 2.5 eq. of azide-functionalised platinum(II) complexes. **C.** Specific T_M values for duplex

sequences when treated with Pt-N_3-Cis, Pt-N_3-Carbo or Pt-N_3-Oxali respectively over 48 h. 135
Figure V-6. A. T_M values of triplex melting observed for TFO3 and TOTFO hybrids. **B.** Thermal melting isotherms showing destabilising and stabilising effects in comparison to alkyne-modified TFO3. Key: ● = TFO3-Carbo; ● = Alkyne-TFO3; ● = TOTFO1-Carbo; and ● = TOTFO2-Carbo represent the respective mid-points of the triplex transitions. 139
Figure V-7. A. Triplex formation for TFO1. Duplex A (1 pmol, lane 2-7) was treated with increasing concentration of TFO1 (2.5-50 eq., lane 3-7). **B.** Triplex formation for TFO2 with similar parameters. Triplex formation is only fully achieved after introduction of approx. 10-25 eq. of TFO (lane 5-6) in comparison to **A.** Samples were prepared in 10 mM phosphate buffer, 150 mM NaCl and 2 mM $MgCl_2$ (pH 6) and incubated over 48 h at 37 ºC, loaded onto 20 % PAGE and subjected to electrophoresis for 4 h at 70 V in 50 mM tris-acetate (TA) buffer (pH 6). Gels were post-stained with SybrGold. 141
Figure V-8. C. Triplex formation for TFO3. Full triplex formation with duplex A (1pmol, lane 2-7) is demonstrated after first stoichiometric loading step (2.5 eq., lane 3). **D-F.** Triplex formation for TFO4, TFO5 and TFO6 respectively. No triplex formation was observed under the PAGE conditions. Conditions and sample preparation was performed as described before (Figure V-7). 142
Figure V-9. A. Triplex formation for TFO2 treated against both a 57 bp target (1 pmol, lane 2, 4-8) and a 40 bp *off*-target (1 pmol, lane 3, 4-8). Increasing stoichiometric ratios of TFO2 was introduced (2.5-50 eq., lane 4-8) and samples incubated over 48 h. **B.** Triplex formation for TFO3 under similar parameters. Neither TFO2 or TFO3 displayed any specificity for the *off*-target. Sample preparation and PAGE conditions were as before. ... 143
Figure V-10. A. TFO3 with modified internal octadinyl-dU nucleobase and respective GFP target sequence. **B.** TFO3-Cis hybrid triplex formation with higher band structures observable. **C.** TFO3-Carbo hybrid. Triplex formation is significant even at lower loadings. **D.** TFO3-Oxali hybrid with higher band triplex formation – slower rate of triplex formation in comparison with TFO3-Carbo. 144
Figure V-11. A. TFO3-Cis hybrid and fluorescently labelled Duplex 3. **B.** NaCN treatment of unmodified triplex system. **C.** NaCN (5,000 eq.) afforded reversal of Pt-triplex system formed by TFO3-Cis hybrid. 146
Figure V-12. A. Denaturing PAGE experimental design. **B.** Terminal and internal nucleobase modification octadinyl-dU and azide-functionalised Pt-N_3-Carbo. **C.** Modified TFO sequences and dsDNA targets. **D.** Denaturing PAGE analysis: TFO-hybrids (50 eq.) were incubated at 37 ºC with duplex targets for a minimum of 48 hours prior to electrophoresis. Upper band (Lanes 3-6) under Cy5 filter is indicative of adduct formation with purine strand. No adduct formation observed for TFO-17C (Lanes 7 and 8). 147
Figure VI-1. Overview of Pt(II)-AA-TOTFO hybrid construction and triplex-mediated crosslinking ability. 157
Figure VI-2. Schematic of AA-TOTFO incorporations. **A.** AP-C3 alkyne-amine nucleobase monomer. **B.** 5-(1-propargylamino)-dU modified nucleobase for TO inclusion. 160

Figure VI-3. A. Preliminary investigation of purity of non-modified AA-TOTFO1-8 sequences. **B**. Triplex formation for AA-TOTFO1-4 with Duplex A (1 pmol, lane 2-5) and AA-TOTFO5-8 with Duplex B (1 pmol, lane 7-10). AA-TOTFO5-8 failed to form triplexes under these conditions. Samples were prepared in 10 mM phosphate buffer, 150 mM NaCl and 2 mM $MgCl_2$ (pH 6) prior to incubation over 24 h at 37 ºC**.** Samples were then loaded onto 20 % PAGE and subjected to electrophoresis for 8 h at 50 V in 50 mM tris-acetate (TA) buffer (pH 6). Gels were post-staiend with SybrGold. 161

Figure VI-4. A. AA-TOTFO1-4 Carbo sequences with modification sites, where X = AP-C3 alkyne-amine monomer and U = 5-(1-propargylamino)-dU nucleobase modification. 57 bp target and 40 bp off-target are shown. **B.** Triplex formation for AA-TOTFO1-4 Carbo treated against target duplex (57 bp) and off-target duplex (40 bp). No off-target selectivity is observed. AA-TOTFO4 Carbo triplex activity is impeded before >10 eq. (AA-TOTFO4 Carbo, lane 4-8). Samples were prepared in 10 mM phosphate buffer, 150 mM NaCl and 2 mM $MgCl_2$ (pH 6) prior to incubation over 48 h at 37 ºC**.** Samples were then loaded onto 20% PAGE and subjected to electrophoresis for 4h at 70 V in 50 mM tris-acetate (TA) buffer (pH 6). Gels were post-stained with SybrGold. ... 162

Figure VI-5. A. AA-TOTFO1 Carbo, X = AP-C3 alkyne-amine monomer. Duplex 3 sequence displayed. **B.** Untreated Pt-triplex gradient (lane 3-5) and NaCN (5,000 eq.) treated Pt-triplex gradient (lane 8-9). AA-TOTFO Carbo crosslink reversal is afforded by NaCN treatment. **C.** TO visualisation at 540 nm without staining. 164

Figure VI-6. A. AA-TOTFO2 Carbo, X = AP-C3 alkyne-amine monomer and U = 5-(1-propargylamino)-dU nucleobase modification. Duplex 3 sequence displayed. **B.** Untreated Pt-triplex gradient (lane 3-5) and NaCN (5,000 eq.) treated Pt-triplex gradient (lane 8-9). AA-TOTFO Carbo crosslink reversal is afforded by NaCN treatment. **C.** TO visualisation at 540 nm without staining. 165

Figure VI-7. A. AA-TOTFO3 Carbo, X = AP-C3 alkyne-amine monomer and U = 5-(1-propargylamino)-dU nucleobase modification. Duplex 3 sequence displayed. **B.** Untreated Pt-triplex gradient (lane 3-5) and NaCN (5,000 eq.) treated Pt-triplex gradient (lane 8-9). AA-TOTFO Carbo crosslink reversal is afforded by NaCN treatment. **C.** TO visualisation at 540 nm without staining. 166

Figure VI-8. A. AA-TOTFO4 Carbo, X = AP-C3 alkyne-amine monomer and U = 5-(1-propargylamino)-dU nucleobase modification. Duplex 3 sequence displayed. **B.** Untreated Pt-triplex gradient (lane 3-5) and NaCN (5,000 eq.) treated Pt-triplex gradient (lane 8-9). AA-TOTFO Carbo crosslink reversal is afforded by NaCN treatment. **C.** TO visualisation at 540 nm without staining. 167

Figure VI-9. Triplex-mediated crosslinking activity for **A.** TFO1-Carbo and **B.** AA-TOTFO1 Carbo. Target (57 bp, 1 pmol, lane 3) and off-target (40 bp, 1 pmol, lane 3) were treated with 1-10 eq. of either TFO1-Carbo or AA-TOTFO1 Carbo. Samples were prepared in 10 mM phosphate buffer, 150 mM NaCl and 2 mM $MgCl_2$ (pH 6) prior to incubation over 48 h at 37 ºC**.** Samples were then loaded onto 20% PAGE and subjected to

electrophoresis for 4h at 70 V in 50 mM tris-acetate (TA) buffer (pH 6). Gels were post-stained with SybrGold. 168
Figure VI-10. TO visualisation of Figure VI-9B at 540 nm with no staining at inverted contrast. TO emission increases with triplex formation. Triplex control is AA-TOTFO1 Carbo at 10 eq. (lane 4). 169
Figure VII-1. Overview of the design of the Cu(II)-AMN-TFO hybrid and potential gene-targeted oxidative DNA damage. 172
Figure VII-2. A. Radical oxidative cleavage by Cu-Phen resulting in direct strand break formation. **B.** Structure of $[Cu(1,10\text{-phenanthroline})_2(H_2O)]^{2+}$. Figure adapted from ref.[2] 175
Figure VII-3. Ligand scaffolds for Cu(II)-AMN-TFO hybrid generation. 176
Figure VII-4. A. TFO2 and duplex target A, where X = 5'-BCN(CEP II)-dC. **B.** Thermal melting analysis of TFO2A-C in comparison to TFO2. **C.** Ligands A-C. **D.** ΔT_M for TFO2 hybrids. **E.** Melting curves for TFO2 hybrids. 182
Figure VII-5. Alkyne-modified TFO2 triplex control. 183
Figure VII-6. A. TFO2 and D_{ON} (57 bp) and D_{OFF} (40 bp) sequences where X = 5'-BCN(CEP II)-dC. Triplex formation for **B**. TFO2A. **C**. TFO2B and **D**. TFO2C. Target (57 bp, 1 pmol, lane 2) and off-target (40 bp, 1 pmol, lane 3) were treated with 2.5-50 eq. of TFO2 hybrid. Samples were prepared in 10 mM phosphate buffer, 150 mM NaCl and 2 mM $MgCl_2$ (pH 6) prior to incubation over 24 h at 37 ºC**.** Samples were then loaded onto 20% PAGE and subjected to electrophoresis for 4h at 70 V in 50 mM tris-acetate (TA) buffer (pH 6). Gels were post-stained with SybrGold. .. 184
Figure VII-7. A. TFO2A cleavage optimisation with increasing ascorbate loading. **B**. Band densitometry analysis of the cleavage reaction. Band intensities were normalised to lane 1 (duplex target) and lane 2 (triplex formation without ascorbate). Samples were prepared in 10 mM phosphate buffer, 150 mM NaCl and 2 mM $MgCl_2$ (pH 6) prior to incubation over 24 h at 37 ºC**.** Samples were then loaded onto 20% PAGE and subjected to electrophoresis for 4h at 70 V in 50 mM tris-acetate (TA) buffer (pH 6). Gels were post-stained with SybrGold. 185
Figure VII-8. TFO2 hybrid cleavage activity. Cleavage for **A**. TFO2A. **B**. TFO2B and **C**. TFO2C. Target (57 bp, 1 pmol, lane 2) and off-target (40 bp, 1 pmol, lane 3) were treated with 10 eq. of TFO2 hybrid and 10 eq. of $CuSO_4$. Increasing concentrations of ascorbate were added to initiate cleavage reaction. **D**. Band densitometry analysis of the cleavage reaction. Band intensities were normalised to lane 2 (duplex target), lane 3 (off-target duplex) and lane 4 (triplex formation without Cu(II)/Na-L-asc). **E**. % Normalised cleavage and % depletion of sample bands. Samples were prepared in 10 mM phosphate buffer, 150 mM NaCl and 2 mM $MgCl_2$ (pH 6) prior to incubation over 24 h at 37 ºC**.** Samples were then loaded onto 20% PAGE and subjected to electrophoresis for 4h at 70 V in 50 mM tris-acetate (TA) buffer (pH 6). Gels were post-stained with SybrGold. 186
Figure VIII-1. ^1H NMR spectra for 1,10-phenanthroline-5,6-epoxide (**1**). 197
Figure VIII-2. ^{13}C NMR spectra for 1,10-phenanthroline-5,6-epoxide (**1**). 197
Figure VIII-3. IR spectrum for 1,10-phenanthroline-5,6-epoxide (**1**). 198
Figure VIII-4. ^1H NMR spectra for 5-azido-1,10-phenanthroline (**2**). 199
Figure VIII-5. ^{13}C NMR spectra for 5-azido-1,10-phenanthroline (**2**). 199

Figure VIII-6. IR spectrum for 5-azido-1,10-phenanthroline (**2**). 200
Figure VIII-7. ^{1}H NMR spectra for [Pt(5-azido-1,10-phenanthroline)Cl_2] (**3**). . 201
Figure VIII-8. ^{195}Pt NMR spectra for [Pt(5-azido-1,10-phenanthroline)Cl_2] (**3**). 201
Figure VIII-9. IR spectrum for [Pt(5-azido-1,10-phenanthroline)Cl_2] (**3**)..... 202
Figure VIII-10. ^{1}H NMR spectra for 1,10-phenanthroline-5,6-dione (**4**). 203
Figure VIII-11. ^{13}C NMR spectra for 1,10-phenanthroline-5,6-dione (**4**). 203
Figure VIII-12. ^{13}C DEPT NMR spectra for 1,10-phenanthroline-5,6-dione (**4**). 204
Figure VIII-13. IR spectrum for 1,10-phenanthroline-5,6-dione (**4**). 204
Figure VIII-14.^{1}H NMR spectra for 11-nitrodipyrido[3,2-a:2',3'-c]phenazine (**5**). 205
Figure VIII-15. ^{13}C NMR spectra for 11-nitrodipyrido[3,2-a:2',3'-c]phenazine (**5**). 205
Figure VIII-16. ^{13}C DEPT NMR spectra for 11-nitrodipyrido[3,2-a:2',3'-c]phenazine (**5**). 206
Figure VIII-17. IR spectrum for 11-nitrodipyrido[3,2-a:2',3'-c]phenazine (**5**). . 206
Figure VIII-18. ^{1}H NMR spectra for 11-aminodipyrido[3,2-a:2',3'-c]phenazine (**6**). 207
Figure VIII-19. ^{13}C NMR spectra for 11-aminodipyrido[3,2-a:2',3'-c]phenazine (**6**)..... 207
Figure VIII-20. ^{13}C DEPT NMR spectra for 11-aminodipyrido[3,2-a:2',3'-c]phenazine (**6**). 208
Figure VIII-21. IR spectrum for 11-aminodipyrido[3,2-a:2',3'-c]phenazine (**6**). 208
Figure VIII-22. ^{1}H NMR spectra for 11-azidodipyrido[3,2-a:2',3'-c]phenazine (**7**). 209
Figure VIII-23. ^{13}C NMR spectra for 11-azidodipyrido[3,2-a:2',3'-c]phenazine (**7**). 209
Figure VIII-24. ^{13}C DEPT NMR spectra for 11-azidodipyrido[3,2-a:2',3'-c]phenazine (**7**). 210
Figure VIII-25. IR spectrum for 11-azidodipyrido[3,2-a:2',3'-c]phenazine (**7**). 210
Figure VIII-26. IR spectrum for [Pt(11-azidodipyrido[3,2-a:2',3'-c]phenazine)Cl_2] (**8**)..... 211
Figure VIII-27. ^{1}H NMR spectra for Di-tert-boc-2-hydroxy-1,3-diaminopropane (**9**)..... 212
Figure VIII-28. ^{13}C NMR spectra for Di-tert-boc-2-hydroxy-1,3-diaminopropane (**9**)..... 212
Figure VIII-29. IR spectrum for Di-tert-boc-2-hydroxy-1,3-diaminopropane (**9**). 213
Figure VIII-30. ^{1}H NMR spectra for Di-tert-boc-2-methanesulfonyl-1,3-diaminopropane (**10**)..... 214
Figure VIII-31. ^{13}C NMR spectra for Di-tert-boc-2-methanesulfonyl-1,3-diaminopropane (**10**)..... 214
Figure VIII-32. ^{13}C NMR spectra for Di-tert-boc-2-methanesulfonyl-1,3-diaminopropane (**10**)..... 215
Figure VIII-33. ^{1}H NMR spectra for Di-tert-boc-2-azido-1,3-diaminopropane (**11**). 216
Figure VIII-34. ^{13}C NMR spectra for Di-tert-boc-2-azido-1,3-diaminopropane (**11**)..... 216

Figure VIII-35. IR spectrum for Di-tert-boc-2-azido-1,3-diaminopropane (**11**). 217
Figure VIII-36. ^{1}H NMR spectra for 2-azidopropane-1,3-diamine dihydrochloride (**12**). 218
Figure VIII-37. ^{13}C NMR spectra for 2-azidopropane-1,3-diamine dihydrochloride (**12**). 218
Figure VIII-38. IR spectrum for 2-azidopropane-1,3-diamine dihydrochloride (**12**). 219
Figure VIII-39. ^{1}H NMR spectra for cis-[Pt(2-azidopropane-1,3-diamine)Cl_2] (**13**). 220
Figure VIII-40. ^{13}C NMR spectra for cis-[Pt(2-azidopropane-1,3-diamine)Cl_2] (**13**). 220
Figure VIII-41. ^{195}Pt NMR spectra for cis-[Pt(2-azidopropane-1,3-diamine)Cl_2] (**13**). 221
Figure VIII-42. IR spectrum for cis-[Pt(2-azidopropane-1,3-diamine)Cl_2] (**13**). 221
Figure VIII-43. ESI-MS for cis-[Pt(2-azidopropane-1,3-diamine)Cl_2] (**13**). 222
Figure VIII-44. ^{1}H NMR spectra for cis-[Pt(2-azidopropane-1,3-diamine)CBDCA] (**15**). 223
Figure VIII-45. ^{13}C NMR spectra for cis-[Pt(2-azidopropane-1,3-diamine)CBDCA] (**15**). 223
Figure VIII-46. ^{195}Pt NMR spectra for cis-[Pt(2-azidopropane-1,3-diamine)CBDCA] (**15**). 224
Figure VIII-47. IR spectrum for cis-[Pt(2-azidopropane-1,3-diamine)CBDCA] (**15**). 224
Figure VIII-48. ESI-MS for cis-[Pt(2-azidopropane-1,3-diamine)CBDCA] (**15**). 225
Figure VIII-49. ^{1}H NMR spectra for cis-[Pt(2-azidopropane-1,3-diamine)Oxalate] (**16**). 226
Figure VIII-50. ^{13}C NMR spectra for cis-[Pt(2-azidopropane-1,3-diamine)Oxalate] (**16**). 226
Figure VIII-51. ^{195}Pt NMR spectra for cis-[Pt(2-azidopropane-1,3-diamine)Oxalate] (**16**). 227
Figure VIII-52. IR spectrum for cis-[Pt(2-azidopropane-1,3-diamine)Oxalate] (**16**). 227
Figure VIII-53. ESI-MS for cis-[Pt(2-azidopropane-1,3-diamine)Oxalate] (**16**). 228
Figure VIII-54. HPLC and ESI-MS spectra for alkyne-TFO1. 234
Figure VIII-55. HPLC and ESI-MS spectra for alkyne-TFO2. 234
Figure VIII-56. HPLC and ESI-MS spectra for alkyne-TFO3. 235
Figure VIII-57. HPLC and ESI-MS spectra for alkyne-TFO4. 235
Figure VIII-58. HPLC and ESI-MS spectra for alkyne-TFO5. 236
Figure VIII-59. HPLC and ESI-MS spectra for alkyne-TFO6. 236
Figure VIII-60. HPLC and ESI-MS spectra for TFO1-Cis. 237
Figure VIII-61. HPLC and ESI-MS spectra for TFO1-Carbo. 237
Figure VIII-62. HPLC and ESI-MS spectra for TFO1-Oxali. 238
Figure VIII-63. HPLC and ESI-MS spectra for TFO2-Cis. 238
Figure VIII-64. HPLC and ESI-MS spectra for TFO2-Carbo. 239
Figure VIII-65. HPLC and ESI-MS spectra for TFO2-Oxali 239
Figure VIII-66. HPLC and ESI-MS spectra for TFO3-Cis. 240

Figure VIII-67. HPLC and ESI-MS spectra for TFO3-Carbo. 240
Figure VIII-68. HPLC and ESI-MS spectra for TFO3-Oxali..... 241
Figure VIII-69. HPLC and ESI-MS spectra for TFO4-Cis..... 241
Figure VIII-70. HPLC and ESI-MS spectra for TFO4-Carbo. 242
Figure VIII-71. HPLC and ESI-MS spectra for TFO4-Oxali..... 242
Figure VIII-72. HPLC and ESI-MS spectra for TFO5-Cis..... 243
Figure VIII-73. HPLC and ESI-MS spectra for TFO5-Carbo. 243
Figure VIII-74. HPLC and ESI-MS spectra for TFO5-Oxali..... 244
Figure VIII-75. HPLC and ESI-MS spectra for TOTFO1. 245
Figure VIII-76. HPLC and ESI-MS spectra for TOTFO2. 245
Figure VIII-77. HPLC and ESI-MS spectra for TOTFO3. 246
Figure VIII-78. HPLC and ESI-MS spectra for TOTFO4. 246
Figure VIII-79. HPLC and ESI-MS spectra for TOTFO5. 247
Figure VIII-80. HPLC and ESI-MS spectra for TOTFO6. 247
Figure VIII-81. HPLC and ESI-MS spectra for TOTFO1-Carbo. 248
Figure VIII-82. HPLC and ESI-MS spectra for TOTFO2-Carbo. 248
Figure VIII-83. HPLC and ESI-MS spectra for TOTFO3-Carbo. 249
Figure VIII-84. HPLC and ESI-MS spectra for TOTFO4-Carbo. 249
Figure VIII-85. HPLC and ESI-MS spectra for TOTFO5-Carbo. 250
Figure VIII-86. HPLC and ESI-MS spectra for TOTFO6-Carbo. 250
Figure VIII-87. HPLC and ESI-MS spectra for AA-TOTFO1. 251
Figure VIII-88. HPLC and ESI-MS spectra for AA-TOTFO2. 251
Figure VIII-89. HPLC and ESI-MS spectra for AA-TOTFO3. 252
Figure VIII-90. HPLC and ESI-MS spectra for AA-TOTFO4. 252
Figure VIII-91. HPLC and ESI-MS spectra for AA-TOTFO5. 253
Figure VIII-92. HPLC and ESI-MS spectra for AA-TOTFO6. 253
Figure VIII-93. HPLC and ESI-MS spectra for AA-TOTFO1-Carbo. 254
Figure VIII-94. HPLC and ESI-MS spectra for AA-TOTFO2-Carbo. 254
Figure VIII-95. HPLC and ESI-MS spectra for AA-TOTFO3-Carbo. 255
Figure VIII-96. HPLC and ESI-MS spectra for AA-TOTFO4-Carbo. 255
Figure VIII-97. HPLC and ESI-MS spectra for AA-TOTFO5-Carbo. 256
Figure VIII-98. HPLC and ESI-MS spectra for AA-TOTFO6-Carbo. 256
Figure VIII-99. HPLC and ESI-MS spectra for AA-TOTFO7-Carbo. 257
Figure VIII-100. HPLC and ESI-MS spectra for AA-TOTFO8-Carbo. 257
Figure VIII-101. High resolution fluorescent melting of Duplex A-C controls with and without cisplatin treatment. Melting curves are normalised with control melts (black) plotted in comparison to duplex melts after 24 h (green) and 48 h (blue) cisplatin incubation. First negative derivative of normalised fluorescence of duplex curves displayed in rows 2 and 4. 258
Figure VIII-102. UV melting curves for Duplex A-C over 24-48 h recorded as a function of temperature. 259
Figure VIII-103. Thermal melting analysis of alkyne-TFO1-5 recorded as a function of temperature (12–90 ºC)..... 263
Figure VIII-104. Thermal melting analysis of *cis*-Pt(II)-TFO hybrids with alkyne-TFO as reference. UV melting curves recorded as a function of temperature, normalised and smoothed. Curves displayed from 20-87 ºC. 264

Figure VIII-105. Thermal melting analysis of *cis*-Pt(II)-TOTFO constructs after 24-48 h incubation with alkyne-TFO1 as reference. Curves displayed from 20-87 ºC. 265
Figure VIII-106. Cell viability expressed as normalized percent of viable cells relative to controls of cisplatin, NaCl and 1,10-phenanthroline. Cell lines treated with platinum complexes and control compounds over 24 h and 48 h incubations. 266
Figure VIII-107. Triple formation and cross-linking for TFO2-Carbo. **24 h**. Triplex formation after 24 hour incubation of duplex target (1 pmol, Lane 6-10) with increasing equivalents of TFO2-Carbo hybrid (2.5-50 eq., Lane 6-10). Triplex formation increases with larger loading while no off-target triplex formation or cross-linking is observed (Off-target duplex, Lane 6-10). **48 h.** Triplex formation after 48 hour incubation. Formation occurs at lower loading of TFO2-Carbo (10-25 eq., Lane 8-9) compared to 24 hour incubation. Samples were prepared in 10 mM phosphate buffer with 150 mM NaCl and 2 mM $MgCl_2$) (pH 6.0) in a volume of 5 μL + 1 μL 6x loading dye. Samples were incubated for either 24 h (left) or 48 h (right) at 37 °C, loaded onto 20% PAGE and subjected to electrophoresis for 4 h at 70 V in 50 mM TA triplex buffer (pH 6.0). 267
Figure VIII-108. A. Alkyne-modified TFO3 and D_{ON} and D_{OFF} target sequences. Triplex-mediated crosslinking for **B.** TFO3-Cis. **C.** TFO3-Carbo and **D.** TFO3-Oxali. Target (57 bp, 1 pmol, lane 3) and off-target (40 bp, 1 pmol, lane 3) were treated with 1-10 eq. of TFO3 hybrid. Samples were prepared in 10 mM phosphate buffer, 150 mM NaCl and 2 mM $MgCl_2$ (pH 6) prior to incubation over 48 h at 37 ºC**.** Samples were then loaded onto 20% PAGE and subjected to electrophoresis for 4h at 70 V in 50 mM tris-acetate (TA) buffer (pH 6). Gels were post-stained with SybrGold. 268
Figure VIII-109. A. Triplex formation for TOTFO1-3 Carbo (50 eq., Lanes 7-9). TOTFO2 displays enhanced triplex formation compared with TOTFO1-Carbo and TOTFO3-Carbo. Gel is post-stained with SYBRGold stain. **B.** Non-stained visualisation of the same gel. TOTFO2-Carbo displays enhanced fluorescent emission. PAGE analysis was performed in TA triplex buffer (10 mM phosphate 150 mM NaCl 2 mM $MgCl_2$, pH 6.0) at 70 V for 240 mins. **C.** Propargylamino-dU nucleobase modification with coupled TO_{B6}. 269
Figure VIII-110. Optimisation of triplex reversal with sodium cyanide. Triplex formation for TFO3 (50 eq.) with fluorescently labelled Duplex 3 (1 eq., 1 pmol) (Lane 3). Introduction of increasing concentrations of NaCN solution (1000-300000 pmol, Lanes 4-13). PAGE performed in TA triplex buffer (10 mM phosphate 150 mM NaCl 2 mM $MgCl_2$, pH 6.0) at 70 V for 240 mins. Gel visualised and imaged using Cy5 filter. 269
Figure VIII-111. ^{1}H NMR spectra for 2-(4-nitrophenyl)-1H-imidazo[4,5-f]-1,10-phenanthroline. 272
Figure VIII-112. ^{13}C NMR spectra for 2-(4-nitrophenyl)-1H-imidazo[4,5-f]-1,10-phenanthroline. 272
Figure VIII-113. ^{1}H NMR spectra for 2-(4-aminophenyl)-1H-imidazo[4,5-f]-1,10-phenanthroline. 273
Figure VIII-114. ^{13}C NMR spectra for 2-(4-aminophenyl)-1H-imidazo[4,5-f]-1,10-phenanthroline. 273

Figure VIII-115. ^{1}H NMR spectra for 2-(4-azidophenyl)-1H-imidazo[4,5-f]-1,10-phenanthroline. 274
Figure VIII-116. ^{13}C NMR spectra for 2-(4-azidophenyl)-1H-imidazo[4,5-f]-1,10-phenanthroline. 274
Figure VIII-117. HPLC and ESI-MS spectra for TFO2A..... 275
Figure VIII-118. HPLC and ESI-MS spectra for TFO2B..... 275

Table of Schemes

Scheme III-1. Synthetic routes for the azide-functionalised cis-platinum(II) complexes 91
Scheme III-2. Synthetic routes to generate Pt-N_3-Phen (**3**)..... 92
Scheme III-3. Reaction mechanism of alkene epoxidation by a peroxy acid reagent. 93
Scheme III-4. Proposed reaction mechanism for epoxide ring-opening through nucleophilic attack of sodium azide. 94
Scheme III-5. Synthetic routes for the generation of Pt-N_3-DPPZ (**8**). 95
Scheme III-6. Reaction mechanism for a general Schiff base condensation. . 95
Scheme III-7. Reaction mechanism for the reduction of aromatic nitro groups to amines proposed by Rozas et al.[17] 96
Scheme III-8. Reaction mechanism demonstrating **A**. the conversion of $NaNO_2$ to nitrous acid prior to **B.** further conversion of the excess HNO_2 to the nitrosonium ion. 97
Scheme III-9. Reaction mechanism depicting the formation of the diazonium ion. 97
Scheme III-10. Synthetic routes for the generation of N_3-DAP.HCl (**12**). 98
Scheme III-11. Reaction mechanism for the addition of BOC protection groups to amines. 99
Scheme III-12. Reaction mechanism for the formation of the mesylated product. 100
Scheme III-13. S_N2 nucleophilic substitution of mesylate group to obtain azide product. 101
Scheme III-14. Reaction mechanism for the deprotection of the BOC-protected amines using 6M HCl and subsequent in-situ formation of the hydrochloride salt. 101
Scheme III-15. Synthetic route for the generation of N_3-Pt-Cis. 102
Scheme III-16. Synthetic routes for the generation of N_3-Pt-Carbo **15** and N_3-Pt-Oxali **16.** 102
Scheme VII-1. Synthetic routes for the generation of N_3-ImPhen (19). 176
Scheme VII-2. Synthetic routes for the generation of N_3-But-DPPZ. 188
Scheme VII-3. Synthetic routes for the generation of Methyl 4-(4-azidophenyl)-7-oxo-7H-pyrido[4,3,2-de][1,10]phenanthroline-5-carboxylate. 189
Scheme VII-4. Synthetic routes for the generation of 5-azidoascididemin. ... 189

Table of Tables

Table I-1. Summary of structural differences between A-, B- and Z-DNA.[9] 5
Table I-2. Derivatised psoralen-hybrids and design linkage..... 38
Table I-3. Current Platinum-DNA Hybrid state of the art. 42
Table IV-1. 5'-dC = 5'-(5)octadinyl-deoxycytidine; **int-dU** = internal-octadinyl-deoxyuridine; **5'-BCN-dC** = 5'-BCN(CEP II)-deoxycytidine; **AP-C3** = alkyne-amine monomer nucleobase; **pdU** = 5-(1-propargylamino)-deoxyuridine; **pdU-TO** = pdU with TO (thiazole orange) coupled; **N_3-Pt(II)-Cis** = cis-[Pt(2-azidopropane-1,3-diamine)Cl_2]; **N_3-Pt(II)-Carbo** = cis-[Pt(2-azidopropane-1,3-diamine)(CBDCA)]; **N_3-Pt(II)-Oxali** = cis-[Pt(2-azidopropane-1,3-diamine)(Oxalate)]; ***** = Yield was not recoverable. 121
Table V-1. IC_{50} values determined for breast cancer cell lines treated over 48 h. 137
Table VI-1. AA-TOTFO sequences clicked with Pt-N_3-Carbo. 159
Table VIII-1. Oligonucleotide, Pt(II)-TFO hybrid oligonucleotide sequences and modifications. Calculated and observed m/z: (a) = -71 m/z caused by loss of the chloride ligands during ionisation process; (b) = -88 m/z caused by loss of oxalate ligand during ionisation process; (c) = ESI-MS displayed additional peak with +56 m/z, corresponding to Fe^{3+} ion. **5'-dC** = 5'-(5)octadinyl-deoxycytidine; **int-dU** = internal-octadinyl-deoxyuridine; **5'-BCN-dC** = 5'-BCN(CEP II)-deoxycytidine; **N_3-Pt(II)-Cis** = *cis*-[Pt(2-azidopropane-1,3-diamine)Cl_2]; **N_3-Pt(II)-Carbo** = *cis*-[Pt(2-azidopropane-1,3-diamine)(CBDCA)]; **N_3-Pt(II)-Oxali** = *cis*-[Pt(2-azidopropane-1,3-diamine)(Oxalate)]; **DA tgt.** = Duplex A polypurine target strand; **DA comp.** = Duplex A polypyrimidine complementary strand. Duplex A is the target sequence for oligos TFO1-TFO3. **DB** and **DC** = Duplex B and Duplex C. Duplex B is the target sequence for oligos TFO4-TFO5. Duplex C is the target sequence for TFO6. The 57 bp target is a target sequence for TFO1-3 used in PAGE analysis. 229
Table VIII-2. Oligonucleotide, Pt(II)-TOTFO and Pt(II)-AA-TOTFO hybrid oligonucleotide sequences and modifications. Calculated and observed m/z: **5'-dC** = 5'-(5)octadinyl-deoxycytidine; **AP-C3** = alkyne-amine monomer nucleobase; **pdU** = 5-(1-propargylamino)-deoxyuridine; **pdU-TO** = pdU with TO (thiazole orange) coupled**; N_3-Pt(II)-Carbo** = *cis*-[Pt(2-azidopropane-1,3-diamine)(CBDCA)]. *** =** ESI-MS data for TOTFO6-Carbo was not obtained. 232
Table VIII-3. Fluorescent thermal melting analysis for Duplex A-C after incubation with cisplatin at 37 ºC. 258
Table VIII-4. Thermal melting analysis for Duplex A-C after incubation with N_3-Pt-Cis at 37 ºC. 259
Table VIII-5. Thermal melting analysis for Duplex A-C after incubation with N_3-Pt-Carbo at 37 ºC. 260
Table VIII-6. Thermal melting analysis for Duplex A-C after incubation with N_3-Pt-Oxali at 37 ºC. 261
Table VIII-7. T_M values were recorded in 10 mM phosphate (PO_4^{3-}), 150 mM NaCl, 2 mM $MgCl_2$, pH 6 buffer. Samples were incubated for 24-48 h prior to melting analysis. T_M temperatures were calculated by the first

derivative of a non-linear sigmoidal regression curve using GraphPad Prism 8.0. Final T_M values are an average of 3 melting cycles. ΔT_M values for Pt(II)-TFOs are relative to the unclicked alkyne TFO precursor (e.g. TFO1 and TFO1-Carbo). **5'-dC** = 5'-(5)octadinyl-deoxycytidine; **int-dU** = internal-octadinyl-deoxyuridine; **5'-BCN-dC** = 5'-BCN(CEP II)-deoxycytidine; **pdU** = 5-(1-propargylamino)-deoxyuridine; **pdU-TO** = pdU with TO (thiazole orange) coupled; **N_3-Pt(II)-Cis** = *cis*-[Pt(2-azidopropane-1,3-diamine)Cl_2]; **N_3-Pt(II)-Carbo** = *cis*-[Pt(2-azidopropane-1,3-diamine)(CBDCA)]; **N_3-Pt(II)-Oxali** = *cis*-[Pt(2-azidopropane-1,3-diamine)(Oxalate)]; **n.t.o.** = no triplex observed; **n.d.** = not determined due to T_M < 12 ºC. 262

Table VIII-8. Cell line characteristics utilised in cell viability studies. Four breast cancer cell lines were selected: MCF-7, T-47D, MDA-MB-231 and MDA-MB-468. MCF-10a is an immortalised non-tumorigenic breast cancer cell line. Results obtained for the treatment of MCF-10a cells are preliminary, 3 biological replicates need to be performed to produce reliable results. 266

Table VIII-9. Raw PAGE analysis images for Chapter V Figure V-10 and Figure V-11. Images were visualised using a Syngene G:Box Mini 9 gel documentation system. Raw PAGE images for: **A.** Figure V-10B. **B.** Figure V-10C. **C.** Figure V-10D. **D.** Figure V-11C (Cy5). **E.** Figure V-11C (FAM). **F.** Figure V-11C (Multiplex). 270

Table VIII-10. Raw PAGE analysis images for Chapter V Figure V-12D. Images were visualised on a Syngene G:Box Mini 9 gel documentation system. Raw PAGE images for: **A.** Figure V-12D (Multiplex). **B.** Figure V-12D (Cy5). **C.** Figure V-12D (FAM)..... 271

List of Abbreviations

A	Adenine
AA	AP-C3 alkyne amine monomer
AGO-2	Argonaute-2
AMN	Artificial metallo-nuclease
AR	Androgen receptor
ASO	Antisense Oligonucleotide
ATP7A	Copper transporter ATPase 7A
ATP7B	Copper transporter ATPase 7B
BCN	Bicyclo[6.1.0]nonyne
BNA	Branched nucleic acid
C	Cytosine
CBDCA	Cyclobutane Dicarboxylic Acid
$CDCl_3$	Deuterated chloroform
$CHCl_3$	Chloroform
Cl	Chloride
CMV	Cytomegalovirus
^{13}C NMR	Carbon-13 nuclear magnetic resonance
CRISPRs	Clustered Regularly Interspaced Short Palindromic Repeats
CTR1	High affinity copper uptake protein 1
Cu	Copper
CuAAC	Copper-catalysed Azide-Alkyne Cycloaddition
DACH	1,2-Diaminocyclohexane
dA	Deoxyadenine
dC	Deoxycytosine
DCM	Dichloromethane
dG	Deoxyguanine
DIBO	Dibenzocyclooctynol
DLT	Dose-limiting toxicity

DMD	Duchenne muscular dystrophy
DMF	Dimethylformamide
DMF-d_7	Deuterated dimethylformamide
DMSO	Dimethylsulfoxide
DMSO-d_6	Deuterated dimethylsulfoxide
DNA	Deoxyribonucleic Acid
DPPZ	Dipyrido[3,2-a:2',3'-c]phenazine
DTD	Drug Targeting and Delivery
DNA	Deoxyribonucleic Acid
dsDNA	Double-stranded DNA
ssDNA	Single-stranded DNA
EDTA	Ethylenediaminetetraacetic acid
EPR	Enhanced permeability and retention
ER	Estrogen receptors
ESI-MS	Electrospray Ionisation Mass Spectrometry
Et_2O	Diethyl ether
EtOH	Ethanol
FDA	Food and Drug Administration
FT-IR	Fourier transform infrared
G	Guanine
GFP	Green Fluorescent Protein
HCl	Hydrochloric acid
HSA	Human serum albumin
HDR	Homologous directed repair
^{1}H NMR	Proton nuclear magnetic resonance
HNO_3	Nitric acid
HSAB	Hard and soft acid and base
H_2SO_4	Sulphuric Acid
IR	Infrared Spectroscopy

KBr	Potassium bromide
KI	Potassium Iodide
LNA	Locked nucleic acid
LG	Leaving group
MeOH	Methanol
$MgCl_2$	Magnesium chloride
$MgSO_4$	Magnesium sulphate
mRNA	Messenger ribonucleic acid
MTD	Maximum Tolerated Dose
2'-MOE	2'-O-methoxyethyl
N	Nitrogen
NA	Nucleic Acid
NaCl	Sodium chloride
Na-*L*-Asc	Sodium-*L*-ascorbate
NaOH	Sodium hydroxide
NaN_3	Sodium azide
$NaNO_2$	Sodium nitrite
NER	Nucleotide Excision Repair
NHEJ	Non-homologous end joining
NSCLC	Non-small cell lung cancer
ON	Oligonucleotide
PCR	Polymerase chain reaction
Pd/C	Palladium on carbon
pdU	Propargylamino deoxyuridine
PMO	Phosphorodiamidate morpholino oligonucleotide
PNA	Peptide nucleic acid
PPC	Polynuclear platinum(II) compounds/complexes
PS	Phosporothioate

Pt	Platinum
Pur	Purine
Py	Pyrimidine
RNA	Ribonucleic Acid
RISC	RNA-induced silencing complex
SCLC	Small cell lung cancer
siRNA	Short-interfering ribonucleic acid
SPAAC	Strain Promoted Azide-Alkyne Cycloaddition
T	Thymine
TA	Tris-acetate
TALENs	Transcription activator-like effector nucleases
TBE	Tris/Borate/EDTA
TBTA	Tris[1(1-benzyl-1H-1,2,3-triazol-4-yl)methyl]amine
THF	Tetrahydrofuran
TFO	Triplex-forming oligonucleotide
T_M	Thermal melting
U	Uracil
ZFN	Zinc-finger nuclease

Abstract

Joseph Hennessy B.Sc.

The Development of Mononuclear Platinum Hybrid Biomaterials for Antigene Therapeutic Application

Since the serendipitous discovery of cisplatin by Rosenberg platinum agents based on the traditional *cis* chemotype are still the cornerstone of platinum therapeutic application with cisplatin, carboplatin and oxaliplatin as the only agents approved globally for use. Past research has focused mainly on elucidating the mechanistic action of these traditional Pt(II) agents with great success and streamed into efforts centred on trying to reduce the potent toxic side-effects such as nephrotoxicity, ototoxicity and poor target selectivity. Classes of platinum complexes such as *trans*-substituted platinum(II) agents, platinum(IV) prodrugs, polynuclear platinum(II) complexes and in particular, platinum(II)-DNA hybrids produced for an antigene strategy, have all observed a significant renewal of interest in recent years.

This thesis focuses on the development of a library of platinum(II)-triplex forming oligonucleotide hybrids that possess targeted antigene applications. Firstly, the synthesis of azide-functionalised ligands and their complexation with platinum to form azide-functionalised *cis*-platinum(II) complexes is reported. Thereafter, the design and synthesis of triplex forming oligonucleotides (TFOs) is reported and followed by the utilisation of the copper-catalysed and strain promoted alkyne-azide cycloaddition or 'click chemistry' to generate gene-directed *cis*-platinum(II)-TFO hybrids. The work reported represents the first example of click chemistry strategies being employed to afford *cis*-platinum(II)-TFO constructs designed this way.

DNA interaction studies identified that the azide-functionalised platinum(II) complexes retain activity against dsDNA targets. The cis-platinum(II)-TFO constructs demonstrated sequence specific triplex recognition with no *off*-target effects observed in the presence of purine rich sequences. However, in general the crosslink formation on target genes of interest by the platinum(II) ion destabilises triplex formation. The introduction of TO – a known intercalating fluorophore – can remediate this destabilisation and this work demonstrates how TO-modified *cis*-Pt(II)-TFOs retain their targeting abilities with enhanced stabilising characteristics.

Finally, TFO constructs containing a novel alkyne-amine nucleobase were developed and investigated for their ability to incorporate TO and Pt(II). This strategy was developed to enhance site-specific metal ion-DNA target interactions whereby the proximity of the complex to the DNA interface was enhanced under the guidance of the neighbouring TO intercalator. The conjugation of Cu(II)-phenanthrene-type scaffolds with alkyne-modifed TFOs to generate novel Cu(II)-AMN-TFOs has afforded unique stabilising properties and represent an innovative class of gene-targeted system.

Chapter I

Platinum – Nucleic Acid Interactions

I. 1. DNA structure and function

I. 1. 1. Canonical DNA structures

Deoxyribonucleic acid (DNA) can be considered the host carrier of natural biological information and in turn acts as both a safe storage and transfer mechanism for the continuance of cellular information. Discovered in 1953, the structure of DNA was elucidated by Watson, Crick and Franklin sparking the advancement of research across numerous biological and chemistry fields.[1] The predominant form of DNA found in nature is known as B-DNA and is composed of two nucleic acid strands that contain multiple repeating nucleotides wherein the nucleotides consist of a nucleobase, a sugar and a linking phosphodiester group (**Figure I-1, A**). The two strands coil around each other in an anti-parallel orientation and afford complimentary base recognition through hydrogen bonding between the nucleobase substituents giving rise to the secondary helical structure of DNA. The nucleobases consist of the purines adenine (A) and guanine (G) and the pyrimidines thymine (T) and cytosine (C), respectively. Bonding between DNA bases follows Chargaff's rules whereby purines and pyrimidines bind in a 1:1 ratio (adenine:thymine and guanine:cytosine) (**Figure I-1, B**).[2] The rigidity and strength of the DNA double helical structure is derived from the internal hydrogen bonding of the base pairs and π-π stacking interactions between nucleobases.

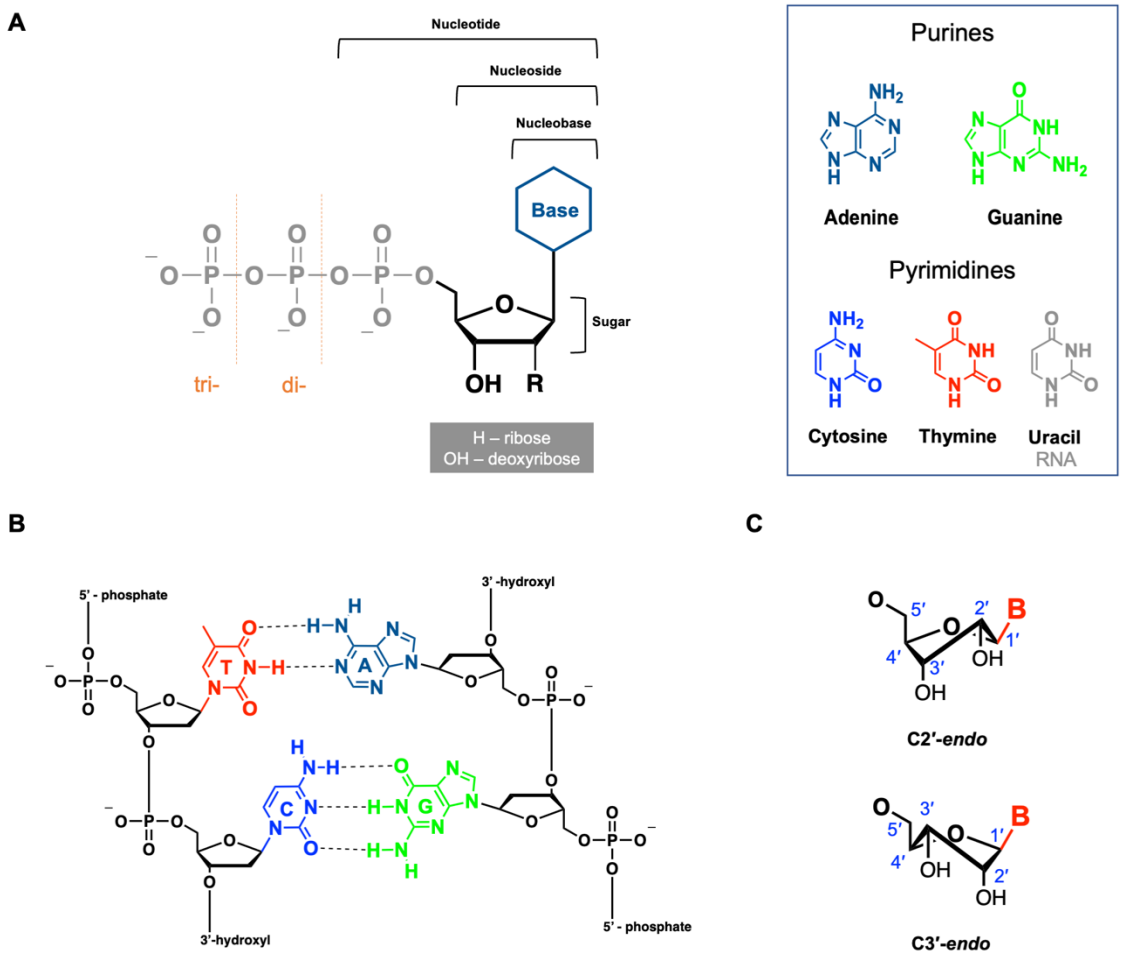

Figure I-1. A. Structural configuration of DNA nucleotides and nucleobases. **B.** Specific base-pair recognition between complimentary strands – Adenine:Thymine and Guanine:Cytosine **C**. Conformational twist geometries of the deoxyribose ring structure within DNA.

In B-DNA, the 2'-deoxyribose ring is found in a locked C2'-endo twist configuration whereas A-DNA and Z-DNA both exhibit C3'-endo twist configurations (**Figure I-1, C**). Due to this the angle between the glycosidic bonds and hydrogen bonds result in unequal grooves in the helical structure known as the minor and major grooves. These structural characteristics are key factors in the targeting of B-DNA – the major groove (10.5 Å) is wider than the minor groove (4.8 Å), although their depths are identical.[3] The hydrophobic environment of the exposed nucleobases within the major groove represents another key distinction compared to the hydrophilic environment in which the phosphate chains can be found in the minor groove. The base pairs of B-DNA display an axial rise of 3.4 Å (0.34 nm) and a 34.5 ° twist angle associated with every residue rotation while the width of the helix diameter is 20 Å.[4] DNA itself is an interestingly flexible

polymeric structure and can be found in other configurations when presented with changing environments or in the presence of certain small molecules. A-DNA is predominantly found within anhydrous environments and although similar to B-DNA, is shorter and more rigid. The conformation of the A-DNA ribose ring – found in a 'puckered' C3'-endo twist configuration – leads to 11 base pairs per helical turn compared to the 10-10.5 of B-DNA and a shorter distance between nucleobases with an axial rise of 2.55 Å.[5]

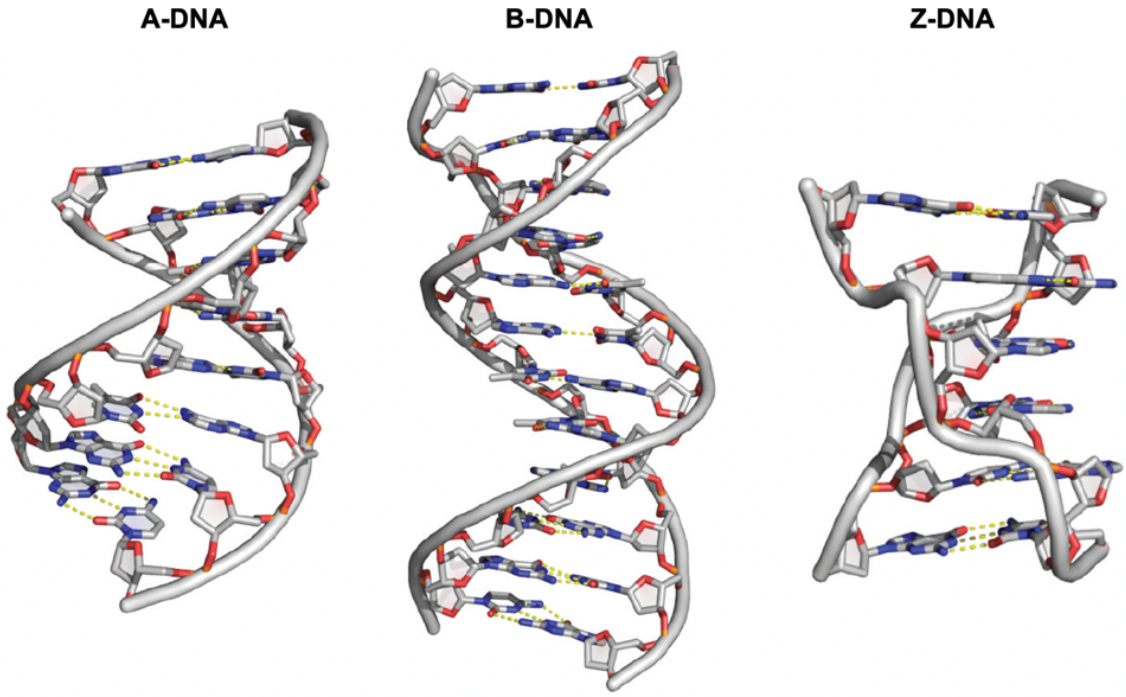

Figure I-2. Three conformational forms dsDNA helix: A-DNA (PDB: 1VJ4), B-DNA (PDB: 1BNA) and Z-DNA (PDB: 2DCG).[6]

Discovered in 1979,[7] Z-DNA displays radical differences compared to A- and B-DNA whereby the helical geometry changes to a left-handed double helical structure in comparison to the normal right-handed nature of DNA. The conformational change occurs from the alternating *syn*- and *anti*-conformations of the purine and pyrimidine nucleobases, respectively, alongside the alternating puckering of the sugar units (C2'-endo for pyrimidines and C3'-endo for purines). Structurally, this leads to a 'zig-zag' patterning where the Z-DNA is elongated and narrow (18 Å in diameter) with a single narrow groove comparable to the minor groove of B-DNA (**Figure I-2**).[8]

Table I-1. Summary of structural differences between A-, B- and Z-DNA.[9]

Parameter	A-DNA	B-DNA	Z-DNA
Helical Sense	Right	Right	Left
Residues per helical turn	11	10	12
Helix Pitch (Å)	28	34	45
Helix Diameter (Å)	23	20	18
Axial Rise (Å)	2.55	3.4	3.7
Rotation per Residue (Å)	33	36	-30

DNA is not only limited to the three canonical conformations described and can be observed to arrange itself in other forms such as triplexes, G-quadruplexes and I-motifs. These forms of DNA have seen significant research efforts undertaken with their importance recognised for gene-specific drug targeting.[10, 11] In particular, triplex motifs are discussed in greater detail in future sections.

I. 2. Platinum Therapeutics

I. 2. 1. Platinum Metallodrug Chemistry

Platinum belongs to the group 10 transition metals with an electronic configuration of $[Xe]4f^{14}5d^{9}6s^{1}$. Platinum is most commonly found in the Pt(II) and Pt(IV) oxidation states. Following HSAB (hard and soft (Lewis) acid and bases), platinum is considered a 'soft' acid metal – whereby 'soft' indicates that the platinum species is considered relatively large, forms low charge states and is strongly polarizable.[12] Due to this soft acid nature, platinum undergoes stable soft-soft interactions with ligands such as sulphur, nitrogen and carbon monoxide.

The 16-electron metal complexes that possess d^8 configurations are found to contravene the general 18 electron rule. Pt(II) is observed to form square planar low-spin d^8 geometries while the more kinetically inert Pt(IV) oxidation state forms complexes consisting of octahedral low spin d^6 geometries (**Figure I-3**). The highest energy orbitals for both geometries – square planar (d_x^2-y^2) and octahedral (d_x^2-y^2, d_z^2) – are unoccupied.

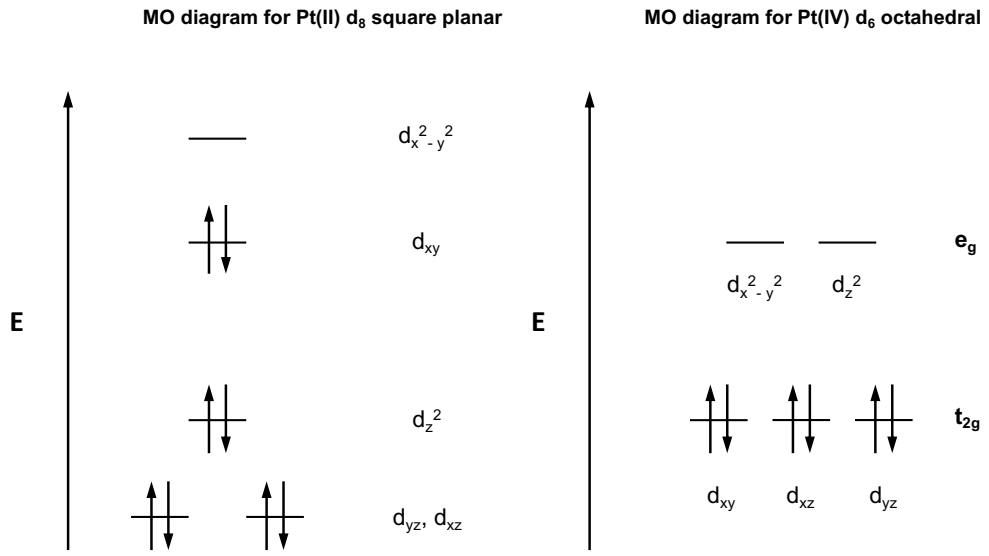

Figure I-3. Molecular orbital diagram for Pt(II) d_8 square planar and d_6 octahedral geometries.

The *trans effect* strongly influences square planar compounds, notably Pt(II) complexes, and plays a dominant role in our current understanding and development of traditional Pt(II) clinical agents. First proposed by Chernyaev,[13] defined as the *ability of a ligand in a complex to direct substitution opposite, or trans, to itself*, the *trans effect* details the reactivity of ligands and allows for prediction of platinum(II) substitution chemistry. Models were introduced to identify the factors that controlled the magnitude of the *trans effect* with the main factors being the electronegativity of the ligand groups and their ability to form π-bonds with the metal ion in the transition state. The *trans effect* series ranks ligands by their increasing ability to direct substitution *trans* to themselves:

$$CN^-, CO, C_2H_2 > PH_3, SH_2 > NO_2^- > I^- > Br^- > Cl^- > NH_3, py > OH^- > H_2O$$

Therefore, CN^- is the ligand with the greatest *trans* directing ability and H_2O is the least. The synthesis of anticancer agent *cis*-diamminedichloroplatinum(II), cisplatin, and a comparison to the synthesis of its *trans*-platinum(II) isomer provides a good illustration of the *trans effect*. The Dhara synthesis[14] is the most commonly employed procedure for the synthesis of cisplatin and uses the commercially available potassium tetrachloroplatinate, $K_2[PtCl_4]$ and proceeds through a reaction with excess KI to first form $[PtI_4]^{2-}$ followed by treatment with ammonia, NH_3, to form the *cis*-$[PtI_2(NH_3)_2]$ product. Displacement of the iodide ligands using $AgNO_3$ replaces these ligands with water molecules which are then finally displaced by the addition of KCl to introduce the chloride ligands and produce cisplatin, *cis*-$[PtCl_2(NH_3)_2]$. The synthesis of transplatin also displays the *trans effect* and proceeds from $K_2[PtCl_4]$. Full substitution by treatment with excess ammonia generates the tetra-ammine complex, $[Pt(NH_3)_4]^{2+}$ and follows the scheme shown (**Figure I-4**). A simplified example of the synthesis can be seen below:

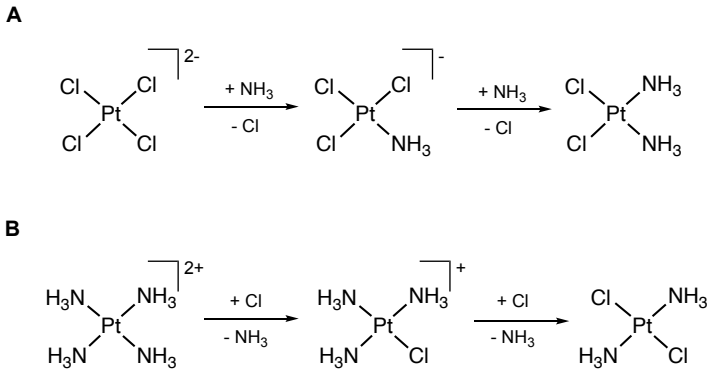

Figure I-4. Demonstration of the *trans*-effect. **A.** Synthesis of cisplatin. **B.** Synthesis of transplatin.

I. 2. 2. Cisplatin – Discovery to Application

Platinum anticancer agents have maintained their status as the mainstay of cancer therapeutics since the serendipitous discovery of cisplatin by Rosenberg[15] and the subsequent approval for its use as an anticancer agent by the FDA in 1978.[16] To this day over a thousand platinum-containing complexes have been produced and started testing, however there are still only three globally approved platinum agents for anti-cancer therapy.[17]

Due to drug resistance, both intrinsic and acquired, and severe dose-limiting toxicity issues related to cisplatin use, there has been a drive to produce other platinum-based agents with similar or improved anti-tumour properties. Further research into generations of cisplatin-like complexes led to the development of carboplatin and oxaliplatin, and are notably the only two other platinum-containing anticancer agents approved for clinical use worldwide.[18] Alongside these second generation chemotherapeutics, a number of platinum drugs have been approved for clinical use in specific regions of Asia (**Figure I-5**).

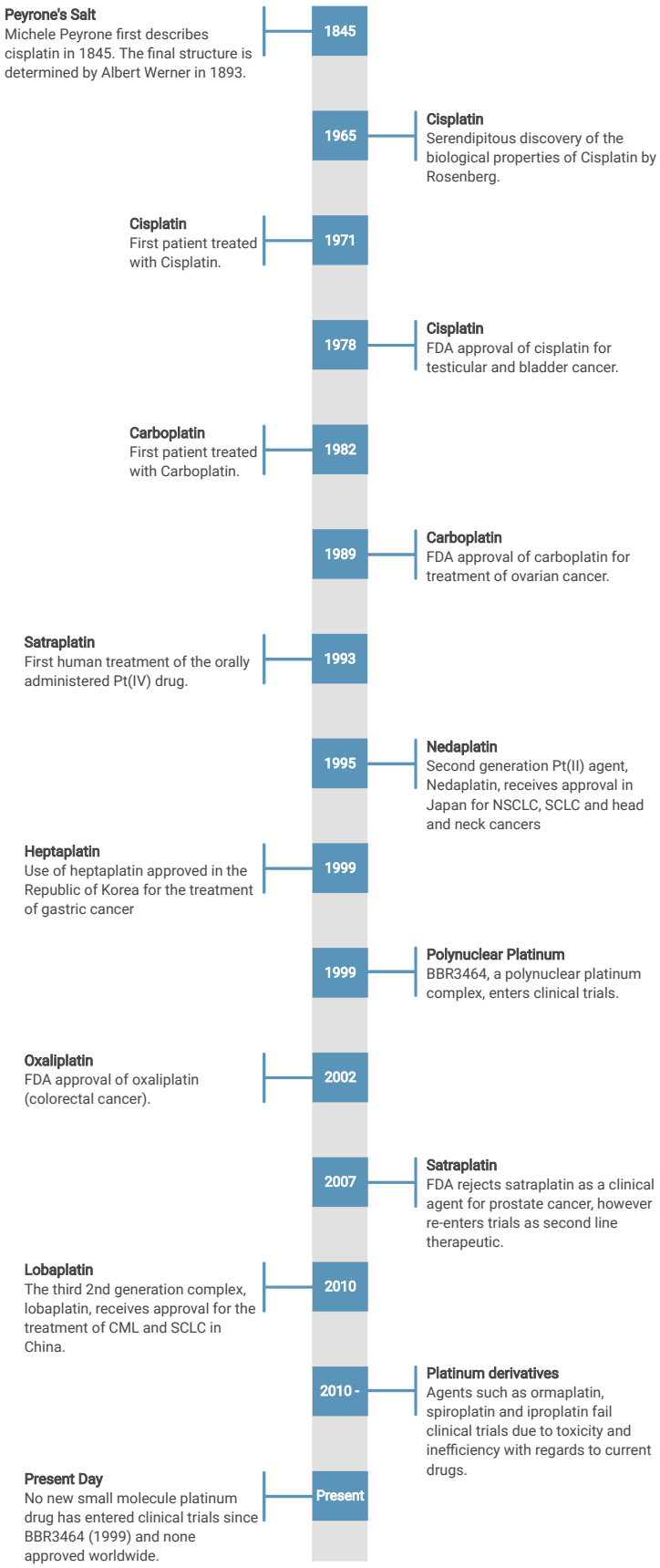

Figure I-5. Timeline of the discovery of cisplatin to the current state of the art regarding platinum(II) therapeutic agents today.

Significant research efforts have been undertaken to elucidate the mechanism of action of cisplatin with particular focus on how the complex and other similar platinum-containing agents cross the cell membrane and elicit an anticancer effect. Consensus within the field identifies the majority of cisplatin most likely enters the cell through a combination of a methods. Traditionally, it was surmised that passive diffusion was a major contributor,[19, 20] however later research pointed towards other methods such as active transport by membrane proteins[21] and uptake and translocation by copper transporters such as CTR1 as major participants.[22, 23]

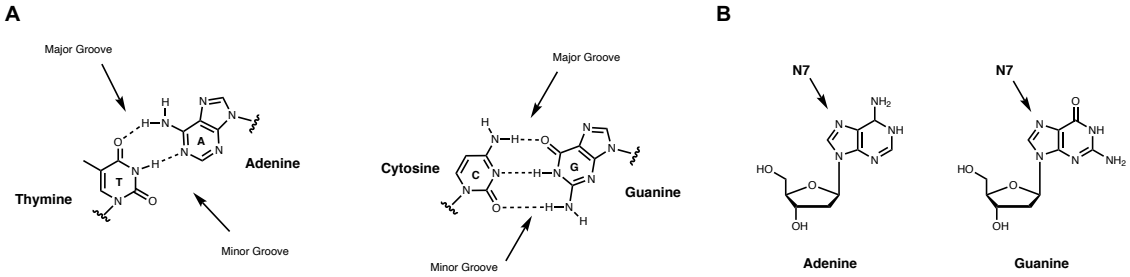

Figure I-6. A. Watson and Crick base pairing between thymine-adenine and cytosine-guanine. Orientation of major and minor groove of the duplex sequence. **B.** N7 position of purine bases deoxyadenosine and deoxyguanosine. N7 is implicated in the majority of platinum(II) lesions.

Once cisplatin is across the cell membrane aquation of the complex occurs wherein one or both of the chloride ligands are lost. The square-planar geometry of cisplatin allows for facile substitution of the chloride ligands – aquation occurs readily in the cytoplasm where chloride ion concentration is low (4-20 mM) in comparison to the bloodstream where chloride concentration is significantly higher (~100 mM) (**Figure I-7, A**).[24] The highly electrophilic Pt(II) aquo complex readily binds to the nucleophilic N7 of the purine bases (**Figure I-6, B**). The binding of cisplatin to DNA predominantly occurs on guanine but will occur to a lesser degree on adenine.

Numerous studies have determined the full extent of the formation of cisplatin-DNA adducts with the 1,2-d(GpG) intrastrand cross-linking adduct being of highest prevalence (*ca*. 65%), followed by 1,2-d(ApG) intrastrand cross-linking (*ca*. 25%) and 1,3-d(GpXpG) intrastrand cross-linking (*ca*. 10%) (**Figure I-7, B**). A very small amount of interstrand cross-linking GpG cross-linking (*ca*. 2%) has

also been demonstrated alongside the prevalent intrastrand adducts.[25-27] Subsequent bending and distortion of the DNA double-helix leads to inhibition of the transcription process followed by eventual cell death by apoptosis.[28]

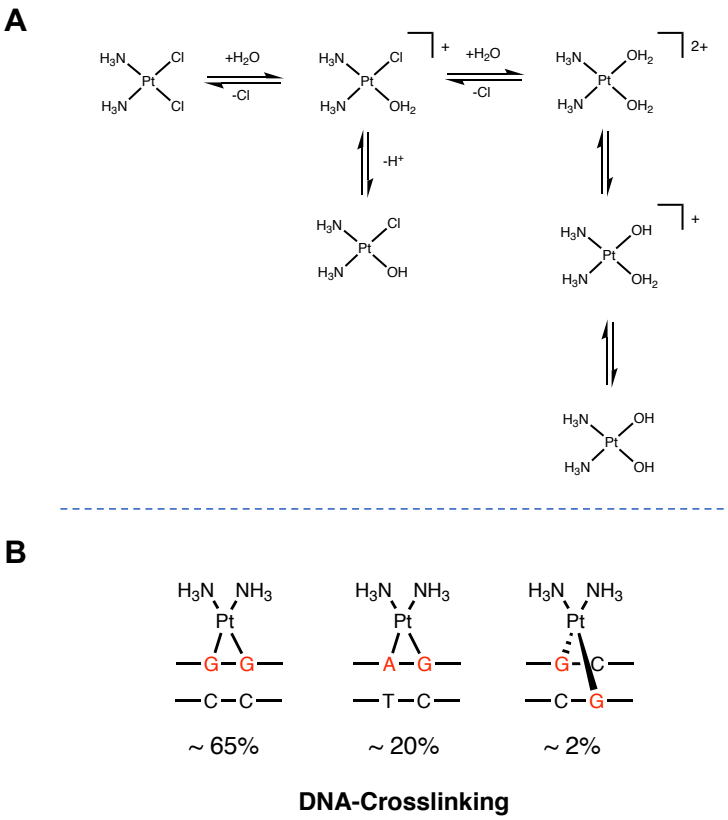

Figure I-7. A. Aquation of *cis* chemotype platinum(II) molecules – initially monosubstituted complex are formed prior to complete conversion under cellular conditions to the final di-aqua cation. **B.** Ratio of dsDNA by *cis*-platinum(II) species.

While cisplatin has seen success in numerous treatments such as bladder, ovarian and lung cancer and is considered a curative success in the treatment of testicular cancer,[29] severe dose-limiting toxic-side effects such as nephrotoxicity,[30] neurotoxicity[31] and ototoxicity[32] have led to a migration in research focus to discover platinum anticancer agents with improved chemotherapeutic properties. Coupled with the toxic side-effects are major resistance factors such as the interactions with plasma proteins[33] and human serum albumin (HSA). Since platinum(II) is a strong Lewis acid it binds avidly with sulphur-rich biomolecules such as methionine and glutathione[34] (HSAB theory). These sulphur-rich form part of the cells natural detoxification process.[35] It has been deduced that cell lines exhibiting an overexpression of copper

transport proteins ATP7A and ATP7B showcase increased cisplatin resistance. Coinciding with this, lower expression of CTR1 influx proteins have also been implicated in resistance.[36] Notably, ATOX1a chaperone protein responsible for transference of copper to ATP7A and ATP7B was shown to coordinate a $[Pt(NH_3)_2]^{2+}$ molecule bound at the Cu-binding site although further revisions dispute the interpretation as either a lone copper or platinum ion.[37, 38]

Consequently, much research effort has focused on designing modern drugs that improve the overall platinum-based therapy for patients. Two avenues of development include i.) increasing the bioavailability of the drug–with an increased focus on oral bioavailability and reduced toxicity and ii.) reducing drug resistance (both intrinsic and acquired). Solutions to these problems are not mutually exclusive and developments to tailor the hydrolysis kinetics and the final structural geometry of the platinum lesion form the bulk of ongoing work.

I. 2. 3. Second Generation Platinum(II) Agents

Efforts to develop newer complexes has focused on redesigning coordinating ligands bound directly to platinum. Generally, platinum complexes are comprised of two ligand types as outlined in **Figure I-8**: i) non-leaving group ligands (NH_3-, DACH, etc) and ii) leaving group ligands (Cl, CBDCA, Oxalate etc) involved in the substitution and aquation kinetics which form DNA adducts. Thus, the nature of the platinum-DNA lesions that form and the subsequent cellular repair response is directly correlated to these non-leaving group ligands whereas the leaving group ligands are responsible for the control of DNA binding kinetics and off-target toxicity. Following this framework, carboplatin and oxaliplatin were realised. Carboplatin incorporates a comparatively stable chelating ligand 1,1-cyclobutanedicarboxylato (CBDCA). As such, carboplatin has lower toxicity and is administered in higher doses compared to cisplatin.[39] However, due to the identical ammine non-leaving group ligands that form the overall platinum-DNA adduct, cross-resistance to cisplatin is a persistent issue.[40, 41]

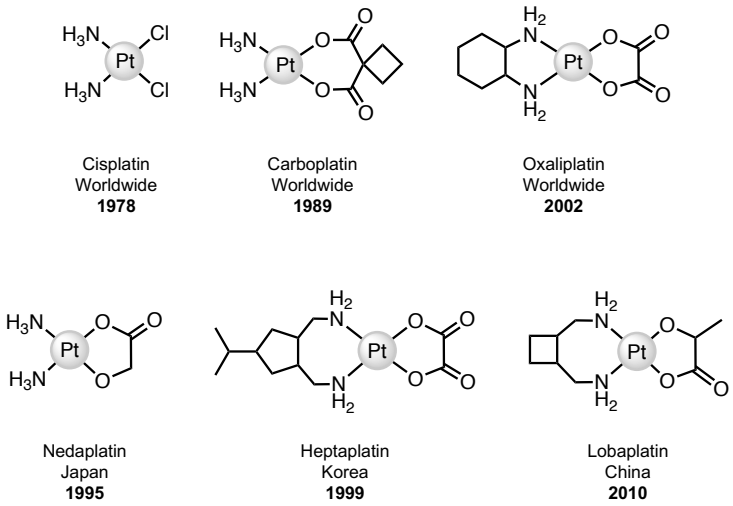

Figure I-8. First, second and regionally approved generations of cisplatin analogues. From **top left** to **bottom right**: cisplatin, carboplatin, oxaliplatin, nedaplatin (Japan), heptaplatin (Korea) and lobaplatin (China). Date shown indicates year of first approval.[42]

On the other hand, oxaliplatin differs quite significantly, with changes to both sets of ligands. The complex features a non-leaving chiral chelating *trans*-1(*R*),2(*R*)-DACH ligand and a leaving group is comprised of an oxalate ligand. Not exclusive to oxaliplatin, DACH ligands have long held interest as additional components for platinum anticancer agents with oxaliplatin being an exhibit of developmental success containing these ligands. Unlike cisplatin and carboplatin which are used to treat various conditions such as testicular, lung and breast cancers, oxaliplatin is used almost predominantly to treat colorectal and gastrointestinal cancers. Displaying a side-effect and off-target toxicity profile quite different to the former two agents, oxaliplatin does not suffer from efficacy or resistance problems against these particular cancers.[41, 43] Notably, the use of oxaliplatin within treatment regimens is based on the activity against these cell lines rather than any noteworthy knowledge of the drugs mechanism of action. It was assumed that oxaliplatin possessed the same mechanism of eliciting a DNA damage response as observed with previous generations, although it was known that the enhanced bulk of the DACH ligand positioned into the major groove inhibits the efficiency of repair proteins.[44]

Recently, Bruno et *al.* published work wherein the mechanism of action of oxaliplatin was investigated and discovered to be unique compared to that of

cisplatin and carboplatin–killing cells by inducing ribosomal biogenesis stress.[45] This work can be considered preeminent within the field and is potentially one of the most important findings since the realisation of the three mainstay clinical agents themselves. While further investigative work is underway to fully understand all aspects concerning how this mechanism differs with cisplatin and carboplatin, it may indicate a paradigm shift exhibited by changes in the pharmacodynamics and pharmacokinetics of future drugs by alterations based on the ligand components.

I. 2. 4. *Trans*-platinum Derivatives

After the preliminary experiments performed by Rosenberg, it was quickly noted that the *cis*-isomer and another Pt(IV) analogue were the compounds responsible for the observed effect and that the *trans*-isomer was relatively inactive.[46, 47] Further studies affirmed this was due to the altered geometry of the complex as the *trans* geometry increased the kinetic lability of the attached chloride ligands. Because of this, the complex promotes undesirable side effects with intra- and extracellular biomolecules.[48] The *trans* isomer is capable of forming 1,3-intrastrand crosslinks and principally monofunctional adducts in comparison to cisplatin–which forms predominantly 1,2-intrastrand purine adducts, a crosslink the *trans*-isomer is stereochemically unable to form. Both of these lesions have been further observed to convert to interstrand crosslinks,[49] which combined with the lethargic conversion process itself, lead to easy excision of *trans*-isomer crosslinks by cellular repair mechanisms. While research has generally disfavoured *trans*-diamminedichloroplatinum(II), biologically active derivatives have been discovered and are centred around the alteration of the am(m)ine ligands through substitution with sterically bulky heteroaromatic ligands (**Figure I-9, A**),[50] asymmetric aliphatic ligands[51] (**Figure I-9, B**) and inminoether ligands (**Figure I-9, C**).[52]

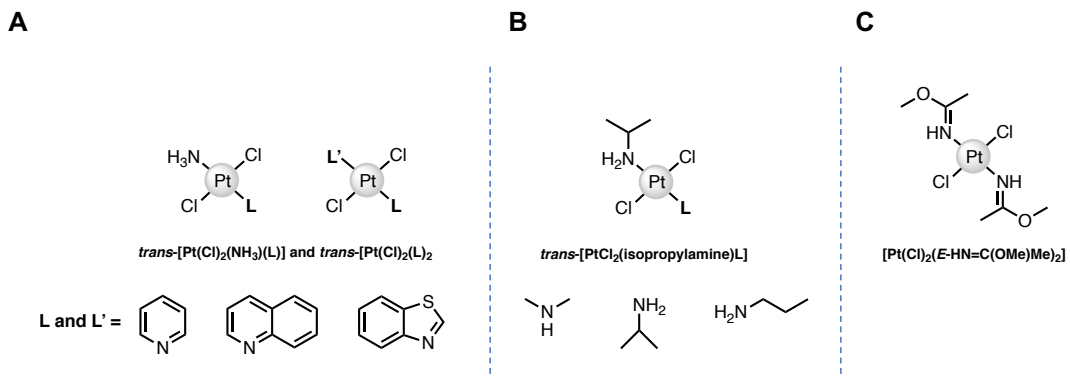

Figure I-9. A. Mono- and bifunctional trans-platinum(II) species with L and L' representing a variety of heteroaromatic ligands such as pyridine, quinoline and benzothiazole. **B.** Examples of *trans*-platinum(II) complexes with substituted asymmetric aliphatic ligands dimethylamine, isopropylamine and propylamine. **C.** An iminoether-substituted trans-platinum(II) complex.

Notably, although intrastrand crosslinks are the hallmark of current clinical platinum drugs, interstrand lesions have been found to exhibit higher toxicity due to the separation required between strands for cellular DNA processes such as transcription.[53] As such, conformational change in the DNA backbone is the trigger for eventual cell apoptosis and invites interest to the idea of developing compounds that can induce greater conformational distortion but not necessarily through traditional *cis*-isomer chemotypic effects.

I. 2. 5. Platinum(IV) Prodrugs

Significantly different to platinum(II) complexes, Pt(IV) complexes are six coordinate and adopt an octahedral geometry (**Figure I-10**). Complexes possessing a low-spin d^6 octahedral metal ion, like those of Pt(IV), are substantially more kinetically inert than those of Pt(II). Therefore, these complexes are generally more resistant to ligand substitution and thus do not exhibit as many undesirable side reactions with extracellular biomolecules prior to eliciting a biological effect. Satraplatin is one such Pt(IV) drug with these properties and it can be administered orally.[54]

In comparison to traditional Pt(II) systems, the introduction of two additional ligands affords tuning of the overall complex towards biological properties such as lipophilicity, cellular uptake, redox stability and cell targeting.[42] Pt(IV) complexes are also prodrugs and will usually undergo reduction to Pt(II)

prior to DNA binding through the loss of two ligands thereby reverting to a square-planar Pt(II) cytotoxin.[55] The generally accepted mechanism is centred on the loss of the axial ligands, however studies have shown that the nature of the reducing agent also plays a role in the composition of the final Pt(II) complex.[56]

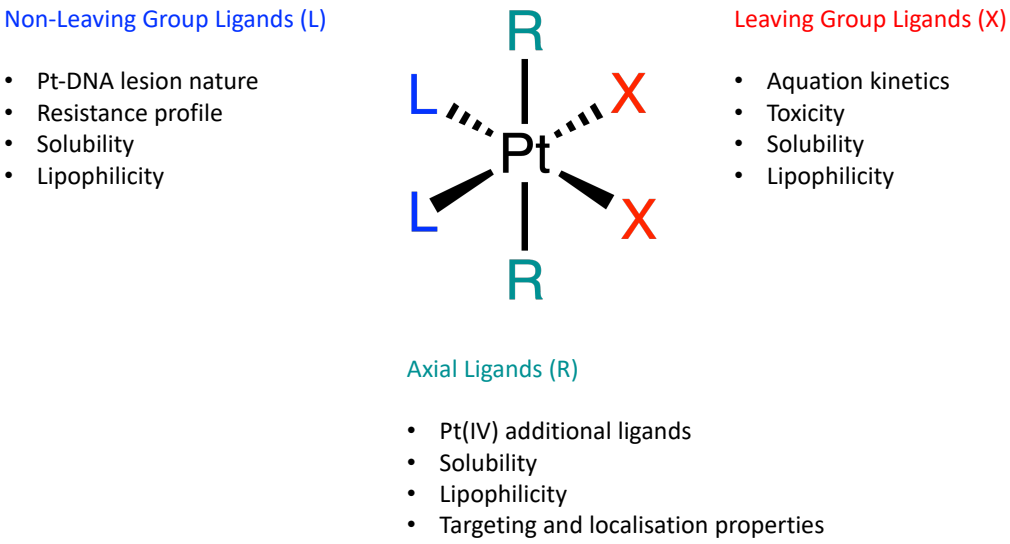

Figure I-10. Nature of Pt(II) and Pt(IV) constituent ligands and the properties that are controlled. Pt(IV) complexes possess axial ligands (R) that can undergo extensive modification to provide a wide range of characteristics.

Notable Pt(IV) complexes that were brought to clinical trials include ormaplatin,[57] also known as tetraplatin, iproplatin (JM9),[58] and satraplatin (JM216)[54] (**Figure I-11**).[59] Unfortunately, ormaplatin did not advance past Phase I trials due to severe and unpredictable neurotoxicity at the maximum tolerated dose (MTD).[60] Despite initial promise, iproplatin was tested against a number of cancers and although Phase III clinical trials were conducted, it was deemed unfeasible to progress further as the overall effectiveness of the drug did not surpass cisplatin or carboplatin.[61] Similarly, satraplatin progressed to Phase III clinical trials and exhibited success in certain combinatorial regimes, although mainly as a second-line therapeutic. FDA approval was denied, based on the overall survival rate and prior patient treatment with docetaxel,[62] and thus to this day, satraplatin remains the closest Pt(IV) complex to have come to the clinic. At present, however, there are numerous Phase I-III clinical trials underway using

satraplatin in association with docetaxel (prostate) and paclitaxel (NSCLC) among others.[63]

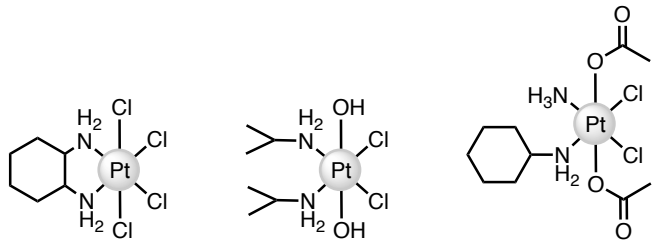

Figure I-11. Prominent Pt(IV) complexes that have participated in clinical trials.

The rational design of newer Pt(IV) complexes through fine-tuning of both the axial and equatorial ligands has become part of an overall shift in emphasis to that of targeted drug discovery and development.[64] The ability to elicit a specific drug action against a specific target without the prevalent side effects synonymous with traditional clinical agents is the central paradigm of modern 'smart' drug design – a so called 'silver bullet' as referenced across the literature.[65]

I. 2. 6. Polynuclear Platinum(II) Complexes

A particularly interesting class of drug are the family of polynuclear platinum(II) compounds (PPCs) developed by the Farrell group and are uniquely different in structure to traditional cisplatin-like agents. Based on a *trans* geometry and structured around a multi-nuclear scaffold, coordination with bridging alkanediamine ligands facilitate long distance interstrand and intrastrand cross-linking.[66] Two notable compounds, BBR3464 and TriplatinNC-A, are leading agents from the trinuclear family (**Figure I-12**) and are the most prominent examples of the paradigm shift towards this field. BBR3464 bis-[*trans*-diamminechloroplatinum(II)][*μ-trans*-diamminebis(hexanediamine)platinum(II)] nitrate is a trinuclear complex that has shown increased uptake in cisplatin resistant cells and has been found to create larger quantities of adducts compared to cisplatin.[48]

Potently cytotoxic, pre-association with DNA and increasing efficiency and specificity of the long-distance unique 1,4-intrastrand cross-links are accepted as the reasons for success. Unlike cisplatin analogues, lesions formed with DNA are undetected by NER machinery while BBR3464 has also been observed to cause B to Z and B to A changes in DNA conformation.[67] For all the benefits associated with BBR3464, high systemic toxicity was prevalent including a reported MTD of 0.12 mg m^{-2} day^{-1} in human patients. An increase to 0.17 mg m^{-2} day^{-1} led to dose-limiting toxicity (DLT) including neutropenia and gastrointestinal toxicity.[68] Although BBR3464 holds the achievement of being the only example of a non-cisplatin chemotype to enter human clinical trials, ultimately, due to pharmacokinetic issues and a narrow therapeutic index, it did not progress beyond Phase II.[65]

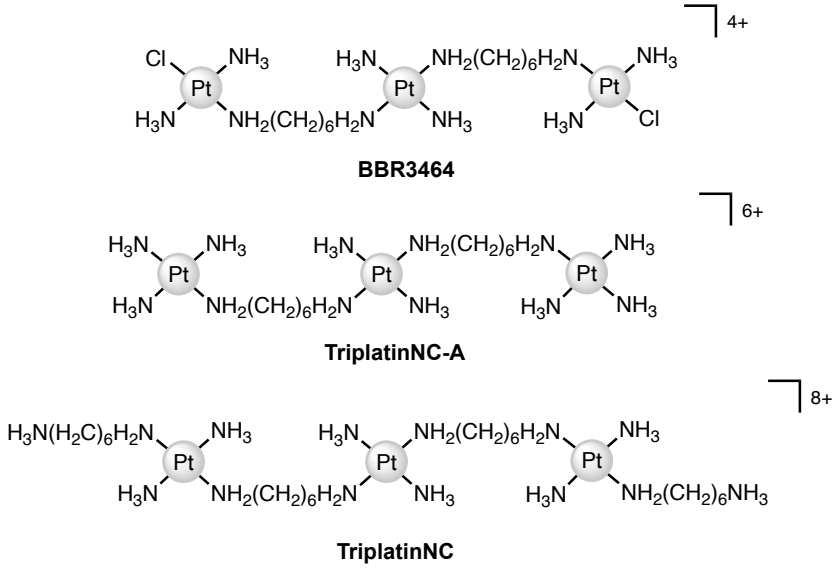

Figure I-12. Polynuclear platinum complexes synthesised by the Farrell group. Note the terminal amines on TriplatinNC-A and amine chains on TriplatinNC-A that interact in a non-covalent fashion.

Advancing the work undertaken with BBR3464, TriplatinNC-A and TriplatinNC were realised. Substitution of the terminal chloride ligands with am(m)ines (TriplatinNC-A) or longer 'dangling' amines (TriplatinNC) afforded complexes which possess unique non-covalent nucleic acid recognition through the use of the 'phosphate clamp' binding motif.[69, 70] Bidentate amine-phosphate-am(m)ine interactions induce similar B to Z and B to A changes[71] while the mechanism of action is believed to be DNA condensation in which

topoisomerase-I enzymatic activity is inhibited.[72] The cationic nature and unique binding of these compounds has been implicated in their efficiency in recent studies against cisplatin-sensitive and resistant ovarian cell lines.[73]

I. 2. 7. Drug Targeting and Delivery

A major concern facing current platinum-based therapy is a distinct lack of tumour specificity. Systemic *off*-target toxicity and inactivation of platinum drugs by extracellular biomolecules are predominant issues that research is constantly trying to curtail.[74] Recent efforts have focused on the delivery of platinum agents to their desired target and are known as drug targeting and delivery (DTD) and can be regarded as either active or passive (**Figure I-13**). Active DTD is dependent on particular interactions between the drug and cellular components and is useful in targeting cells that possess biomolecules that are quantifiably or functionally different than typical cells *i.e*. overexpression of a particular protein or receptor by cancerous cells.[75] Passive DTD harnesses the inherent enhanced permeability and retention (EPR) effect associated with tumour tissues since, for example, tumour vasculature is discernibly disorganised and perforated due to the rapid proliferation of the tumour.[76] Numerous apertures and a lack of a viable lymphatic system combine to create a hyperpermeable environment within the tumour leading to increased passive influx of any surrounding biomolecules. Targeting biomolecules of specific sizes are thus able to access and elicit an effect within the tumour itself and have been found to remain on location for long periods of time mainly due to the decrease in efflux efficacy arising from the crippled lymphatic network.[77]

Notable examples of Active DTD include:

- Estrogen hybrids: targeting of estrogen receptors (ER) which are implicated in growth modulation of both healthy and malignant breast tissues. Croy and co-workers have generated estrogen-hybrids designed to transport platinum(II) warheads to cancer cells with overexpression of ER.[78]
- Carbohydrate carriers: studies show that tumours display altered sugar metabolisms, namely increased consumption due to their hypoxic environment, allowing for targeting with tailored hybrids. Keppler *et al*.

have developed numerous glucose derived platinum hybrids with similar activity as oxaliplatin.[79]

- Peptide hybrids: cancer proliferation is founded in angiogenesis and as such targeting of upregulated peptide receptors in endothelial cells of tumour vasculature is an interesting avenue of investigation. Conjugation of a 36 amino acid peptide, CTX, to a platinum core has shown preferential binding to glioma and non-glioma tumour cells in certain cancers including lung and prostate.[80]

The comparatively recent field of Passive DTD includes:

- Polymer conjugates: non-toxic polymers exploit the EPR mechanism for greater cellular uptake before enacting safe delivery of the platinum moiety or 'warhead' through enzymatic or pH driven cleavage reactions. Examples include acid responsive hybrids which release the platinum agent once within the intracellular acidic environment.[81]
- Nanoparticles: similar 'piggybacking' of the EPR effect allow for increased accumulation of nanoparticles in cancerous cells. Enhanced targeting and sustained release are prominent aspects of nanoparticle technology alongside the protection of the drug from external metabolites. Interestingly, nanoparticle-anticancer drugs have been approved by the FDA, although research into effective platinum incorporation continues.[82]

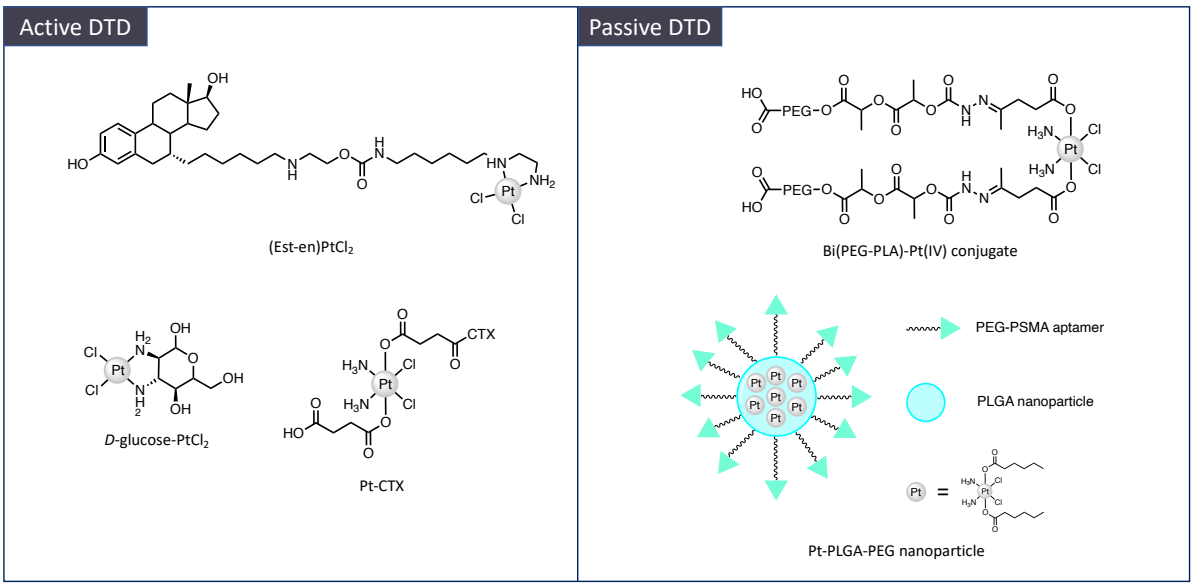

Figure I-13. Left – Examples of Active-DTD platinum-hybrids. (Est-en)$PtCl_2$, a platinum(II)-hybrid which possess affinity for ER. D-glucose-$PtCl_2$, developed by Keppler and co-workers, showcases similar activity to oxaliplatin analogues. Pt-CTX is a peptide conjugated hybrid exploits unregulated peptide receptor proliferation in tumour vasculature. **Right** – Passive-DTD platinum-hybrids. Bi(PEG-PLA)-Pt(IV) polymer hybrid which showcases excellent drug release kinetics and enhanced activity in comparison to cisplatin. Pt-PLGA-PEG nanoparticles developed by Lippard et. al.[83] that greatly improve the therapeutic index of cisplatin for prostate cancer.

I. 3. Click Chemistry

First coined by K.B. Sharpless in 1998, although not fully detailed until 2001,[84] 'click' chemistry envelops a wide variety of powerful, selective and reliable reactions that endeavour to generate products through combination of small units with heteroatom links. A stringent set of criteria was laid out by Sharpless in order to define what constitutes 'click' chemistry – the reactions must be modular, exhibit wide scope, display high yields while remaining stereospecific and generate negligible by-products. Simple reaction conditions are a must with readily available starting materials and should allow for no solvent or a benign solvent to be utilised. Product isolation must be facile and if purification is required, methods to be employed would ideally be crystallisation or distillation. The most common examples of carbon-heteroatom bond formation include:

- Cycloadditions – particularly 1,3-dipolar cycloadditions
- Nucleophilic ring opening chemistry
- Non-aldol carbonyl chemistry
- Carbon-carbon bond additions such as epoxidations and aziridinations

Cycloadditions, principally the 1,3-dipolar cycloaddition, is perhaps the most widely utilised example of click chemistry. Reimagined by Rolf Huisgen and extensively investigated starting in the 1960s,[85] the azide-alkyne reaction initially required high temperatures or pressure and was not regioselective. Although incompatible with biological systems, the general concept was undeniably significant and was revisited over time. Independently, both Sharpless[86] and Meldal[87] discovered and optimised conditions that used a Cu(I) catalyst to produce 1,4-disubstituted 1,2,3-triazoles. This reaction has been known since as the copper-catalysed azide-alkyne cycloaddition (CuAAC) (**Figure I-14, A**). Additionally, ruthenium(II) has been utilised to a lesser extent as a catalyst in the synthesis of 1,5-disubstituted 1,2,3-triazole products.[88]

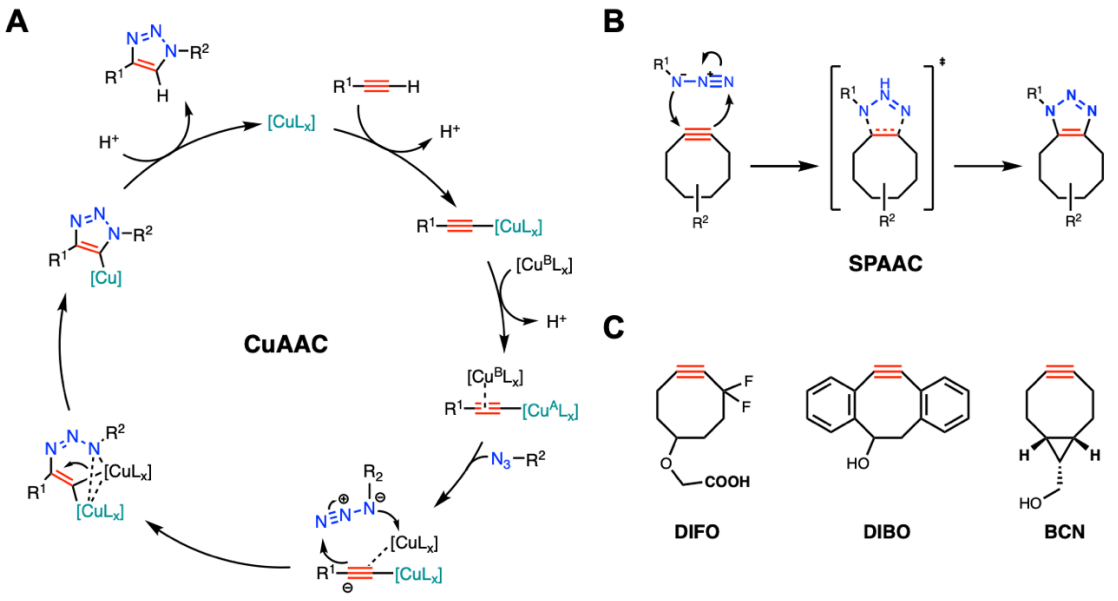

Figure I-14. A. Schematic of copper catalysed alkyne-azide cycloaddition reaction. **B.** Strain promoted alkyne-azide cycloaddition reaction. **C.** Cycloalkynes utilised as strain promoting click reagents: DIFO, DIBO and BCN.

For all the benefits of CuAAC, its use within biological systems has been deterred by the apparent toxicity of the copper(I) catalyst with multiple studies showing acute cellular sensitivity once introduced.[89, 90] Methods such as strain promoted azide cycloadditions have been intensively studied and have allowed for alternative pathways to conjugate units within living systems (**Figure I-14, B**).[91] Catalyst-free [3+2] cycloaddition of azides and cyclooctyne derivatives has been reported to occur readily in ambient conditions.[92, 93] Notable cyclooctyne substituents include i.) DIFO , a cyclooctyne substituted with a *gem*-difluoro group which demonstrates comparable rates to CuAAC, ii.) DIBO, or dibenzocyclooctynol where extension of the aromatic system produces greater ring strain, and iii.) BCN, bicyclo[6.1.0]nonyne, a highly hydrophilic probe that allows for enhanced non-toxic bioorthogonal conjugation (**Figure I-14, C**).

I. 3. 1. Nucleic Acid Click Chemistry

Following the advent of the CuAAC 'click' reaction, the significant potential for this application was swiftly realised in biochemistry. Carell and co-workers produced seminal work that demonstrated that reliable and efficient post-synthetic click functionalisation could be performed on alkyne-modified DNA.[94] The labelling of biomolecules without disturbing biophysical properties was recognised as an ideal benefit of utilising this approach. Thus the scope of click chemistry has expanded to include areas such as bioconjugation of polymers, hydrogel biomaterials, nanoparticles, biosensors and perhaps the most widely studied: biochemistry – with an emphasis on DNA modification. El-Sagheer & Brown[95] then laid out potential uses of click chemistry within the field of nucleic acids given:

- The addition of azide and alkyne moieties do not alter target biophysical properties.
- Azide and alkynes are relatively unreactive and will seldom react with anything other than themselves in nature - an important characteristic for intracellular research.
- The triazole moiety is stable and non-toxic in cellular environments.

Nucleic acid functionalisation is well documented within the literature.[95-97] A key topic within the field is the comparison between pre- and post-synthetic modification of DNA. In general, pre-synthetic modification is less favoured due to the inability of labelled precursors to survive the synthesis process intact. On the other hand, post-synthetic labelling of the completed oligonucleotide has shown to be efficient.[98] In this process alkyne-modified oligonucleotide materials are post-labelled with azide-bearing groups. The incorporation of alkyne groups onto DNA is chosen rather than azide moieties due to the propensity for azide functional groups to react with P^{III} during the phosphoramidite oligonucleotide synthesis (**Figure I-15**).[99]

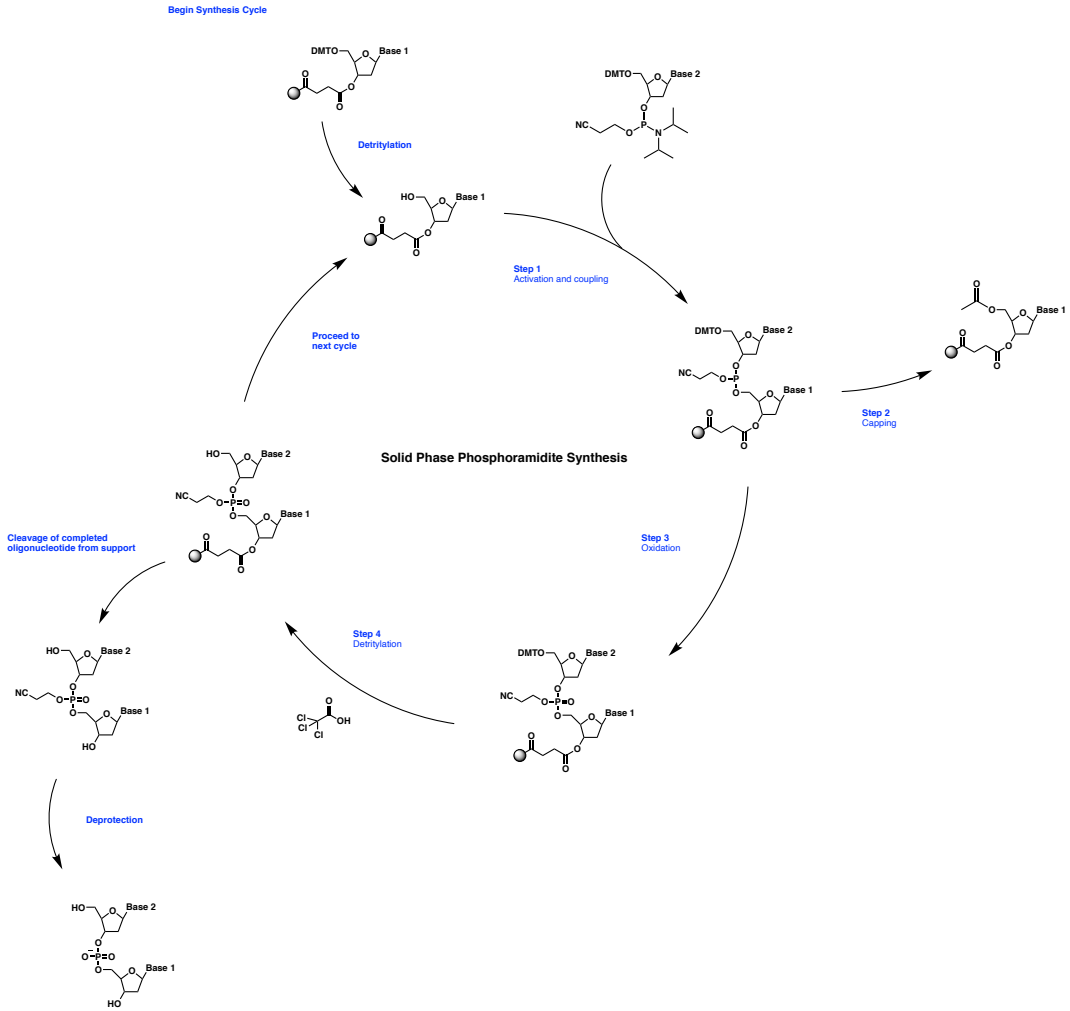

Figure I-15. Schematic of solid-phase phosphoramidite synthesis cycle. In general, azide substituents are not well received in the synthesis as reaction with phosphorus have been documented – thus alkyne moieties are the preferred reactive handle to introduce onto the oligo. Solid-phase phosphoramidite synthesis with platinum constituents is also poorly accepted with the inactivation of the metal core observed in some instances.

It is known that modification of the 5-position of pyrimidine and the 7-position of deazapurine nucleosides are the best positions to incorporate functionalities such as alkynyl moieties, to enhance DNA stability and base hydrophobicity, as these areas lie in the major groove of the DNA duplex and thus have significantly greater freedom of movement.[100] Building on this work, Seela *et al.* then investigated the effect of introducing a variety of longer chained alkynyl groups as scaffolds for eventual click labelling. It was determined that as chain length increased from propynyl to hexynyl linkers the hydrophobicity was increased to such an extent as to cause duplex instability. Incorporation of carbon-carbon triple bonds into the chain provided a reliable decrease in

hydrophobicity whist retaining stability of the duplex.[101] Subsequent work showcased the synthesis of analogues of canonical DNA: dC, DG, and dA bases bearing modified octadinyl side chains. Notably, these derivatives still possess the same Watson-Crick base recognition sites as traditional DNA and were further clicked to reporter fluorophores and, in turn, displayed the ability to generate reporter-labelled bases without distorting or disturbing the DNA duplex.[102]

Brown and co-workers have demonstrated several strategies to prepare cyclic DNA structures through the use of both alkyne and azide modifications on an oligonucleotide strand.[103] For example, generation of a 5'-terminal alkyne coinciding with placement of an azide at the 3'-terminal affords modified ssDNA that has been found to react with itself in high dilution conditions to produce a cyclic ssDNA structure. Furthermore, introduction of a similarly clicked complementary strand has been shown to form catenated dsDNA structures that display increased resistance to exonuclease activity.[104]

In a similar line of investigation, oligonucleotide analogues were developed that possessed clicked backbones. Oligo units bearing 3'-AZT and 5'-propargylamido modifications were successfully click to create an oligonucleotide with a triazole linkage as a backbone scaffold (**Figure I-16**). Notably, recognition and replication of these unnatural backbones is recognised and replicated by PCR with a number of polymerases showing suitable efficiency. This work was the first demonstration of efficient nonenzymatic DNA ligation to afford reproducible amplification.[105]

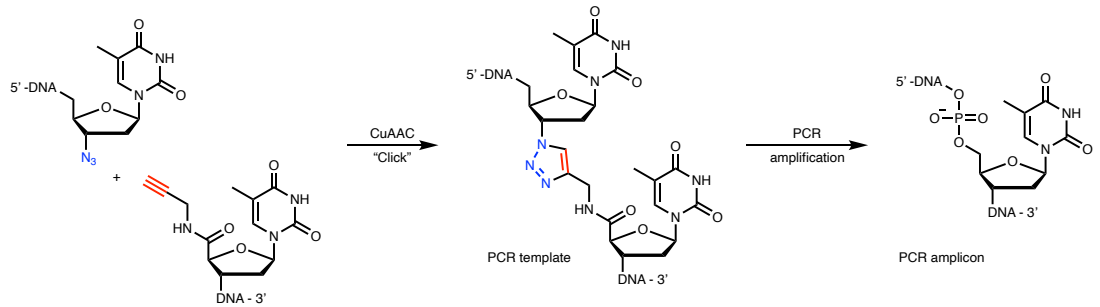

Figure I-16. Click reaction of an azide and alkyne modified nucleobase to form unnatural clicked PCR template. Recognition by polymerases produce amplified product.

Covalent crosslinking between complimentary strands has been achieved by incorporating alkyne-modified deoxyuridine nucleosides into a probe strand. Two different bases were examined: 5-ethynl- and 5-(octa-1,7-dinyl)- 2'-deoxyuridine phosphoramidites that were incorporated and clicked with a similarly modified azide-bearing deoxyuridine base in an adjacent strand (**Figure I-17**).[106] Work performed in this study and separate work by the Carell group[94] emphasises that octadinyl linkers provide the best yields with longer linkers being less efficient – an indication that longer linkers are most likely inhibited by steric factors.[94]

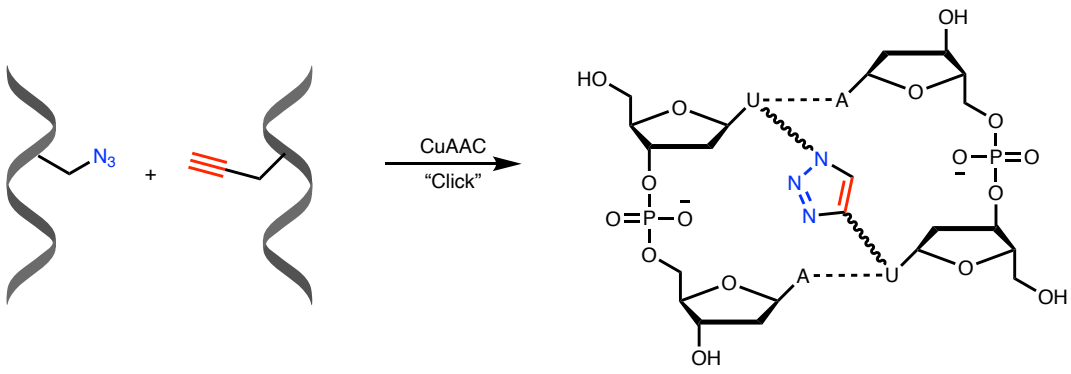
N3
+
CuAAC
"Click"
HO
O
U
A
OH
O
O
O

was one of the first cases in which two separate drug units were preassembled before combination to yield the final target. In similar fashion research has expanded towards the use of clickable fluorophores in order to investigate the cellular interactions of platinum(II) agents. Griffith *et al.* have reported the use of SPAAC to conjugate a near infrared fluorophore onto a platinum scaffold in order to track real-time imaging of *in vitro* processes such as cell localisation, mechanism of action and cellular resistance.[110]

The DeRose group has performed notable work regarding conjugation of azide and alkyne handles onto platinum substrates. Arising from intracellular interactions between platinum agents and RNA species, clickable reagents were envisaged to provide some elucidation of these mechanisms that are still unknown to the platinum community.[111] Picazoplatin, an azide-modified reimagining of the drug picoplatin, was synthesised and conjugated with alkyne-fluorophores to further determine the binding characteristics of the compound with both DNA and RNA substrates.[112] The complex was then used to showcase possible ribotoxic responses to platinum therapy and accessing RNA substructures by metal complexes *in vivo*.[113] Experiments depicting the merits of either azide or alkyne functionalisation of platinum complexes have also been carried out with the aim of increasing the accessibility of these complexes to a wider range of analytical techniques and cell lines.[114]

I. 4. Gene-Editing

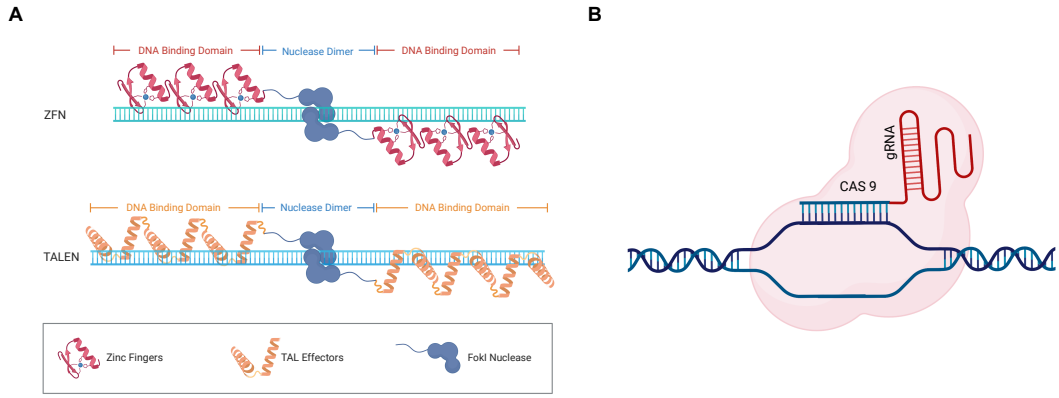

Figure I-18. A. Schematical representation of sequence-targeted Zinc Finger Nucelases (ZFNs) and Transcription Activator-like Effector Nucleases (TALENs). **B.** Clustered Regularly Interspaced Short Palindromic Repeats (CRISPRs). Scheme is derived from ref[115] and created using BioRender.com.

Gene-editing or genome editing is a method of genetic engineering defined by its various functions such as i.) inactivation of a particular mutated gene, ii.) replacement of a mutated gene, or iii.) introduction of a genetic therapeutic to treat disease. Gene editing methods can exploit natural biological repair processes such as non-homologous end joining (NHEJ) and homologous directed repair (HDR). In NHEJ, first coined by Moore and Haber,[116] two cleaved ends of damaged DNA are recombined by ligase enzymes without the need for a homologous template sequence. If the cleaved overhang regions are not completely compatible, errors may occur upon repair — NHEJ anomalies are consistent markers within tumorous cells.[117] On the other hand, HDR is considered more efficient and accurate, whereby a homologuos template guides repair of the damaged sequence.[118] The methods can both be used to successfully introduce either single nucleotide incisions or exogenous sequences in order to influence inactivation, replacement or site-specific gene creation.[119] Initial methods of genome editing such as homologous recombination[120] generally suffered from poor site selectivity and efficiency. Sequence-specific DNA binding domains such as zinc-finger nucleases (ZFNs)[121, 122] and transcription activator-like effector nucleases (TALENS)[123] are major gene-editing technologies that have pioneered the application of site-selective cleavage within the field and led to increased focus over recent years.

The rise of clustered regularly interspaced short palindromic repeats (CRISPRs)[124, 125] as an alternative has seen it take a prominent role in the current state of art within gene-editing and affords key advantages over the former including simple design and development (**Figure I-18**).[126]

I. 4. 1. Antisense Technology

Antisense therapy is a gene silencing technique developed to bind 'antisense' oligonucleotides complementary to a target nucleic acid — generally mRNA — by Watson-Crick base pairing which inhibits subsequent expression or translation of the gene in question. An antisense oligonucleotide (ASO) is a single stranded oligomer that typically contains 18-21 nucleotides, although ranges of between 12-25 bases are also common. The silencing of gene expression is achieved mainly through steric hindrance of ribosomal interactions along the mRNA or by inducing enzymatic mRNA degradation via RNaseH.[127] Notably, interest in this field was heralded by ground breaking work by Stephenson *et al.* when inhibition of viral replication of the Rous sarcoma virus was achieved through the use of ASOs.[128]

The rise to prominence of nucleic acid vectors within the field of antisense technology has provided an avenue for renewed promise in effectively targeting stubborn diseases that at one stage were viewed as 'undruggable'. A paradigm shift in treating target RNAs as receptors for antisense oligonucleotides (ASOs) proved an interesting concept in which was once considered the purview of small molecules. A key advantage in the development of antisense oligonucleotides is that the primary mechanic behind their mode of action – Watson-Crick binding – is well elucidated and provides an edge over traditional drug discovery where rational design is curtailed by incomplete information on targeting mechanisms.

I. 4. 2. Therapeutic Oligonucleotides

To date there are nine single-stranded ASOs representing four chemical modification classes that have been approved for commercial use. Additionally, there are four siRNAs (short-interfering RNAs) that have also received regulatory approval.[129] The primary aim of ASOs is to present excellent affinity and specificity for the receptor sequence of choice. This is achieved by i.) mimicking traditional DNA through structural isomorphism, ii.) display non-sequence off-target toxicity, and iii.) ability to cross cellular membranes and present high resistance to nuclease degradation.

Investigation into the development of ASOs is primarily concerned with the modification of backbones structures and sugar groups.[130] Nucleobase modification is generally uncommon as retention of Watson-Crick base pairing is paramount. As such only modifications such as 5-methylcytosine, displaying increased stabilising properties, are generally found. The prevention of nuclease degradation was the primary concern upon the advent of the field. The use of phosphorothioate oligonucleotides (PS) (**Figure I-19, PS**) wherein a non-bridging oxygen is substituted for a sulphur atom represented the initial generation of ASOs.[131] Formivirsen, a 21 mer PS-ASO, was the first antisense oligonucleotide to be approved by the FDA in 1998 for the treatment of cytomegalovirus (CMV) retinitis.

Introduction of the sulphur atom was found to slightly decrease the binding affinity of the ASO and thus limit therapeutic potency.[132] From this, the second generation developed in which PS-ASOs underwent further sugar modifications such as the introduction of 2'-O-methoxyethyl (2'-MOE) or by constraining the ribose structure through tethering of the 2' positon to the 4' carbon using a 2'-constrained ethyl group (2'-cEt).[133] A 2'-MOE PS antisense oligonucleotide, Mipomersen, developed by Ionis Pharmaceuticals received FDA approval in 2013 for the treatment of familial hypercholesterolemia.[134] DYN101 is a 2'-cEt modified PS ASO currently undergoing Phase I/II trials for the treatment of centronuclear myopathy.

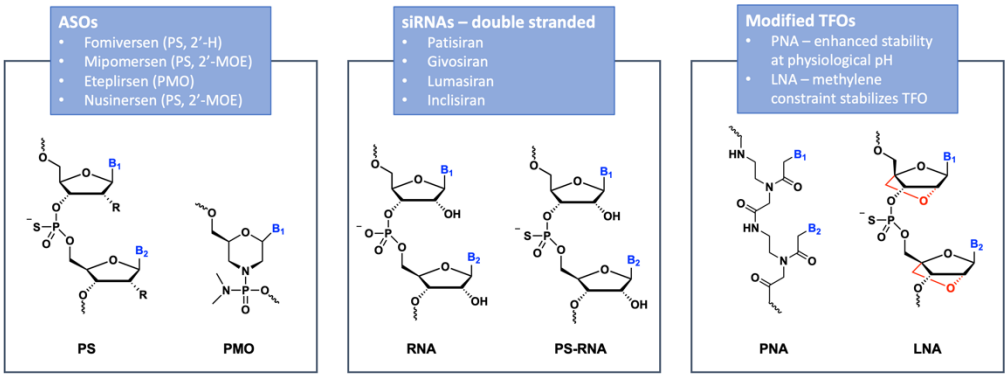

Figure I-19. Therapeutic oligonucleotide modifications within the clinic and under development. Phosphorothioate linkages (**PS**) improves the nuclease stability of ASOs and are generally found combined with 2-MOE modifications, as the 2' position is most commonly used in nuclease degradation processes.[135] **PMO** ASOs represent a class of ASOs that retain the nuclease stability of typical PS ASOs without any of the consequential loss of affinity for target substrates.[136] **PS-RNA** modifications represent the most widely used clinical SiRNA constructs.[137] **PNA** significantly changes the application of oligos at physiological pHs due to the inherent neutral backbone. **LNA**s are a growing class of modified nucleic acids that prevent degradation through the 2' position similar to 2-MOE modifications. Miraversen is an innovative hepatitis treatment representative of this class.[138]

Phosphorodiamidate morpholino oligonucleotides (PMOs) represent another class of ASO in which the complete substitution of the ribose ring by morpholine is achieved. The phosphodiester backbone is further altered by the introduction of phosphoroamidate subunits (**Figure I-19, PMO**).[139] Sarepta Therapeutics developed Eteplirsen, a PMO-ASO, which received accelerated approval by the FDA in 2016 for the treatment of Duchenne muscular dystrophy (DMD).[140]

Of the nine ASOs currently approved for treatment regimens, four are modified PMOs while PS modifications are found in the other five. PS modifications are also the most widely used moiety in siRNAs. Patisiran (2018), givosiran (2019), lumasiran (2020) and inclisiran (2020) are the four siRNAs that are currently approved.[129] siRNAs are short double stranded RNA fragments (19-21 nucleotides) that undergo Watson-Crick base pairing with target RNA similar to other ASOs. A notable distinction between siRNAs and ASOs is the increased hydrophilic nature of siRNAs – as the therapeutic is double stranded the nucleobases are in effect protected in a duplex motif with a concerted backbone encompassing it and thus have a significant effect on the resultant

pharmacokinetic properties.[141] Recognition of the siRNA by proteins known as the RNA-induced silencing complex (RISC) occurs prior to binding with the target RNA sequence. The guide siRNA strand incorporates into the RISC whilst the complimentary or 'passenger' strand is discarded. The RISC brings the guide strand into contact with the target RNA sequence followed by Argonaute-2 (AGO-2) cleavage of the target RNA and subsequent degradation.

Alternative approaches involving the use of triplex-forming oligonucleotides (TFOs) are also gaining traction within the antisense community. In contrast to ASOs, TFOs are designed as DNA targeting triplex invasion oligonucleotides in which the target is double stranded DNA rather than RNA.

I. 4. 3. Triplex Forming Oligonucleotides

Recent research has focused on the application of antisense technology to target dsDNA through the use of triplex-forming oligonucleotides (TFOs).[142] The technology is termed 'antigene' therapy whereby transcription to mRNA is inhibited rather than by translation. TFOs bind in the major groove of the duplex through hydrogen bond formation with the Watson-Crick bases forming a triple helix otherwise known as a triplex. Oligonucleotides can bind in one of two ways dependent on its own composition alongside that of the target sequence. Pyrimidine-rich oligonucleotides bind in a parallel orientation through hydrogen bonding, known as Hoogsteen bonding, with T and C forming bonds with AT and GC in turn creating T-AT and C^+-GC triplex motifs.[143] Purine-rich sequences form anti-parallel conformations (reverse Hoogsteen bonding) through A-AT and G-GC triplexes although these are generally less-favoured due to the variety of triplex distortions associated along with undesirable self-bonding of the anti-parallel TFO and resultant features such as G-quadruplexes (**Figure I-20**). Interestingly, G-GC and T-AT triplex motifs can be produced in both triplex orientations, although stability is dependent on the amount of GpT and TpG triplets present.[144]

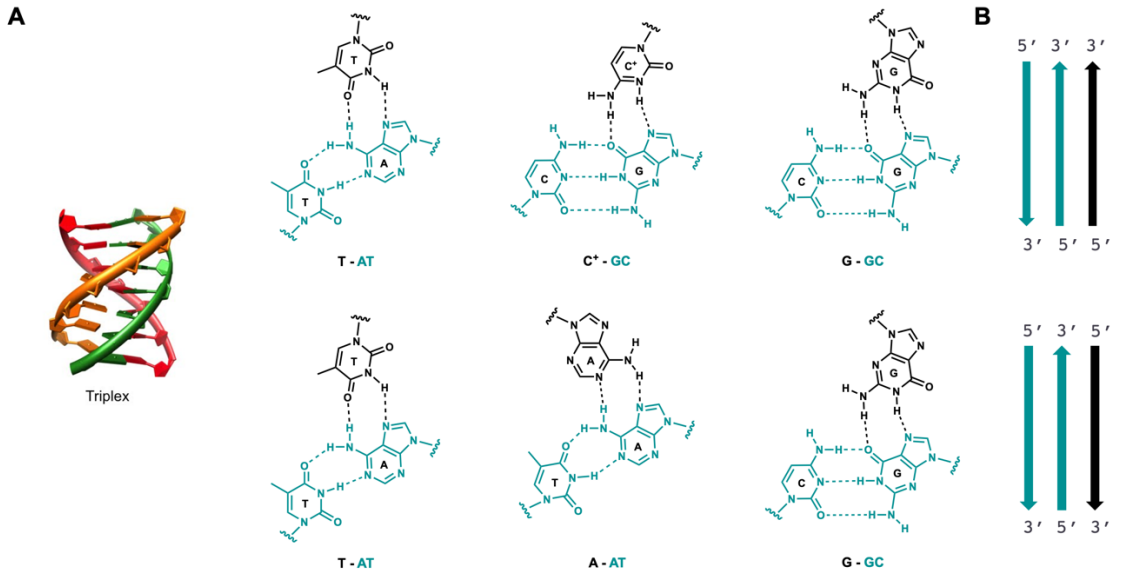

Figure I-20. A. Structure of a parallel DNA triplex. **Top.** Triplets generated by parallel triplex formation (T-AT, C^+-GC and G-GC). **Bottom.** Antiparallel triplets (T-AT, A-AT and G-GC). Note that both T-AT and G-GC triplets are possible in either configuration. **B.** Illustration of parallel and antiparallel triplex formation.

A core tenet of antisense research is the drive to increase the binding affinity and stability of the oligonucleotides and their target. Numerous problems face TFO technology including i.) pH dependence, ii.) stability and resistance to cellular nuclease activity and iii.) poor cellular uptake due to their anionic nature. Prominent adaptations to solve these issues include base, sugar and phosphate backbone modifications.[142] 5-methylcytosine is a notable base substitute that has been reported to improve the pH dependence of parallel triplexes.[145] Other examples include the base analogue 5-propargylamino deoxyuridine which incorporates an alkyne moiety and a positive charge has shown increased stability when utilised as a base substitute.[146] In comparison to its control TFO (no alkyne modification) has shown that the added stacking interactions from the alkyne group within the major groove lead to increased binding affinity. It was further demonstrated that by replacing the cationic charge from the ring system and moving it into the major groove had a considerable effect on triplex stabilisation compared to prototypical triplexes with protonated cytosines.[146] Phosphate backbone modifications have also been investigated whereby resident phosphate groups were replaced with cationic substitutes such as *N,N*-diethyl-ethylenediamine.[147] The cationic linkages minimised charge repulsion between the probe and target strand thus increasing triplex stability. Across the

literature, sugar modifications are perhaps the most thoroughly explored. Similar to phosphate modifications, the addition of specific cationic amino side chains to the sugar moiety enhanced stability significantly. For example, 5' modifications with cationically-modified sugar backbones have been shown to increase stability in comparison to 3' and central oligonucleotide base sites.[148]

Another type of modification includes the conjugation of adjuvants to TFOs which provide secondary interactions to the duplex thereby helping to anchor the probe to its target. Several studies have investigated different adjuvants including crosslinking *via* alkylating agents such as bromoacetamide[149] and chlorambucil.[150] In addition, crosslinking has been achieved *via* photoactivation with psoralen[151] or through the use of intercalating molecules combined with nucleic acids.[152] Markedly, the ability of metal ions such as platinum to generate crosslinks between TFOs and target nucleic acid strands was quickly identified as another means to achieve increased affinity.[153]

I. 4. 4. DNA-Crosslinking Hybrids

I. 4. 4. 1. Psoralen Hybrids

Targeted oligonucleotides are mainly believed to elicit their effects through hybridisation mechanisms with complimentary target sequences. The oligonucleotide will bind to the target dsDNA or mRNA and prevent transcription and translation respectively through steric obstruction of ribosomal entities. A significant portion of previous research however was aimed at evaluating the exact targets of these oligonucleotide vectors once within the cellular environment. Thus, crosslinking agents found a place going forward within the field as the use of adduct formation by these conjugates would enhance the elucidation of exact cellular targets. Additionally, the use of crosslinking hybrids would in theory allow for lower quantities of drug to be used as the crosslink/H-bonding combination would allow for more effective inhibition than traditional hybridisation alone.

Psoralens represent an important class of photochemical crosslinking agents that have been used in the investigation of nucleic acid structure and

function. A planar and aromatic compound, psoralen maintains the ability to intercalate into dsDNA regions and form bifunctional covalent bonds with the pyrimidine bases (**Figure I-21**).[154] Covalent interstrand adduct formation can occur at either the furan or coumarin end of the molecule. Crosslinking of single stranded nucleic acid targets is possible although less prevalent than interactions with dsDNA sequences.[155] Adduct formation occurs through irradiation of the compound with long wavelength UV light and is significant as it leaves the DNA moiety untouched aside from the site of the chemical modification. Therefore psoralen and derivatives have found innovative use as probes of nucleic acid secondary and tertiary structure in both *in vivo* and *in vitro* conditions.[156, 157]

Significantly, a key aspect of the use of psoralen is the ability to control and modulate the degree of crosslinking through regulation of compound concentration, light intensity and timed application of the light source. Furthermore, the crosslink is reversed through introduction of a shorter wavelength UV light treatment.[156]

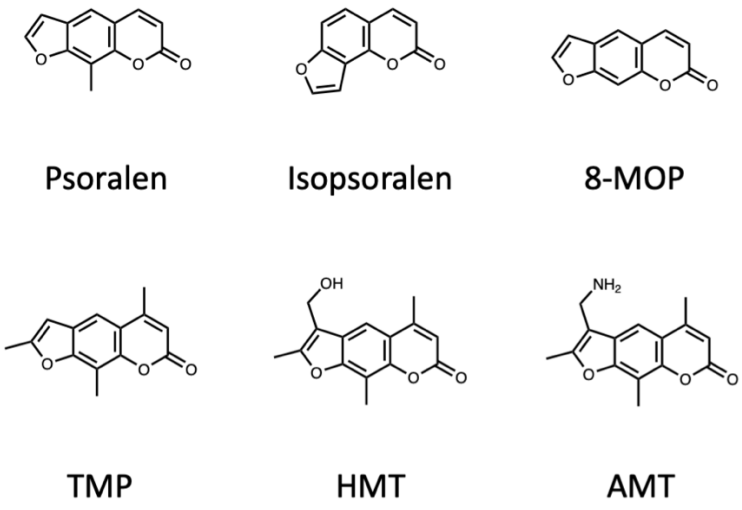

Figure I-21. Psoralen and significant derivatives. Isopsoralen, 8-methoxypsoralen (8-MOP), 4,5',8-trimethylpsoralen (TMP), 4'-hydroxymethyl-4,5',8-trimethylpsoralen (HMT) and 4'-aminomethyl-4,5',8-trimethylpsoralen (AMT).[158]

With their therapeutic and diagnostic application proving notable, the evolution of psoralen application to incorporate targeting nucleic acid vectors followed soon after. Miller and colleagues demonstrated the ability to successfully conjugate AMT-derivatised psoralen molecules with oligomers via phosphoramidate bonds followed by hybridisation and photo-initiated crosslinking with a complimentary target system.[159] Similarly Englisch showcased psoralen-TFO hybrid generation and photo-adduct formation with a HMT psoralen derivative.[160] Advancing the research of these psoralen hybrids even further Hélène and co-workers demonstrated the first example of a psoralen-TFO construct successfully targeting and crosslinking a duplex sequence and creating a crosslinked triplex system[161] and was quickly followed by similar work performed by Glazer *et al*. using a HMT derivative.[162] The use of psoralen-derived hybrid constructs led to interest in platinum-conjugated systems and the crosslinking affinity they possess. Although research detailing the use of psoralen-hybrids has slowed as of recently, innovative work still proceeds including the generation of TMP-derived nucleosides and subsequent employment through solid-phase synthesis to form a psoralen-oligomer that retains the ability to form photoadducts.[163]

Table I-2. Derivatised psoralen-hybrids and design linkage.

Binding	Psoralen		Reference
Phosphoramidate	AMT	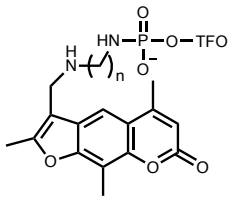	Miller 1988[159]
Phosphoramidite	TMP	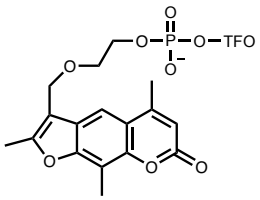	Englisch 1989[160]
5'-thiophosphate	8-MOP	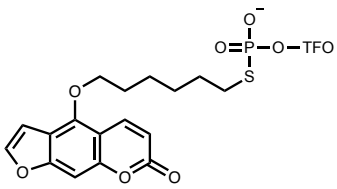	Helene 1991[161]
Phosphoramidite	HMT	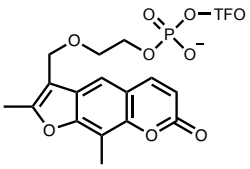	Glazer 1993[162]
Nucleoside	TMP	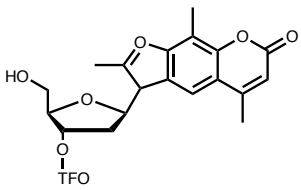	Murakami 2009[163]

I. 4. 4. 2. Platinum-DNA Hybrids

The use of platinum complexes to act as directed crosslinking reagents has been known for some time. Mononuclear transplatin compounds were shown to bind with specific oligonucleotide targets[164] where their geometry and coordination behaviour make them ideal candidates for crosslinking oligonucleotides without any resultant local steric distortions. This work was followed by binuclear platinum(II) complexes being shown to favourably crosslink with oligo-5'-phosphorothioate derivatives prior to targeting of polypurine tracts in triple stranded DNA.[165] Progressing from this, Lippert *et al.* then investigated whether transplatin could appropriately crosslink triplexes.[166] Hybrid TFOs with transplatin modifications at either the 5'-terminus or internal positions were generated and results demonstrated that a *trans*-platinum(II) molecule hybridised to a homopyrimidine ON could react with a complimentary duplex and form an interstrand crosslink once bound. Significantly, no crosslinking was observed between the *trans*-Pt(II)-TFO and non-complementary dsDNA. Additional experiments have shown the transplatin crosslink to increase the stability of the triplex system.[167] Preliminary studies such as these led researchers to believe that platinum-facilitated crosslinking could form a core aspect of future antisense strategies and technology. Indeed, the inhibition of translation *in vitro* and within *E. coli.* cells by a transplatin-conjugated oligonucleotide crosslinked to a target was further reported.[168]

Extensive research efforts have focused on generating easier preparative methods for generating platinum-modified oligonucleotides. Using solid-phase DNA synthesis, platinated building blocks have been added and incorporated into nucleic acid sequences, however, these methods are far from effective (**Figure I-22, A**).[169, 170] Subsequently, Reedijk and Lippert showed that solid-phase synthesis can be used to create libraries of trans-platinum(II) modified PNA (peptide nucleic acids) oligomers and this method can be applied to produce a range of desired probes.[171]

A common problem encountered in triplex formation involves pyrimidine interruptions in the target purine strand.[142] Research has shown that even a single pyrimidine base interruption can significantly perturb triplex stability. To

address this problem, the use of base analogues that recognise the interruption and facilitate stabilisation have been generated.[172] A relatively new approach has involved the use of transplatin conjugated to these base analogues to facilitate crosslinking across the major groove at the purine mismatch site. Although this concept of crosslinking has been demonstrated, probe binding is inferior to that of standard base analogues.[173]

The generation of *cis*-platinum(II) derivatives by solid-phase DNA synthesis are known,[174] however substitution with NH_3^+ during the deprotection step leads to an inactive species being produced.[175] Other methods were therefore investigated to develop oligonucleotides incorporating *cis* complexes. Sharma and McLaughlin have shown how an oligonucleotide tethered to a 2-(2-aminoethylamino) ethanol chelator can be post-synthetically reacted with platinum to obtain a viable *cis* derivatised sequence that exhibits effective intrastrand cross-linking to a polypurine target (**Figure I-22, B**).[176] The targeting of interruptions within the target polypurine tract was revisited utilising similar *cis* derivatives and was shown to afford highly stable adduct formation.[177] More recently, Miller *et al.* have shown that specific mono and 3',5'-bis-*trans*-platinated TFOs can form highly stable interstrand crosslinks with both strands of the target duplex (**Figure I-22, C-D**). Binding of plasmid DNA and subsequent *in vitro* inhibition of transcription was further observed by these conjugates.[178] Recent work has showcased the ability of these Pt-TFOs to target the human androgen receptor (AR) gene causing knockdown of AR mRNA and associated protein in LAPC-4 prostate cancer cells after transfection.[179] Results such as this show the potential that Pt-TFO hybrids have as antigene therapeutic agents. A complete summary of past and current platinum crosslink hybrids including binding modes and motifs can be found in **Table I-3**.

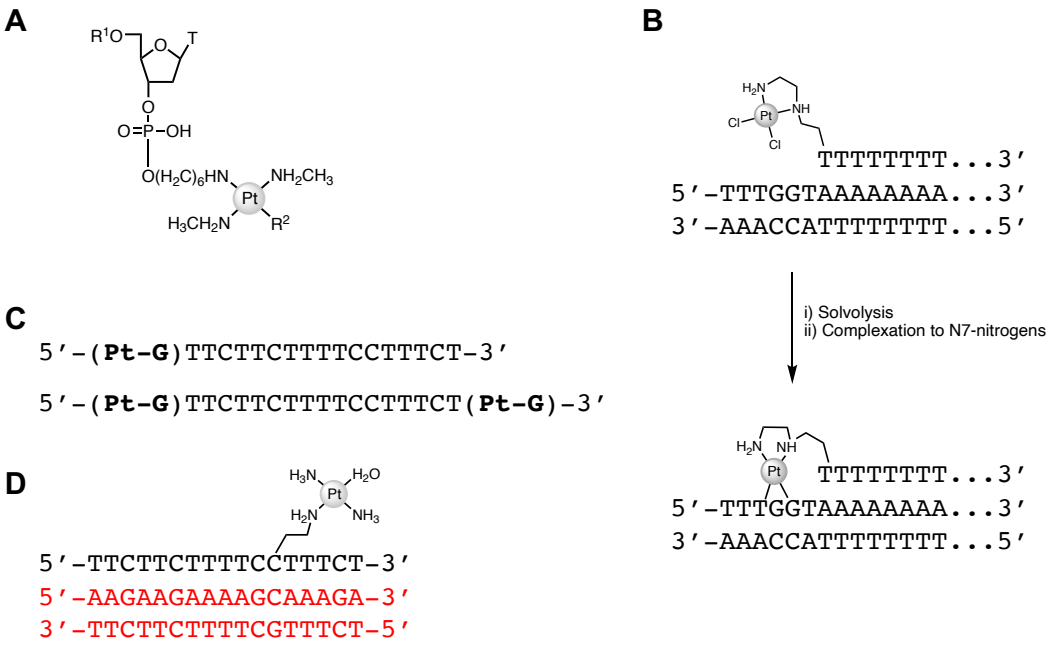

Figure I-22. A. Platinated building block developed by Reedijk and co-workers for implementation in solid-phase synthesis.[170] **B.** Cis-platinum(II) derived TFO hybrid designed by Sharma and DNA McLaughlin.[176] **C.** Example of a mono-and bis-functionalised trans-platinum(II) TFO hybrid developed by Miller and colleagues,[168] where (**Pt-G**) denotes a guanine nucleobase coupled at the N7 position to a trans-platinum(II) reagent. **D.** Internally modified N^4-(aminoalkyl) cytosine TFO with a trans-platinum(II) derived reagent coupled.[180]

Table I-3. Current Platinum-DNA Hybrid state of the art.

Binding Mode	Platinum Structure	Reference
Direct platination	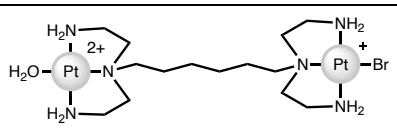 Vlassov 1983 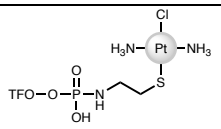 Orgel 1989 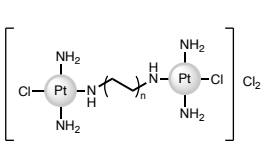 Orgel 1991 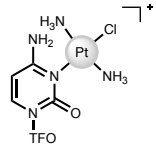 Leng 1998 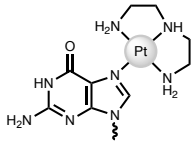 Siegel 2001 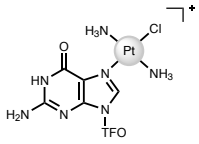 Miller 2009, 2015	Vlassov 1983[153] Orgel 1989,[181] 1991[165] Leng 1996,[166] 1998[169] Sigel 2001[182] Miller 2009,[180] 2015[179]
Direct platination/ Solid Phase Synthesis	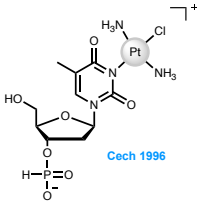 Cech 1996 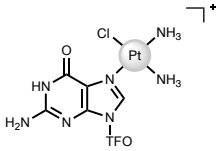 Lippard 1996 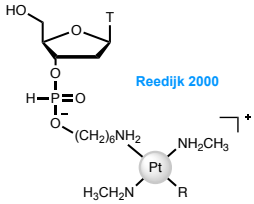 Reedijk 2000	Cech 1996[175] Lippard 1996[174] Reedijk 2000[170]
N-4 Aminoethyl linker	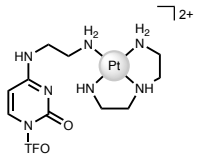 Miller 2007 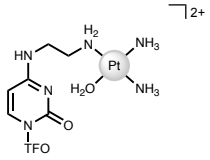 Miller 2007	Miller 2007[173]
N-4 Aminopentyl linker	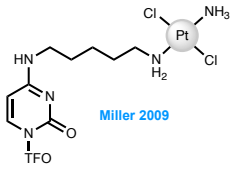 Miller 2009 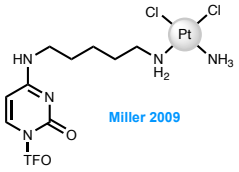 Miller 2009	Miller 2009[168]
C-5 Aminoethyl linker	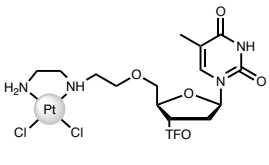 McLaughlin 2002, 2004 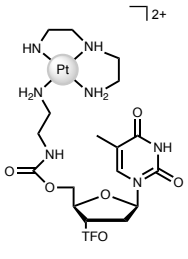 Miller 2007	McLaughlin 2002,[176] 2004[177] Miller 2007[173]

I. 5. Conclusion

Almost forty years have passed since the discovery of the medicinal properties of cisplatin and other platinum drugs – yet only three remain approved around the world today. This has led to a great amount of interest in improving upon the associated drawbacks and modulating the strengths of platinum agents to be applicable in other fields. Antisense technology is an intriguing approach that through the use of click chemistry strategies has shown how small molecules can be conjoined with discrete targeting nucleic acid vectors. The chapter has focused in particular on the advent of platinum-nucleic acid combination chemistry and the pathways that have been explored in their generation and application. The use of click chemistry is an excellent strategy that herein is shown to be highly applicable in developing new targeted platinum agents.

I. 6. References

1. Watson, J. D. C. F. H. C., Molecular Structure of Nucleic Acids: A Structure for Deoxyribose Nucleic Acid. *Nature* **1953,** *171*, 737-738.
2. Chargaff, E.; Lipshitz, R.; Green, C., Composition of the desoxypentose nucleic acids of four genera of sea-urchin. *J. Biol. Chem.* **1952,** *195* (1), 155-160.
3. Wing, R. D., H.; Takano, T.; Broka, C.; Tanaka, S.; Itakura, K.; Dickerson, R. E., Crystal structure analysis of a complete turn of B-DNA. *Nature* **1980,** *287*, 755-758.
4. Drew, H. R.; Wing, R. M.; Takano, T.; Broka, C.; Tanaka, S.; Itakura, K.; Dickerson, R. E., Structure of a B-DNA dodecamer: conformation and dynamics. *Proc. Natl. Acad. Sci.* **1981,** *78* (4), 2179-2183.
5. Harteis, S.; Schneider, S., Making the Bend: DNA Tertiary Structure and Protein-DNA Interactions. *Int. J. Mol. Sci.* **2014,** *15* (7), 12335-12363.
6. Kellett, A.; Molphy, Z.; Slator, C.; McKee, V.; Farrell, N. P., Molecular methods for assessment of non-covalent metallodrug–DNA interactions. *Chem. Soc. Rev.* **2019,** *48* (4), 971-988.
7. Wang, A. H.-J. Q., G. J.; Kolpak, F. J.; Crawford, J. L.; van Boom, J. H.; van der Marel, G.; Rich, A., Molecular structure of a left-handed double helical DNA fragment at atomic resolution. *Nature* **1979,** *282*, 680-686.
8. Drew, H. R. D., R. E., Conformation and dynamics in a Z-DNA tetramer. *J. Mol. Biol.* **1981,** *152* (4), 723-736.
9. Dickerson, R. E. D., H. R.; Conner, B. N.; Wing, R. M.; Fratini, A. V.; Kopka, M. L., The anatomy of A-, B- and Z-DNA. *Science* **1982,** *216* (4545), 475-485.
10. Zhao, J.; Bacolla, A.; Wang, G.; Vasquez, K. M., Non-B DNA structure-induced genetic instability and evolution. *Cell. Mol. Life. Sci.* **2010,** *67* (1), 43-62.
11. Zeraati, M.; Langley, D. B.; Schofield, P.; Moye, A. L.; Rouet, R.; Hughes, W. E.; Bryan, T. M.; Dinger, M. E.; Christ, D., I-motif DNA structures are formed in the nuclei of human cells. *Nat. Chem.* **2018,** *10* (6), 631-637.
12. Pearson, R. G., Hard and Soft Acids and Bases. *J. Am. Chem. Soc.* **1963,** *85* (22), 3533-3539.

13. Coe, B. J.; Glenwright, S. J., Trans-effects in octahedral transition metal complexes. *Coord. Chem. Rev.* **2000,** *203* (1), 5-80.
14. Dhara, S. C., A rapid method for the synthesis of cisplatin. *Indian J. Chem.* **1970,** *8*, 193-194.
15. Rosenberg, B.; Van Camp, L.; Krigas, T., Inhibition of Cell Division in Escherichia coli by Electrolysis Products from a Platinum Electrode. *Nature* **1965,** *205* (207), 835-837.
16. Lebwohl, D.; Canetta, R., Clinical Development of Platinum Complexes in Cancer Therapy: an Historical Perspective and an Update. *Eur. J. Cancer.* **1998,** *34* (10), 1522-1534.
17. Wong, E.; Giandomenio, C. M., Current Status of Platinum-Based Antitumor Drugs. *Chem. Rev.* **1999,** *99*, 2451-2466.
18. Kelland, L., The resurgence of platinum-based cancer chemotherapy. *Nat. Rev. Cancer.* **2007,** *7* (8), 573-584.
19. Gale, G. R.; Morris, C. R.; Atkins, L. M.; Smith, A. B., Binding of an Antitumor Platinum Compound to Cells as Influenced by Physical Factors and Pharmacologically Active Agents. *Cancer Res.* **1973,** *33*, 813-818.
20. Hromas, R. A.; North, J. A.; Burns, C. P., Decreased cisplatin uptake by resistant L1210 leukemia cells. *Cancer Lett.* **1987,** *36* (2), 197-201.
21. Gately, D. P.; Howell, S. B., Cellular accumulation of the anticancer agent cisplatin: A review. *Br. J. Cancer* **1993,** *67*, 1171-1176.
22. Naredi, P.; Heath, D. D.; Enns, R. E.; Howell, S. B., Cross-Resistance between Cisplatin and Antimony in a Human Ovarian Carcinoma Cell Line. *Cancer Res.* **1994,** *54*, 6464-6468.
23. Safaei, R.; Howell, S. B., Copper transporters regulate the cellular pharmacology and sensitivity to Pt drugs. *Crit. Rev. Oncol. Hematol.* **2005,** *53* (1), 13-23.
24. Reishus, J. W.; Martin, D. S. J., cis-Dichlorodiammineplatinum(II). Acid Hydrolysis and Isotopic Exchange of the Chloride Ligands. *J. Am. Chem. Soc.* **1961,** *83*, 2457-2462.
25. Eastman, A., Characterization of the adducts produced in DNA by cis-diamminedichloroplatinum(II) and cis-dichloro(ethylenediamine)platinum(II). *Biochemistry* **1983,** *22* (16), 3927-3933.

26. Eastman, A., Interstrand crosslinks and sequence specificity in the reaction of cis-dichloro(ethylenediamine)platinum(II) with DNA. *Biochemistry* **1985,** *24* (19), 5027-5032.
27. Fichtinger-Schepman, A. M. J.; van der Veer, J. L.; den Hartog, J. H. J.; Lohman, P. H. M.; Reedijk, J., Adducts of the Antitumor Drug cis-Diamminedichloroplatinum(II) with DNA: Formation, Identification, and Quantitation. *Biochemistry* **1985,** *24*, 707-713.
28. Todd, R. C.; Lippard, S. J., Inhibition of transcription by platinum antitumor compounds. *Metallomics* **2009,** *1* (4), 280.
29. Howlander, N.; Noone, A. M.; Krapcho, M.; Miller, D.; Brest, A.; Yu, M.; Ruhl, J.; Tatalovich, Z.; Mariotto, A.; Lewis, D. R.; Chen, H. S.; Feuer, E. J.; Cronin, K. A., SEER Cancer Statistics Review, 1975-2017. National Cancer Institute: Bethesda, MD: 2020.
30. Daugaard, G.; Abildgaard, U., Cisplatin nephrotoxicity. A review. *Cancer Chemother. Pharmacol.* **1989,** *25* (1), 1-9.
31. Screnci, D.; McKeage, M. J., Platinum neurotoxicity: clinical profiles, experimental models and neuroprotective approaches. *J. Inorg. Biochem.* **1999,** *77* (1-2), 105-10.
32. Sheth, S.; Mukherjea, D.; Rybak, L. P.; Ramkumar, V., Mechanisms of Cisplatin-Induced Ototoxicity and Otoprotection. *Front. Cell. Neurosci.* **2017,** *11*, 338.
33. Johnstone, T. C.; Wilson, J. J.; Lippard, S. J., Monofunctional and Higher-Valent Platinum Anticancer Agents. *Inorg. Chem.* **2013,** *52* (21), 12234-12249.
34. Espósito, B. P.; Najjar, R., Interactions of antitumoral platinum-group metallodrugs with albumin. *Coord. Chem. Rev.* **2002,** *232*, 137-149.
35. Rabik, C. A.; Dolan, M. E., Molecular mechanisms of resistance and toxicity associated with platinating agents. *Cancer Treat. Rev.* **2007,** *33* (1), 9-23.
36. Howell, S. B.; Safaei, R.; Larson, C. A.; Sailor, M. J., Copper Transporters and the Cellular Pharmacology of the Platinum-Containing Cancer Drugs. *Mol. Pharmacol.* **2010,** *77* (6), 887-894.
37. Shabalin, I.; Dauter, Z.; Jaskolski, M.; Minor, W.; Wlodawer, A., Crystallography and chemistry should always go together: a cautionary tale

of protein complexes with cisplatin and carboplatin. *Acta Crystallogr. D.* **2015,** *71* (9), 1965-1979.

38. Boal, A. K.; Rosenzweig, A. C., Response from Boal and Rosenzweig toCrystallography and chemistry should always go together: a cautionary tale of protein complexes with cisplatin and carboplatin. *Acta Crystallogr. D.* **2015,** *71* (9), 1984-1986.
39. van der Vijgh, W. J., Clinical pharmacokinetics of carboplatin. *Clin. Pharmacokinet.* **1991,** *21* (4), 242-61.
40. Gore, M. E.; Fryatt, I.; Wiltshaw, E.; Dawson, T.; Robinson, B. A.; Calvert, A. H., Cisplatin/carboplatin cross-resistance in ovarian cancer. *Br. J. Cancer* **1989,** *60* (5), 767-9.
41. Rixe, O.; Ortuzar, W.; Alvarez, M.; Parker, R.; Reed, E.; Paull, K.; Fojo, T., Oxaliplatin, Tetraplatin, Cisplatin, and Carboplatin- Spectrum of Activity in Drug-Resistant Cell Lines and in the Cell Lines of the National Cancer Institute's Anticancer Drug Screen Panel. *Biochem. Pharmacol.* **1996,** *52*, 1855-1865.
42. Johnstone, T. C.; Suntharalingam, K.; Lippard, S. J., The Next Generation of Platinum Drugs: Targeted Pt(II) Agents, Nanoparticle Delivery, and Pt(IV) Prodrugs. *Chem. Rev.* **2016,** *116* (5), 3436-86.
43. Boulikas, T.; Vougiouka, M., Cisplatin and platinum drugs at the molecular level. (Review). *Oncol. Rep.* **2003,** *10* (6), 1663-82.
44. Malina, J.; Natile, G.; Brabec, V., Spontaneous Translocation of Antitumor Oxaliplatin, its Enantiomeric Analogue, and Cisplatin from One Strand to Another in Double-Helical DNA. *Chem. Eur. J.* **2013,** *19* (36), 11984-11991.
45. Bruno, P. M.; Liu, Y.; Park, G. Y.; Murai, J.; Koch, C. E.; Eisen, T. J.; Pritchard, J. R.; Pommier, Y.; Lippard, S. J.; Hemann, M. T., A subset of platinum-containing chemotherapeutic agents kills cells by inducing ribosome biogenesis stress. *Nat. Med.* **2017,** *23* (4), 461-471.
46. Rosenberg, B.; Van Camp, L.; Grimley, E. B.; Thomson, A. J., The Inhibition of Growth or Cell Division in Escherichia coli by Different Ionic Species of Platinum(IV) Complexes. *J. Biol. Chem.* **1967,** *242*, 1347-1352.
47. Rosenberg, B.; Van Camp, L.; Trosko, J., Platinum Compounds: a New Class of Potent Antitumour Agents. *Nature* **1969,** *223*, 582-587.

48. Farrell, N., Current status of structure-activity relationships of platinum anticancer drugs: activation of the trans geometry. *Met. Ions. Biol. Syst.* **1996,** *32*, 603-39.
49. Brabec, V.; Leng, M., DNA interstrand cross-links of trans-diamminedichloroplatinum(II) are preferentially formed between guanine and complementary cytosine residues. *Proc. Natl. Acad. Sci.* **1993,** *90* (11), 5345-5349.
50. Kelland, L. R.; Barnard, C. F. J.; Mellish, K. J.; Jones, M.; Goddard, P. M.; Valenti, M.; Bryant, A.; Murrer, B. A.; Harrap, K. R., A Novel trans-Platinum Coordination Complex Possessing in Vitro and in Vivo Antitumor Activity. *Cancer Res.* **1994,** *54* (21), 5618-5622.
51. Montero, E. I.; Díaz, S.; González-Vadillo, A. M.; Pérez, J. M.; Alonso, C.; Navarro-Ranninger, C., Preparation and Characterization of Novel trans -[PtCl 2 (amine)(isopropylamine)] Compounds: Cytotoxic Activity and Apoptosis Induction in r as- Transformed Cells. *J. Med. Chem.* **1999,** *42* (20), 4264-4268.
52. Coluccia, M.; Nassi, A.; Boccarelli, A.; Giordano, D.; Cardellicchio, N.; Locker, D.; Leng, M.; Sivo, M.; Intini, F. P.; Natile, G., In vitro and in vivo antitumour activity and cellular pharmacological properties of new platinum–iminoether complexes with different configuration at the iminoether ligands. *J. Biol.* **1999,** *77*, 31-35.
53. Li, W.; Jiang, M.; Cao, Y.; Yan, L.; Qi, R.; Li, Y.; Jing, X., Turning Ineffective Transplatin into a Highly Potent Anticancer Drug via a Prodrug Strategy for Drug Delivery and Inhibiting Cisplatin Drug Resistance. *Bioconjug. Chem.* **2016,** *27* (8), 1802-1806.
54. Kelland, L. R.; Abel, G.; McKeage, M. J.; Jones, M.; Goddard, P. M.; Valent, M.; Murrer, B. A.; Harrap, K. R., Preclinical Antitumor Evaluation of Bis-acetato-ammine-dichloro-cyclohexylamine Platinum(IV)- an Orally Active Platinum Drug. *Cancer Res.* **1993,** *53*, 2581-2586.
55. Hall, M. D.; Mellor, H. R.; Callaghan, R.; Hambley, T. W., Basis for Design and Development of Platinum(IV) Anticancer Complexes. *J. Med. Chem.* **2007,** *50* (15), 3403-3411.
56. Sinisi, M.; Intini, F. P.; Natile, G., Dependence of the Reduction Products of Platinum(IV) Prodrugs upon the Configuration of the Substrate, Bulk of

the Carrier Ligands, and Nature of the Reducing Agent. *Inorg. Chem.* **2012,** *51* (18), 9694-9704.

57. Plaxe, S. C.; Braly, P. S.; Freddo, J. L.; McClay, E.; Christen, R. D.; Kirmani, S.; Kim, S.; Heath, D.; Howell, S. B., Phase I and pharmacokinetic study of intraperitoneal ormaplatin. *Gynecol. Oncol.* **1993,** *51* (1), 72-7.
58. Bramwell, V. H.; Crowther, D.; O'Malley, S.; Swindell, R.; Johnson, R.; Cooper, E. H.; Thatcher, N.; Howell, A., Activity of JM9 in advanced ovarian cancer: a phase I-II trial. *Cancer Treat. Rep.* **1985,** *69*, 409-416.
59. Wheate, N. J.; Walker, S.; Craig, G. E.; Oun, R., The status of platinum anticancer drugs in the clinic and in clinical trials. *Dalton Trans.* **2010,** *39* (35), 8113-27.
60. Tutsch, K. D.; Arzoomanian, R. Z.; Alberti, D.; Tombes, M. B.; Feierabend, C.; Robins, H. I.; Spriggs, D. R.; Wilding, G., Phase I clinical and pharmacokinetic study of an one-hour infusion of ormaplatin (NSC 363812). *Invest. New Drug.* **1999,** *17* (1), 63-72.
61. Anderson, H.; Wagstaff, J.; Crowther, D.; Swindell, R.; Lind, M. J.; McGregor, J.; Timms, M. S.; Brown, D.; Palmer, P., Comparative toxicity of cisplatin, carboplatin (CBDCA) and iproplatin (CHIP) in combination with cyclophosphamide in patients with advanced epithelial ovarian cancer. *Eur. J. Cancer. Clin. Oncol.* **1988,** *24* (9), 1471-9.
62. GPC Biotech Inc. "ORPLATNA Satraplatin Capsules: Advisory Commiitee Briefing Document, NDA 21-801". USA Food and Drug Administration. 2007.
63. U.S. National Library of Medicine. http://www.clinicaltrials.gov/satraplatin (accessed 2020).
64. Kelland, L. R.; Sharp, S. Y.; O'Neill, C. F.; Raynaud, F. I.; Beale, P. J.; Judson, I. R., Mini-review: discovery and development of platinum complexes designed to circumvent cisplatin resistance. *J. Inorg. Biochem.* **1999,** *77* (1-2), 111-5.
65. Farrell, N. P., Multi-platinum anti-cancer agents. Substitution-inert compounds for tumor selectivity and new targets. *Chem. Soc. Rev.* **2015,** *44* (24), 8773-8785.
66. Mangrum, J. B.; Farrell, N. P., Excursions in polynuclear platinum DNA binding. *Chem. Commun. (Camb).* **2010,** *46* (36), 6640-50.

67. McGregor, T. D.; Balcarova, Z.; Qu, Y.; Tran, M. C.; Zaludova, R.; Brabec, V.; Farrell, N., Sequence-dependent conformational changes in DNA induced by polynuclear platinum complexes. *J. Inorg. Biochem.* **1999,** *77* (1-2), 43-6.
68. Sessa, C.; Capri, G.; Gianni, L.; Peccatori, F.; Grasselli, G.; Bauer, J.; Zucchetti, M.; Vigano, L.; Gatti, A.; Minoia, C.; Liati, P.; Van den Bosch, S.; Bernareggi, A.; Camboni, G.; Marsoni, S., Clinical and pharmacological phase I study with accelerated titration design of a daily times five schedule of BBR3464, a novel cationic triplatinum complex. *Ann. Oncol.* **2000,** *11* (8), 977-83.
69. Komeda, S.; Moulaei, T.; Woods, K. K.; Chikuma, M.; Farrell, N. P.; Williams, L. D., A Third Mode of DNA Binding: Phosphate Clamps by a Polynuclear Platinum Complex. *J. Am. Chem. Soc.* **2006,** *128* (50), 16092-16103.
70. Prisecaru, A.; Molphy, Z.; Kipping, R. G.; Peterson, E. J.; Qu, Y.; Kellett, A.; Farrell, N. P., The phosphate clamp: sequence selective nucleic acid binding profiles and conformational induction of endonuclease inhibition by cationic Triplatin complexes. *Nucleic Acids Res.* **2014,** *42* (22), 13474-13487.
71. Qu, Y.; Harris, A.; Hegmans, A.; Petz, A.; Kabolizadeh, P.; Penazova, H.; Farrell, N., Synthesis and DNA conformational changes of non-covalent polynuclear platinum complexes. *J. Inorg. Biochem.* **2004,** *98* (10), 1591-8.
72. Malina, J.; Farrell, N. P.; Brabec, V., Substitution-inert trinuclear platinum complexes efficiently condense/aggregate nucleic acids and inhibit enzymatic activity. *Angew. Chem. Int. Ed.* **2014,** *53* (47), 12812-6.
73. Harris, A. L.; Yang, X.; Hegmans, A.; Povirk, L.; Ryan, J. J.; Kelland, L.; Farrell, N. P., Synthesis, characterization, and cytotoxicity of a novel highly charged trinuclear platinum compound. Enhancement of cellular uptake with charge. *Inorg. Chem.* **2005,** *44* (26), 9598-600.
74. Bruijnincx, P. C.; Sadler, P. J., New trends for metal complexes with anticancer activity. *Curr. Opin. Chem. Biol.* **2008,** *12* (2), 197-206.
75. Dancey, J. E.; Chen, H. X., Strategies for optimizing combinations of molecularly targeted anticancer agents. *Nat. Rev. Drug Discov.* **2006,** *5* (8), 649-659.

76. Wang, X.; Guo, Z., Targeting and delivery of platinum-based anticancer drugs. *Chem. Soc. Rev.* **2013,** *42* (1), 202-24.
77. Fang, J.; Nakamura, H.; Maeda, H., The EPR effect: Unique features of tumor blood vessels for drug delivery, factors involved, and limitations and augmentation of the effect. *Adv. Drug. Deliv. Rev.* **2011,** *63* (3), 136-51.
78. Kim, E.; Rye, P. T.; Essigmann, J. M.; Croy, R. G., A bifunctional platinum(II) antitumor agent that forms DNA adducts with affinity for the estrogen receptor. *J. Inorg. Biochem.* **2009,** *103* (2), 256-61.
79. Berger, I.; Nazarov, A. A.; Hartinger, C. G.; Groessl, M.; Valiahdi, S.-M.; Jakupec, M. A.; Keppler, B. K., A glucose derivative as natural alternative to the cyclohexane-1,2-diamine ligand in the anticancer drug oxaliplatin? *ChemMedChem* **2007,** *2* (4), 505-514.
80. Graf, N.; Mokhtari, T. E.; Papayannopoulos, I. A.; Lippard, S. J., Platinum(IV)-chlorotoxin (CTX) conjugates for targeting cancer cells. *J. Inorg. Biochem.* **2012,** *110*, 58-63.
81. Aryal, S.; Hu, C. M.; Zhang, L., Polymer--cisplatin conjugate nanoparticles for acid-responsive drug delivery. *ACS Nano* **2010,** *4* (1), 251-8.
82. Peer, D.; Karp, J. M.; Hong, S.; Farokhzad, O. C.; Margalit, R.; Langer, R., Nanocarriers as an emerging platform for cancer therapy. *Nat. Nanotechnol.* **2007,** *2* (12), 751-760.
83. Dhar, S.; Kolishetti, N.; Lippard, S. J.; Farokhzad, O. C., Targeted delivery of a cisplatin prodrug for safer and more effective prostate cancer therapy in vivo. *Proc. Natl. Acad. Sci.* **2011,** *108* (5), 1850-1855.
84. Kolb, H. C.; Finn, M. G.; Sharpless, K. B., Click Chemistry: Diverse Chemical Function from a Few Good Reactions. *Angew. Chem. Int. Ed.* **2001,** *40* (11), 2004-2021.
85. Huisgen, R., 1,3-Dipolar Cycloadditions. Past and Future. *Angew. Chem. Int. Ed.* **1963,** *2* (10), 565-598.
86. Rostovtsev, V. V.; Green, L. G.; Fokin, V. V.; Sharpless, K. B., A stepwise huisgen cycloaddition process: copper(I)-catalyzed regioselective "ligation" of azides and terminal alkynes. *Angew. Chem. Int. Ed.* **2002,** *41* (14), 2596-9.
87. Tornoe, C. W.; Christensen, C.; Meldal, M., Peptidotriazoles on solid phase: [1,2,3]-triazoles by regiospecific copper(i)-catalyzed 1,3-dipolar

cycloadditions of terminal alkynes to azides. *J. Org. Chem.* **2002,** *67* (9), 3057-64.

88. Johansson, J. R.; Beke-Somfai, T.; Said Stalsmeden, A.; Kann, N., Ruthenium-Catalyzed Azide Alkyne Cycloaddition Reaction: Scope, Mechanism, and Applications. *Chem. Rev.* **2016,** *116* (23), 14726-14768.
89. Speers, A. E.; Adam, G. C.; Cravatt, B. F., Activity-Based Protein Profiling in Vivo Using a Copper(I)-Catalyzed Azide-Alkyne [3 + 2] Cycloaddition. *J. Am. Chem. Soc.* **2003,** *125* (16), 4686-4687.
90. Wolbers, F.; ter Braak, P.; Le Gac, S.; Luttge, R.; Andersson, H.; Vermes, I.; van den Berg, A., Viability study of HL60 cells in contact with commonly used microchip materials. *Electrophoresis* **2006,** *27* (24), 5073-80.
91. Sletten, E. M.; Bertozzi, C. R., Bioorthogonal Chemistry: Fishing for Selectivity in a Sea of Functionality. *Angew. Chem. Int. Ed.* **2009,** *48* (38), 6974-6998.
92. Agard, N. J.; Baskin, J. M.; Prescher, J. A.; Lo, A.; Bertozzi, C. R., A Comparative Study of Bioorthogonal Reactions with Azides. *ACS Chem. Biol.* **2006,** *1* (10), 644-648.
93. Baskin, J. M.; Prescher, J. A.; Laughlin, S. T.; Agard, N. J.; Chang, P. V.; Miller, I. A.; Lo, A.; Codelli, J. A.; Bertozzi, C. R., Copper-free click chemistry for dynamic in vivo imaging. *Proc. Natl. Acad. Sci.* **2007,** *104* (43), 16793-16797.
94. Gierlich, J.; Burley, G. A.; Gramlich, P. M. E.; Hammond, D. M.; Carell, T., Click Chemistry as a Reliable Method for the High-Density Postsynthetic Functionalization of Alkyne-Modified DNA. *Org. Lett.* **2006,** *8* (17), 3639-3642.
95. El-Sagheer, A. H.; Brown, T., Click chemistry with DNA. *Chem. Soc. Rev.* **2010,** *39* (4), 1388.
96. Gramlich, P. M.; Warncke, S.; Gierlich, J.; Carell, T., Click-click-click: single to triple modification of DNA. *Angew. Chem. Int. Ed.* **2008,** *47* (18), 3442-4.
97. Gutsmiedl, K.; Fazio, D.; Carell, T., High-density DNA functionalization by a combination of Cu-catalyzed and cu-free click chemistry. *Chemistry* **2010,** *16* (23), 6877-83.

98. Gramlich, P. M. E.; Wirges, C. T.; Manetto, A.; Carell, T., Postsynthetic DNA Modification through the Copper-Catalyzed Azide-Alkyne Cycloaddition Reaction. *Angew. Chem. Int. Ed.* **2008,** *47* (44), 8350-8358.
99. Staudinger, H.; Meyer, J., Über neue organische Phosphorverbindungen III. Phosphinmethylenderivate und Phosphinimine. *Helv. Chim. Acta* **1919,** *2*, 635-646.
100. Sági, J.; Szemzö, A.; Ébinger, K.; Szabolcs, A.; Sági, G.; Ruff, E.; Ötvös, L., Base-modified oligodeoxynucleotides. I. effect of 5-alkyl, 5-(1-alkenyl) and 5-(1-alkynyl) substitution of the pyrimidines on duplex stability and hydrophobicity. *Tetrahedron Lett.* **1993,** *34* (13), 2191-2194.
101. Seela, F.; Sirivolu, V. R., DNA Containing Side Chains with Terminal Triple Bonds: Base-Pair Stability and Functionalization of Alkynylated Pyrimidines and 7-Deazapurines. *Chem. Biodivers.* **2006,** *3* (5), 509-514.
102. Seela, F.; Sirivolu, V. R.; Chittepu, P., Modification of DNA with Octadiynyl Side Chains: Synthesis, Base Pairing, and Formation of Fluorescent Coumarin Dye Conjugates of Four Nucleobases by the Alkyne−Azide "Click" Reaction. *Bioconjug. Chem.* **2008,** *19* (1), 211-224.
103. El-Sagheer, A. H.; Brown, T., Click Nucleic Acid Ligation: Applications in Biology and Nanotechnology. *Acc. Chem. Res.* **2012,** *45* (8), 1258-1267.
104. Kumar, R.; El-Sagheer, A.; Tumpane, J.; Lincoln, P.; Wilhelmsson, L. M.; Brown, T., Template-Directed Oligonucleotide Strand Ligation, Covalent Intramolecular DNA Circularization and Catenation Using Click Chemistry. *J. Am. Chem. Soc.* **2007,** *129* (21), 6859-6864.
105. El-Sagheer, A. H.; Brown, T., Synthesis and Polymerase Chain Reaction Amplification of DNA Strands Containing an Unnatural Triazole Linkage. *J. Am. Chem. Soc.* **2009,** *131* (11), 3958-3964.
106. Kočalka, P.; El-Sagheer, A. H.; Brown, T., Rapid and Efficient DNA Strand Cross-Linking by Click Chemistry. *ChemBioChem* **2008,** *9* (8), 1280-1285.
107. Lauria, T.; Slator, C.; McKee, V.; Müller, M.; Stazzoni, S.; Crisp, A. L.; Carell, T.; Kellett, A., A Click Chemistry Approach to Developing Molecularly Targeted DNA Scissors. *Chem. Eur. J.* **2020,** *26* (70), 16782-16792.
108. Zuin Fantoni, N.; McGorman, B.; Molphy, Z.; Singleton, D.; Walsh, S.; El-Sagheer, A. H.; McKee, V.; Brown, T.; Kellett, A., Development of

Gene-Targeted Polypyridyl Triplex-Forming Oligonucleotide Hybrids. *ChemBioChem* **2020,** *21* (24), 3563-3574.

109. Urankar, D.; Košmrlj, J., Preparation of diazenecarboxamide–carboplatin conjugates by click chemistry. *Inorg. Chim. Acta.* **2010,** *363* (14), 3817-3822.
110. Kitteringham, E.; Wu, D.; Cheung, S.; Twamley, B.; O'Shea, D. F.; Griffith, D. M., Development of a novel carboplatin like cytoplasmic trackable near infrared fluorophore conjugate via strain-promoted azide alkyne cycloaddition. *J. Inorg. Biochem.* **2018,** *182*, 150-157.
111. Hostetter, A. A.; Osborn, M. F.; Derose, V. J., RNA-Pt Adducts Following Cisplatin Treatment of Saccharomyces cerevisiae. *ACS Chem. Biol.* **2012,** *7* (1), 218-225.
112. White, J. D.; Osborn, M. F.; Moghaddam, A. D.; Guzman, L. E.; Haley, M. M.; DeRose, V. J., Picazoplatin, an Azide-Containing Platinum(II) Derivative for Target Analysis by Click Chemistry. *J. Am. Chem. Soc.* **2013,** *135* (32), 11680-11683.
113. Osborn, M. F.; White, J. D.; Haley, M. M.; DeRose, V. J., Platinum-RNA Modifications Following Drug Treatment in S. cerevisiae Identified by Click Chemistry and Enzymatic Mapping. *ACS Chem. Biol.* **2014,** *9* (10), 2404-2411.
114. Wirth, R.; White, J. D.; Moghaddam, A. D.; Ginzburg, A. L.; Zakharov, L. N.; Haley, M. M.; DeRose, V. J., Azide vs Alkyne Functionalization in Pt(II) Complexes for Post-treatment Click Modification: Solid-State Structure, Fluorescent Labeling, and Cellular Fate. *J. Am. Chem. Soc.* **2015,** *137* (48), 15169-15175.
115. Chen, L.; Tang, L.; Xiang, H.; Jin, L.; Li, Q.; Dong, Y.; Wang, W.; Zhang, G., Advances in genome editing technology and its promising application in evolutionary and ecological studies. *GigaScience* **2014,** *3* (1), 24.
116. Moore, J. K.; Haber, J. E., Cell cycle and genetic requirements of two pathways of nonhomologous end-joining repair of double-strand breaks in Saccharomyces cerevisiae. *Mol. Cell. Biol.* **1996,** *16* (5), 2164-2173.
117. Espejel, S.; Franco, S.; Rodríguez-Perales, S.; Bouffler, S. D.; Cigudosa, J. C.; Blasco, M. A., Mammalian Ku86 mediates chromosomal fusions and

apoptosis caused by critically short telomeres. *EMBO J.* **2002,** *21* (9), 2207-2219.

118. Li, X.; Heyer, W.-D., Homologous recombination in DNA repair and DNA damage tolerance. *Cell Res.* **2008,** *18* (1), 99-113.
119. Thurtle-Schmidt, D. M.; Lo, T.-W., Molecular biology at the cutting edge: A review on CRISPR/CAS9 gene editing for undergraduates. *Biochem. Mol. Biol. Edu.* **2018,** *46* (2), 195-205.
120. Capecchi, M. R., Altering the Genome by Homologous Recombination. *Science* **1989,** *244* (4910), 1288-1292.
121. Kim, Y. G.; Cha, J.; Chandrasegaran, S., Hybrid restriction enzymes: zinc finger fusions to Fok I cleavage domain. *Proc. Natl. Acad. Sci.* **1996,** *93* (3), 1156-1160.
122. Kim, Y.-G.; Shi, Y.; Berg, J. M.; Chandrasegaran, S., Site-specific cleavage of DNA–RNA hybrids by zinc finger/FokI cleavage domain fusions. *Gene* **1997,** *203* (1), 43-49.
123. Joung, J. K.; Sander, J. D., TALENs: a widely applicable technology for targeted genome editing. *Nat. Rev. Mol. Cell Biol.* **2013,** *14* (1), 49-55.
124. Garneau, J. E.; Dupuis, M.-È.; Villion, M.; Romero, D. A.; Barrangou, R.; Boyaval, P.; Fremaux, C.; Horvath, P.; Magadán, A. H.; Moineau, S., The CRISPR/Cas bacterial immune system cleaves bacteriophage and plasmid DNA. *Nature* **2010,** *468* (7320), 67-71.
125. Ran, F. A.; Hsu, P. D.; Wright, J.; Agarwala, V.; Scott, D. A.; Zhang, F., Genome engineering using the CRISPR-Cas9 system. *Nat. Protoc.* **2013,** *8* (11), 2281-2308.
126. Lino, C. A.; Harper, J. C.; Carney, J. P.; Timlin, J. A., Delivering CRISPR: a review of the challenges and approaches. *Drug Delivery* **2018,** *25* (1), 1234-1257.
127. Dean, N. M.; Bennett, C. F., Antisense oligonucleotide-based therapeutics for cancer. *Oncogene* **2003,** *22* (56), 9087-9096.
128. Zamecnik, P. C.; Stephenson, M. L., Inhibition of Rous sarcoma virus replication and cell transformation by a specific oligodeoxynucleotide. *Proc. Natl. Acad. Sci.* **1978,** *75* (1), 280-284.
129. Crooke, S. T.; Baker, B. F.; Crooke, R. M.; Liang, X.-H., Antisense technology: an overview and prospectus. *Nat. Rev. Drug Discov.* **2021**.

130. Wan, W. B.; Seth, P. P., The Medicinal Chemistry of Therapeutic Oligonucleotides. *J. Med. Chem.* **2016,** *59* (21), 9645-9667.
131. Bennett, C. F., Therapeutic Antisense Oligonucleotides Are Coming of Age. *Annu. Rev. Med.* **2019,** *70* (1), 307-321.
132. Freier, S.; Altmann, K.-H., The ups and downs of nucleic acid duplex stability: structure-stability studies on chemically-modified DNA:RNA duplexes. *nucleic Acids Res.* **1997,** *25* (22), 4429-4443.
133. Hong, D.; Kurzrock, R.; Kim, Y.; Woessner, R.; Younes, A.; Nemunaitis, J.; Fowler, N.; Zhou, T.; Schmidt, J.; Jo, M.; Lee, S. J.; Yamashita, M.; Hughes, S. G.; Fayad, L.; Piha-Paul, S.; Nadella, M. V. P.; Mohseni, M.; Lawson, D.; Reimer, C.; Blakey, D. C.; Xiao, X.; Hsu, J.; Revenko, A.; Monia, B. P.; Macleod, A. R., AZD9150, a next-generation antisense oligonucleotide inhibitor of STAT3 with early evidence of clinical activity in lymphoma and lung cancer. *Sci. Transl Med.* **2015,** *7* (314).
134. Raal, F. J.; Santos, R. D.; Blom, D. J.; Marais, A. D.; Charng, M.-J.; Cromwell, W. C.; Lachmann, R. H.; Gaudet, D.; Tan, J. L.; Chasan-Taber, S.; Tribble, D. L.; Flaim, J. D.; Crooke, S. T., Mipomersen, an apolipoprotein B synthesis inhibitor, for lowering of LDL cholesterol concentrations in patients with homozygous familial hypercholesterolaemia: a randomised, double-blind, placebo-controlled trial. *Lancet* **2010,** *375* (9719), 998-1006.
135. Crooke, S. T., Antisense therapeutics. *Biotechnol. Genet. Eng. Rev.* **1998,** *15*, 121-57.
136. Iversen, P. L., Phosphorodiamidate morpholino oligomers: favorable properties for sequence-specific gene inactivation. *Curr. Opin. Mol. Ther.* **2001,** *3* (3), 235-8.
137. Crooke, S. T.; Vickers, T. A.; Liang, X.-H., Phosphorothioate modified oligonucleotide–protein interactions. *Nucleic Acids Res.* **2020,** *48* (10), 5235-5253.
138. Gebert, L. F. R.; Rebhan, M. A. E.; Crivelli, S. E. M.; Denzler, R.; Stoffel, M.; Hall, J., Miravirsen (SPC3649) can inhibit the biogenesis of miR-122. *Nucleic Acids Res.* **2014,** *42* (1), 609-621.

139. Popplewell, L. J.; Trollet, C.; Dickson, G.; Graham, I. R., Design of Phosphorodiamidate Morpholino Oligomers (PMOs) for the Induction of Exon Skipping of the Human DMD Gene. *Mol. Ther.* **2009,** *17* (3), 554-561.
140. Cirak, S.; Arechavala-Gomeza, V.; Guglieri, M.; Feng, L.; Torelli, S.; Anthony, K.; Abbs, S.; Garralda, M. E.; Bourke, J.; Wells, D. J.; Dickson, G.; Wood, M. J.; Wilton, S. D.; Straub, V.; Kole, R.; Shrewsbury, S. B.; Sewry, C.; Morgan, J. E.; Bushby, K.; Muntoni, F., Exon skipping and dystrophin restoration in patients with Duchenne muscular dystrophy after systemic phosphorodiamidate morpholino oligomer treatment: an open-label, phase 2, dose-escalation study. *Lancet* **2011,** *378* (9791), 595-605.
141. Rüger, J.; Ioannou, S.; Castanotto, D.; Stein, C. A., Oligonucleotides to the (Gene) Rescue: FDA Approvals 2017–2019. *Trends Pharmacol. Sci.* **2020,** *41* (1), 27-41.
142. Fox, K. R.; Brown, T.; Rusling, D. A., *DNA Recognition by Parallel Triplex Formation*. 2018.
143. Faria, M.; Giovannangeli, C., Triplex-forming molecules: from concepts to applications. *J. Gene. Med.* **2001,** *3* (4), 299-310.
144. Giovannangeli, C.; Rougee, M.; Garestier, T.; Thuong, N. T.; Helene, C., Triple-helix formation by oligonucleotides containing the three bases thymine, cytosine, and guanine. *Proc. Natl. Acad. Sci.* **1992,** *89* (18), 8631-8635.
145. Leitner, D.; Schröder, W.; Weisz, K., Influence of Sequence-Dependent Cytosine Protonation and Methylation on DNA Triplex Stability†. *Biochemistry* **2000,** *39* (19), 5886-5892.
146. Bijapur, J.; Bergqvist, S.; Brown, T.; Keppler, M. D.; Fox, K. R., 5-(1-propargylamino)-2'-deoxyuridine (UP): A novel thymidine analogue for generating DNA triplexes with increased stability. *Nucleic Acids Res.* **1999,** *27* (8), 1802-1809.
147. Dagle, J., Positively charged oligonucleotides overcome potassium-mediated inhibition of triplex DNA formation. *Nucleic Acids Res.* **1996,** *24* (11), 2143-2149.
148. Hari, Y.; Ijitsu, S.; Akabane-Nakata, M.; Yoshida, T.; Obika, S., Kinetic study of the binding of triplex-forming oligonucleotides containing partial

cationic modifications to double-stranded DNA. *Bioorg. Med. Chem. Lett.* **2014,** *24* (14), 3046-9.

149. Grant, K. B.; Dervan, P. B., Sequence-Specific Alkylation and Cleavage of DNA Mediated by Purine Motif Triple Helix Formation. *Biochemistry* **1996,** *35* (38), 12313-12319.
150. Kutyavin, I. V.; Gamper, H. B.; Gall, A. A.; Meyer, R. B., Efficient, specific interstrand cross-linking of double-stranded DNA by a chlorambucil-modified, triplex-forming oligonucleotide. *J. Am. Chem. Soc.* **1993,** *115* (20), 9303-9304.
151. Oh, D., Triple helix-forming oligonucleotides target psoralen adducts to specific chromosomal sequences in human cells. *Nucleic Acids Res.* **1999,** *27* (24), 4734-4742.
152. Helene, C.; Montenay-Garestier, T.; Saison, T.; Takasugi, M.; Toulme, J. J.; Asseline, U.; Lancelot, G.; Maurizot, J. C.; Toulme, F.; Thuong, N. T., Oligodeoxynucleotides covalently linked to intercalating agents: a new class of gene regulatory substances. *Biochimie* **1985,** *67* (7-8), 777-83.
153. Vlassov, V. V.; Gorn, V. V.; Ivanova, E. M.; Kazakov, S. A.; Mamaev, S. V., Complementary addressed modification of oligonucleotide d(pGpGpCpGpGpA) with platinum derivative of oligonucleotide d(pTpCpCpGpCpCpTpTpT). *FEBS Lett.* **1983,** *162* (2), 286-289.
154. Hearst, J. E.; Isaacs, S. T.; Kanne, D.; Rapoport, H.; Straub, K., The reaction of the psoralens with deoxyribonucleic acid. *Q. Rev. Biophys* **1984,** *17* (1), 1-44.
155. Thompson, J. F.; Bachellerie, J.; Hall, K.; Hearst, J. E., Dependence of 4'-(Hydroxymethyl)-4,5',8-trimethylpsoralen Photoaddition on the Conformation of Ribonucleic Acid. *Biochemistry* **1982,** *21*, 1363-1368.
156. Thompson, J. F.; Hearst, J. E., Structure of E. coli 16S RNA elucidated by psoralen crosslinking. *Cell* **1983,** *32* (4), 1355-1365.
157. Zolan, M. E.; Smith, C. A.; Hanawalt, P. C., Formation and Repair of Furocoumarin Adducts in a-Deoxyribonucleic Acid and Bulk Deoxyribonucliec Acid of Monkey Cells. *Biochemistry* **1984,** *23*, 63-69.
158. Cimino, G. D.; Gamper, H. B.; Isaacs, S. T.; Hearst, J. E., Psoralens as Photoactive Probes of Nucleic Acid Structure and Function: Organic

Chemistry, Photochemistry, and Biochemistry. *Ann. Rev. Biochem.* **1985,** *54*, 1151-1193.

159. Lee, B. L.; Murakami, A.; Blake, K. R.; Lin, S.; Miller, P. S., Interaction of Psoralen-Derivatized Oligodeoxyribonucleoside Methylphosphonates with Single-Stranded DNA. *Biochemistry* **1988,** *27*, 3197-3203.
160. Pieles, U.; Englisch, U., Psoralen covalently linked to oligodeoxyribonucleotides: synthesis, sequence specific recognition of DNA and photo-cross-linking to pyrimidine residues of DNA. *Nucleic Acids Res* **1989,** *17* (1), 285-299.
161. Takasugi, M.; Guendouz, A.; Chassignol, M.; Decout, J. L.; Lhomme, J.; Thuong, N. T.; Helene, C., Sequence-specific photo-induced cross-linking of the two strands of double-helical DNA by a psoralen covalently linked to a triple helix-forming oligonucleotide. *Proc. Natl. Acad. Sci. U.S.A.* **1991,** *88* (13), 5602-5606.
162. Havre, P. A.; Gunther, E. J.; Gasparro, F. P.; Glazer, P. M., Targeted mutagenesis of DNA using triple helix-forming oligonucleotides linked to psoralen. *Proc. Natl. Acad. Sci. U.S.A.* **1993,** *90* (16), 7879-7883.
163. Kobori, A.; Takaya, K.; Higuchi, M.; Yamayoshi, A.; Murakami, A., Synthesis and Photoinduced Cross-linking Reactions of 4,5′,8-Trimethylpsoralen-incorporated Oligodeoxyribonucleotide. *Chem. Lett.* **2009,** *38* (3), 272-273.
164. Chu, B. C. F.; Orgel, L. E., Optimization of the efficiency of cross-linking Pt II oligonucleotide phosphorothioate complexes to complementary oligonucleotides. *Nucleic Acids Res.* **1990,** *18* (17), 5163-5171.
165. Gruff, E. S.; Orgel, L. E., An efficient, sequence-specific method for crosslinking complementary oligonucleotides using binuclear platinum complexes. *Nucleic Acids Res.* **1991,** *19* (24), 6849-6854.
166. Colombier, C.; Lippert, B.; Leng, M., Interstrand Cross-linking Reaction in Triplexes Containing a Monofunctional Transplatin-Adduct. *Nucleic Acids Res.* **1996,** *24* (22), 4519-4524.
167. Müller, J.; Drumm, M.; Boudvillain, M.; Leng, M.; Sletten, E.; Lippert, B., Parallel-stranded DNA with Hoogsteen base pairing stabilized by a trans-[Pt(NH3)2]2+ cross-link: characterization and conversion into a homodimer

and a triplex. *JBIC Journal of Biological Inorganic Chemistry* **2000,** *5* (5), 603-611.

168. Campbell, M. A.; Miller, P. S., Transplatin-Conjugated Triplex-Forming Oligonucleotides Form Adducts with Both Strands of DNA. *Bioconjug. Chem.* **2009,** *20* (12), 2222-2230.
169. Bernal-Méndez, E.; Sun, J.-S.; González-Vílchez, F.; Leng, M., Reactivity of transplatin-modified oligonucleotides in triple-helical DNA complexes. *New. J. Chem.* **1998,** *22* (12), 1479-1483.
170. Schmidt, K. S.; Filippov, D. V.; Meeuwenoord, N. J.; van der Marel, G. A.; van Boom, J. H.; Lippert, B.; Reedijk, J., Solid-Phase Synthesis of a Monofunctional *trans*-a2PtII Complex Tethered to a Single-Stranded Oligonucleotide. *Angew. Chem. Int. Ed.* **2000,** *39* (2), 375-377.
171. Schmidt, K. S.; Boudvillain, M.; Schwartz, A.; van der Marel, G. A.; van Boom, J. H.; Reedijk, J.; Lippert, B., Monofunctionally *trans*-Diammine Platinum(II)-Modified peptide Nucleic Acid Oligomers: A New Generation of Potential Antisense Drugs. *Chem. Eur. J.* **2002,** *8*, 5566-5570.
172. Kiessling, L. L.; Griffin, L. C.; Dervan, P. B., Flanking sequence effects within the pyrimidine triple-helix motif characterized by affinity cleaving. *Biochemistry* **1992,** *31* (10), 2829-34.
173. Campbell, M. A.; Mason, T. M.; Miller, P. S., Interactions of platinum(II)-derivatized triplex-forming oligonucleotides with DNA. *Can. J. Chem.* **2007,** *85* (4), 241-248.
174. Manchanda, R.; Dunham, S. U.; Lippard, S. J., Automated Solid-Phase Synthesis of Site-Specifically Platinated Oligodeoxyribonucleotides. *J. Am. Chem. Soc.* **1996,** *118* (21), 5144-5145.
175. Cech, D.; Schliepe, J.; Berghoff, U.; Lippert, B., Automated Solid Phase Synthesis of Platinated Oligonucleotides via Nucleoside Phosphonates. *Angew. Chem. Int. Ed.* **1996,** *35* (6), 646-648.
176. Sharma, S. K.; McLaughlin, L. W., Cross-Linking of a DNA Conjugate Tethering a cis-Bifunctional Platinated Complex to a Target DNA Duplex. *J. Am. Chem. Soc.* **2002,** *124*, 9658-9659.
177. Sharma, S. K.; McLaughlin, L. W., Triplex mediated delivery of a platinum complex to a specific DNA target site. *J. Inorg. Biochem.* **2004,** *98* (10), 1570-7.

178. Graham, M. K.; Miller, P. S., Inhibition of transcription by platinated triplex-forming oligonucleotides. *J. Biol. Inorg. Chem.* **2012,** *17* (8), 1197-1208.
179. Graham, M. K.; Brown, T. R.; Miller, P. S., Targeting the Human Androgen Receptor Gene with Platinated Triplex-Forming Oligonucleotides. *Biochemistry* **2015,** *54* (13), 2270-2282.
180. Campbell, M. A.; Miller, P. S., Cross-linking to an interrupted polypurine sequence with a platinum-modified triplex-forming oligonucleotide. *J. Biol. Inorg. Chem.* **2009,** *14* (6), 873-881.
181. Chu, B. C. F.; Orgel, L. E., Inhibition of DNA synthesis by cross-linking the template to platinum-thiol derivatives of complementary oligodeoxynucleotides. *Nucleic Acids Research* **1989,** *17* (12), 4783-4798.
182. Kampf, G.; Lüth, M. S.; Kapinos, L. E.; Müller, J.; Holy, A.; Lippert, B.; Sigel, H., Formation of Ternary Complexes by Coordination of (Diethylenetriamine)-Platinum(II) to N1 or N7 of the Adenine Moiety of the Antiviral NucleotideAnalogue 9-[2-(Phosphonomethoxy)ethyl]adenine (PMEA):Comparison of the Acid - Base and Metal-Ion-Binding Properties of PMEA,(Dien)Pt(PMEA-N1), and (Dien)Pt(PMEA-N7). *Chem. Eur. J.* **2001,** *7* (9), 1899-1908.

Chapter II

Project Rationale

II. 1. Rationale

Cisplatin and derivatives display efficient anticancer activity through their ability to bind with DNA. Binding primarily with the N7 nitrogen of purine bases, *cis*-Pt(II) agents can interact in suitable ratios with nucleic acid targets. However, the binding is indiscriminate and non-sequence specific with off-target toxicity being the greatest hindrance to the application of platinum anticancer therapeutics. Triplex-forming oligonucleotides (TFO) have long been considered exceptional tools in antisense applications for targeting specific nucleic acid (NA) sequences and so the application of therapeutic oligonucleotides to discretely deliver a platinum agent to an intended target was envisioned. Our group has previously shown that TFO sequences modified through nucleic acid click chemistry with both caging polypyridyl[1] and phenanthrene-like ligands[2] demonstrate effective affinity for and oxidative cleaving of target genes of interest. The application of redox chemistry mediated oxidative damage was further extended to bifunctional 'clip-phen' TFO-AMN systems which further proved the applicability of TFO vectors as suitable guides for targeted AMN constructs.[3]

Early work by Lippert and co-workers showed the delivery of a platinum complex to a precise target was possible using this approach.[4] As such, a large amount of modern research has focused on the conjugation of platinum materials with ONs by traditional chemical means. The majority of platinum-ON hybrids consist of a *trans*-Pt(II) derivative produced by a labelling reaction between the Pt(II) complex and the oligo prior to the targeting of DNA. As a result there are few examples of *cis* analogues being combined with ONs in this fashion. To overcome this problem, another avenue was to synthesise an ON with a tethered chelator which can then be complexed with a suitable *cis*-platinum agent. Although the tethering of a Pt(II) chelator has allowed for post-complexation, this method is only feasible if the ON is designed not to include the other common purines which greatly constrains the scope of possible TFO targeting sequences.[5]

From a design perspective, there are notable obstacles that restrain the full potential of existing Pt-TFO hybrid motifs including: i.) parallel TFOs

containing guanine nucleobases provide lower stability due to Hoogsteen base mismatching and *trans*-Pt(II)-TFOs are limited by their need to incorporate a G base to which the *trans*-platinum(II) reagent is couped; ii.) *cis*-platinum(II) complexes fail to form interstrand crosslinks in appreciable quantities and thus the initial TFO adduct formation is ineffective as a pathway for hybrid generation; iii.) the rigid design of trans-Pt-TFOs means that hybrids have a very narrow target window dependent on purine location; iv.) post-synthetic procedures involving tethered chelators can alleviate rigidity problems but are still not compatible with ONs that contain purine nucleobases; and v.) solid-phase synthetic methods have, to date, been unsuccessful in generating functional Pt(II)-TFOs.

To address these limitations, the aim of this thesis was to synthesise a family of azide-bearing mononuclear platinum(II) complexes capable of undergoing click chemistry to an alkyne modified TFOs. This family of complexes consisted of Pt-N_3-Cis (*cis*-[Pt(2-azidopropane-1,3-diamine)Cl_2]), Pt-N_3-Carbo (*cis*-[Pt(2-azidopropane-1,3-diamine)(CBDCA)]), Pt-N_3-Oxali (*cis*-[Pt(2-azidopropane-1,3-diamine)(Oxalate)]), Pt-N_3-Phenazide ([Pt(5-azido-1,10-phenanthroline)Cl_2]) and Pt-N_3-DPPZ ([Pt(11-azidodipyrido[3,2,*a*:2',3'-*c*]phenazine)Cl_2]). The first three complexes are based on traditional agents cisplatin, carboplatin and oxaliplatin which are known for their proficient crosslinking ability, while the latter contain known phenanthrene (Phen and DPPZ) DNA intercalating ligands. Firstly, DNA interaction profiles of the complexes was investigated prior to preliminary cytotoxicity assays performed against a selection of triple-negative breast cancer cell lines. This work involved direct comparisons to the activity of cisplatin in order to gauge their *in vitro* activity. Subsequently, a selection of TFOs bearing octadinyl and BCN modified nucleobases were prepared through solid-phase phosphoramidite synthesis. These TFOs were then conjugated to the azide-bearing platinum(II) complexes through click chemistry strategies in order to generate a new class of *cis*-Pt(II)-TFO hybrids. Conjugation was achieved using nucleic acid click chemistry and proved to be an efficient method to prepare a library of Pt(II)-TFO hybrids with minimal purification needed. In order to identify the most suitable potential crosslinking position(s), both 5' and internal modifications were generated.

TFOs were designed to target the green fluorescent protein (GFP) gene by forming parallel triplexes with the Hoogsteen face of target sequences. By exploiting the unique base-triplet recognition properties of TFOs and the crosslinking ability of the 'clicked' *cis*-Pt(II) groups, this strategy sought to target purine-rich genetic elements of the GFP gene (**Figure II-1**). UV thermal melting and PAGE analysis were performed to identify triplex formation and crosslinking by the hybrids to their intended targets. Crosslink reversal by sodium cyanide treatment was investigated alongside the use of denaturing PAGE experiments with fluorescently labelled target sequences to identify the sequence specific crosslinking of the GFP targets.

Chapter I outlined the existing state of the art in current platinum drug therapy followed by recent research efforts in modulating the advantages and disadvantages of their use. The advent of nucleic acid click chemistry and its use in recent gene knockout applications arising from the conjugation of oxidatively active metal complexes to TFOs. Furthermore, the background of platinum(II)-DNA hybrids has been described and how research has led to the development of targeted platinum(II)-TFO constructs.

Chapter III describes the design, methodology and synthetic routes behind the development of the azide-modified *cis*-platinum(II) complexes.

Chapter IV describes the development of the alkyne-modified TFO, thiazole orange (TO)-TFOs and alkyne-amine (AA)-TOTFO sequences. Furthermore, subsequent click chemistry experiments to afford the platinum(II)-TFO hybrids are discussed.

Chapter V describes the work performed in identifying the DNA binding properties of the azide-modified *cis*-platinum(II) complexes. The chapter then progresses to an investigation of the triplex formation and crosslinking ability of the Pt(II)-TFO hybrids and their viability as antigene agents.

Chapter VI describes the incorporation of a unique bifunctional nucleobase containing the AA modification. This modification was investigated

for its ability to incorporate TO proximate to a Pt(II). The strategy was developed to enhance site-specific interactions whereby the affinity of complex-DNA interactions are augmented under the guidance of a neighbouring TO intercalator.

Chapter VII describes the conjugation of phenanthrene-type scaffolds with BCN-modified TFOs to generate Cu(II)-AMN-TFO hybrids. These hybrids were investigated for their ability to coordinate copper(II) ions and form stable triplex systems. Finally, the sequence-specific gene-targeting and oxidative DNA damage was investigated.

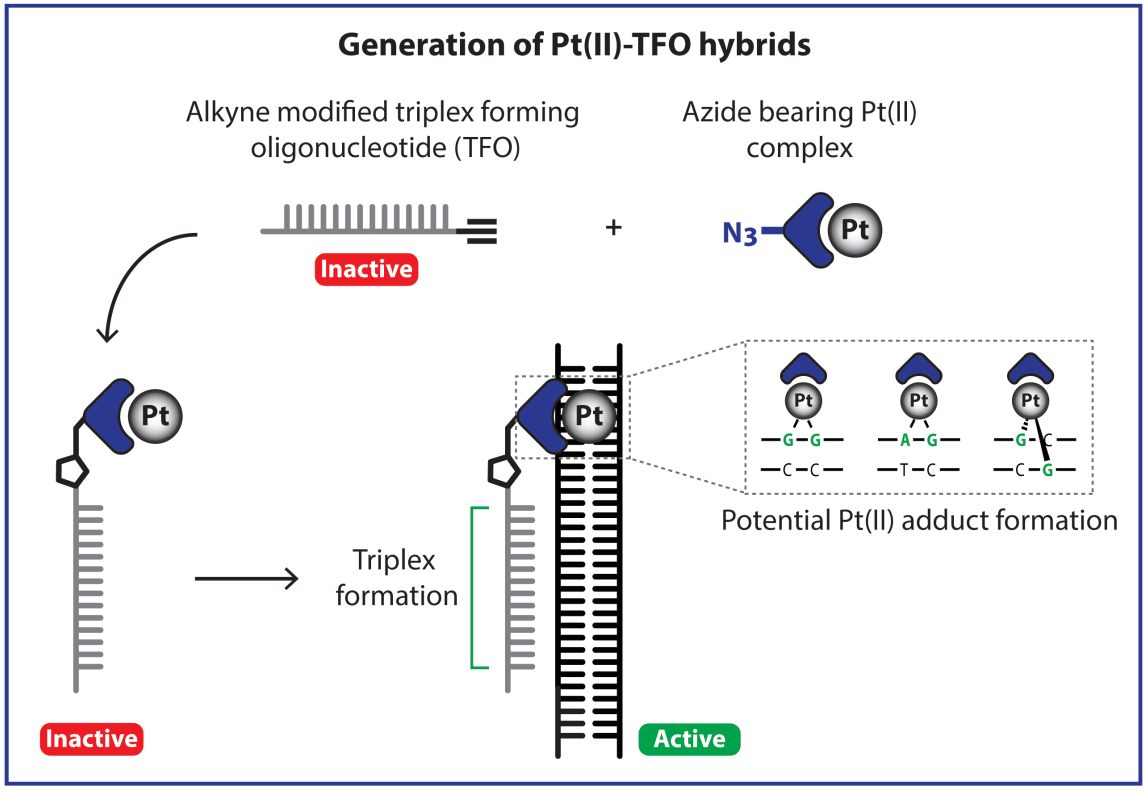

Figure II-1. Project Overview – Generation of Platinum(II)-TFO Hybrid Biomaterials with specific triplex formation and crosslinking to intended duplex targets.

II. 2. References

1. Zuin Fantoni, N.; McGorman, B.; Molphy, Z.; Singleton, D.; Walsh, S.; El-Sagheer, A. H.; McKee, V.; Brown, T.; Kellett, A., Development of Gene-Targeted Polypyridyl Triplex-Forming Oligonucleotide Hybrids. *ChemBioChem* **2020,** *21* (24), 3563-3574.
2. Lauria, T.; Slator, C.; McKee, V.; Müller, M.; Stazzoni, S.; Crisp, A. L.; Carell, T.; Kellett, A., A Click Chemistry Approach to Developing Molecularly Targeted DNA Scissors. *Chem. Eur. J.* **2020,** *26* (70), 16782-16792.
3. Panattoni, A.; El-Sagheer, A. H.; Brown, T.; Kellett, A.; Hocek, M., Oxidative DNA Cleavage with Clip-Phenanthroline Triplex-Forming Oligonucleotide Hybrids. *ChemBioChem* **2020,** *21* (7), 991-1000.
4. Dieter-Wurm, I.; Sabat, M.; Lippert, B., Model for a platinated DNA triplex: Watson-Crick and metal-modified Hoogsteen pairing. *J. Am. Chem. Soc.* **1992,** *114* (1), 357-359.
5. Sharma, S. K.; McLaughlin, L. W., Cross-Linking of a DNA Conjugate Tethering a cis-Bifunctional Platinated Complex to a Target DNA Duplex. *J. Am. Chem. Soc.* **2002,** *124*, 9658-9659.

Chapter III

Design and Synthesis of Azide-Modified *cis*-Platinum(II) complexes

The work presented in this chapter has been submitted as part of a patent application: Patent application filed for “A cis-platinum(II)-oligomer hybrid”. Application number GB2113541.3. (Date filed: 22/09/2021)

III. 1. Abstract

The design and development of azide-functionalised *cis*-platinum(II) complexes *via* azide-modified phenanthroline and diaminopropane ligand scaffolds is reported. Complexation of the ligand scaffolds with platinum(II) reagents afforded the *cis*-platinum(II) products for future use in nucleic acid click chemistry applications. The synthesis of [Pt(5-azido-1,10-phenanthroline)Cl_2] (Pt-N_3-Phen) and Pt(11-azidodipyrido[3,2,*a*:2',3'-*c*]phenazine)Cl_2] (Pt-N_3-DPPZ) represent the first known reported series of azide-functionalised *cis*-Pt(II) phenanthroline-like complexes that possess nucleic acid click chemistry applications. Furthermore, the synthesis of *cis*-[Pt(2-azidopropane-1,3-diamine)oxalate] is for the first time reported and represents the first known example of an azide-modified *cis*-platinum(II) complex based on the oxaliplatin structure.

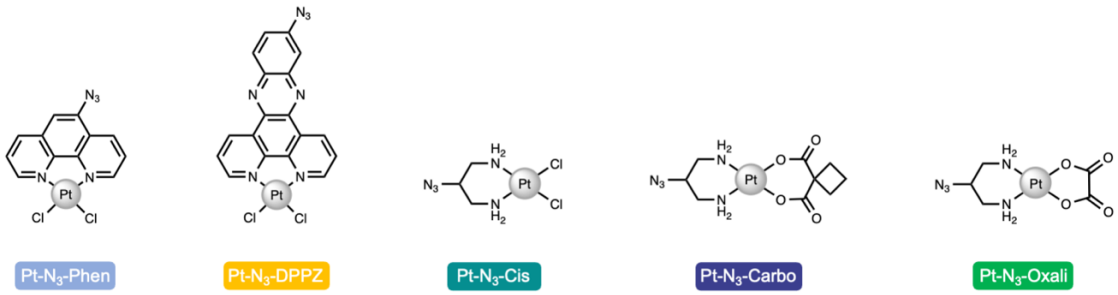

Figure III-1. Azide-functionalised *cis*-platinum(II) complexes designed and developed in Chapter III.

III. 2. Organic and Inorganic Synthesis

III. 2. 1. Chapter Aims

- To synthesise and characterise a series of azide-functionalised ligand scaffolds for coordinating with platinum(II) and copper(II) metal ions.

- To design and synthesise a series of azide-functionalised *cis*-platinum(II) derivatised complexes for future use in platinum(II)-TFO hybrid construction.

III. 2. 2. Rationale

The primary aim of this synthetic work was to develop a series of *cis*-platinum(II) complexes with azide-modified handles that can be combined with nucleic acids vectors to afford Pt(II)-TFO constructs in a facile manner. Phenanthroline scaffolds bearing an azide handle, generated through the 1,10-phenanthroline starting material and proceeding through an epoxide (N_3-Phen) and phendione (N_3-DPPZ) derivative, were developed. The extended aromatic systems were identified as potential stabilising aids once triplex formation and stability was to be investigated. N_3-DAP was selected due to its recent reporting in the generation of azide-modified platinum(II) constructs and the relative ease that it undergoes click chemistry without interfering steric effects.

III. 2. 3. General Information and Methods

All commercially available reagents, chemicals and HPLC grade solvents were sourced from Sigma-Aldrich Ireland Ltd. or TCI Chemicals and, unless otherwise stated, were used without any further purification. All other solvents were used as supplied. **Important Note:** Organic azides are hazardous materials and are known to be heat- and shock-sensitive. Explosive decomposition can potentially occur with very little energy input. To ensure safe manipulation and non-explosiveness for organic azides, the rule is that the number of nitrogen atoms must not exceed that of carbon, where $(N_C + N_O)/N_N \geq 3$. (N = number of atoms).[1] **12** is a potentially hazardous material, however all relevant safety precautions were undertaken while working with the material.

Nuclear Magnetic Resonance Spectroscopy (NMR spectroscopy)

^{1}H-NMR (600 MHz), ^{13}C-NMR (151 MHz) and ^{195}Pt-NMR (129 MHz) spectra were obtained on a Bruker AC 600 MHz NMR Spectrometer. All experiments were performed at room temperature in either $CDCl_3$, DMSO-d_6 or DMF-d_7 where indicated. Chemical shift signals (δ) are given in parts per million (ppm) using the residual proton signals in the indicated solvents as internal standards. Coupling constants (*J*) are quoted in hertz (Hz) and proton multiplicities were assigned using the analysis software. Signal peak multiplicities are assigned with the following: singlet (s), doublet (d), doublet of doublets (dd), doublet of doublet of doublets (ddd), triplet (t), doublet of triplets (dt), quartet (q), quintuplet (qn) and multiplet (m). Experimental spectra were analysed using MestReNova software (v. 14.2.0-26256, Mestrelab Research S.L.)

Fourier-Transform Infrared Spectroscopy

FT-IR experimental spectra were obtained from neat solids on a Perkin Elmer Spectrum Two Spectrometer. Spectra were recorded from 400-4000 cm^{-1} and analysed for signal peak determination using PerkinElmer Spectrum (v. 10.5.3, PerkinElmer, Inc) and graphed and formatted with GraphPad Prism (v. 8.4.0, GraphPad Software, LLC).

Melting Point Analysis

Experimental melting points were obtained on a Stanford Research Systems MPA100 Optimelt apparatus. KIMBLE KIMAX melting point capillary tubes were used for sample loading.

Elemental Analysis

Elemental analysis (C, H, N) were analysed using a Flash EA Elemental Analyser with integrated PTFE Multiseparation Column and Thermal Conductivity Detector (TCD). Resultant data was analysed using Eager 300 software. Analysis was performed by Mr. Walter Walsh in the Department of Chemistry, Science Building, Maynooth University, Ireland.

Mass Spectrometry (MS)

Accurate mass spectrometry analyses were conducted using a MaXis HD quadrupole electrospray time-of-flight (ESI-QTOF) mass spectrometer (Bruker Daltonik GmbH, Bremen, Germany), using a glass syringe (Hamilton) and syringe pump (KD Scientific, Model 781100) for infusions at a flow rate of 3 µL/min. Analyses were performed in ESI positive mode with the capillary voltage was set to 4500 V, nebulizing gas at 0.6 bar, drying gas at 4 L/min at 180°C in each case. The TOF scan range was from 100 – 1000 mass-to-charge ratio (*m/z*). The MS instrument was calibrated using an infusion of sodium formate calibrant solution. The calibrant solution consisted of 3 parts of 1 M NaOH to 97 parts of 50:50 water:isopropanol with 2% formic acid. Data processing was performed using the Compass Data Analysis software v. 4.3 (Bruker Daltonik GmbH, Bremen, Germany).

III. 2. 4. Synthesis

1,10-phenanthroline-5,6-epoxide (1)

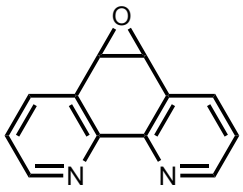

1

1,10-phenanthroline monohydrate (1.982 g, 10.00 mmol) and tetrabutylammonium bisulfate (TBAHS) (1.70 g, 5.00 mmol) were dissolved in 50 ml $CHCl_3$. To this solution was added 50 ml commercial bleach and the entire mixture was stirred vigourously for 24 h. The organic layer was separated and washed with excess H_2O (4 x 50 ml portions), dried over $MgSO_4$ and evaporated to obtain an off-white pure product. Yield: 1.69 g, 82%.

^{1}H NMR (600 MHz, $CDCl_3$) δ 8.88 (dd, *J* = 4.7, 1.7 Hz, 2H, N=CH), 7.97 (dd, *J* = 7.6, 1.7 Hz, 2H, CH), 7.37 (dd, *J* = 7.6, 4.7 Hz, 2H, CH), 4.59 (s, 2H, O-CH). ^{13}C NMR (151 MHz, Chloroform-*d*) δ 151.96 (C=N), 150.68 (CH=N), 139.30 (C=C), 130.18 (CH), 124.81 (CH), 56.36 (CH, Epoxide). IR (ATR, cm^{-1}): 3005, 1579, 1559, 1431, 1215, 1011, 881, 797, 749, 614. Melting point (mp): 182 °C.

5-azido-1,10-phenanthroline (2)

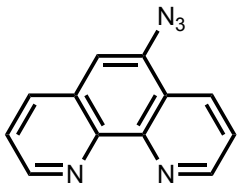

2

5-azido-1,10-phenanthroline was prepared in accordance with a method reported by Lauria *et al*.[2] 1,10-phenanthroline-5,6-epoxide (0.300 g, 1.54 mmol, 1 eq.) was dissolved in a MeOH:H_2O mixture (4:1, 15 ml) with stirring. To this solution was added NaN_3 (0.350 g, 5.39 mmol, 3.5 eq.) and the mixture was heated at 110 °C for approx. 18 h. MeOH was removed *in vacuo* prior to the addition of approx. 20 ml of deionised water to the reaction and cooled at 5 °C overnight. The solution was vacuum filtered to yield a yellow solid and washed with 3 x 5 ml deionised water and Et_2O before drying over vacuum in darkness to afford the pure product. Yield: 0.320 g, 94%.

^{1}H NMR (600 MHz, DMSO-d_6) δ 9.16 (dd, *J* = 4.3, 1.7 Hz, 1H, CH), 9.03 (dd, *J* = 4.3, 1.7 Hz, 1H, CH), 8.49 (ddd, *J* = 17.0, 8.2, 1.8 Hz, 2H, N=CH), 7.94 (s, 1H, CH), 7.82 (dd, *J* = 8.3, 4.2 Hz, 1H, CH), 7.77 (dd, *J* = 8.0, 4.3 Hz, 1H, CH). ^{13}C NMR (151 MHz, DMSO-d_6) δ 150.82, 149.31, 145.86, 143.40, 135.09, 134.38, 130.82, 128.24, 123.78, 123.41, 122.65, 113.48, 40.06. IR (ATR, cm^{-1}): 3013, 2110 (N_3), 1610, 1486, 1417, 1386, 1315, 1251, 819, 736, 621.

[Pt(5-azido-1,10-phenanthroline)Cl_2] (3)

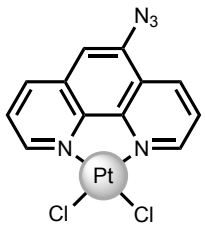

3

Into a solution of K_2PtCl_4 (0.100 g, 0.241 mmol, 1 eq.) in deionised water (10 ml), a solution of 5-azido-1,10-phenanthroline (0.053 g, 0.241 mmol, 1 eq.) in 6 ml EtOH was added dropwise. The entire mixture was stirred at 50 °C for approx. 18 h in darkness. The solution was cooled gradually to r.t. and vacuum filtered to yield a green precipitate. The precipitate was washed with 3 x 3 ml portions of ice-cold EtOH and Et_2O. The product was dried over vacuum in darkness to afford a green solid. Yield: 0.089 g, 76 %.

^{1}H NMR (600 MHz, DMSO-d_6) δ 9.66 (d, J = 5.4 Hz, 1H, N=CH), 9.50 (d, J = 5.4 Hz, 1H, N=CH), 8.90 (d, J = 8.3 Hz, 2H, CH), 8.26 (s, 1H, CH), 8.10 (ddd, J = 19.7, 8.3, 5.4 Hz, 2H, CH). ^{195}Pt NMR (129 MHz, DMSO-d_6) δ -2316. IR (ATR, cm^{-1}): 3064, 2112 (N_3), 1427, 1275, 800, 715.

1,10-Phenanthroline-5,6-dione (4)

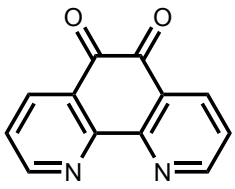

4

1,10-phenanthroline-5,6-dione was prepared in accordance with the literature method previously reported by Molphy et *al*.[3] 1,10-Phenanthroline (4.00 g, 22.19 mmol) and potassium bromide (4.00 g, 33.60 mmol) were thoroughly mixed and slowly added to an ice-cold mixture of H_2SO_4 (40ml) and HNO_3 (20 ml). The solution was refluxed for 4 h at 160 °C, and cooled to r.t. before pouring onto approx. 400 ml crushed ice and neutralised with a 5M NaOH solution (80 g in 400 ml) to pH 4-5. This solution was extracted with $CHCl_3$ (4 x 250 ml portions) and organic fractions combined and dried over $MgSO_4$. Solvent was removed *in vacuo*, with the product being obtained as a yellow solid. The product was further purified by recrystallisation from HPLC grade methanol. Yield: 3.38 g, 72.5 %.

^{1}H NMR (600 MHz, $CDCl_3$) δ 9.06 (dd, *J* = 4.7, 1.8 Hz, 2H, N=CH), 8.45 (dd, *J* = 7.8, 1.8 Hz, 2H, CH), 7.55 (dd, *J* = 7.8, 4.7 Hz, 2H, CH). ^{13}C NMR (151 MHz, $CDCl_3$) δ 178.67, 156.43, 152.91, 137.33, 128.09, 125.66. IR (ATR, cm^{-1}): 1684, 1562, 1460, 1413, 1285, 1206, 806, 735. Melting point (mp): 259-262 °C.

11-nitrodipyrido[3,2-*a*:2',3'-*c*] phenazine (5)

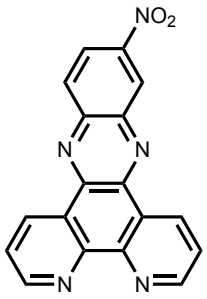

5

11-nitrodipyrido[3,2-*a*:2',3'-*c*] phenazine was prepared according to the literature method reported by Jones et *al*.,[4] with slight modifications. 4-nitro-*o*-phenylenediamine (1.37 g, 8.93 mmol, 1.5 eq.) was dissolved in 60 ml EtOAc by reflux at 90°C. Upon dissolution, a warm EtOAc/MeOH (30 ml:10 ml) solution of phendione (1.25 g, 5.95 mmol, 1 eq.) was added. The mixture was refluxed at 90 °C for 2 h and a yellow/orange precipitate was observed forming during reflux. Solution cooled to r.t. before further cooling at 0 °C. The precipitate was collected by vacuum filtration and washed with Et_2O (3 x 5 ml portions) to obtain a pure pale yellow product. Yield: 1.69 g, 87%.

^{1}H NMR (600 MHz, $CDCl_3$) δ 9.52 (ddd, *J* = 14.3, 8.0, 1.8 Hz, 2H, CH), 9.28 (ddd, *J* = 9.2, 4.4, 1.8 Hz, 2H, CH), 9.18 (d, *J* = 2.5 Hz, 1H, CH), 8.63 (dd, *J* = 9.2, 2.5 Hz, 1H), 8.42 (d, *J* = 9.2 Hz, 1H, CH), 7.79 (dt, *J* = 8.1, 4.1 Hz, 2H, CH). ^{13}C NMR (151 MHz, $CDCl_3$) δ 152.65, 152.47, 148.02, 147.67, 147.12, 143.13, 142.43, 142.01, 139.78, 133.25, 132.99, 130.18, 125.75, 125.70, 124.96, 123.50, 123.42, 122.66. IR (ATR, cm^{-1}): 3098, 1618, 1577, 1520, 1481, 1406, 1342, 1142, 1063, 812, 737, 723, 618. Melting point (mp): 327-335 °C.

11-aminodipyrido[3,2,*a*:2',3'-*c*]phenazine (6)

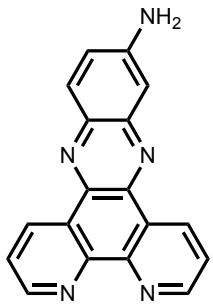

6

11-aminodipyrido[3,2-*a*:2',3'-*c*] phenazine was synthesised according to the literature method described by Lin et *al*.[5] 11-nitrodipyrido[3,2-*a*:2',3'-*c*] phenazine (0.300 g, 0.916 mmol, 1 eq.) was dissolved in 150 ml EtOH. To this solution was added hydrazine hydrate (10 ml) and 10 % Pd/C (0.030 g) and the mixture was refluxed at 90°C for 4 h. The hot solution was filtered through celite and solvent reduced *in vacuo* to approx. 5 ml. The solution was cooled at 5 °C prior to filtration. Precipitate was washed with ice-cold ethanol (3 x 3 ml) and dried to afford product as red powder. Yield: 0.217 g, 80%.

^{1}H NMR (600 MHz, DMSO-d_6): 9.49 (dd, *J* = 8.1, 1.8 Hz, 1H, CH), 9.41 (dd, *J* = 8.1, 1.8 Hz, 1H, CH), 9.17 (dd, *J* = 4.3, 1.8 Hz, 1H, CH), 9.11 (dd, *J* = 4.3, 1.8 Hz, 1H, CH), 8.05 (d, *J* = 9.1 Hz, 1H, CH), 7.88 (ddd, *J* = 12.6, 8.1, 4.3 Hz, 2H, CH), 7.49 (dd, *J* = 9.1, 2.4 Hz, 1H, CH), 7.15 (d, *J* = 2.4 Hz, 1H, CH), 6.55 (s, 2H, NH_2). ^{13}C NMR (151 MHz, DMSO-d_6): 151.78, 151.69, 150.69, 147.59, 146.40, 144.82, 140.18, 137.17, 135.34, 132.82, 131.77, 130.03, 127.57, 127.09, 125.21, 124.21, 124.09, 103.13. IR (ATR, cm^{-1}): 3273, 3161, 1623, 1495, 1408, 1358, 1273, 817, 740, 654, 564. Anal. Calcd for $C_{18}H_{11}N_5$: C, 72.72; H, 3.73; N, 23.56. Found: C, 72.42; H, 3.68; N, 23.80. Melting point (mp): 365-370 °C.

11-azidodipyrido[3,2,*a*:2',3'-*c*]phenazine (7)

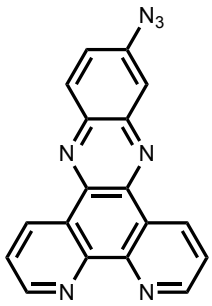

7

11-azidodipyrido[3,2-*a*:2',3'-*c*] phenazine was prepared according to the literature method previously reported by Lauria *et al*.[2] 11-aminodipyrido[3,2,*a*:2',3'-*c*]phenazine (0.100 g, 0.34 mmol, 1 eq.) was dissolved in a 6M HCl solution (10 ml) with stirring and heated at 95 °C for 30 mins. The solution was cooled to 0 °C and an aqueous solution of $NaNO_2$ (0.047 g, 0.68 mmol, 2 eq.) in 5 ml of deionised water was added dropwise and stirred for 60 mins at 0 °C. A solution of NaN_3 (0.133 g, 2.04 mmol, 6 eq.) in 10 ml deionised water was prepared and cooled to 0 °C. The diazonium mixture was slowly added dropw4ise to the NaN_3 mixture at 0 °C and the entire mixture was stirred for 2 h at 0 °C. 10 ml of a 6M NaOH solution was added and the mixture stirred overnight. Precipitate was vacuum filtered and washed with 3 x 5 ml portions of deionised water and Et_2O before drying over vacuum in darkness. Yield: 0.079 g, 72%.

^{1}H NMR (600 MHz, $CDCl_3$: 9.56 (ddd, *J* = 9.8, 8.1, 1.8 Hz, 2H, CH), 9.27 (ddd, *J* = 9.3, 4.4, 1.8 Hz, 2H, CH), 8.30 (dd, *J* = 9.0, 0.5 Hz, 1H, CH), 7.93 (dd, *J* = 2.5, 0.5 Hz, 1H, CH), 7.78 (dt, *J* = 8.1, 4.6 Hz, 2H, CH), 7.54 (dd, *J* = 9.0, 2.5 Hz, 1H, CH). ^{13}C NMR (151 MHz, DMSO-d_6): 152.80, 152.53, 148.56, 148.21, 142.98, 142.85, 141.75, 140.46, 140.43, 133.82, 133.55, 131.32, 127.47, 127.30, 124.41, 124.20, 124.17, 116.30. IR (ATR, cm^{-1}): 2111 (N_3), 1615, 1573, 1489, 1406, 1360, 1262, 1207, 1108, 1062, 819, 738.

[Pt(11-azidodipyrido[3,2,*a*:2',3'-*c*]phenazine)Cl_2] (8)

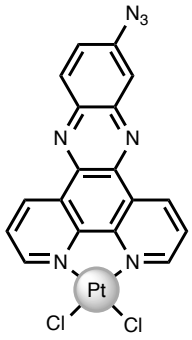

8

The reaction protocol followed was similar to (**3**) with minor alterations. Into a solution of *cis*-Pt(DMSO)$_2$Cl$_2$ (0.065 g, 0.155 mmol, 1 eq.) in 7 ml DMSO was added 11-azidodipyrido[3,2,*a*:2',3'-*c*]phenazine (0.050 g, 0.155 mmol, 1 eq.) dissolved in 10 ml DMSO. The entire mixture was stirred at 50 °C for 24 h in darkness. The solution was cooled to r.t. and vacuum filtered to yield a green-brown precipitate. The product was washed sequentially with 5 x 5 ml potions of H_2O, EtOH and Et_2O prior to drying over vacuum in darkness. Yield: 0.065 g, 38%.

^{1}H NMR, ^{13}C NMR and ^{195}Pt NMR spectroscopy proved difficult due to solubility issues of the final complex. IR (ATR, cm^{-1}): 3052, 2108 (N_3), 1601, 1493, 1413, 1279, 1078, 819, 720.

Di-*tert*-boc-2-hydroxy-1,3-diaminopropane (9)

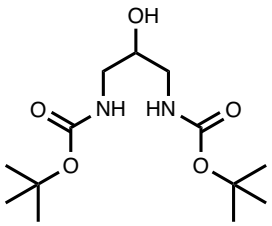

9

Di-tert-boc-2-hydroxy-1,3-diaminepropane was prepared, with adaptation, from the literature method previously reported by Kane *et* al.[6] To a solution of 1,3-diamino-2-propanol (2.000 g, 22.19 mmol, 1 eq.) and triethylamine (4.49 g, 44.38 mmol, 2 eq.) in a 1:1 THF/H_2O mix (80 ml) stirring at 0 °C was added di-*tert*-butyl dicarbonate (12.11 g, 55.48 mmol, 2.5 eq.) in THF (40 ml). The resulting solution was stirred at r.t. overnight (approx. 18 h). THF was removed *in vacuo* and approx. 40 ml of distilled H_2O was added to the solution before extraction with EtOAc (3 x 50 ml). Organic layer was dried over $MgSO_4$ and solvent removed *in vacuo* to yield the desired product as a clear pale oil, which subsequently solidified to white solid. Yield: 5.617 g, 87%.

^{1}H NMR (600 MHz, $CDCl_3$): 5.14 (s, 2H, NH), 3.78 – 3.73 (m, 1H, CH), 3.31 – 3.14 (m, 4H, $(CH_2)_2$), 1.46 (s, 18H, Boc). ^{13}C NMR (151 MHz, $CDCl_3$): 157.27 (C, carbonyl), 79.81 (C, Boc), 71.14 (CH), 43.57 (CH_2), 28.36 (CH_3, Boc). IR (ATR, cm^{-1}): 3490, 3369, 3313, 2983, 2933, 1681, 1659, 1524, 1274, 1253, 1164, 1084, 970, 865, 581. mp 91-93 °C. Anal. Calcd for $C_{13}H_{26}N_2O_5$: C, 53.78; H, 9.03; N, 9.65. Found: C, 53.88; H, 9.19; N, 9.59.

Di-*tert*-boc-2-methanesulfonyl-1,3-diaminopropane (10)

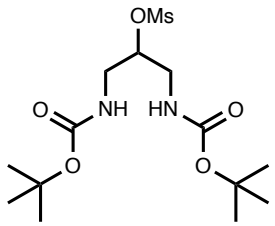

10

Di-*tert*-boc-2-methanesulfonyl-1,3-diaminopropane was synthesised, with slight adaptation, according to a procedure reported by Abd Karim *et al*.[7] Di-*tert*-boc-2-hydroxy-1,3-diaminopropane (5.000 g, 17.22 mmol, 1 eq.) and triethylamine (5.23 g, 51.66 mmol, 3 eq.) were dissolved in 80 ml anhydrous DCM and purged with argon for 20 mins. Methanesulfonyl chloride (3.95 g, 34.44 mmol, 2 eq.) was dissolved in approx. 8 ml anhydrous DCM and added dropwise to the degassed solution with stirring over 30 minutes at 0 °C. The mixture was allowed to gradually warm to r.t. and stirred overnight (approx. 18 h). 70 ml DI water was added to the mixture to react with excess MsCl and stirred for 3 h. Organic layer was separated and washed sequentially with 100 ml 10% $NaHCO_3$ and 100 ml brine (x2). Organic layer was dried over $MgSO_4$ and solvent removed *in vacuo* to afford a pale yellow/beige solid and recrystallised using hexane, to yield white solid. Yield: 4.755 g, 75%.

^{1}H NMR (600 MHz, $CDCl_3$): 5.18 (t, *J* = 6.6 Hz, 2H, NH), 4.66 (p, *J* = 5.2 Hz, 1H, CH), 3.49 (ddd, *J* = 14.8, 7.5, 4.5 Hz, 2H, CH_2), 3.30 (dt, *J* = 14.9, 5.8 Hz, 2H, CH_2), 3.09 (s, 3H, CH_3), 1.44 (s, 18H, Boc). ^{13}C NMR (151 MHz, $CDCl_3$): 156.47 (C, carbonyl), 80.19 (C, Boc), 79.20 (CH), 40.96 (CH_2), 38.31(CH_3, OMs), 28.46 (CH_3, Boc). IR (ATR, cm^{-1}): 3448, 3379, 2976, 2937, 1704, 1516, 1345, 1251, 1172, 1116, 1045, 950, 917, 800, 529, 460. mp 138-140 °C. Anal. Calcd for $C_{14}H_{28}N_2O_7S$: C, 45.64; H, 7.66; N, 7.60. Found: C, 45.44; H, 7.42; N, 7.31.

Di-*tert*-boc-2-azido-1,3-diaminopropane (11)

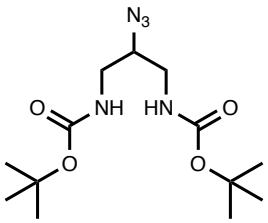

11

Di-*tert*-boc-2-azido-1,3-diaminopropane was synthesised, with slight adaptation, according to a procedure reported by Veerendhar *et al*.[8] To a solution of di-*tert*-boc-2-methanesulfonyl-1,3-diaminopropane (2.000 g, 5.43 mmol, 1 eq.) in 30 ml anhydrous DMF, NaN_3 (1.412 g, 21.72 mmol, 4 eq.) was added and the mixture stirred at 80 °C for 18 h. The mixture was allowed to cool to ambient temperature, poured into approx. 50 ml DI water and further cooled at to 0 °C prior to filtering to obtain white solid product. Yield: 1.38 g, 81 %.

^{1}H NMR (600 MHz, $CDCl_3$): 5.06 (s, 2H, NH), 3.64 (s, 1H, CH), 3.43 – 3.31 (m, 2H, CH_2), 3.18 – 3.07 (m, 2H, CH_2), 1.44 (s, 18H, Boc). ^{13}C NMR (151 MHz, $CDCl_3$): 156.20 (C, carbonyl), 79.91 (C, Boc), 60.92 (CH), 40.80 (CH_2), 28.35 (CH_3, Boc). IR (ATR, cm^{-1}): 3340, 2966, 2936, 2110 (N_3), 1680, 1517, 1363, 1267, 1239, 1153, 963, 862, 635.

2-azidopropane-1,3-diamine dihydrochloride (12)

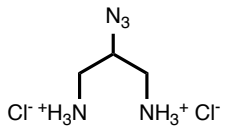

12

2-azidopropane-1,3-diamine dihydrochloride was synthesised according to the literature method previously reported by Urankar *et al*.[9] To a solution of di-*tert*-boc-2-azido-1,3-diaminopropane (0.400 g, 1.27 mmol, 1 eq.) in EtOAc (3 ml) was added aqueous 6 M HCl (approx. 1.5 ml) dropwise with stirring. The reaction mixture was stirred at 0 °C for 30 mins followed by stirring for approximately 18 h at r.t. before cooling at 5 °C overnight. The resulting white precipitate was filtered and washed several times with EtOAc to afford the product as a white crystalline solid. Yield: 0.221 g, 93 %.

^{1}H NMR (600 MHz, DMSO-d_6): 8.38 (s, 6H, $(NH_3)_2$), 4.23 (tt, J = 8.6, 4.0 Hz, 1H, CH), 3.15 (dd, J = 13.5, 4.0 Hz, 2H, CH_2), 2.90 (dd, J = 13.4, 8.9 Hz, 2H, CH_2). ^{13}C-NMR (151 MHz, DMSO-d_6): 57.70 (CH), 40.49 (CH_2). IR (ATR, cm^{-1}): 2946, 2851, 2127 (N_3), 1503, 1462, 1361, 1279, 1203, 1081, 957, 933, 606. mp 227-233 °C.

***cis*-[Pt(2-azidopropane-1,3-diamine)Cl_2] (13)**

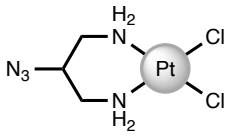

13

cis-[Pt(2-azidopropane-1,3-diamine)Cl_2] was prepared from an adjusted literature method previously reported by Urankar *et al*.[9] 1,8-Diazabicyclo[5.4.0]undec-7-ene (DBU) (0.081 g, 0.53 mmol, 2 eq.) was added to a solution of 2-azidopropane-1,3-diamine dihydrochloride (0.050 g, 0.265 mmol, 1 eq.) in 0.7 ml anhydrous DMF with stirring. To this solution was added *cis*-[Pt$(DMSO)_2Cl_2$] (0.112 g, 0.265 mmol, 1 eq.) and the solution was stirred at r.t. for 3 days. Approximately 2 ml DI H_2O was added and the mixture was cooled at 5 °C overnight. A grey precipitate was collected by filtration, and the product washed with DI H_2O (2 x 2 ml). Yield: 0.027 g, 27 %.

^{1}H NMR (600 MHz, DMF-d_7) δ 5.26-5.18 (d, J = 45.3 Hz, 4H, NH_2), 4.19 (m, 1H, CH), 2.93 (m, 2H, CH_2), 2.85 (ddq, J = 13.1, 6.7, 3.9 Hz, 2H, CH_2). ^{13}C NMR (151 MHz, DMF-d_7) δ 59.88 (CH), 46.54 (CH_2). ^{195}Pt NMR (129 MHz, DMF-d_7) δ -2272. IR (ATR, cm^{-1}): 3324, 3182, 3118, 2108 (N_3), 1586, 1258, 1172, 1027, 821. ESI-MS: m/z. 403.9 $[M+Na]^+$, 784.9 $[2M+Na]^+$. $C_3H_9Cl_2N_5{}^{195}Pt^+$ $[M+Na]^+$: 402.9781. Found: 403.9758 .

***cis*-[Pt(2-azidopropane-1,3-diamine)I_2] (14) (Intermediate)**

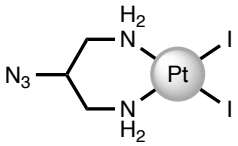

14

Reaction protocol was followed as previously reported by Urankar *et a*l.[9] with slight deviations. To a solution of K_2PtCl_4 (0.300 g, 0.723 mmol, 1 eq.) in approx. 8 ml DI H_2O was added KI (1.20 g, 7.23 mmol, 10 eq.) and the mixture was stirred for 2 h. A solution of 2-azidopropane-1,3-diamine dihydrochloride (0.0.136 g, 0.723 mmol, 1 eq.) in 3 ml aqueous NaOH (0.058 g, 1.45 mmol, 2 eq.) was then added dropwise to the stirring mixture. Subsequently, the entire mixture was then heated at 60 °C for 10 mins, cooled to 0 °C and filtered to obtain brown/ tan solid product. Sequential washes with DI H_2O, MeOH and Et_2O (5 x 5 ml) followed by drying over vacuum afforded *cis*-[Pt(2-azidopropane-1,3-diamine)I_2] as a brown solid. Yield: 0.352 g, 86% (from K_2PtCl_4).

***cis*-[Pt(2-azidopropane-1,3-diamine)(CBDCA)] (15)**

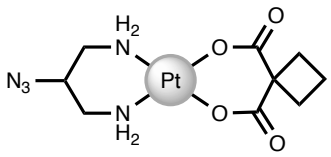

15

Cis-[Pt(2-azidopropane-1,3-diamine)(CBDCA)] was synthesised, with slight adaptation, according to the literature method previously reported by Urankar *et al*.[9] *Cis*-[Pt(2-azidopropane-1,3-diamine)I_2] (0.352 g, 0.624 mmol, 1 eq.) was suspended in approx. 30 ml DI H_2O and a 5 ml aqueous solution of $AgNO_3$ (0.212 g, 1.25 mmol, 2 eq.) was then added dropwise with stirring. The solution was stirred for 3 h before filtering through a 0.22 μm Millipore pad to remove AgI. To the filtrate was added 3 ml of an aqueous solution of cyclobutane-1,1-dicarboxylic acid (CBCDA) (0.090 g, 0.624 mmol, 1 eq.) and NaOH (0.050 g, 1.25 mmol, 2 eq.). The solution was stirred for approx. 18 h in darkness and filtered through a 0.22 μm Millipore pad prior to the removal of solvent to yield a crude grey residue. 5 ml DI H_2O was added to the residue and cooled at 5 °C before vacuum filtration, washed with 5x5 ml H_2O, MeOH and Et_2O and finally dried to obtain an off-white solid. Yield: 0.118 g, 36 % (from K_2PtCl_4).

^{1}H NMR (600 MHz, DMSO-d_6) δ 5.45 (s, 2H, NH_2), 5.28 (s, 2H, NH_2), 3.91 (s, 1H, CH), 2.65 (qn, 4H, $(CH_2)_2$), 2.53 (m, 2H, CH_2), 2.48 (m, 2H, CH_2), 1.64 (qn, 2H, CH_2). ^{13}C NMR (151 MHz, DMSO-d_6): 177.89 (C, carbonyl), 59.16 (CH, N_3), 56.06 (C, CBDCA), 45.86 (CH_2, N_3), 31.04 (CH_2, CBDCA), 30.71 (CH_2, CBDCA), 15.45 (CH_2, CBDCA). ^{195}Pt NMR (129 MHz, DMSO-d_6) δ -1942. IR (ATR, cm^{-1}): 3217, 3092, 2938, 2120 (N_3), 1622, 1576, 1342, 1268, 1106, 1024, 900, 768. ESI-MS: m/z. 453.1 $[M+H]^+$, 475.1 $[M+Na]^+$. ESI-MS calc. for $C_9H_{15}N_5O_4{}^{195}Pt^+$ $[M+H]^+$: 453.0850. Found: 453.0846.

***cis*-[Pt(2-azidopropane-1,3-diamine)(Oxalate)] (16)**

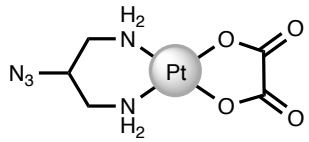

16

Reaction protocol was performed as reported in **(7)** with only minor changes. After the removal of AgI, an aqueous solution (4 ml) of sodium oxalate (0.188 g, 1.40 mmol, 1 eq.) was added to the retained filtrate and the entire solution was stirred for approx. 18 h in darkness. The solution was filtered through a 0.45 μm Millipore pad to obtain a grey solid. Yield: 0.405 g, 72% (from K_2PtCl_4).

^{1}H NMR (600 MHz, DMSO-d_6) δ 5.76 (dt, J = 10.5, 4.5 Hz, 2H, NH_2), 5.46 (dt, J = 15.3, 5.1 Hz, 2H, NH_2), 3.99 (m, 1H, CH), 2.63-2.56 (m, 2H, CH_2), 2.55-2.51 (m, 2H, CH_2). ^{13}C NMR (151 MHz, DMSO-d_6): 166.57 (C, carbonyl), 58.89 (CH), 45.48 (CH_2). ^{195}Pt NMR (129 MHz, DMSO-d_6) δ -1968. IR (ATR, cm^{-1}): 3182, 3092, 2106 (N_3), 1654, 1388, 1248, 1212, 818. . ESI-MS: m/z. 399.0 $[M+H]^+$, 421.0 $[M+Na]^+$. ESI-MS calc. for $C_5H_9N_5O_4{}^{195}Pt^+$ $[M+H]^+$: 399.0380. Found: 399.0374.

III. 2. 5. Development of Synthetic Routes

Azide-functionalised *cis*-platinum(II) complexes were prepared using a family of three azide-modified ligands (**Figure III-2**, **A**) prior to their complexation with platinum to afford the final five *cis*-platinum(II) complexes (**Figure III-2**, **B**). Ligands **2** (N_3-Phen), **7** (N_3-DPPZ), and **12** (N_3-DAP) contain a single azide functional group and each ligand possess an N,N donor that can chelate a platinum(II) metal ion. The synthesis of **2** and **7** has recently been reported by the Kellett group[2] and were applied here for their chelating and intercalating properties. Additionally, van Wezel *et al*.[10] have demonstrated that similar phenanthroline derivatives such as phendione (**4)** and DPPZ are effective substrates for the chelation of platinum(II) metal ions and displayed good intercalative potential. The enhanced planarity and thus increased aromatic base stacking potential was also expected to enhance triplex stability. Another aspect that was considered with regards to future studies is the potential shielding that the steric bulk of the phenanthrene ligands can provide to the adducts that may form. Phenathriplatin, a novel platinum(II) agent developed by Lippard and co-workers,[11] harbours a bulky ligand that has demonstrated the ability to shield DNA lesions from repair. **12** is a ligand that has previously been demonstrated to undergo successful complexation with platinum(II) metal ions and retain the ability to conjugate using click chemistry with various substrates. To date, however, **12** has not yet been explored for platinum(II)-TFO hybrid applications. The ligands were reacted with various platinum(II) precursors to obtain the final azide-functionalised *cis*-platinum(II) complexes **3** (Pt-N_3-Phen), **8** (Pt-N_3-DPPZ), **13** (Pt-N_3-Cis), **15** (Pt-N_3-Carbo) and **16** (Pt-N_3-Oxali). The synthetic routes towards the generation of this series are displayed in **Scheme III-1**. The azide-functionalised complexes maintain their cisplatin-like structural properties.

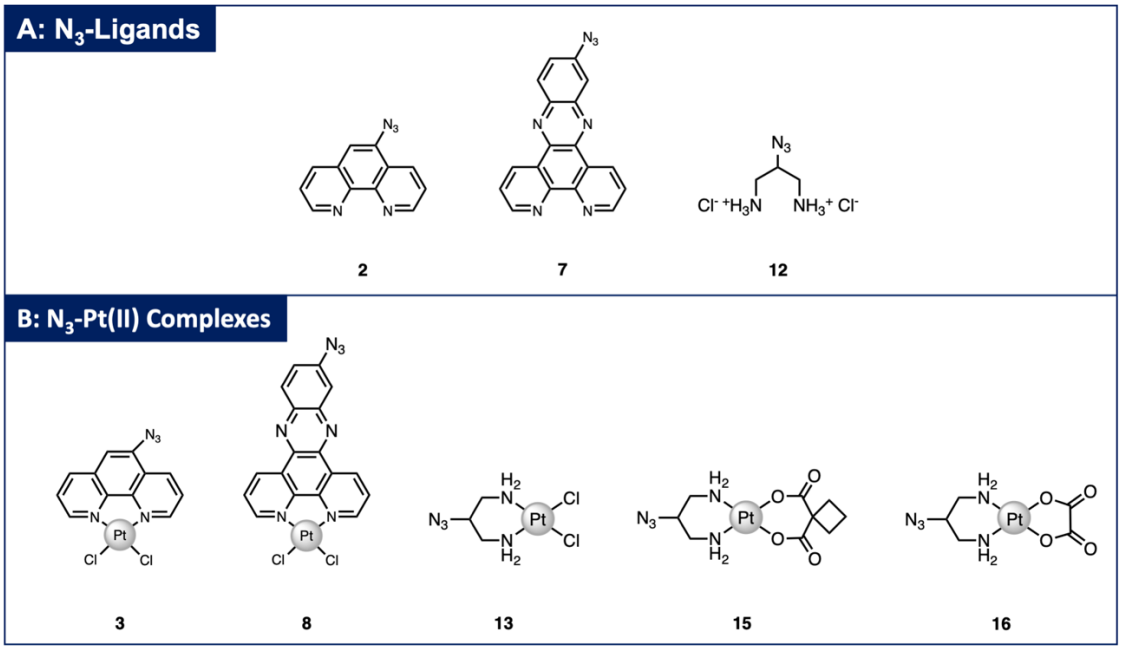

Figure III-2. A. Azide-modified N,N chelating ligands generated. **B.** *cis*-platinum(II) complexes with azide handles for future click chemistry applications.

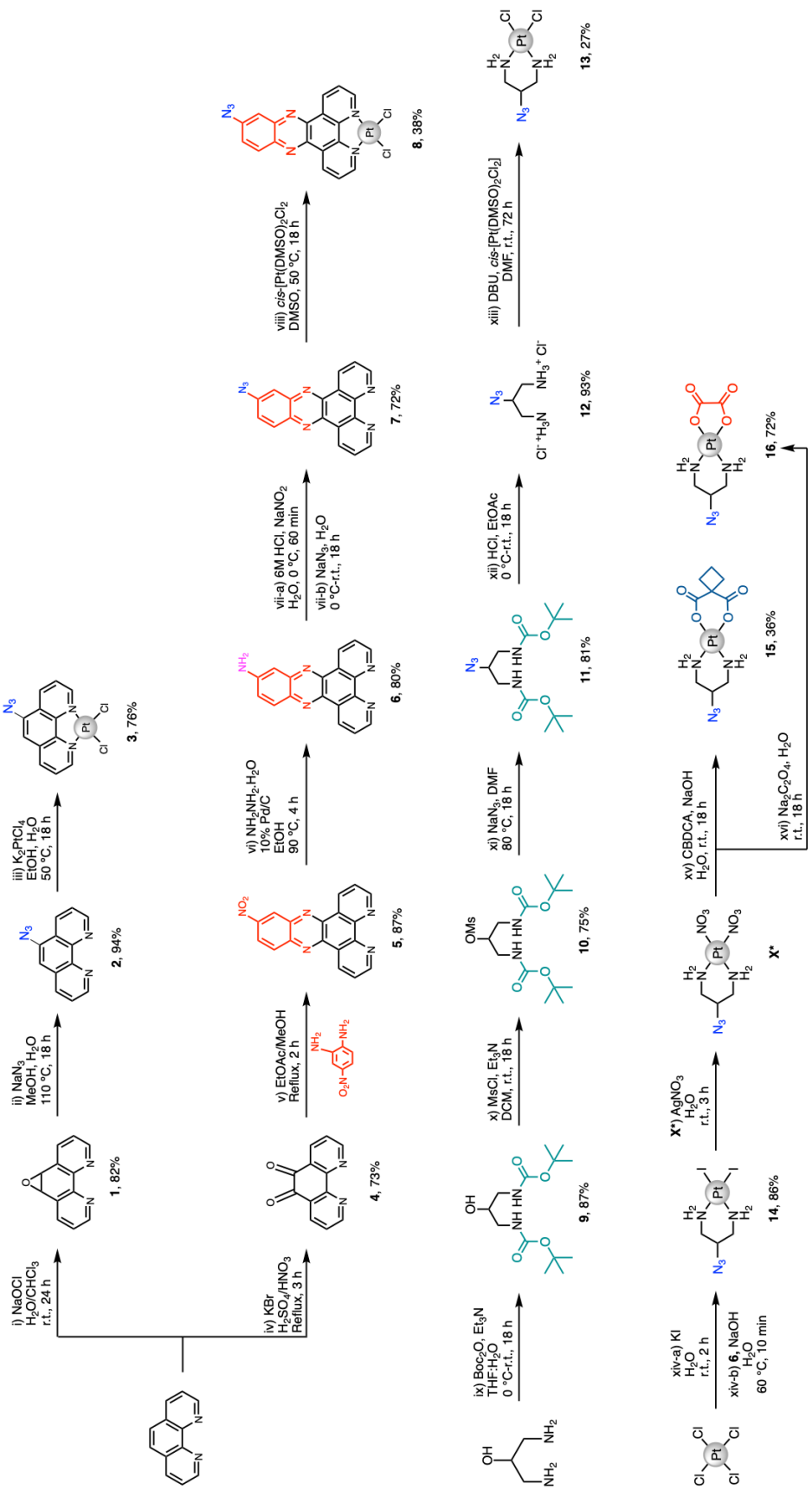

Scheme III-1. Synthetic routes for the azide-functionalised *cis*-platinum(II) complexes

[Pt(5-azido-1,10-phenanthroline)Cl_2] (Pt-N_3-Phen)

The synthesis of Pt-N_3-Phen (**4**) was performed in three steps from the starting material 1,10-phenanthroline (**Scheme III-2**). The procedure has previously been reported and refined by the Kellett group and proceeds through an epoxide intermediate.[2]

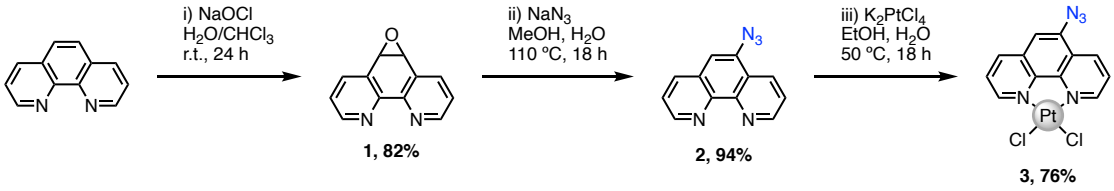

Scheme III-2. Synthetic routes to generate Pt-N_3-Phen (**3**).

The synthetic procedure to obtain **3** involves the epoxidation of commercially available 1,10-phenanthroline prior to nucleophilic substitution with sodium azide under reflux to acquire **2**. Subsequent complexation using potassium tetrachloroplatinate yields the desired product in high yields (76%). Initial attempts at nucleophilic substitution reactions using Br- and Cl- derivatised 1,10-phenanthrolines were unsuccessful – the carbo-halogen bonds of aryl halides are considered much stronger than alkyl halides thus are quite resistant to nucleophilic attack. In general, strong electron-withdrawing groups in *ortho* or *para* configurations can induce substitution however. As such the use of an epoxide intermediate was chosen to facilitate the reaction.

1,10-phenanthroline-5,6-epoxide (**1**, Epoxy-phen) was obtained by initial hypochloride-oxidation of 1,10-phenanthroline (1,10-phen) under phase transfer catalyst conditions in a biphasic solvent setup at room temperature. The pH of the reaction was carefully monitored throughout and maintained between pH 8-9 to ensure optimal oxidations conditions. Epoxidation reactions are commonly performed using bleaching agents such as peroxy acids like *meta*-Chloroperoxybenzoic acid (mCPBA) or sodium hypochlorite solutions alone or in the presence of metal catalysts. The reaction of epoxidation using peroxy acids can be seen below (**Scheme III-3**).

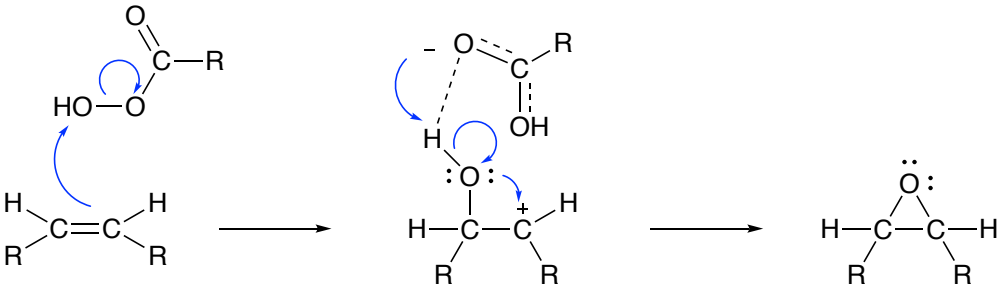

Scheme III-3. Reaction mechanism of alkene epoxidation by a peroxy acid reagent.

Another commonly used method involves the use of sodium hypochlorite in the presence of metal catalysts. Jacobsen *et al.*[12] have produced significant research into this methodology with considerable results – the Jacobsen-Katsuki epoxidation mechanism is attributed as such although it is not fully elucidated to date.[13] Epoxidation by sodium hypochlorite without the need for catalyst has been demonstrated before,[14, 15] and it is most likely that the reaction above follows a similar mechanism. The reaction was monitored by ^{1}H-NMR over the duration of the experiment. The middle six carbon ring of 1,10-phen displays a notable singlet signal at approx. 7.8 ppm for the two protons adjacent to the carbon-carbon double bond that undergoes epoxidation. The signal intensity reduces as the epoxy-phen product forms and thus complete elimination of the proton peak indicates full conversion of the starting material. A new singlet peak at 4.59 ppm (**Appendix A, Figure VIII-1**) represents the two protons adjacent to the epoxide moiety and is a key diagnostic signal in the monitoring of the reaction.

The epoxide moiety is a notably good leaving group and so is susceptible to nucleophilic attack. This is due to the increased ring strain present within the epoxide and makes the epoxide carbons strong electrophiles – reaction with nucleophiles is key to opening the ring and relieving the strain. Considering that the proposed leaving group is a hydroxyl and that sodium azide is itself a powerful nucleophile, the ring-opening will most likely proceed through a combined S_N1- S_N2 mechanism under acidic conditions. In the case of epoxide ring openings, the least substituted electrophilic carbon is attacked. Our group has previously shown that performing the reaction at increased temperatures leads to complete elimination of the diol sub-product through reformation of the

aromatic double bond and gives **2** as the sole isolated product (**Proposed Mechanism, Scheme III-4**).[2]

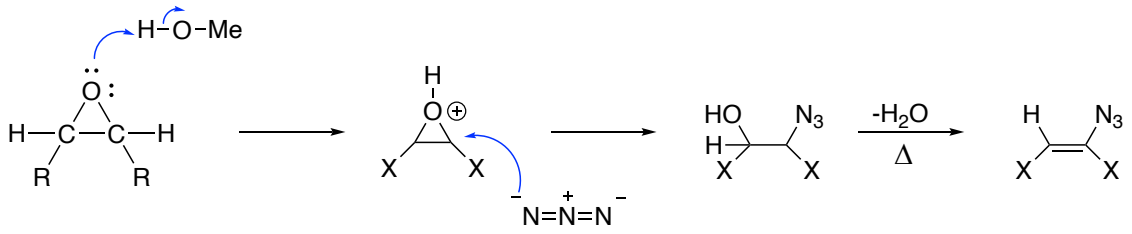

Scheme III-4. Proposed reaction mechanism for epoxide ring-opening through nucleophilic attack of sodium azide.

Product formation was detectable through ^{1}H-NMR in $CDCl_3$ through the diagnostic signal of the proton adjacent to the newly formed double bond of the central ring at 7.94 ppm and is relatively more intense in comparison (**Appendix A, Figure VIII-4**). No indication of diol by-product presence is observed. In addition, FT-IR spectroscopy was used to identify **3** through the distinct strong azide stretching frequency at 2110 cm^{-1} (**Appendix A, Figure VIII-6**). To obtain **3**, and the final product of this particular pathway, **2** was reacted with a solution of potassium tetrachloroplatinate at 50 °C in darkness. The product was observed as a green precipitate as the reaction proceeded prior to filtration and collection. Primary characterisation of the product was performed by ^{195}Pt NMR spectroscopy with a signal peak at -2316 ppm (**Appendix A, Figure VIII-8**). FT-IR characterisation determined the retention of the azide moiety after complexation with a strong azide band at 2112 cm^{-1} (**Appendix A, Figure VIII-9**) whilst ^{1}H-NMR (DMSO-d_6) displayed a downfield shift for all proton signals of the phenanthroline system (**Appendix A, Figure VIII-7**) in comparison to the uncoordinated precursor **2**.

Pt(11-azidodipyrido[3,2,*a*:2',3'-*c*]phenazine)Cl_2] (Pt-N_3-DPPZ)

1,10-phenanthroline was also used as the starting material for the synthesis of Pt-N_3-DPPZ (**8**). This synthetic route proceeds through the generation of 1,10-Phenanthroline-5,6-dione (**4**, Phendione) prior to a Schiff-base reaction with 4-nitro-*o*-phenylenediamine to generate 11-nitrodipyrido[3,2-*a*:2',3'-*c*] phenazine (**5**, NO_2-DPPZ). Further reduction of the NO_2 group yields the amino-derivative, 11-nitrodipyrido[3,2-*a*:2',3'-*c*] phenazine (**6**, NH_2-DPPZ). The protocol then uses

diazonium chemistry to obtain the azide-substituted derivative, 11-azidodipyrido[3,2-*a*:2',3'-*c*] phenazine (**7**, N_3-DPPZ) and final complexation using a *cis*-[Pt(DMSO)$_2$Cl$_2$] reagent produces the final platinum(II) product in medium yield, [Pt(11-azidodipyrido[3,2,*a*:2',3'-*c*]phenazine)Cl$_2$] (**8**, Pt-N_3-DPPZ). (**Scheme III-5**)

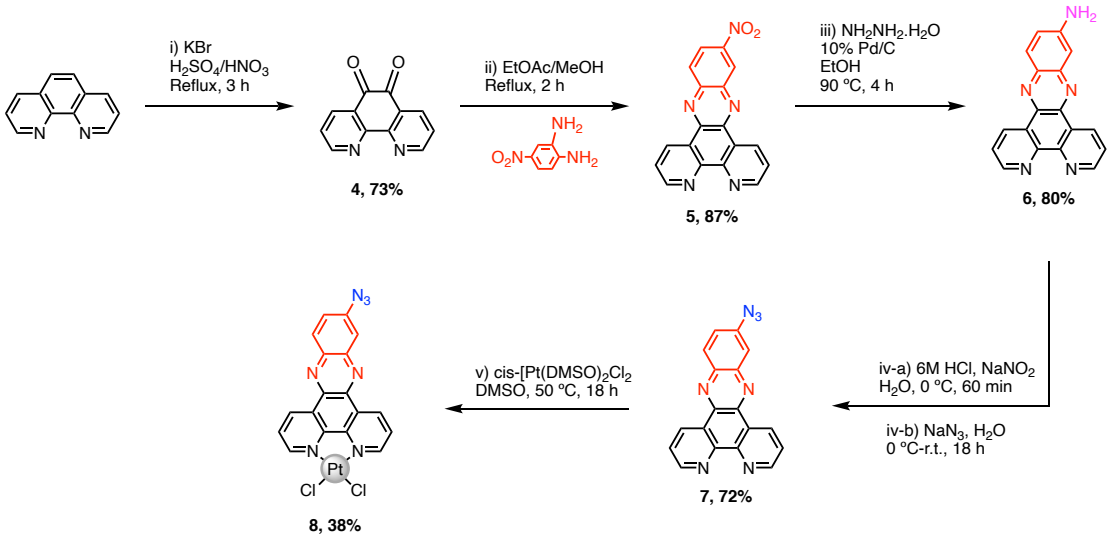

Scheme III-5. Synthetic routes for the generation of Pt-N_3-DPPZ (**8**).

Phendione (**4**) has previously been synthesised within our group[16] and is obtained through oxidative addition under harsh acidic conditions. A Schiff-base condensation reaction (**Scheme III-6**) under reflux with 4-nitro-*o*-phenylenediamine yields the NO_2-DPPZ derivative (**5**) as an off-brown solid.

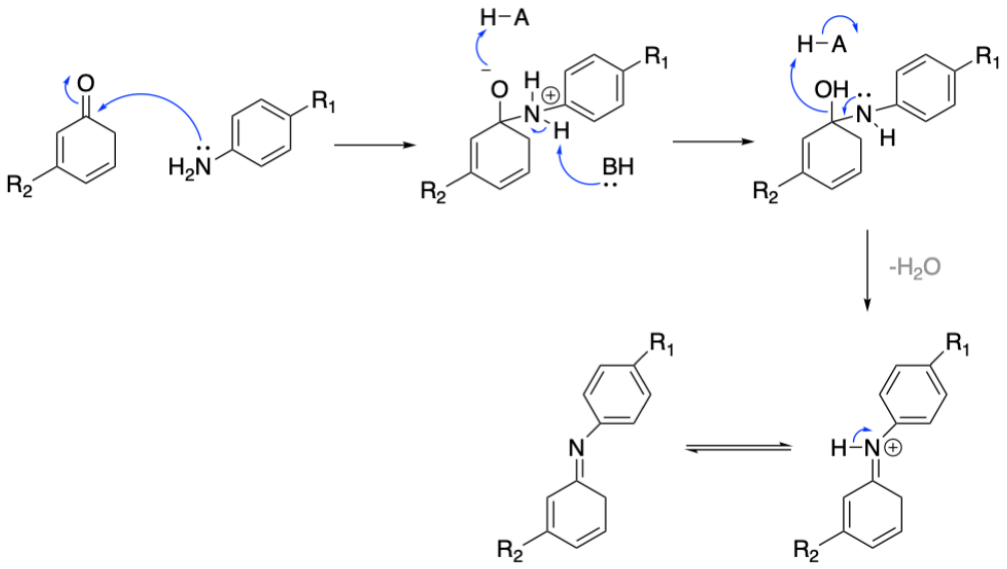

Scheme III-6. Reaction mechanism for a general Schiff base condensation.

Hydrazine hydrate ($NH_2NH_2.H_2O$) in conjuction with Pd/C catalyst at high temperature was used as the reducing agent to afford the amino derivative NH_2-DPPZ (**6**) from reduction of the NO_2 moiety (**Scheme III-7**). The conditions used are typical of a traditional catalytic hydrogenation. The proposed mechanism was suggested by Rozas et al.[17] in which the use of a base such as KOH is used, although the protocol followed allows for the use of EtOH as a weak base. The proposal is an example of a modified Wolff-Kishner reaction. The reaction was closely monitored by ^{1}H-NMR (DMSO-d_6) with the distinct signal of the two amino protons at 6.55 ppm increasing in intensity as the product forms.

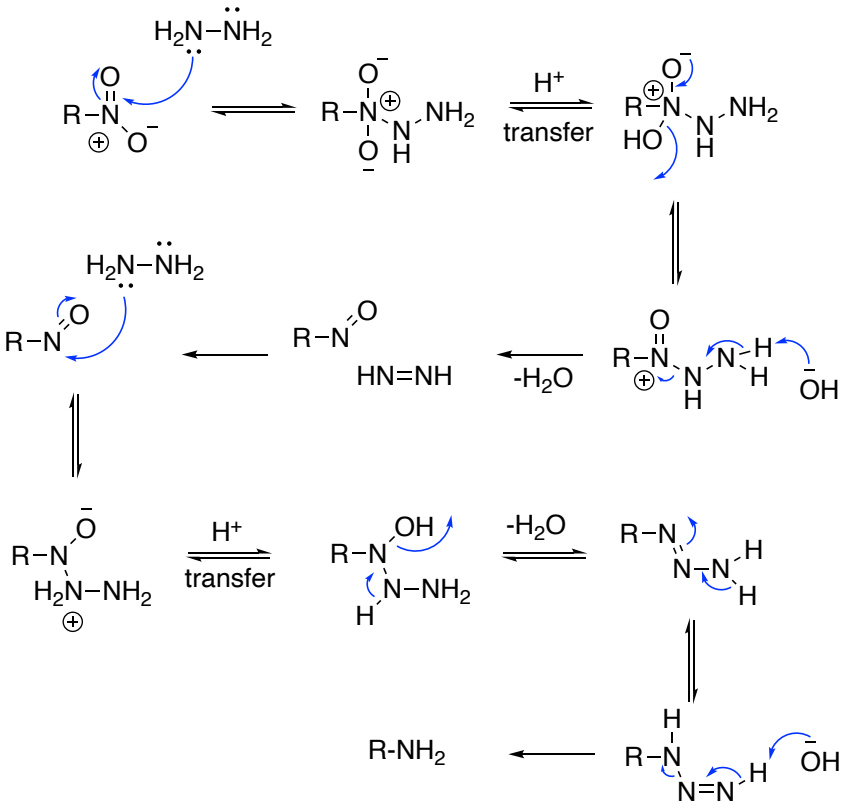

Scheme III-7. Reaction mechanism for the reduction of aromatic nitro groups to amines proposed by Rozas et al.[17]

In general, aromatic amines make poor leaving groups for nucleophilic substitution reactions. Thus, it is often required that the amino group is converted into a substituent that will easily undergo substitution in order to incorporate the azide click handle. Conversion of the amine into a diazonium ion (N_2) presents a good leaving group for nucleophilic substitution – particularly for aromatic amines. This reaction is known as a diazotization. The use of HCl is highly important in this reaction and provides two functions. Firstly it is used to convert

the sodium nitrite ($NaNO_2$) reagent to nitrous acid (HNO_2) and subsequently converts the excess HNO_2 *in-situ* to the electrophilic NO^+ or 'nitrosonium ion' which forms the diazonium salt (**Scheme III-8**).

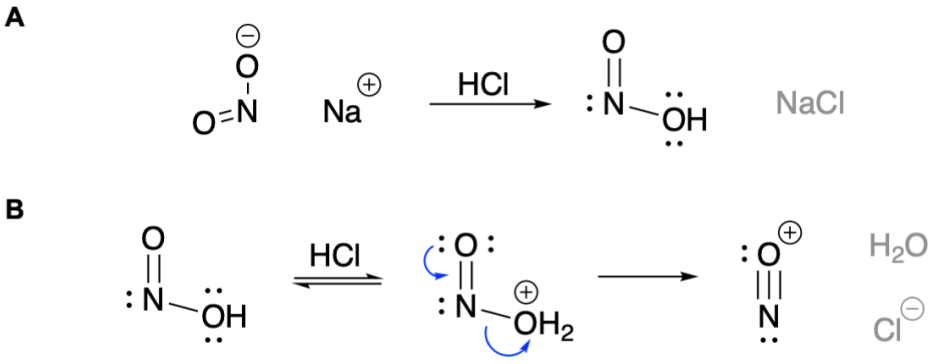

Scheme III-8. Reaction mechanism demonstrating **A**. the conversion of $NaNO_2$ to nitrous acid prior to **B.** further conversion of the excess HNO_2 to the nitrosonium ion.

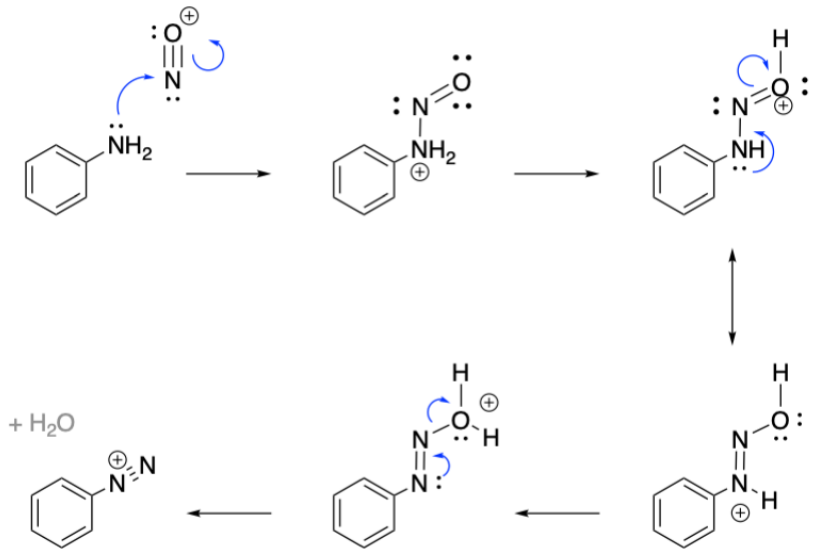

Scheme III-9. Reaction mechanism depicting the formation of the diazonium ion.

Formation of the diazonium salt proceeds through the addition of the nitrosonium ion and subsequent elimination of water (H_2O) (**Scheme III-9**). The diazonium ion itself is relatively unstable and thus sodium azide (NaN_3) is used to displace it in solution to produce the desired azide derivative, N3-DPPZ (**7**). Complexation with *cis*-[$Pt(DMSO)_2Cl_2$] in darkness at 50 °C yields the dark green-brown product, Pt-N_3-DPPZ (**8**).

Synthesis of the azide-functionalised *cis*-platinum(II) analogues

2-azidopropane-1,3-diamine dihydrochloride (N_3-DAP.HCl)

The synthetic route to obtain N_3-DAP. HCl (**12**) was performed through a four step process starting from the commercially available reagent 1,3-diamino-2-propanol (**Scheme III-10**). In order to adequately convert the alcohol substituent into an azide handle, an appropriate leaving group was required. Thus BOC protection chemistry was required on the amines to facilitate this. After BOC protection, a mesylate was generated from the alcohol and substitution with sodium azide afforded the azide derivative N_3-BOC-DAP (**11**). Deprotection using concentrated acid (6 M HCl) afforded the final N_3-DAP.HCl salt (**12**) in high yield (93%) (**Scheme III-10**).

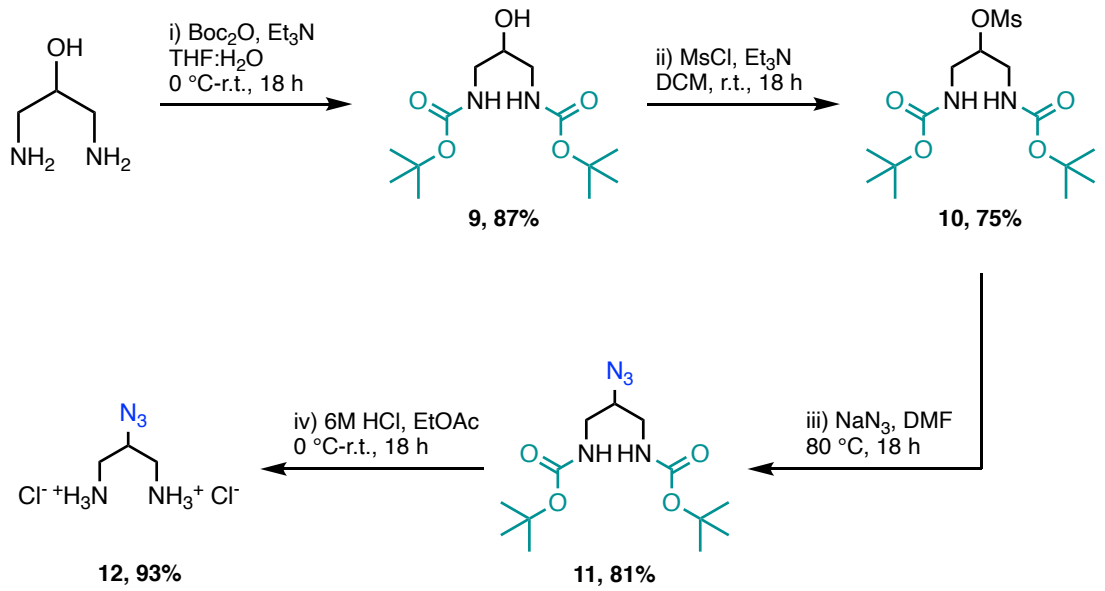

Scheme III-10. Synthetic routes for the generation of N_3-DAP.HCl (**12**).

Generation of the hydrochloride salt (**12**) served a number of purposes. Azides are hazardous materials and are known to be heat- and shock-sensitive and can also undergo explosive decomposition with very little external energy input. A general rule of thumb is to ensure that the number of nitrogen in the organic azide do not exceed that of carbon (and oxygen) atoms.[1] The equation below can be followed as a good example whereby:

$$(N_{carbon} + N_{oxygen})/ (N_{nitrogen}) \geq 3$$

- (C/N = 3): the smallest azide that can be safely isolated and stored in a pure form.
- (C/N = 1-3): generally can be isolated but needs to be stored below r.t and under concentrations of 1 M and 5 grams.
- (C/N <1): should never be isolated, unless it is a transient intermediate, or stored in quantities greater than 1 g.

Use of the hydrochloride salt allows for safe synthesis and isolation of the material. The ability to apportion quantities for subsequent reactions allowed for azide portions to be used safely and easily. Attempts to synthesise 2-azidopropane-1,3-diamine in a pure form were successful on test scales, however the resultant oil was difficult to work with and proved hard to divide into quantifiable amounts for future experiments. BOC-DAP (**1**) was obtained through the BOC protection of the two amines present on 1,3-diamino-2-propanol at 0 ºC in a nucleophilic acyl substitution reaction. Initial addition of the amine to the carbonyl group of the *tert*-butyloxycarbonyl protecting group (BOC_2O) is followed by elimination of the *tert*-butanoic anion. Further decomposition leads to the formation of CO_2 and the alkoxy ion of *tert*-butanol. The use of triethylamine (TEA) as a base picks the proton from the amino *tert*-butyl derivative forming the carbamate or "BOC" (**Scheme III-11**).

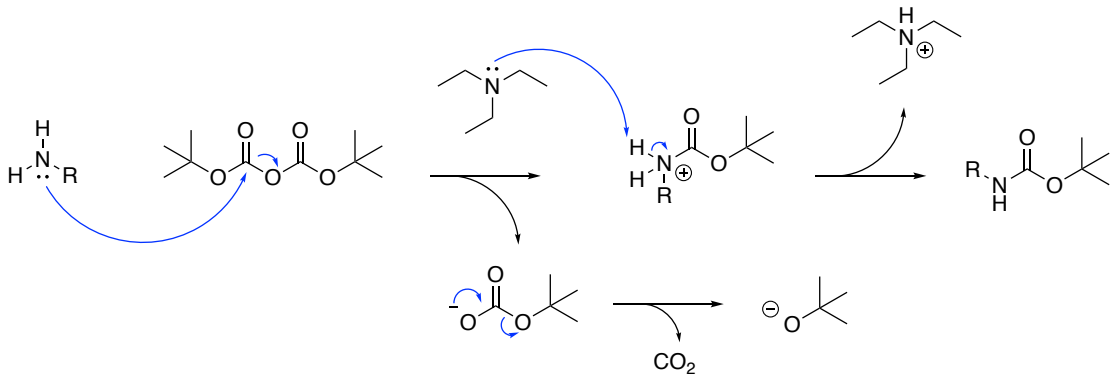

Scheme III-11. Reaction mechanism for the addition of BOC protection groups to amines.

The BOC product was obtained initially as an oil which subsequently solidified to a pale off-white solid upon exposure to air. The protons of the *tert*-butyl groups represent the primary ^1H NMR ($CDCl_3$) signal for the product wherein a distinct single peak of strong intensity is present at approx. 1.46 ppm

which correlates to the 18 protons of the protecting groups (**Appendix A, Figure VIII-27**). With the reactive amine groups protected it was now possible to proceed with the reactions to convert the alcohol to the required azide click handle. As mentioned previously, alcohol groups (-OH) are poor leaving groups and thus require conversion to suitable groups for possible azide substitution. Conversion of the alcohol to an alkyl mesylate by introduction of methanesulfonyl chloride in the presence of TEA was performed successfully. Unlike tosyl chlorides (TsCl), wherein addition proceeds through a charged intermediate, mesylation occurs through the formation of a sulfene (**Scheme III-12**). Deprotonation of the a-proton of the -CH_3 group by TEA leads to expulsion of chloride and formation of the aforementioned sulfene. Nucleophilic attack by the alcohol on the highly electrophilic sulfene swiftly follows and rearrangement affords the mesylate product, MsCl-BOC-DAP (**10**).

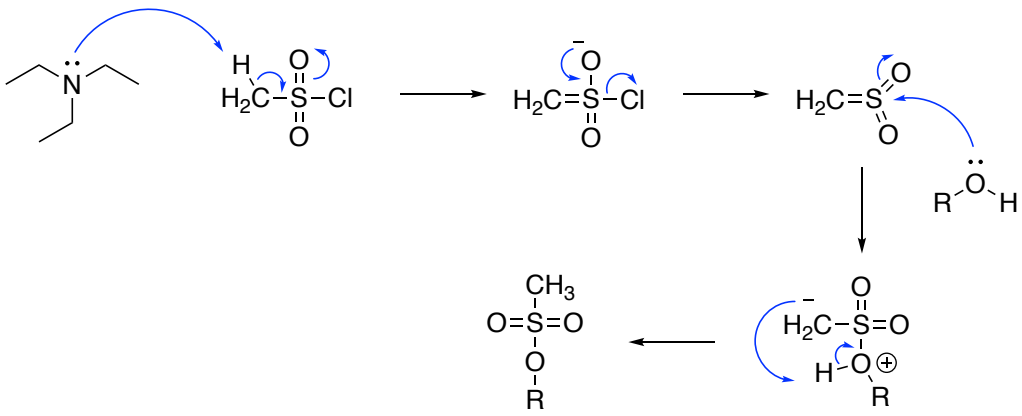

Scheme III-12. Reaction mechanism for the formation of the mesylated product.

MsCl-BOC-DAP (**10**) formation was characterised by ^{1}H NMR ($CDCl_3$) which displayed a distinct singlet diagnostic peak at 3.09ppm representing the three protons of the methyl group (**Appendix A, Figure VIII-30**). Characterisation by ^{13}C NMR ($CDCl_3$) displayed a distinct peak at 38.31ppm representing the carbon of the methyl group (**Appendix A, Figure VIII-31**). To afford the first azide product, N_3-BOC-DAP (**11**), a nucleophilic S_N2 substitution was performed (**Scheme III-13**). An S_N2 substitution reaction mechanism is dependent on the concentration of both the substrate and nucleophile. Sodium azide (NaN_3) was reacted in excess with **10** at 80 ºC prior to precipitation with H_2O to obtain the product **11** as a white solid.

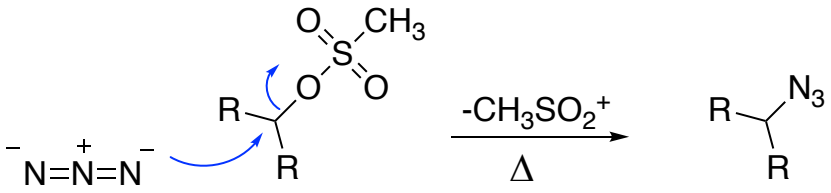

Scheme III-13. S_N2 nucleophilic substitution of mesylate group to obtain azide product.

Both ^1H NMR and ^{13}C NMR characterisation (**Appendix A, Figure VIII-33 and Figure VIII-34**) displayed the loss of the methyl proton and carbon singlet signals respectively while FT-IR spectroscopy confirmed the presence of the azide by the strong band at 2110 cm^{-1} (**Appendix A, Figure VIII-35**). The final reaction to afford the N_3-DAP .HCl product **12** was two-fold (**Scheme III-14**). The first step of the reaction was the deprotection of the amine groups using concentrated hydrochloric acid dissolved in ethyl acetate followed by *in-situ* conversion to the hydrochloride salt. 6 M hydrochloric acid was used to protonate the oxygen of the *tert*-butyl carbamate moiety and subsequent elimination of the *tert*-butyl cation is achieved. Deprotonation by the chloride ion, which acts as a base, of the carbamic acid occurs leading to the loss of CO_2. The free amine reacts with the excess HCl to form the hydrochloride salt which consequently precipitates from the ethyl acetate solution at approx. 5 ºC. Characterisation by ^1H NMR (DMSO-d_6) dislayed a distinct peak at 8.38 ppm that correlates to the six protons of the amine groups. Coinciding with this, the loss of the intense singlet corresponding to the eighteen protons of the BOC protecting groups is observed (**Appendix A, Figure VIII-36**). FT-IT spectroscopy confirms retention of the azide handle throughout the deprotection process by the strong band observed at 2127 cm^{-1} (**Appendix A, Figure VIII-38**).

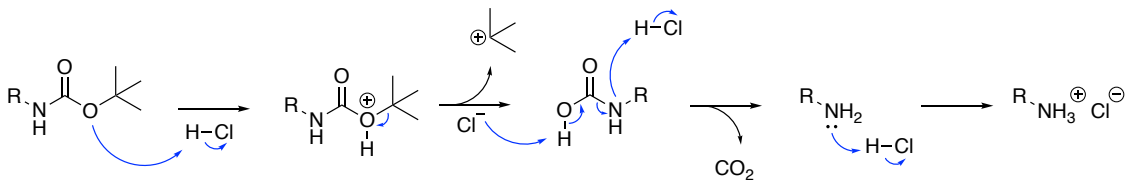

Scheme III-14. Reaction mechanism for the deprotection of the BOC-protected amines using 6M HCl and subsequent *in-situ* formation of the hydrochloride salt.

Synthesis of *cis*-[Pt(2-azidopropane-1,3-diamine)Cl_2]

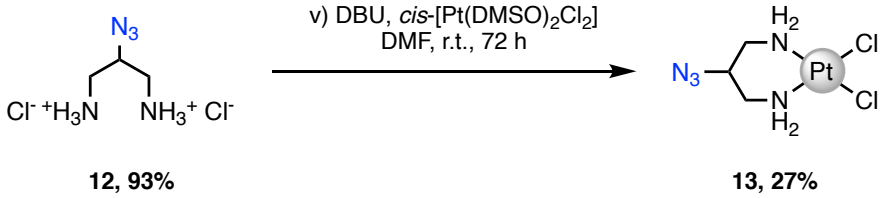

12, 93% **13, 27%**

Scheme III-15. Synthetic route for the generation of N_3-Pt-Cis.

Pt-N_3-Cis **13** was synthesised according to a method previously reported by Urankar *et al*.[9] **12** was treated with an equivalent quantity of *cis*-[Pt(DMSO)$_2$Cl$_2$] in the presence of DBU at r.t. over the course of three days in darkness. The product **13** was obtained by precipitation with H_2O and cooling to 5 ºC prior to filtration to afford the grey crystalline solid (**Scheme III-15**). ^{1}H NMR, ^{13}C NMR and ^{195}Pt NMR spectroscopy was used to characterise the product and closely correlates with the literature data published previously. Additionally, ESI-MS spectrometry and FT-IR spectroscopy confirmed the presence of the complex and azide handle (2108 cm^{-1}) respectively.

Synthesis of *cis*-[Pt(2-azidopropane-1,3-diamine)CBDCA] and *cis*-[Pt(2-azidopropane-1,3-diamine)Oxalate]

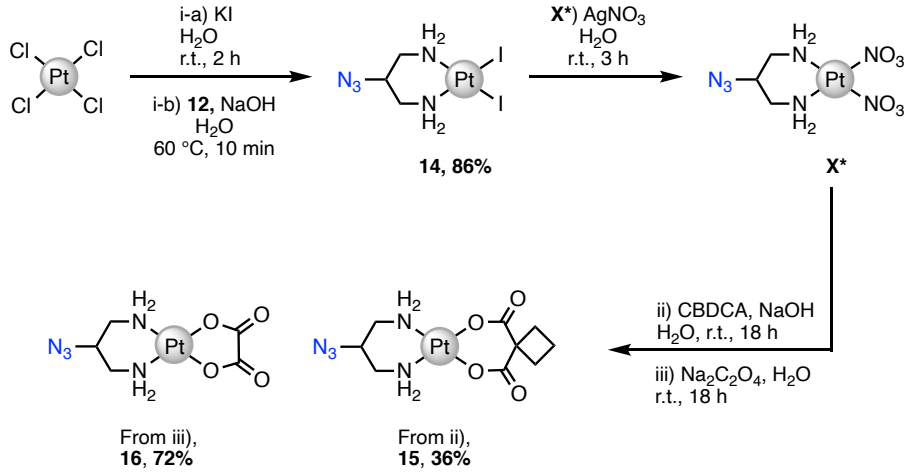

14, 86% **X***

From iii), **16, 72%** From ii), **15, 36%**

Scheme III-16. Synthetic routes for the generation of N_3-Pt-Carbo **15** and N_3-Pt-Oxali **16.**

Pt-N_3-Carbo **15** and Pt-N_3-Oxali **16** were synthesised according to the previously reported method by Urankar *et al*.[9] with minor deviation for the synthesis of **16** (**Scheme III-16**). The synthesis of **15** proceeded through the commercially available $K_2[PtCl_4]$ which was converted to the tetra-iodo complex $[PtI_4]^{2-}$ by treatement with excess potassium iodide (KI). Introduction of N_3-DAP.HCl **12** in combination with sodium hydroxide generates N_3-DAP *in-situ* prior to complexation to form the *cis*-[Pt(2-azidopropane-1,3-diamine)I_2] derivative. This was followed by treatment with excess $AgNO_3$ and subsequent removal of the AgI by-product by celite filtration techniques. Cyclobutane-1,1-dicarboxylic acid (CBDCA) was added in the presence of two equivalents of NaOH and stirred in darkness for approx. 18 h. Concentration of the solution under reduced pressure caused precipitation of the N_3-Pt-Carbo product, **15**, which was collected by 0.22 μm Millipore filtration.

^{1}H NMR, ^{13}C NMR and ^{195}Pt NMR and FT-IR spectroscopy confirmed the obtained product and correlated with the data published previously by Urankar *et al*.[9] N_3-Pt-Oxali was obtained by following protocol above with slight deviations. After AgI removal, sodium oxalate ($Na_2C_2O_4$) was added and the solution was stirred in darkness for 18-24 h (**Scheme III-16**). The off-white solid was collected in a manner similar to above. The product was characterised and confirmed by ^{1}H NMR and ^{13}C NMR. ^{195}Pt NMR displayed a distinct platinum diagnostic signal at -1968 ppm (**Appendix A, Figure VIII-51**). The azide handle was confirmed by the presence of a strong azide band at 2106 cm^{-1}. Further analysis by ESI-MS provided confirmation of the complex generation. To the best of our knowledge, this is the first reported synthesis of *cis*-[Pt(2-azidopropane-1,3-diamine)Oxalate] (**16**).

III. 3. References

1. Bräse, S.; Gil, C.; Knepper, K.; Zimmermann, V., Organic Azides: An Exploding Diversity of a Unique Class of Compounds. *Angew. Chem. Int. Ed.* **2005,** *44* (33), 5188-5240.
2. Lauria, T.; Slator, C.; McKee, V.; Müller, M.; Stazzoni, S.; Crisp, A. L.; Carell, T.; Kellett, A., A Click Chemistry Approach to Developing Molecularly Targeted DNA Scissors. *Chem. Eur. J.* **2020,** *26* (70), 16782-16792.
3. Fantoni, N.; McGorman, B.; Molphy, Z.; Singleton, D.; Walsh, S.; El-Sagheer, A. H.; McKee, V.; Brown, T.; Kellett, A., Development of Gene-Targeted Polypyridyl Triplex Forming Oligonucleotide Hybrids. *ChemBioChem* **2020**.
4. Jones, J. E.; Jenkins, R. L.; Hicks, R. S.; Hallett, A. J.; Pope, S. J. A., Water-soluble, luminescent iridium(iii)–ytterbium(iii) complexes using dipyrido[3,2-a:2′,3′-c]phenazine derivatives as bridging units. *Dalton Trans.* **2012,** *41* (34), 10372.
5. Lin, G.-J.; Jiang, G.-B.; Xie, Y.-Y.; Huang, H.-L.; Liang, Z.-H.; Liu, Y.-J., Cytotoxicity, apoptosis, cell cycle arrest, reactive oxygen species, mitochondrial membrane potential, and Western blotting analysis of ruthenium(II) complexes. *J. Biol. Inorg. Chem.* **2013,** *18* (8), 873-882.
6. Kane, S. A.; Sasaki, H.; Hecht, S. M., Guanosine-Specific DNA Damage by a Co(II) Bithiazole Complex. *J. Am. Chem. Soc.* **1995,** *117* (36), 9107-9118.
7. Abd Karim, K. J.; Binauld, S.; Scarano, W.; Stenzel, M. H., Macromolecular platinum-drugs based on statistical and block copolymer structures and their DNA binding ability. *Polym. Chem.* **2013,** *4* (22), 5542-5554.
8. Veerendhar, A.; Cohen, S.; Frant, J.; Supuran, C. T.; Reich, R.; Breuer, E., Synthesis of Enantiomeric Aminoalkylcarbamoylphosphonates and Their Evaluation as Dual-Action Anticancer MMP and Carbonic Anhydrase Inhibitors. *Heteroat. Chem.* **2015,** *26* (4), 257-269.
9. Urankar, D.; Košmrlj, J., Preparation of diazenecarboxamide–carboplatin conjugates by click chemistry. *Inorg. Chim. Acta.* **2010,** *363* (14), 3817-3822.

10. Roy, S.; Hagen, K. D.; Maheswari, P. U.; Lutz, M.; Spek, A. L.; Reedijk, J.; Van Wezel, G. P., Phenanthroline Derivatives with Improved Selectivity as DNA-Targeting Anticancer or Antimicrobial Drugs. *ChemMedChem* **2008,** *3* (9), 1427-1434.
11. Park, G. Y.; Wilson, J. J.; Song, Y.; Lippard, S. J., Phenanthriplatin, a monofunctional DNA-binding platinum anticancer drug candidate with unusual potency and cellular activity profile. *Proc. Natl. Acad. Sci.* **2012,** *109* (30), 11987-11992.
12. Zhang, W.; Loebach, J. L.; Wilson, S. R.; Jacobsen, E. N., Enantioselective epoxidation of unfunctionalized olefins catalyzed by salen manganese complexes. *J. Am. Chem. Soc.* **1990,** *112* (7), 2801-2803.
13. Linker, T., The Jacobsen–Katsuki Epoxidation and Its Controversial Mechanism. *Angew. Chem. Int. Ed.* **1997,** *36* (19), 2060-2062.
14. Krishnan, S.; Kuhn, D. G.; Hamilton, G. A., Direct oxidation in high yield of some polycyclic aromatic compounds to arene oxides using hypochlorite and phase transfer catalysts. *J. Am. Chem. Soc.* **1977,** *99* (24), 8121-8123.
15. Klawonn, M.; Bhor, S.; Mehltretter, G.; Döbler, C.; Fischer, C.; Beller, M., A Simple and Convenient Method for Epoxidation of Olefins without Metal Catalysts. *Adv. Synth. Catal.* **2003,** *345* (3), 389-392.
16. Molphy, Z.; Prisecaru, A.; Slator, C.; Barron, N.; McCann, M.; Colleran, J.; Chandran, D.; Gathergood, N.; Kellett, A., Copper Phenanthrene Oxidative Chemical Nucleases. *Inorg. Chem.* **2014,** *53* (10), 5392-5404.
17. Diez-Cecilia, E.; Kelly, B.; Rozas, I., One-step double reduction of aryl nitro and carbonyl groups using hydrazine. *Tetrahedron Lett.* **2011,** *52* (50), 6702-6704.

Chapter IV

Oligonucleotide and Hybrid Development

The work presented in this chapter has been submitted as part of a patent application: Patent application filed for “A cis-platinum(II)-oligomer hybrid”. Application number GB2113541.3. (Date filed: 22/09/2021)

IV. 1. Abstract

The successful design and generation of alkyne-modified triplex-forming oligonucleotides (TFOs), thiazole orange TFOs (TOTFOs), and alkyne-amine modified TFOs (AA-TOTFOs) is reported. The use of both the copper-catalysed (CuAAC) and strain-promoted (SPAAC) azide alkyne cycloaddition strategies has afforded the generation of a family of *cis*-platinum(II)-TFOs with future targeted triplex formation and crosslinking abilities. These hybrid constructs are the first examples of Pt(II)-TFOs designed using these strategies and overcome numerous limitations currently present in the state-of-the-art. Furthermore, labelling with TO intercalating units has allowed for hybrid development that possess greater stabilising abilities. The design of AA-TOTFO constructs, wherein both *cis*-platinum(II) reagent and TO unit are present on the same nucleobase, represent the first in class for this innovative hybrid nucleic acid hybrid technology.

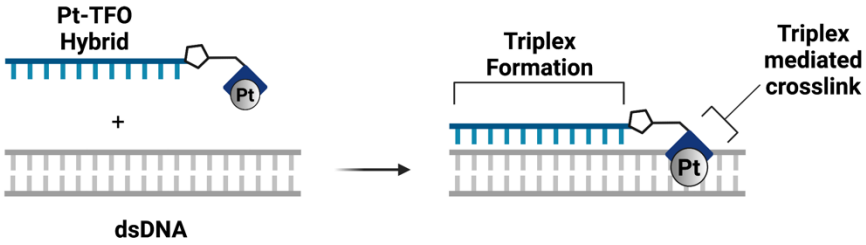

Figure IV-1. Representation of triplex formation and crosslinking afforded by the click chemistry generated *cis*-platinum(II) TFO hybrids.

IV. 2. Oligonucleotide Generation

IV. 2. 1. Chapter Aims

- The generation of a library of alkyne-modified TFOs, TOTFOs, and AA-TOTFOs through solid-phase oligonucleotide synthesis.

- The generation of a library of *cis*-platinum(II)-TFO constructs through the use of CuAAC and SPAAC strategies.

- The development of a library of platinum(II) AA-TOTFO constructs and copper-AMN-TFOs

IV. 2. 2. Rationale

The current state-of-art involved in designing Pt(II) nucleic acid vectors has focused on methods generally involving complexation of transplatin-like complexes to oligonucleotides or post-synthetic methods wherein oligonucleotide vectors with attached chelating linkers are treated with either *trans*- or *cis*-platinum(II) reagents. Both pathways present multiple problems with the main challenge involving oligonucleotide design limitations. To date, there have been no reported attempts to generate these hybrids using click chemistry strategies. Therefore the aim of this work was to create a library of TFOs possessing modified alkyne handles that will allow for facile click chemistry generation of *cis*-platinum(II) TFO hybrids. By developing a library of TFOS of varying length and base modification location, the ideal parameters for hybrid generation can be investigated. Furthermore, the use of CuAAC and SPAAC strategies will provide information on the best methodology to follow for future hybrid development with regards to reaction ease, yield and purities. Finally, the design of nucleic acid vectors that allow for the incorporation of stabilising agents such as TO and introduce bifunctional nucleobases like the AP-C3 monomer will aid the investigation into final TFO design. Combined, the multiple *cis*-platinum(II) complexes available, the varying TFO sequences and the availability of intercalating TO units will provide a multitude of options to probe the ideal composition of next-generation Pt(II)-TFO hybrids.

IV. 2. 3. General Information

Oligonucleotide synthesis and purification was performed in collaboration with Dr. Daniel Singleton in ATDBio Ltd., University of Southampton under the supervision of Prof. Tom Brown, University of Oxford, UK. The 17 mer TFO sequences and associated 21 bp duplex targets and 17 bp duplex targets were bought from Integrated DNA Technologies (IDT), BVBA, Leuven, Belgium. 3-(5-carboxypentyl)-2-((1'-methylquinolin-4'(1H)-ylidene)methyl)benzo-[*d*]-thiazol-3-ium hexafluorophosphate (TO_{B6}) was kindly provided by the research group of Prof. Tom Brown, University of Oxford, UK.

Oligonucleotide Synthesis

Solid supports, standard DNA phosphoramidites and all other reagents used in the synthesis were purchased from Sigma Aldrich. Modified phosphoramidites were purchased from Glen Research. Oligonucleotides (ODNs) were synthesised on a K&A Laborgeräte H-8-SE LNA,DNA/RNA synthesiser using the standard 1.0 μmol phosphoramidite cycle. Coupling efficiencies were monitored by the trityl cation conductivity monitoring facility and was >98% for all oligonucleotides. Standard monomers (A, G, C and T) were coupled for 35 s and non-standard monomers were coupled for 360 s. ODNs were deprotected and cleaved from the solid support using a concentrated ammonia solution for 1 h at r.t., followed by heating in sealed vials for 5 h at 55 °C. ODNs were purified using reverse-phase HPLC on a Gilson HPLC system using a Luna 10 μm C8 100 Å 250 x 10 mm column. For standard alkyne-modified ODNs, the gradient was 10-45 % buffer B over 20 min with flow rate of 4 mL/min (buffer A: 0.1 M triethylammonium acetate (TEAA), buffer B: 0.1 M TEAA with 50% MeCN). Fraction volumes were reduced by rotary evaporation prior to redissolution in water and desalted using NAP-10 gel filtration columns purchased from GE Healthcare. All ODNs were characterised by negative-mode HPLC-mass spectrometry using a Waters Xevo G2-XS QT mass spectrometer with an Acquity UPLC system equipped with an Acquity UPLC oligonucleotide BEH C18 column (particle size: 1.7 μm; pore size 130 Å; column dimensions: 2.1 x 50 mm). Data was deconvoluted and analysed using Waters Mass Lynx software.

Oligonucleotide synthesis with modified nucleobases was performed as described above with some minor deviations. Standard monomers (A, G, C, and T) were coupled for 35 s and non-standard monomers were coupled for 360 s. ODNs with incorporated pdU additions and those that were labelled with thiazole orange (TO_{B6}) or fluorescein/cyanine-5 dyes were purified with ammonium acetate (NH_4OAc) with a gradient of 15-45% buffer B over 25 min, flow rate of 4mL/min (buffer A: 0.1 M NH_4OAc, buffer B: 0.1 M NH_4OAc 50% MeCN).

Thiazole orange (TO) TFO:TO-NHS ester labelling

In a total volume of approx. 350 μL, 2000 nmol (10 eq.) of TO_{B6} NHS ester in DMF was added to 200 nmol of oligonucleotide dissolved in carbonate buffer ($NaHCO_3/Na_2CO_3$, 0.5 M, pH 8.74). The solution was shaken at 20 ºC for 2 h prior to desalting by NAP column and purified by gradient reverse-phase HPLC (C8 column) in 0.1 M NH_4OAc (Buffer A) with CH_3CN (50%) (Buffer B). Gradients of 15-45% were used over 20 mins. ESI-MS analysis, as previously described, was used to determine the purity of the labelled oligonucleotide. For ODNs that contained two labelling sites, 20 eq. of TO_{B6} NHS ester was used. For three or four sites, 30 eq. of TO_{B6} NHS ester was used. For TOTFOs and AA-TOTFOs that were clicked to N_3-platinum(II) complexes, no purification of the TO labelled TFO was performed. Purification was only performed after click conjugation to ensure optimum yield.

Platinum(II)-TFO hybrid generation using click chemistry

In a total volume of 500 μL (50:50 H_2O:DMSO or DMF, complex dependent) 500 nmol of Pt(II)-azide complex was added to 50 nmol of the alkyne-modified TFO. The solutions were degassed with argon and 500 nmol of Cu-TBTA complex in 50:50 H_2O:DMSO was added prior to final addition of 1000 nmol of Na-*L*-ascorbate. The click solutions were further degassed and stirred at 25 °C for 3-6 h prior to desalting by elution through a NAP-10 column. For click reactions concerning the 5'-BCN(CEP II)-dC modified TFO, the reaction was performed as above without the use of Cu-TBTA or Na-*L*-ascorbate. Platinum(II)-TFO hybrids were purified and characterised following the protocol described above. Data was deconvoluted and analysed using Waters Mass Lynx software.

UV-Thermal Melting Studies

Standard oligonucleotides and hybrids were quantified on a NanoDropND-1000 UV-Vis Spectrophotometer using the Beer-Lambert Law and the nearest neighbour DNA model (nn). Characterisation data and analysis was provided by the respective suppliers. Thermal melting studies were performed on a Varian Cary 100 UV-Visible Spectrophotometer equipped with a 6 x 6 Peltier multicell system with temperature controller in Starna Scientific black-walled quartz cuvettes of 10 mm path length and 100 μL sample volume. Experimental measurements were monitored at 260 nm using Cary WinUV thermal application software. The TFO/Pt(II)-TFO hybrid and duplex samples were combined in a 2.5:1 μM ratio and dissolved in triplex buffer - 10 mM phosphate, 150 mM NaCl and 2 mM $MgCl_2$ (pH 6). Pt-N_3-Complex/duplex melting samples were prepared similarly. Samples were initially denatured by heating to 90 ºC at 10 ºC/min. The samples were held at this temperature for 5 min prior to annealing at 0.5 ºC/min. Thermal melting was recorded between 12-90 ºC (0.5 ºC/min with 2 min hold). In total, 3 heating ramps were performed. T_M was calculated as an average of the first derivative of sigmoidal non-linear regression analysis of the triplex melting curve using GraphPad Prism 8 software. Instrument incremental temperature increases were closely monitored to endure accurate recording of measurements (i.e. 0.5 ºC/min) .

Fluorescent Thermal Melting

Cisplatin and duplex samples were combined in a 2.5:1 μM ratio and dissolved in triplex buffer - 10 mM phosphate, 150 mM NaCl and 2 mM $MgCl_2$ (pH 6) prior to incubation at 37 ºC for 48 hours. SYBR green I (1 mL, Roche) was added to each sample and the melting profile for the triplex was analysed on a LightCycler® 480 II (Roche). Samples were heated to 99 ºC with 10 fluorescence measurements recorded per ºC. A plot of sample fluorescence versus temperature is obtained, normalised and the first negative derivative of the sample was calculated. Samples were analysed in triplicate and T_M was calculated as an average of the first negative derivative of the melting curve. Melting curves were analysed and graphed using GraphPad Prism 8 software.

Cell culture and Cell Viability Assays

MCF-7, MDA-MB-231 and MDA-MB-468 cells were maintained in high glucose DMEM and T47D were maintained n RPMI-1640. All media was supplemented with 10% FBS, 1% L-glutamine and 50 units/mL penicillin and 50 mg/mL streptomycin. MCF-10a were maintained in DMEM/F-12 supplemented with 5% horse serum, 20 ng/ml epidermal growth factor, 100 ng/mL cholera toxin, 0.01 mg/mL insulin and 500 ng/mL hydrocortisone. Cells were maintained at 37 ºC and 5% CO_2 in a humidified atmosphere. Stock solutions were prepared in 0.9% saline (w/v) and stored at 4 ºC for up to 1 week. Further dilutions were prepared in culture media daily.

Seeding densities and resazurin (alamar blue) incubation times where predetermined based on Z-score analysis (> 0.6). MCF-7, MDA-MB-231, MDA-MB-468 and MCF-10a cells were seeded at 5000 cells per well in a 96-well plate, while T47D cells were seeded at 7500 cells per well for 18 h prior to drug treatment. Cells were exposed to platinum complexes at 1-100 μM using an automated liquid handling system (JANUS Automated Workstation) and incubated at 24 or 48 h. A 1:10 dilution of resazurin reagent (5.6 mM, Sigma R7017) was added and incubated for a further 4 h (MCF-7) or 6 h (MDA-MB-231, MDA-MB-468, T47D and MCF-10a) Fluorescence was measured on an intergrated Victor X5 Multilabel Reader (ex: 530 nm, em: 620 nM). Cell viability was expressed as normalised percent of viable cells relative to controls and IC_{50} values were calculated using GraphPad Prism8 software.

Triplex Formation

Triplex formation was analysed by native PAGE. In a total volume of 5 μL triplex buffer (10 mM phosphate, 150 mM NaCl, 2 mM $MgCl_2$ (pH 6)), duplex target (40 bp, 1pmol) was treated with increasing concentrations of alkyne-modified TFO (2.5-50 eq.). Samples were incubated at 37 ºC for 0-48 h prior to addition of 6X loading dye (Thermo Scientific) and loaded onto a 20% polyacrylamide gel (50 mM Tris acetate, 150 mM NaCl, 2 mM $MgCl_2$, pH 6). Electrophoresis was performed at 70 V for 240 mins in triplex running buffer (50 mM Tris acetate, pH 6). Polyacrylamide gels were post-stained with SybrGold and visualised and imaged on a Syngene G:Box Mini 9 gel documentation system.

Triplex-mediated crosslink activity

In a total volume of 5 μL triplex buffer, target duplex (57 bp, 1 pmol) and off-target sequence (40 bp, 1 pmol) were treated with increasing concentrations of platinum(II)-TFO hybrid (2.5-50 eq.) and incubated at 37 ºC for up to 48 h. Electrophoresis and visualisation was performed as previously reported.

Reversal of triplex formation and crosslinking by sodium cyanide

Fluorescently labelled duplex target (57 bp, 1 pmol) was treated with alkyne-modified TFO (50 eq.) and separately with platinum(II)-TFO hybrid (50eq.). Samples were incubated at 37 ºC for 48 h prior to addition of increasing concentrations of NaCN solution (1,000-300,000 eq.). Combined samples were incubated at r.t. for 18 h and quenched with 30% glycerol solution. Electrophoresis was performed as before. Gel visualisation and imaging was performed on a Syngene G:Box Mini 9 gel documentation system with integral Cy5 and 6-FAM filters.

Crosslink investigation by denaturing PAGE

In a total volume of 5 μL, fluorescently labelled duplex sequences (21/17 bp, 21 bp, 1 pmol) were treated with platinum(II)-TFO hybrid (TFO-17A – C, 50 eq.) Samples were incubated at 37 ºC for a minimum of 48 h prior to quenching with 2X denaturing loading dye. Samples were loaded onto 20% denaturing PAGE (1X TBE, 7.4 M urea, pH 8.2) and subjected to electrophoresis at 300 V for 60 mins in 1X TBE running buffer.

IV. 2. 4. Oligonucleotide Development

IV. 2. 4. 1. Alkyne-Modified TFOs

A range of sequences targeting a specific location of green fluorescent protein (GFP) coding gene were selected. These triplex-forming oligonucleotides were designed to incorporate alkyne-modified bases for further functionalisation through click chemistry with azide-modified platinum(II) complexes. A library of six TFOs were developed ranging between 21-29 nt in length (**Figure IV-2, A**).

To investigate the effectiveness of platinum cross-linking and triplex stability, terminal 5' (TFO1, 2, 4 and 6) and internal alkyne modifications (TFO3 and 5) were incorporated. TFO6 was designed as a purine-rich antiparallel probe. The base modifications incorporated are octadinyl-deoxycytosine (TFO1 and 4), octadinyl-deoxyuridine (TFO3, 5 and 6) and a 5'-phosphate modified bicyclo[6.1.0]nonyne deoxycytosine derivative (TFO2) (**Figure IV-3, B**). TFO1-3 and 6 contain one mismatch each whereas TFO4 and 5 contain two. Three duplex targets were synthesised corresponding to particular portions of the GFP gene with an eight nt 'overhang' found on the 5' side of the target sequence. Similarly, a 3 nt 'overhang' was produced at the 3' terminal end of the sequence. The full table of ESI-MS analysis for the alkyne-modified TFOs and Pt(II)-TFO hybrids is available in **Appendix B, Table VII-1.**

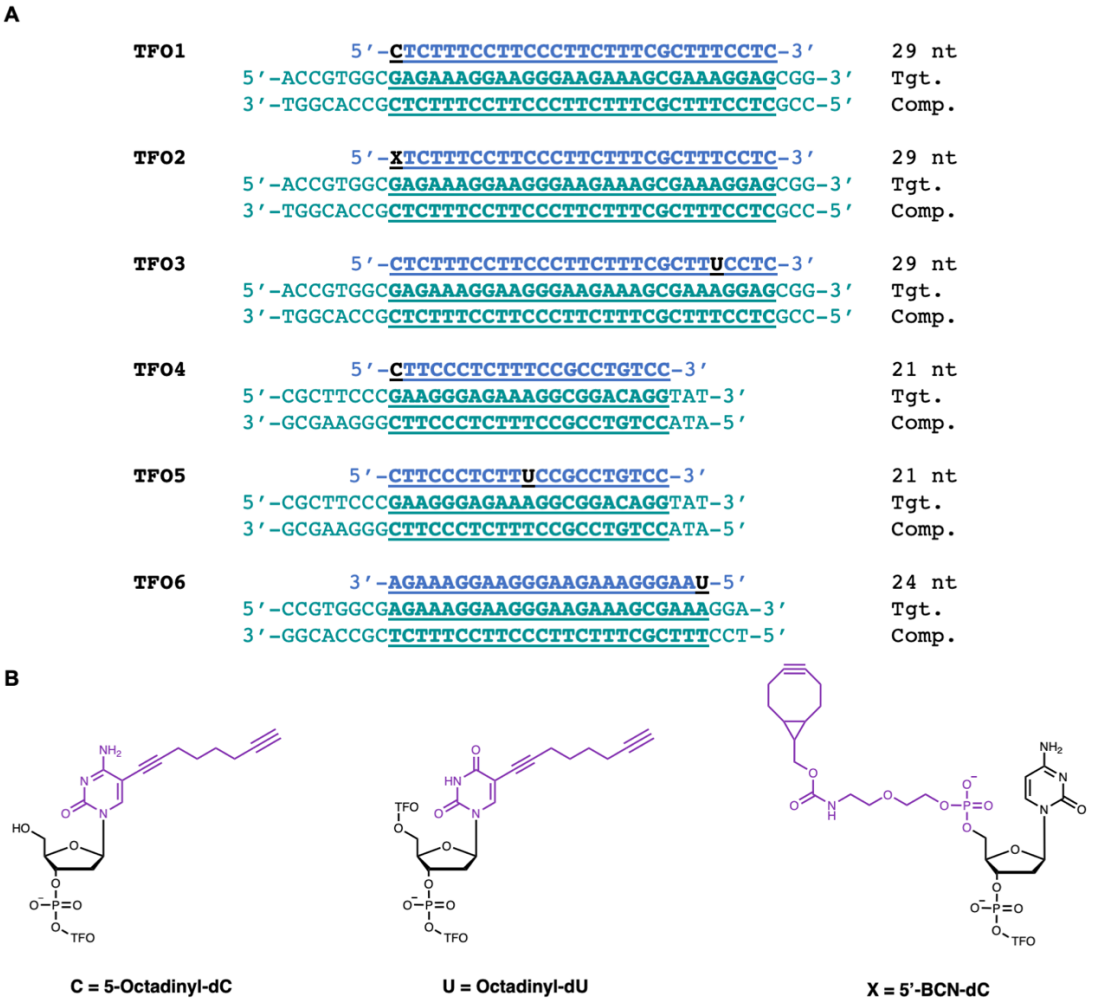

Figure IV-2. A. Library of alkyne-modified TFO1-6 with associated sequence length, base modification, location and target duplex sequence. **B.** Alkyne-modified nucleobases where C = Octadinyl-dC, U= Octadinyl-dU and X = 5'-BCN-dC.

IV. 2. 4. 2. TOTFOs and AA-TOTFOs

The duplex-binding affinity of parallel TFOs has long been a point of investigation – at neutral and higher pH binding is severely reduced mainly due to the need for cytosine protonation. Thus efforts have focused on developing innovative means to overcome this limitation including the use of modified sugar and phosphate backbones and modified nucleobases. Additionally, the use of intercalating molecules has shown to be effective in stabilising triplexes. An interesting molecule that has seen its prominence rise in the field is thiazole orange (TO). An intercalative fluorophore, TO has been shown to possess triplex stabilising capabilities while maintaining its fluorogenic properties.[1] Enhancement of the molecules inherent fluorescence is increased significantly upon intercalation with a duplex target. The use of TO in conjunction with Pt(II)-

TFO hybrids is an innovative idea to enhance the triplex stability of the hybrid oligonucleotides and allow for detection of target sequences. A series of alkyne-modified TFOs were designed based off the template of TFO1 and TFO4 previously discussed (**Figure IV-3, A**). The TFOs retain the octadinyl-dC modified nucleobase as a site for click conjugation and have undergone further modification to incorporate between 1-3 5(1-propargylamino)-dU (pdU) nucleobases for TO coupling (**Figure IV-3, B**)

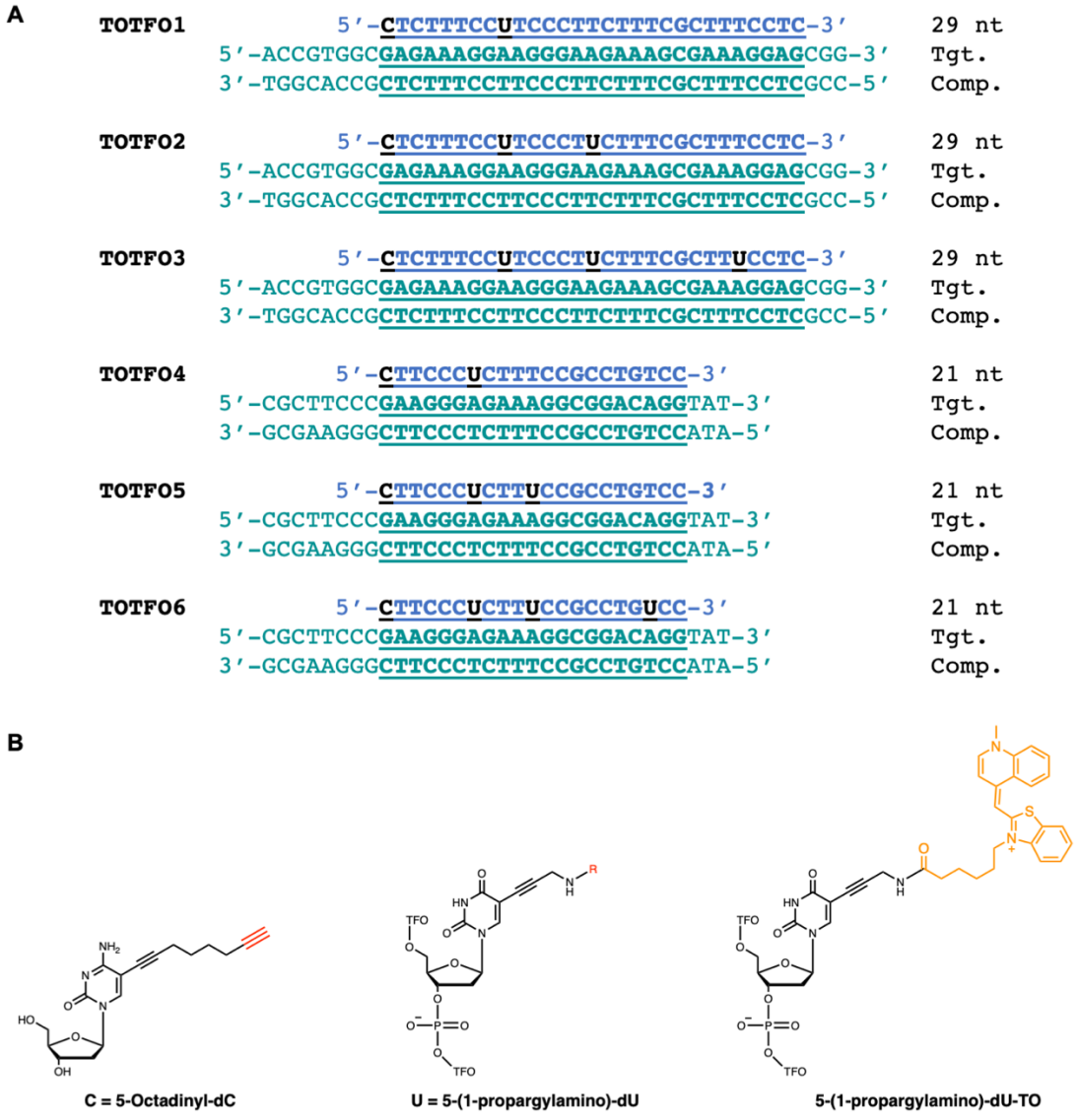

Figure IV-3. A. Alkyne-modified TOTFOs with octadinyl-dC and 5-(1-propargylamino)-dU nucleobase incorporations **B.** Octadinyl-dC modified nucleobase, 5-(1-propargylamino)-dU and schematic depicting TO coupled pdU nucleobase.

Additionally, a second series of TOTFOs have been generated. In this study, the TFOs have been shortened at the 5'-terminal by removal of the octadinyl-dC nucleobase. The adjacent thymine has furthermore been substituted for a unique deoxyuridine modified alkyne-amine nucleobase (**AP-C3**) (**Figure IV-4, B**). This innovative nucleobase incorporates both an alkyne for click conjugation with azide-bearing molecules and an amine for TO coupling. Similarly the rest of the sequences have been modified to incorporate up to **3** 5-(1-propargylamino)-dU nucleobases to allow for TO modification. As such, these alkyne-amine TOTFOs (AA-TOTFOs) will allow for conjugation with a variety of azide functionalised compounds and up to **4** TO molecules (**Figure IV-4, A**). Notably the first TO coupling will be found on the same base site as the clicked compound. ESI-MS analysis for the alkyne-modified TOTFOs and AA-TOTFOs can be found in **Appendix B, Table VII-2.**

A

AA-TOTFO1	5′-**X**CTTTCCTTCCCTTCTTTCGCTTTCCTC-3′	28 nt
	5′-ACCGTGGCGAGAAAGGAAGGGAAGAAAGCGAAAGGAGCGG-3′	Tgt.
	3′-TGGCACCGCTCTTTCCTTCCCTTCTTTCGCTTTCCTCGCC-5′	Comp.
AA-TOTFO2	5′-**X**CTTTCC**U**TCCCTTCTTTCGCTTTCCTC-3′	28 nt
	5′-ACCGTGGCGAGAAAGGAAGGGAAGAAAGCGAAAGGAGCGG-3′	Tgt.
	3′-TGGCACCGCTCTTTCCTTCCCTTCTTTCGCTTTCCTCGCC-5′	Comp.
AA-TOTFO3	5′-**X**CTTTCC**U**TCCCT**U**CTTTCGCTTTCCTC-3′	28 nt
	5′-ACCGTGGCGAGAAAGGAAGGGAAGAAAGCGAAAGGAGCGG-3′	Tgt.
	3′-TGGCACCGCTCTTTCCTTCCCTTCTTTCGCTTTCCTCGCC-5′	Comp.
AA-TOTFO4	5′-**X**CTTTCC**U**TCCCT**U**CTTTCGCTT**U**CCTC-3′	28 nt
	5′-ACCGTGGCGAGAAAGGAAGGGAAGAAAGCGAAAGGAGCGG-3′	Tgt.
	3′-TGGCACCGCTCTTTCCTTCCCTTCTTTCGCTTTCCTCGCC-5′	Comp.
AA-TOTFO5	5′-**X**TCCCTCTTTCCGCCTGTCC-3′	20 nt
	5′-CGCTTCCCGAAGGGAGAAAGGCGGACAGGTAT-3′	Tgt.
	3′-GCGAAGGGCTTCCCTCTTTCCGCCTGTCCATA-5′	Comp.
AA-TOTFO6	5′-**X**TCCC**U**CTTTCCGCCTGTCC-3′	20 nt
	5′-CGCTTCCCGAAGGGAGAAAGGCGGACAGGTAT-3′	Tgt.
	3′-GCGAAGGGCTTCCCTCTTTCCGCCTGTCCATA-5′	Comp.
AA-TOTFO7	5′-**X**TCCC**U**CTT**U**CCGCCTGTCC-3′	20 nt
	5′-CGCTTCCCGAAGGGAGAAAGGCGGACAGGTAT-3′	Tgt.
	3′-GCGAAGGGCTTCCCTCTTTCCGCCTGTCCATA-5′	Comp.
AA-TOTFO8	5′-**X**TCCC**U**CTT**U**CCGCCTG**U**CC-3′	20 nt
	5′-CGCTTCCCGAAGGGAGAAAGGCGGACAGGTAT-3′	Tgt.
	3′-GCGAAGGGCTTCCCTCTTTCCGCCTGTCCATA-5′	Comp.

B

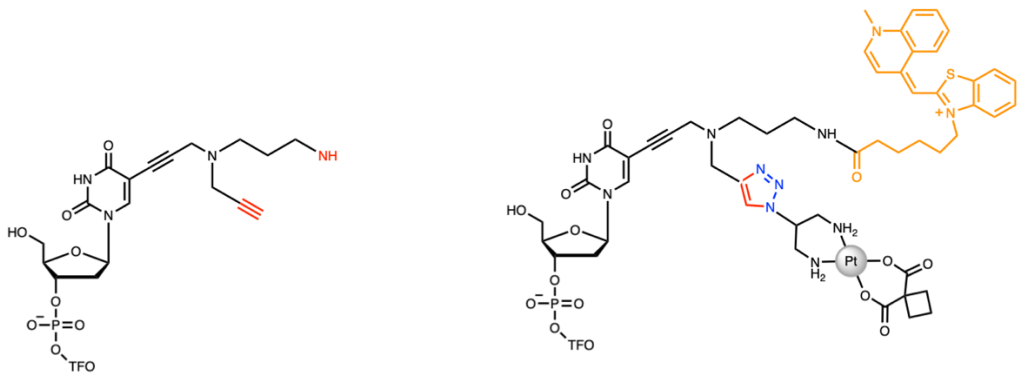

X = AP-C3 alkyne-amine nucleobase **AP-C3 TO-Pt(II) conjugate**

Figure IV-4. A. AA-TOTFO series where X = AP-C3 monomer and U = pdU nucleobase modification. **B.** AP-C3 alkyne-amine monomer and schematic of the nucleobase once conjugated with both TO and N_3-Pt-Carbo.

IV. 2. 4. 3. Click chemistry using CuAAC and SPAAC strategies

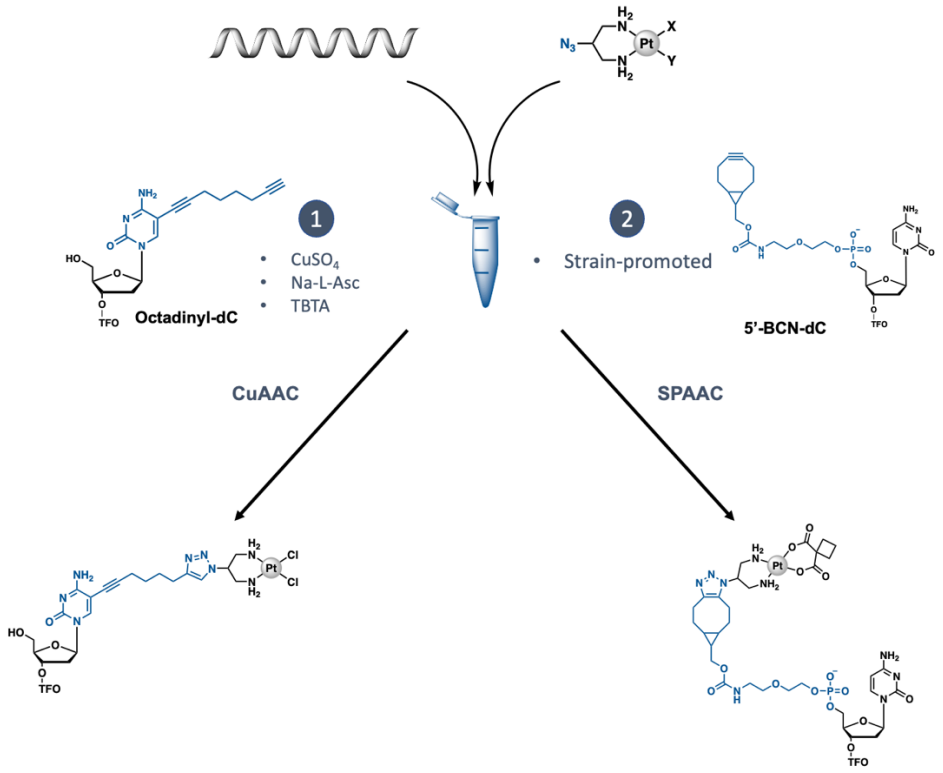

Figure IV-5. Schematic representation of the CuAAC and SPAAC click strategies.

Generation of the cis-platinum(II) TFO hybrids was facilitated through the use of copper-catalysed (CuAAC) and strain promoted alkyne-azide cycloaddition (SPAAC) (**Figure IV-5**). The CuAAC method utilised Cu(II) as a catalyst, which is converted to Cu(I) in situ through the addition of Na-L-ascorbate reductant and further stabilised by the addition of tris((1-benzyl-4-triazoyl)methyl)amine) (TBTA)—a tertiary amine ligand that chelates and stabilises the copper(I) oxidative state while promoting the catalytic cycle. TBTA is soluble in a variety of solvents including both DMSO and DMF which are essential for working with the azide-Pt(II) complexes since they are insoluble in water.

Ethylenediaminetetraacetic acid (EDTA) was added to quench the reaction and to sequester any free copper that may damage the alkyne-modified TFOs or the Pt(II)-TFO hybrids themselves. For click reactions concerning TFO2, which bears a 5'-BCN-dC for SPAAC, similar buffer and incubation conditions were used except with the absence of Cu(II), TBTA and Na-L-ascorbate. Finally, reverse-phase HPLC was used to purify the products prior to redissolution in

water before desalting by elution through NAP-10 columns. Click experiments involving the Pt(II)-phenanthrene derivatives **3** (**Pt-N_3-Phen**) and **8** (**Pt-N_3-DPPZ**) proved ineffective as the solubility of both Pt(II) complexes was poor even in DMSO and DMF. Constant precipitation was observed upon addition of the aqueous alkyne-TFO solution. Furthermore, EDTA sequestration of copper may have led to possible decomposition of the platinum(II)-phenanthrene binding as evidenced by results during HPLC purification attempts and ESI-MS analysis. As such, Pt(II)-TFO hybrids consisting of azide complexes **3** and **8** were not obtained and thus excluded from subsequent experiments. However, TFO-hybrids consisting of these phenanthrene ligands have been generated for potential future applications including coupling with thiazole orange. Similarly, no Pt(II)-TFO hybrids were obtained using TFO6 as analysis after the purification stage revealed numerous click products that could not be separated and exhibited cases of platination of the TFO sequence. Furthermore, it was suspected that self-assembly of this TFO into hairpin or G-quadruplex structures was possible upon observing the HPLC and ESI-MS results. Yields for the click reactions are displayed in **Table IV-1.**

Table IV-1. 5'-dC = 5'-(5)octadinyl-deoxycytidine; **int-dU** = internal-octadinyl-deoxyuridine; **5'-BCN-dC** = 5'-BCN(CEP II)-deoxycytidine; **AP-C3** = alkyne-amine monomer nucleobase; **pdU** = 5-(1-propargylamino)-deoxyuridine; **pdU-TO** = pdU with TO (thiazole orange) coupled; **N_3-Pt(II)-Cis** = *cis*-[Pt(2-azidopropane-1,3-diamine)Cl_2]; **N_3-Pt(II)-Carbo** = *cis*-[Pt(2-azidopropane-1,3-diamine)(CBDCA)]; **N_3-Pt(II)-Oxali** = *cis*-[Pt(2-azidopropane-1,3-diamine)(Oxalate)]; ***** = Yield was not recoverable.

Oligo	Modification	Yield (%)
TFO1-Cis	5'-dC-N_3-Pt(II)-Cis	18.7
TFO1-Carbo	5'-dC-N_3-Pt(II)-Carbo	28.3
TFO1-Oxali	5'-dC-N_3-Pt(II)-Oxali	48.2
TFO2-Cis	5'-BCN-dC-N_3-Pt(II)-Cis	-*
TFO2-Carbo	5'-BCN-dC-N_3-Pt(II)-Carbo	63.5
TFO2-Oxali	5'-BCN-dC-N_3-Pt(II)-Oxali	57.1
TFO3-Cis	Int-dU-N_3-Pt(II)-Cis	34.4
TFO3-Carbo	Int-dU-N_3-Pt(II)-Carbo	35.7
TFO3-Oxali	Int-dU-N_3-Pt(II)-Oxali	49.1
TFO4-Cis	5'-dC-N_3-Pt(II)-Cis	21.0
TFO4-Carbo	5'-dC-N_3-Pt(II)-Carbo	18.1
TFO4-Oxali	5'-dC-N_3-Pt(II)-Oxali	49.5
TFO5-Cis	Int-dU-N_3-Pt(II)-Cis	34.1
TFO5-Carbo	Int-dU-N_3-Pt(II)-Carbo	37.9
TFO5-Oxali	Int-dU-N_3-Pt(II)-Oxali	41.3
TOTFO1-Carbo	5'-dC-N_3-Pt(II)-Carbo pdU-TO (x1)	43.4
TOTFO2-Carbo	5'-dC-N_3-Pt(II)-Carbo pdU-TO (x2)	32.7
TOTFO3-Carbo	5'-dC-N_3-Pt(II)-Carbo pdU-TO (x3)	30.6
TOTFO4-Carbo	5'-dC-N_3-Pt(II)-Carbo pdU-TO (x1)	41.8
TOTFO5-Carbo	5'-dC-N_3-Pt(II)-Carbo pdU-TO (x2)	37.0
TOTFO6-Carbo	5'-dC-N_3-Pt(II)-Carbo pdU-TO (x3)	28.2
AA-TOTOFO1-Carbo	AP-C3-TO (x1), AP-C3-N_3-Pt(II)-Carbo	42.4
AA-TOTOFO2-Carbo	AP-C3-TO (x1), pdU-TO (x1), AP-C3-N_3-Pt(II)-Carbo	31.1
AA-TOTOFO3-Carbo	AP-C3-TO (x1), pdU-TO (x2), AP-C3-N_3-Pt(II)-Carbo	35.5
AA-TOTOFO4-Carbo	AP-C3-TO (x1), pdU-TO (x3), AP-C3-N_3-Pt(II)-Carbo	18.9
AA-TOTOFO5-Carbo	AP-C3-TO (x1), AP-C3-N_3-Pt(II)-Carbo	37.2

AA-TOTOFO6-Carbo	AP-C3-TO (x1), pdU-TO (x1), AP-C3-N_3-Pt(II)-Carbo	34.0
AA-TOTOFO7-Carbo	AP-C3-TO (x1), pdU-TO (x2), AP-C3-N_3-Pt(II)-Carbo	14.8
AA-TOTOFO8-Carbo	AP-C3-TO (x1), pdU-TO (x3), AP-C3-N_3-Pt(II)-Carbo	15.2

IV. 3. Conclusion

A series of azide-functionalised *cis*-platinum(II) complexes based on phenazine scaffolds and traditional *cis*-platinum analogues have been developed and characterised through organic , inorganic and platinum chemistry methods. *cis*-[Pt(2-azidopropane-1,3-diamine)Oxalate] (**16**) has been synthesised and characterised, and represents a novel azide-functionalised Oxaliplatin-like derivative that can undergo click chemistry reactions. Alkyne-TFO sequences targeting specific tracts of the GFP gene have been developed though solid-phase synthesis using the standard phosphoramidite method. Similarly, thiazole-orange labelled alkyne-TFOs have been developed that will allow for investigation into the stabilisation and targeting properties of the conjugated TFO systems. A unique monomeric alkyne-amine nucleobase, AP-C3, has been further incorporated into the TOTFO sequences to create a series of AA-TOTFOs that will form a core part of future studies whereby the introduction of an intercalant onto the same nucleobase as a platinum(II) moiety or AMN is of particular interest. We investigated both CuAAC and SPAAC click chemistry strategies to generate platinum(II) hybrids with the latter displaying higher reaction yields. The use of an ascorbate reductant (required for the CuAAC reaction) may be responsible for lower yields due to unwanted side reaction with both the platinum(II) complex and the TFO probe. The use of strain-promoted azide-alkyne cycloaddition (SPAAC) may therefore offer advantages in the design of future probes offering potential assembly in living systems.[2] This work has demonstrated the development and application of a potential new class of platinum(II)-TFO hybrid. To our knowledge, the use of nucleic acid click chemistry to combine a TFO vector with azide-functionalised *cis*-platinum(II) complexes represents the first example of platinum(II)-TFO hybrids designed in this way

IV. 4. References

1. Zuin Fantoni, N.; McGorman, B.; Molphy, Z.; Singleton, D.; Walsh, S.; El-Sagheer, A. H.; McKee, V.; Brown, T.; Kellett, A., Development of Gene-Targeted Polypyridyl Triplex-Forming Oligonucleotide Hybrids. *ChemBioChem* **2020,** *21* (24), 3563-3574.
2. Sletten, E. M.; Bertozzi, C. R., Bioorthogonal Chemistry: Fishing for Selectivity in a Sea of Functionality. *Angew. Chem. Int. Ed.* **2009,** *48* (38), 6974-6998.

Chapter V

Investigation of *cis*-Platinum(II)-TFO Hybrid Triplex Formation

The work presented in this chapter has been submitted as part of a patent application: Patent application filed for "A cis-platinum(II)-oligomer hybrid". Application number GB2113541.3. (Date filed: 22/09/2021)

Additionally, this chapter was recently accepted for publication as 'A Click Chemistry Approach to Targeted DNA Crosslinking with *cis*-Platinum(II) Modified Triplex Forming Oligonucleotides', Joseph Hennessy, Bríonna McGorman, Zara Molphy, Nicholas P. Farrell, Daniel Singleton, Tom Brown and Andrew Kellett, *Angew. Chem. Int. Ed.* **2021**, *60*, 2-9. DOI: anie.2021110455.

My contribution to this publication was to design and synthesise the series of azide-modified platinum(II) complexes (reported in chapters III and IV). Solid phase synthesis of the oligonucleotides was carried out in collaboration with Dr. Daniel Singleton at ATDBio Ltd. Hybrid generation, complex-DNA binding assays and thermal melting was conducted by me. Preliminary PAGE experiments were conducted in collaboration with Bríonna McGorman.

Cytotoxicity assays were conducted in collaboration with the Apoptosis Research Centre, National University of Ireland Galway, Ireland by Dr. Creina Slator and Dr. Katarzyna Mnich under the supervision of Prof. Afshin Samali and Prof. Adrienne M. Gorman. I would like to acknowledge the technical support provided by Enda O'Connell in the Biosciences Screening Core.

V. 1. Abstract

Limitations of clinical platinum(II) therapeutics consist of abundant systemic toxicity and inherent resistance. Modern approaches therefore seek to deliver active platinum(II) to discrete nucleic acid targets. In the field of antigene therapy, triplex forming oligonucleotides (TFOs) have attracted significant interest for their ability to sequence specifically recognise extended duplex DNA targets. Here, we report a click chemistry-based approach that combines alkyne-modified TFOs with azide-bearing *cis*-platinum(II) complexes—based on cisplatin, oxaliplatin and carboplatin motifs—to generate a library of Pt(II)-TFO hybrids. These constructs can be assembled modularly and enable directed platinum(II) crosslinking to purine nucleobases on the target sequence under the guidance of the TFO probe. By incorporating modifications of thiazole orange—a known DNA intercalating fluorophore—into Pt(II)-TFOs constructs, enhanced target binding and high discrimination between target and *off*-target sequences was achieved. To the best of our knowledge, this is the first example of click chemistry generated platinum(II) nucleic acid hybrids and represents a starting point in the design of a new class of targeted platinum therapy.

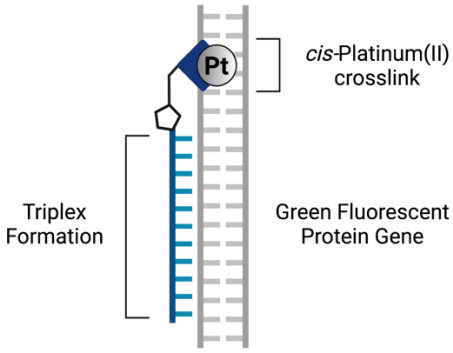

Figure V-1. Representation of the triplex-mediated crosslinking of the GFP gene by *cis*-platinum(II) TFO hybrids.

V. 1. 1. Chapter Aims

- To investigate the DNA binding capabilities of the azide-functionalised *cis*-Pt(II) complexes.

- To investigate the *in vitro* cytotoxicity properties of the azide-functionalised *cis*-Pt(Ii) complexes: Pt-N_3-Cis, Pt-N_3-Carbo, and Pt-N_3-Oxali against recalcitrant breast cancer cell lines MCF-7, T-47D, MDA-MB-231, MDA-MB-468 and MCF-10a.

- To identify the thermal stability of *cis*-Pt(II)-TFO hybrids and their ability to crosslink with dsDNA target sequences.

- To investigate the ability of thiazole orange to stabilise triplex formation and in effect influence crosslink formation.

V. 1. 2. Rationale

Here, a new strategy for the generation of *cis*-platinum(II)-TFO hybrids that possess dsDNA binding and crosslinking activity is presented. Pt(II)-TFO hybrids were generated by conjugating an azide-modified *cis*-platinum(II) chemotype with an alkyne-modified TFO using both the copper catalysed azide-alkyne cycloaddition (CuAAC) and strain promoted azide-alkyne cycloaddition (SPAAC) methodologies (**Figure V-2**). Our group has recently demonstrated how nucleic acid click chemistry can be applied to generate hybrid TFO molecular scissors that afford reliable targeted oxidative cleavage[1, 2] and elegant work by DeRose et al. demonstrated how azide-functionalised Pt(II) complexes can undergo click conjugation with alkyne-fluorophores to enable identification of DNA crosslinking activity and cellular localisation properties.[3]

In the current work, azide groups were incorporated into *cis*-platinum(II) scaffolds to afford suitable handles for click chemistry coupling with alkyne-modified TFOs. In order to maximise crosslinking potential, platinum(II) complexes were designed to be geometrically and structurally similar to clinical agents cisplatin, carboplatin, and oxaliplatin. We targeted purine rich tracts of the

green fluorescent protein (GFP) gene and assessed Pt-TFO hybrid stability and crosslinking through thermal melting studies and native and denaturing PAGE analysis. The use of intercalator thiazole orange (TO) was further employed to develop a Pt(II)-TO-TFO higher order class of hybrid oligonucleotide probe.

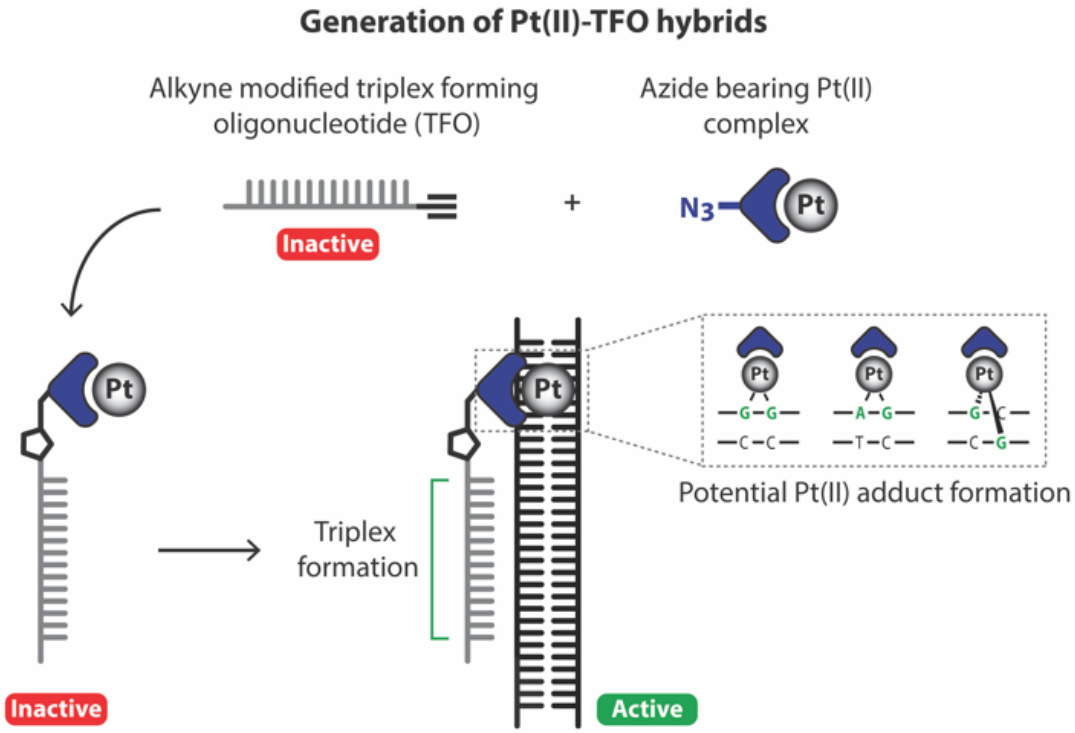

Figure V-2. Overview of *cis*-Pt(II)-TFO hybrid design and application. Development of azide bearing platinum(II) complex prior to click chemistry generation of Pt(II)-TFO hybrids. Triplex formation is obtained through parallel Hoogsteen binding to the target dsDNA. Crosslink formation with the duplex target is facilitated by the triplex formation.

V. 2. Introduction

Therapies that target the downstream inhibition of gene expression are of great current research significance with considerable efforts now dedicated to the discovery of new antisense oligonucleotides (ASOs).[4] The development of nucleic acid probes targeting DNA, such as triplex-forming oligonucleotides (TFOs),[5] offer an alternative strategy whereby gene expression is directly inhibited at the genomic level. Here, we present a click chemistry strategy for the generation of a new class of *cis*-platinum(II)-TFO hybrid biomaterial that possess DNA binding and crosslinking activity. Homopyrimidine TFOs (containing T and C bases only) bind non-covalently in the major groove of duplex DNA to purine target strands through Hoogsteen hydrogen bond formation with AT and GC base pairs producing T-AT and C+-GC parallel triplex motifs.[6] Antiparallel triplexes are also possible whereby homopurine TFOs bind in reverse-Hoogsteen orientation to produce A-AT and G-GC triplets but as their stability is lower compared with parallel motifs, they are not widely adopted.

One of the main challenges confronting the application of TFOs is their binding affinity and *in vitro* and *in vivo* stability.[7, 8] Recent work has therefore focused on enhancing target binding properties to maximise their lifetimes in cellular environments. As part of this effort, the introduction of a covalent crosslinking agent such as psoralen into TFO constructs has showed significant promise (**Figure V-2**).[9, 10] Here, crosslinking is initiated by UV light[11] to produce gene-specific mutations[12] that inhibit transcriptional activity.[13] Alternatively, the use of TFOs as targeting probes that discretely transport platinum(II) crosslinking agents to selected duplex targets has also been explored.[14-17]

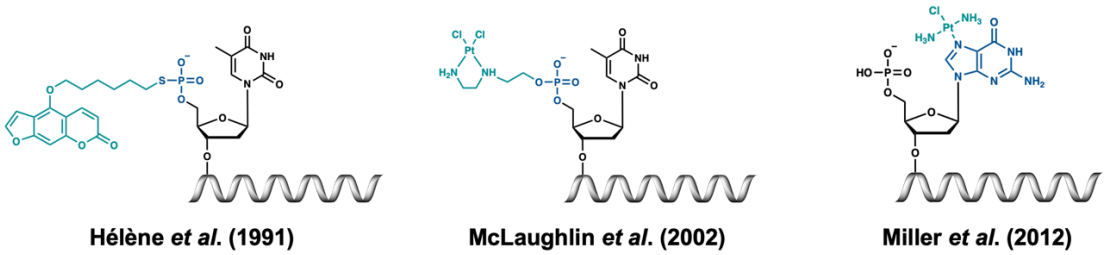

Figure V-3. Recent crosslinking constructs introduced into nucleic acid systems. Psoralen-derivatised constructs (1991),[9] tethered *cis*-platinum(II) units (2002)[18, 19] and mono-functional *trans*-platinum(II) TFO adducts (2012).[20]

Several motifs exist but sustained efforts to coordinate *trans*-Pt(II) complexes—such as *trans*-dichlorodiammineplatinum(II)—to a guanine (mismatch) base within TFO constructs has enabled the generation of mono-functional crosslinking hybrids (**Figure V-1**).[20-24] Here, a single labile trans site on the probe-bound Pt(II) complex is available to crosslink a single purine base on the target duplex. Although monofunctional Pt(II)-TFOs have previously been generated through platinum-derivatised phosphoramidites,[25] and solid-phase synthesis of tethered *trans*-Pt(II) motifs,[26] surprisingly little research has been attempted to extend this concept towards the construction of bifunctional cisplatin(II)-TFO motifs. Further attempts to incorporate platinated nucleotide building blocks into oligonucleotides (ON) using solid-phase synthesis have yielded inactive platinum products[27] although a cis-platinum(II) tethered ON was shown to retain its crosslinking ability and displayed adduct formation against a 25:29 mer target (**Figure V-2**).[18, 19]

From a design perspective, there are notable obstacles that restrict the full potential of existing Pt-TFO hybrid motifs including: i.) *trans*-Pt(II)-TFOs are limited by their need to incorporate a mismatched guanine base to which the *trans*-platinum(II) reagent is coupled; ii.) the geometry of cis-platinum(II) complexes is not optimal for coordinating a DNA base within a TFO probe strand and crosslinking to a specific duplex target; iii.) the rigid design of *trans*-Pt-TFOs means that hybrids have a very narrow target window dependent on the precise purine base location in the target strand; iv.) post-synthetic procedures involving tethered chelators can alleviate rigidity problems but they are not compatible with ONs that contain purine nucleobases; and v.) solid-phase synthetic methods have, to date, been unsuccessful in generating functional Pt(II)-TFOs.

V. 2. 1. Preparation of Azide-Modified *cis*-Platinum(II) Complexes

Azide-modified platinum(II) complexes possessing click chemistry potential while maintaining traditional *cis*-platinum(II) structural properties were developed. Pt(II) complexes *cis*-[Pt(2-azidopropane-1,3-diamine)Cl_2] (**13**, Pt-N_3-Cis), *cis*-[Pt(2-azidopropane-1,3-diamine)(CBDCA)] (**15**, Pt-N_3-Carbo, CBDCA = cyclobutene-1,1-dicarboxylate) and *cis*-[Pt(2-azidopropane-1,3-diamine)(Oxalate) (**16**,Pt-N_3-Oxali) were generated according to **III. 1. 3**. 2-Azidopropane-1,3-diamine hydrochloride (**12**) was selected as a suitable bidentate ligand scaffold as it has been previously shown to be an efficient chelator for platinum while maintaining excellent click orthogonality.[3] Although **13** and **15** have previously been reported in the development of diazenecarboxamide-extended conjugates,[28, 29] **13** in the identification of platinum cellular protein targets[30] and **15** further afield in mitochondrial localisation[31] and clicked estrogen-hybrid generation,[32] this concept is extended to the oxaliplatin-like derivative **16** to our knowledge, not yet been reported. Additionally, no work has yet been performed to construct gene-targeting hybrids involving azide-Pt(II) and alkyne-modified TFOs. All three target complexes were accessed through a common ligand di-*tert*-boc-2-hydroxy-1,3-diaminopropane which was obtained in excellent yields (**12**, 93%) and allowed facile handling in subsequent reactions. Pt-N_3-Cis (**5**) was obtained through the treatment of **12** with *cis*-[$PtCl_2(DMSO)_2$] in the presence of DBU in darkness (**III. 1. 3. (13)**). In order to obtain **15** and **16**, K_2PtI_4 (generated via K_2PtCl_4) was treated with **4** and substituted with either cyclobutene-1,1-dicarboxylic acid (CBDCA) or sodium oxalate to afford Pt-N_3-Carbo (**15**) or Pt-N_3-Oxali (**16**) in moderate (36%) or high (72%) respective yields (**III. 1. 3. (15 and 16)**). The complexes were characterised by ^{1}H, ^{13}C, and ^{195}Pt multinuclear NMR, FTIR, and ESI-MS.

A range of ONs targeting a specific location of GFP plasmid DNA were selected. These TFOs were designed to incorporate alkyne-modified bases for functionalisation through click chemistry with azide-modified *cis*-platinum(II) complexes. The design of the TFOs included several considerations that have previously demonstrated effective triplex formation including: i.) TFOs were

generated as homopyrimidine oligomers to afford effective Hoogsteen base recognition of the target duplex; ii.) a low number of triplet inversions and mismatches were included to prevent destabilization; and iii.) the number of consecutive C^+-GC triplets was minimized to avoid electronic repulsion reducing their stabilities at low pH. Pt(II)-TFOs hybrids were generated by clicking Pt-N_3-Cis (**13**), Pt-N_3-Carbo (**15**), or Pt-N_3-Oxali (**16**) to the alkyne modified TFOs (**Figure V-4**) as described in **III 2. 1. 1**. A library of five TFOs were developed that were between 21-29 nt in length (**Figure V-4, B**). To investigate the effectiveness of platinum crosslinking and triplex stability, terminal modified 5' (TFO1, 2, and 4), internal alkyne modifications (TFO3 and 5), base modifications of 5'-(5)octadinyl-deoxycytidine (TFO1 and 4), and internal-octadinyl-deoxyuridine (TFO3 and 5) and 5'-bicyclo[6.1.0]nonyne-deoxycytidine (5'-BCN(CEP II)-dC) were employed (TFO2) (**Figure V-4, B**). Triplexes formed by TFO1, 2, and 3 contained a single G-CG inversion whereas TFO4 and 5 contained two G-CG inversion sites. Three target duplexes were synthesised corresponding to the recognition elements of the GFP gene with an eight-nucleobase overhang introduced on the 5' side and a three-nucleotide overhang on the 3' side of the target purine sequence. These overhangs were designed to facilitate possible crosslinking activity and harbor numerous GG and/or AG steps—the preferred purine tract for traditional *cis*-platinum(II) adduct formation. Additionally, for use in PAGE experiments, a 57 bp duplex target possessing the same recognition region as Duplex A was generated. TFOs containing either octadinyl-dC (TFO1 and 4) or octadinyl-dU (TFO3 and 5) were clicked using the CuAAC method while TFO2, containing the 5'-BCN(CEP-II)-dC, was generated following a SPAAC protocol (**IV 1. 1.**).

A

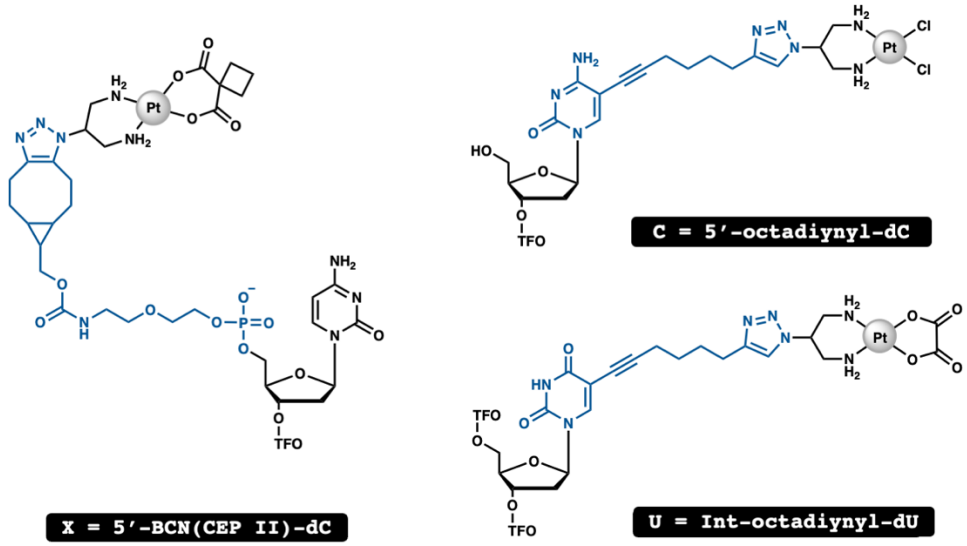

B

```
TFO1                5′-CTCTTTCCTTCCCTTCTTTCGCTTTCCTC-3′          29 b
          5′-ACCGTGGCGAGAAAGGAAGGGAAGAAAGCGAAAGGAGCGG-3′        Tgt.
          3′-TGGCACCGCTCTTTCCTTCCCTTCTTTCGCTTTCCTCGCC-5′        Comp.

TFO2                5′-XTCTTTCCTTCCCTTCTTTCGCTTTCCTC-3′          29 b
          5′-ACCGTGGCGAGAAAGGAAGGGAAGAAAGCGAAAGGAGCGG-3′        Tgt.
          3′-TGGCACCGCTCTTTCCTTCCCTTCTTTCGCTTTCCTCGCC-5′        Comp.

TFO3                5′-CTCTTTCCTTCCCTTCTTTCGCTTUCCTC-3′          29 b
          5′-ACCGTGGCGAGAAAGGAAGGGAAGAAAGCGAAAGGAGCGG-3′        Tgt.
          3′-TGGCACCGCTCTTTCCTTCCCTTCTTTCGCTTTCCTCGCC-5′        Comp.

TFO4                5′-CTTCCCTCTTTCCGCCTGTCC-3′                  21 b
          5′-CGCTTCCCGAAGGGAGAAAGGCGGACAGGTAT-3′                Tgt.
          3′-GCGAAGGGCTTCCCTCTTTCCGCCTGTCCATA-5′                Comp.

TFO5                5′-CTTCCCTCTTUCCGCCTGTCC-3′                  21 b
          5′-CGCTTCCCGAAGGGAGAAAGGCGGACAGGTAT-3′                Tgt.
          3′-GCGAAGGGCTTCCCTCTTTCCGCCTGTCCATA-5′                Comp.

57bp duplex
     5′-AAGCCGGCGAACGTGGCGAGAAAGGAAGGGAAGAAAGCGAAAGGAGCGGGCGCTAGG-3   Tgt.
     3′-TTCGGCCGCTTGCACCGCTCTTTCCTTCCCTTCTTTCGCTTTCCTCGCCCGCGATCC-5′  Comp.
```

Figure V-4. A. Alkyne-modified nucleobases. Click combination with each of the azide-functionalised platinum(II) complexes. **B**. TFO sequences with nucleobases modifications denoted and specific recognition sites indicated within the respective duplex target.

V. 2. 2. DNA Binding Ability of N_3-Pt(II) Complexes

The binding ability of the azide-functionalised *cis*-platinum(II) complexes Pt-N_3-Cis, Pt-N_3-Carbo and Pt-N_3-Oxali was investigated against target dsDNA sequences that would also serve as the target GFP tracts for future triplex formation (**Figure V-5, A**). Thermal melting was chosen as the technique to identify any changes in the thermal stability of the underlying duplex targets. Thermal melting is a biophysical technique that provides a simple qualitative demonstration of DNA binding and is key to investigate the interaction between a compound and a nucleic acid. In general, the technique is widely used to identify the increase in melting temperature of nucleic acids upon interaction with the molecule.[33, 34] However, thermal melting can also be used to identify the destabilising nature of certain small molecules such as alkylating agents and also platinum complexes that bind through adduct formation.[35]

Nucleic acids display high absorbance at and around 260 nm and this signal can change significantly when the secondary DNA structure denatures or reconfigures.[36] The melting temperature (T_M) relates to the equilibrium temperature where half of the sample is in its folded or associated form and half is unfolded or disassociated. Determination of the first derivative of this temperature midpoint yields the melting T_M value of the nucleic acid sample. Generally, consideration needs to be given to the choice of thermal melting buffer. Cacodylate (pKa 6.14 at 25 ºC) and acetate (pKa 4.62 at 25 ºC) are accepted as appropriate buffers to use for neutral or slightly acidic pH experiments as they are temperature independent. Phosphate buffer is considered acceptable, but less optimal, due to a slight temperature dependent pKa of 6.81 at 25 ºC.[37] Prior to triplex formation studies, thermal melting analysis was performed to investigate the binding interaction between the azide-functionalised *cis*-platinum(II) complexes and duplex target sequences from the GFP gene (**Figure V-5, A**). Melting experiments were performed under physiological conditions (10 mM phosphate, 150 mM NaCl and 2 mM $MgCl_2$, pH 6). Native duplex melting temperatures were compared to those treated with the *cis*-platinum(II) complexes over 48 h (**Figure V-5, B).**

A

Target A
5′-ACCGTGGCGAGAAAGGAAGGGAAGAAAGCGAAAGGAGCGG-3′
3′-TGGCACCGCTCTTTCCTTCCCTTCTTTCGCTTTCCTCGCC-5′

Target B
5′-CGCTTCCCGAAGGGAGAAAGGCGGACAGGTAT-3′
3′-GCGAAGGGCTTCCCTCTTTCCGCCTGTCCATA-5′

Target C
5′-CCGTGGCGAGAAAGGAAGGGAAGAAAGCGAAAGGA-3′
3′-GGCACCGCTCTTTCCTTCCCTTCTTTCGCTTTCCT-5′

B

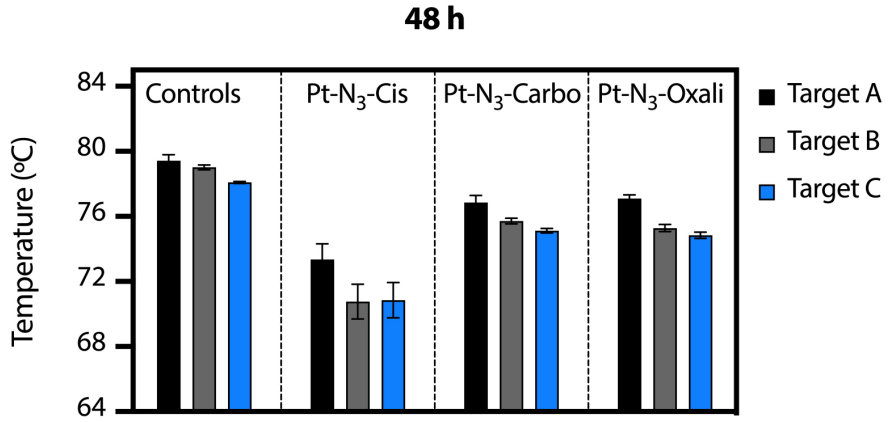

C

Oligo	T_M (°C)	ΔT_M (°C) +Pt-N_3-Cis	ΔT_M (°C) +Pt-N_3-Carbo	ΔT_M (°C) +Pt-N_3-Oxali
Target A	79.4 ± 0.4	-6.0	-2.5	-2.3
Target B	79.0 ± 0.2	-5.6	-3.3	-3.7
Target C	78.1 ± 0.1	-7.2	-3.0	-3.3

Figure V-5. A. dsDNA sequences of the GFP gene with triplex recognition site in red. **B.** ΔT_M of target dsDNA sequences treated with 2.5 eq. of azide-functionalised platinum(II) complexes. **C.** Specific T_M values for duplex sequences when treated with Pt-N_3-Cis, Pt-N_3-Carbo or Pt-N_3-Oxali respectively over 48 h.

All complexes destabilised the melting transition of the target duplexes to varying extents. Pt-N_3-Cis was found to have the greatest destabilising effect with decreases of between 5.6-7.2 °C observed. Pt-N_3-Oxali and Pt-N_3-Carbo also reduced the melting temperatures of all three targets but had notably lower destabilising effects compared with Pt-N_3-Cis. The observed thermal destabilisation effects can be ascribed to the binding of the *cis*-platinum(II) agents followed by kinking or conformational disruption of the duplex.[38] Similarly, the greater activity of Pt-N_3-Cis relative to both Pt-N_3-Carbo and Pt-N_3-Oxali is in line with observations of the crosslinking effects of these clinical agents (**Appendix C, Table VIII-3 and Figure VIII-101**).[39]

Interestingly, ΔT_M changes are roughly similar after 24 h incubation in comparison to 48 h, save a few melting profiles (**Appendix C, Table VIII-4**). Only **Pt-N_3-Cis-Target C** and **Pt-N_3-Oxali-Target B/C** exhibit larger decreases in ΔT_M in comparison to the 24 h incubation. This may be due to inactivation of the Pt(II) species after a certain period of time in solution as it appears the greatest extent of adduct formation is produced before 48 h. Regardless, these results show that target duplex stability is negatively impacted by the presence of the N_3-Pt(II) species and that the azide moiety has little interference with the complexes ability to interact with dsDNA.

V. 2. 3. *In-vitro* cytotoxicity analysis

With the ability of the azide-functionalised complexes to target dsDNA now known, it was decided to investigate their cytotoxicity profiles against a range of breast cancer cell lines and to identify whether the complexes by themselves may represent an interesting class of agents that could have potential as anticancer drugs. Recalcitrant breast cancer cell lines MCF-7, T-47D, MDA-MB-231, MDA-MB-468 and an immortalised non-tumorigenic cell line MCF-10a that display intrinsic resistance properties were exposed to cisplatin, 1,10-phenanthroline and NaCl controls and Pt-N_3-Cis, Pt-N_3-Carbo and Pt-N_3-Oxali at concentrations of 1-100 μM with cell viability and IC_{50} values determined over 24 and 48 h**,** whereby IC_{50} values are the quantitative measure of how much drug is required to inhibit cell growth by 50% (**Appendix D, Table VIII-8**). Stock solutions were prepared in 0.9% saline (w/v) with further dilutions prepared fresh in culture media. Cisplatin is still a mainstay choice in the treatment of a multitude of cancers[40, 41] whereas 1,10-phen[42] and derivatives[43, 44] have demonstrated effective anticancer properties against a number of cell lines that display cisplatin resistance. Cisplatin, unsurprisingly, exhibited greater activity against the cell lines in comparison to the N_3-platinum(II) complexes. Compared to a cisplatin control (IC_{50} = 18.5 μM), Pt-N_3-Cis displayed lower inhibition of proliferation in MCF-7 cells (IC_{50} = 51.3 μM). Pt-N_3-Carbo and Pt-N_3-Oxali were inactive across all cell lines except MDA-MB-468 where Pt-N_3-Oxali was observed to have moderate activity (IC_{50} = 20.6 μM) after 48 h. None of the complexes displayed activity against MDA-MB-231 cells at concentrations below 50 μM and the only

complex that was active is Pt-N_3-Cis after 48 h of incubation (IC_{50} = 61.7 μM). It should be noted that cell viability is quite similar for cisplatin (IC_{50} = 3.5 μM) and Pt-N_3-Cis (IC_{50} = 11.4 μM) after 48 h in MDA-MB-468 cells. whereas poor activity was identified by both after 24 h in the T-47D cell line at low concentrations and only present activity after 48 h. IC_{50} values were recorded for complexes treated against MCF-10a cells in comparison to cisplatin (IC_{50} = 25.1 μM) (**Table V-1**).

Table V-1. IC_{50} values determined for breast cancer cell lines treated over 48 h.

IC_{50} (μM)	**24 h**				**48 h**			
Cell Line	Cisplatin	Pt-N_3-Cis	Pt-N_3-Carbo	Pt-N_3-Oxali	Cisplatin	Pt-N_3-Cis	Pt-N_3-Carbo	Pt-N_3-Oxali
MCF-7	40.3	82.4	>100	>100	18.5	51.3	>100	>100
MDA-MB-231	>100	>100	>100	>100	61.7	>100	>100	>100
MDA-MB-468	22.2	45.1	>100	86.1	3.5	11.4	65.4	20.6
T47D	>100	>100	>100	>100	40.7	50.4	>100	>100
MCF-10a	56.1	>100	>100	>100	25.1	88.2	>100	>100

It is well known that the character of the non-leaving group ligands play a significant role in the nature of the platinum lesions created and the subsequent response from cellular repair mechanisms.[45] From this perspective, it is not surprising that in cell lines were cisplatin produces a cytotoxic effect, activity was also observed for Pt-N_3-Cis. The cell viability dose-response plots can be found in **Appendix D**, **Figure VIII-106**.

Overall, it can be reliably stated that the azide moiety appears to impact the activity of the complex somewhat though not enough to completely inactivate the molecule. Extending from this, it is not surprising that both Pt-N_3-Carbo and Pt-N_3-Oxali were less active since the kinetic rates of aquation of the respective labile ligands are recognised to alter their activity profiles. These results also show that addition of an azide moiety does not completely eliminate the anticancer profile of these platinum(II) derivatives and may afford opportunities to retain the antineoplastic character whilst affording the ability to conjugate

molecules such as fluorophores[46] or other targeting moieties that could enhance investigations in areas such as cellular transportation and localisation.[47] The use of guiding nucleic acid vectors thus represents a viable alternative to deliver *cis*-platinum(II) agents in an efficient manner that retains the targeting profile of the platinum itself alongside the possibility to modulate the transportation and accumulation properties.

V. 2. 4. Triplex Formation by Pt(II)-TFO hybrids

Triplex formation was investigated using UV thermal melting and analysis was performed in 10 mM phosphate, 150 mM NaCl, and 2 mM $MgCl_2$ at pH 6. Alkyne- and Pt(II)-TFOs were incubated for 24 and 48 h in triplex buffer. Triplex melting profiles were recorded for all the alkyne-modified TFOs other than TFO4—a 21 nt terminal octadinyl-dC—which melted below 12 °C. No differences were found in the melting profiles of the alkyne-TFOs over 24 and 48 h incubation periods. Melting analysis of Pt(II)-TFO hybrids resulted in pronounced results after 48 h of continuous incubation. Firstly, not all Pt(II) hybrids were capable of triplex formation including TFO1-Cis, TFO2-Cis, TFO4-Cis, and TFO5-Cis indicating the cisplatin-type moiety, in the majority of cases, precludes triplex formation. TFO3-Cis was identified to form a DNA triplex after 24 h and the melting temperature was significantly lower than the control alkyne-TFO3. By 48 h, the melting temperature difference enhanced with TFO3-Cis melting at 42.6 °C in comparison to 52.0 °C for the alkyne-TFO3 (ΔT_M = -9.4 °C) (**Figure V-6, A**). Unlike the TFO-Cis family, Pt-N_3-Carbo and Pt-N_3-Oxali hybrids did not inhibition triplex formation but their melting temperatures were reduced compared to the alkyne-TFO controls (**Appendix C, Table VIII-7**). Here, destabilisation was less pronounced than triplex-forming N_3-Cis hybrids although it was still substantial compared to the respective controls. Overall, the destabilisation induced by Pt(II)-TFO hybrids alludes to potential crosslinking interactions between the platinum(II) ion and the target duplex since destabilisation is a key feature of platinum(II) crosslinking identified in earlier experiments (**Figure V-5, C**).

A

Oligo	T_M (°C)	ΔT_M (°C)
Alkyne-TFO3	52.0 ± 0.1	0
TFO3-Cis	42.6 ± 0.5	-9.4
TFO3-Oxali	44.1 ± 0.6	-7.9
TFO3-Carbo	45.5 ± 0.5	-6.5
TOTFO1-Carbo	57.2 ± 0.7	5.2
TOTFO2-Carbo	> 65	>13

B

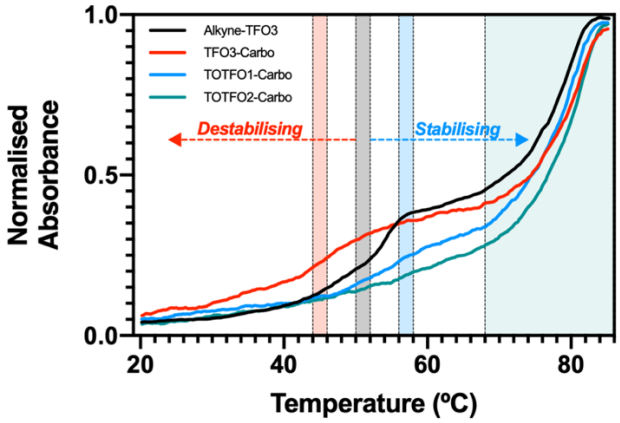

Figure V-6. A. T_M values of triplex melting observed for TFO3 and TOTFO hybrids. **B.** Thermal melting isotherms showing destabilising and stabilising effects in comparison to alkyne-modified TFO3. Key: ● = TFO3-Carbo; ● = Alkyne-TFO3; ● = TOTFO1-Carbo; and ● = TOTFO2-Carbo represent the respective mid-points of the triplex transitions.

To overcome stability limitations associated with Pt(II)-TFOs, TO-modified constructs were developed with carboplatin-type derivatives. TO-TFOs have previously demonstrated an ability to significantly enhance triplex stability[48] through intercalation within the major groove of duplex targets—particularly the TO_{B6} modification. Here, TFO hybrids were designed to incorporate both a carboplatin moiety and TO_{B6} modifications. Prior to click conjugation with N_3-Pt-Carbo, TO_{B6} was coupled to propargylamino dU (pdU) nucleobases as increased base stacking from the pdU triple bond has been shown to further improve triplex stabilisation.[49] TOTFO1-Carbo, containing a single TO modification, displayed increased triplex stability (ΔT_M = +5.2 ºC) compared to the alkyne-TFO3 (**Figure V-6, A**). Significantly, triplex stability increased by +11.7 ºC compared to TFO3-Carbo demonstrating that Pt(II)-TFO triplex formation can be stabilised by the addition of a single TO unit. TOTFO2-Carbo, which incorporates two TO_{B6} units, was then identified to push triplex melting to a similar temperature as the underlying duplex transition (**Figure V-6, B**) with PAGE analysis confirming combined triplex formation and fluorescence emission by the TO_{B6} units (**Appendix E, Figure VIII-109**).

V. 2. 5. PAGE analysis of Pt(II)-hybrids

Polyacrylamide gel electrophoresis is a commonly used technique employed for the separation of nucleic sequences. Once a charge is applied, biomolecules will migrate through the gel system with velocities determined by their charge and the strength of the electric field applied. The nature and composition of the polyacrylamide matrix and buffer system are vital to the separation of the substrates. Generally, in native PAGE, the size and conformation of the nucleic acid is responsible for the resultant mobility achieved on the gel.[50] With regards denaturing PAGE analysis, only the size of the molecule is responsible for the separation characteristics as the reagents present ensure that all nucleic acid molecules are found in a single denatured form.[51] The concentration of the acrylamide and the acrylamide:bisacrylamide ratio are the main determinants of the system pore size. As acrylamide concentration increases, pore size decreases. The pore size is directly responsible for the separation properties of the gel.[52]

PAGE analysis is an effective method of separation for triplex systems. Triplex constructs are distinctly larger and structurally unique compared to dsDNA sequences and therefore are relatively easy to separate by PAGE. Additionally, the extent of triplex formation can be visually determined as the degradation of duplex substrate and formation of the triplex constructs are quite evident using post-staining techniques. In turn, denaturing PAGE is an effective technique for the determination of crosslinked nucleic acid structures. It has been demonstrated recently that crosslinking a platinum(II)-TFO hybrid to a dsDNA duplex target will afford an adduct with either the purine or pyrimidine strand.[19] Denaturing conditions have been employed to successfully separate the non-bound sequence as the migration properties are distinctly different to those of the crosslinked tract.[22] This method allows for the identification of the precise sequence selectivity of the hybrid when presented with multiple adduct opportunities.

V. 2. 5. 1. Alkyne TFO triplex formation

To further supplement the results from the thermal melting analysis, the alkyne-TFO controls were investigated for triplex formation by native PAGE electrophoresis against the duplex GFP targets (**Appendix B, Table VIII-1**). Duplex target (1 pmol) was treated with increasing concentrations of alkyne-TFO whereby triplex formation was observed for TFO1-3. Notably, TFO2 triplex formation appears to be controlled by the stoichiometric ratio of TFO whereas TFO1 and TFO3 display full triplex formation at the lowest loading concentration. The discrepancy may be due to the steric bulk of the BCN alkyne handle of TFO2 and it is possible that triplex formation is hindered by this (**Figure V-7, B**). Under the experimental conditions, TFO4-6 failed to demonstrate triplex formation which correlates with the thermal melting results from before. TFO6 did not form a triplex and thus did not present thermal melting data (**Appendix C, Table VIII-7).**

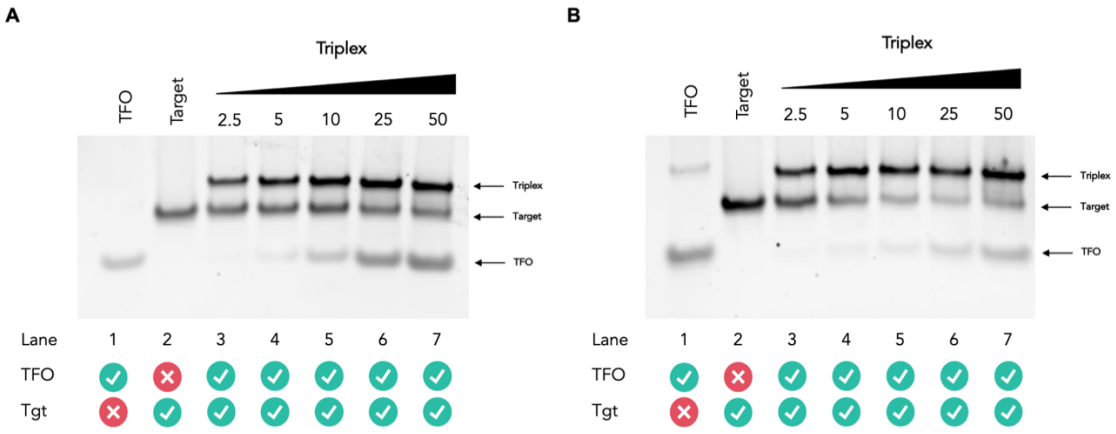

Figure V-7. A. Triplex formation for TFO1. Duplex A (1 pmol, lane 2-7) was treated with increasing concentration of TFO1 (2.5-50 eq., lane 3-7). **B.** Triplex formation for TFO2 with similar parameters. Triplex formation is only fully achieved after introduction of approx. 10-25 eq. of TFO (lane 5-6) in comparison to **A.** Samples were prepared in 10 mM phosphate buffer, 150 mM NaCl and 2 mM $MgCl_2$ (pH 6) and incubated over 48 h at 37 ºC, loaded onto 20 % PAGE and subjected to electrophoresis for 4 h at 70 V in 50 mM tris-acetate (TA) buffer (pH 6). Gels were post-stained with SybrGold.

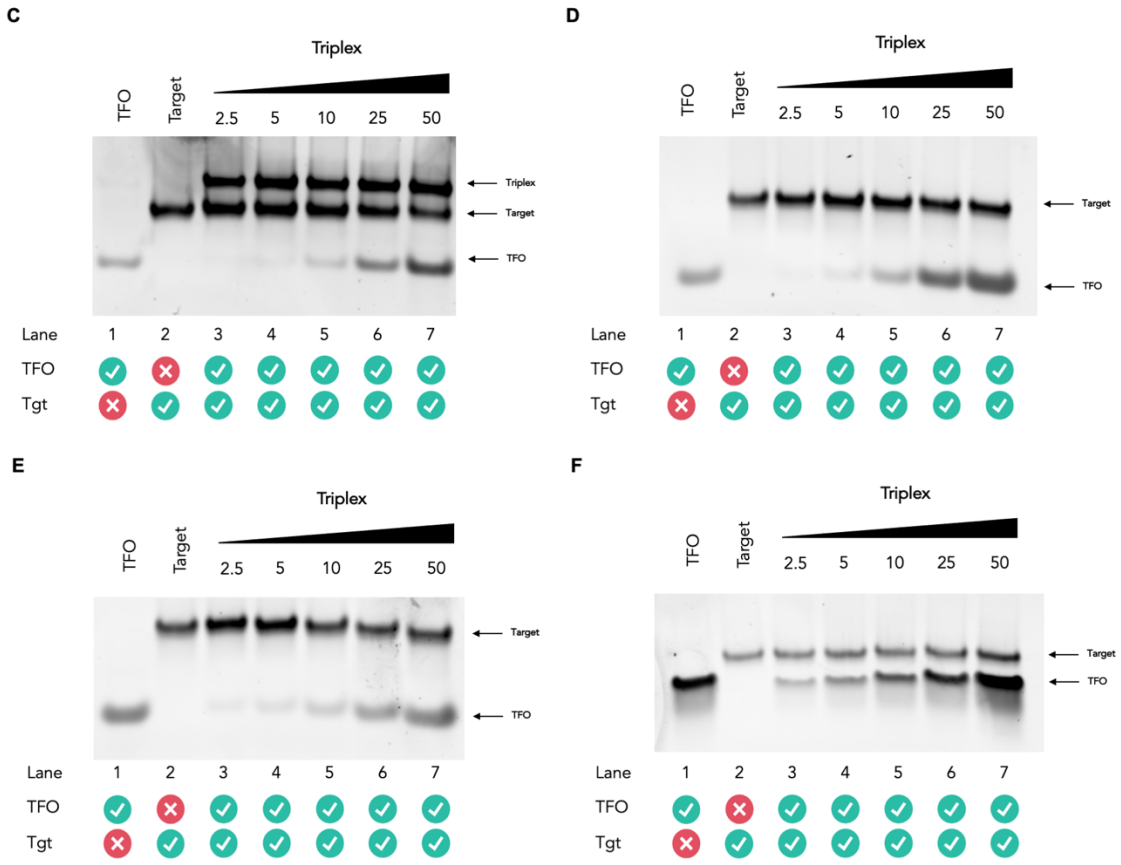

Figure V-8. C. Triplex formation for TFO3. Full triplex formation with duplex A (1pmol, lane 2-7) is demonstrated after first stoichiometric loading step (2.5 eq., lane 3). **D-F.** Triplex formation for TFO4, TFO5 and TFO6 respectively. No triplex formation was observed under the PAGE conditions. Conditions and sample preparation was performed as described before (Figure V-7).

As an additional control to identify any unwarranted specificity problems for Triplex recognition, alkyne- TFO2 and TFO3 were further treated against a 57 bp target and a 40 bp *off*-target (**Figure V-9**). TFO2 and 3 were chosen as they are the control analogues for the *cis*-platinum(II)-TFO hybrids that displayed the greatest thermal instability. TFO2 and TF3 displayed no affinity for the 40 bp *off*-target and notably, TFO2 demonstrated full triplex formation at much lower loadings (**Figure V-9, A, lane 4**) in comparison to the triplex formation displayed previously when treated against the 40 bp target (**Figure V-7, B**).

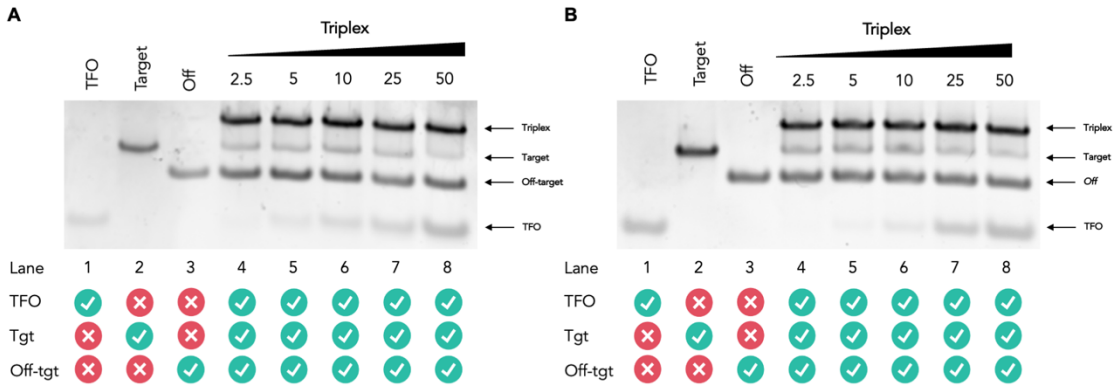

Figure V-9. A. Triplex formation for TFO2 treated against both a 57 bp target (1 pmol, lane 2, 4-8) and a 40 bp *off*-target (1 pmol, lane 3, 4-8). Increasing stoichiometric ratios of TFO2 was introduced (2.5-50 eq., lane 4-8) and samples incubated over 48 h. **B.** Triplex formation for TFO3 under similar parameters. Neither TFO2 or TFO3 displayed any specificity for the *off*-target. Sample preparation and PAGE conditions were as before.

As hybrids of TFO3 displayed the greatest thermal destabilisation upon triplex formation, these constructs were investigated for crosslinking activity. Triplex formation was performed in the presence of a 57 bp target duplex and an *off*-target 40 bp duplex sequence (**Figure V-10**). The *off*-target sequence retains numerous GG and AG base steps to encourage adduct formation, however, it does not possess the triplex recognition site. Target and *off*-target were mixed together in triplex buffer in a 1:1 ratio (1 pmol each) prior to the introduction of increasing concentrations of the hybrid (2.5 – 50 eq., **Figure V-10**, Lanes 6-10) and incubated at 37 ºC for 48 h. Evidence of concentration-dependent triplex formation can be seen in all three of the sample treated experiments while, notably, no diminishment of *off*-target duplex was observed. The ablation of target duplex can be seen as triplex formation increases and this reduction coincides with the respective thermal destabilising capabilities of the hybrids whereby TFO3-Carbo triplex formation occurs at the lowest loading (**Figure V-10, C, lane 6**), followed thereafter by TFO3-Oxali and TFO3-Cis. Significantly, TFO3-Cis and TFO3-Oxali (**Figure V-10, B, lane 6-10** and **D, lane 6-10**) displayed higher order triplex banding patterns compared to the alkyne-TFO (lane 5) indicating a variety of crosslinked triplexes have formed. Taken together, it is likely that the most active hybrid, TFO3-Carbo, forms one predominant crosslink with the target duplex while the Cis and Oxali derivatives form a variety of adducts. These observations are also seen at lower TFO loadings (**Appendix**

E, Figure VIII-108). Similarly TFO2-Carbo is also observed to form only one predominant crosslink structure (**Appendix E, Figure VIII-107**).

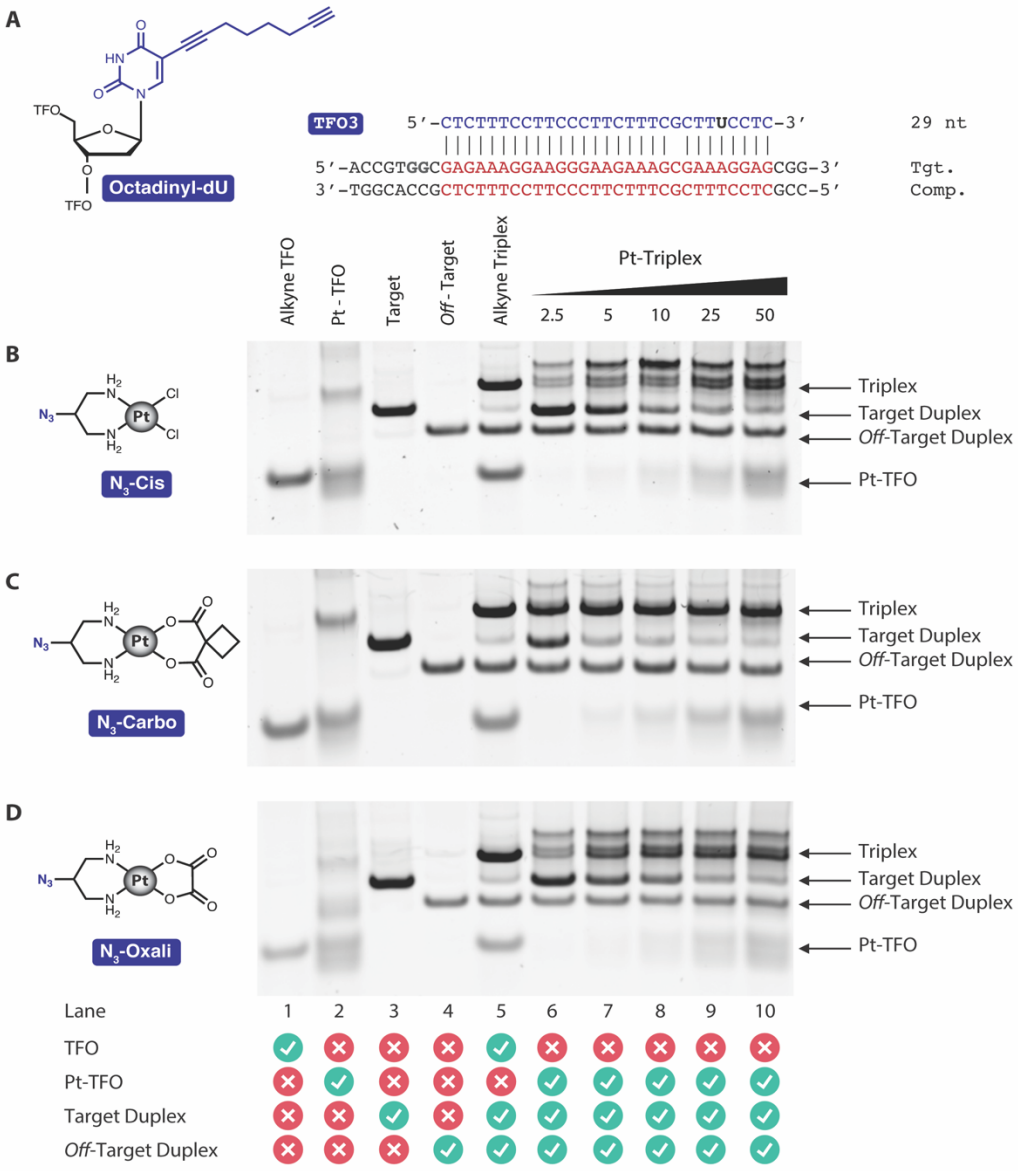

Figure V-10. A. TFO3 with modified internal octadinyl-dU nucleobase and respective GFP target sequence. **B.** TFO3-Cis hybrid triplex formation with higher band structures observable. **C.** TFO3-Carbo hybrid. Triplex formation is significant even at lower loadings. **D.** TFO3-Oxali hybrid with higher band triplex formation – slower rate of triplex formation in comparison with TFO3-Carbo.

In order to elucidate the crosslinking activity of the Pt(II)-TFO hybrids further, PAGE analysis was performed with the added treatment of sodium cyanide. The cyanido anion CN^- exercises a strong *trans* effect and is known to form the extremely stable $[Pt(CN)_4]^{2-}$ anion upon reaction with almost all platinum(II) species that contain N or O donor atoms.[53]. As a strong ligand for

platinum, cyanide is capable of displacing covalent bonds that platinum(II) species form with DNA therefore it is possible to remove a Pt(II) adduct from the N7 position of guanine nucleobases.[54] Treatment of crosslinked DNA with a NaCN solution results in a return to the native state for the target duplex sequence.

Prior to verifying crosslinking between Pt(II)-TFO hybrids and the duplex target, optimisation was performed to identify the extent of triplex reversal by cyanide treatment (**Appendix E, Figure VIII-110**). Alkyne-TFO3 (50 pmol) was incubated with target duplex 3 (D3; 1 pmol) (**Figure V-11, A**) over 48 h in triplex buffer prior to the addition of up to 25,000 eq. of NaCN to identify its effect on triplex formation (**Figure V-11, B**). The probe used in this study (D3) is a 40 bp target sequence with a 6-FAM fluorescent tag located at the 5' terminus of the purine strand and a Cy5 fluorescent tag adjoined to the 5' terminus of the complementary pyrimidine strand and contains the TFO binding region. At the higher loading of NaCN (>10,000 eq.), triplex stability was demonstrably affected with progressive triplex depletion and reformation of the duplex notable (**Figure V-11, B, lanes 3-6**). Treating D3 with TFO3-Cis (2.5-50 eq.) in the absence of NaCN revealed crosslinking activity with a banding pattern indicative of multiple higher-order triplex structures (**Figure V-11, C, lanes 2-4**). Upon treatment with NaCN (5,000 eq.) complete reversal of TFO-Cis crosslinking and triplex formation was observed (**Figure V-11, C, lanes 6-8**). Comparison of this result with the unmodified alkyne-TFO3 control under identical conditions (**Figure V-11, B, lane 4**) provides strong evidence of crosslinking activity by the hybrid.

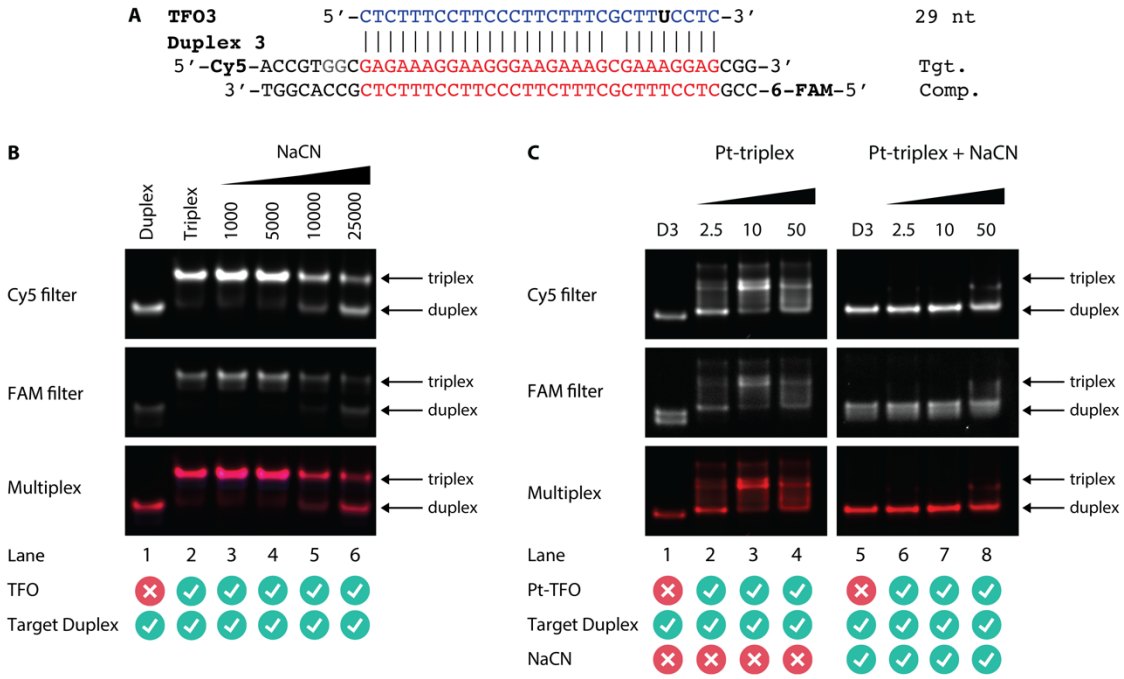

Figure V-11. A. TFO3-Cis hybrid and fluorescently labelled Duplex 3. **B.** NaCN treatment of unmodified triplex system. **C.** NaCN (5,000 eq.) afforded reversal of Pt-triplex system formed by TFO3-Cis hybrid.

Since triplex-mediated crosslinking activity has been established, further analysis of sequence-specific binding was examined using denaturing PAGE experiments outlined in **Figure V-12**. Here, 17 mer alkyne-TFO sequences were designed and clicked to the Pt-N_3-Carbo complex (**Figure V-12, B**). TFOs were designed to incorporate 5'-, 3'-, and internal alkyne base modifications (**Figure V-12, C**). A duplex target consisting of a 21 nt purine sequence with a Cy-5 fluorescent label at the 5'-terminus, and a 17 nt pyrimidine complementary strand labelled with a 6-FAM fluorophore was employed. Similarly, a duplex target consisting of complimentary 21 mer strands was employed, however, the denaturing of this duplex sequence proved to be ineffective. The target duplexes (21:17D and 21:21D) (1 pmol) were treated with 50 eq. of each hybrid and incubated for at least 48h at 37 ºC. Denaturing PAGE identified crosslinking with only the purine strand of the target duplex as verified by Cy-5 filter emission for terminally modified TFO-17A-Carbo and TFO-17B-Carbo (**Figure V-12, D**). TFO-17C Carbo did not display any crosslink activity and this may be due to the centrally located alkyne modification site. Thus, in the case of shorter Pt(II)-TFO hybrids, it appears that terminal modifications are required for appropriate crosslinking activity.

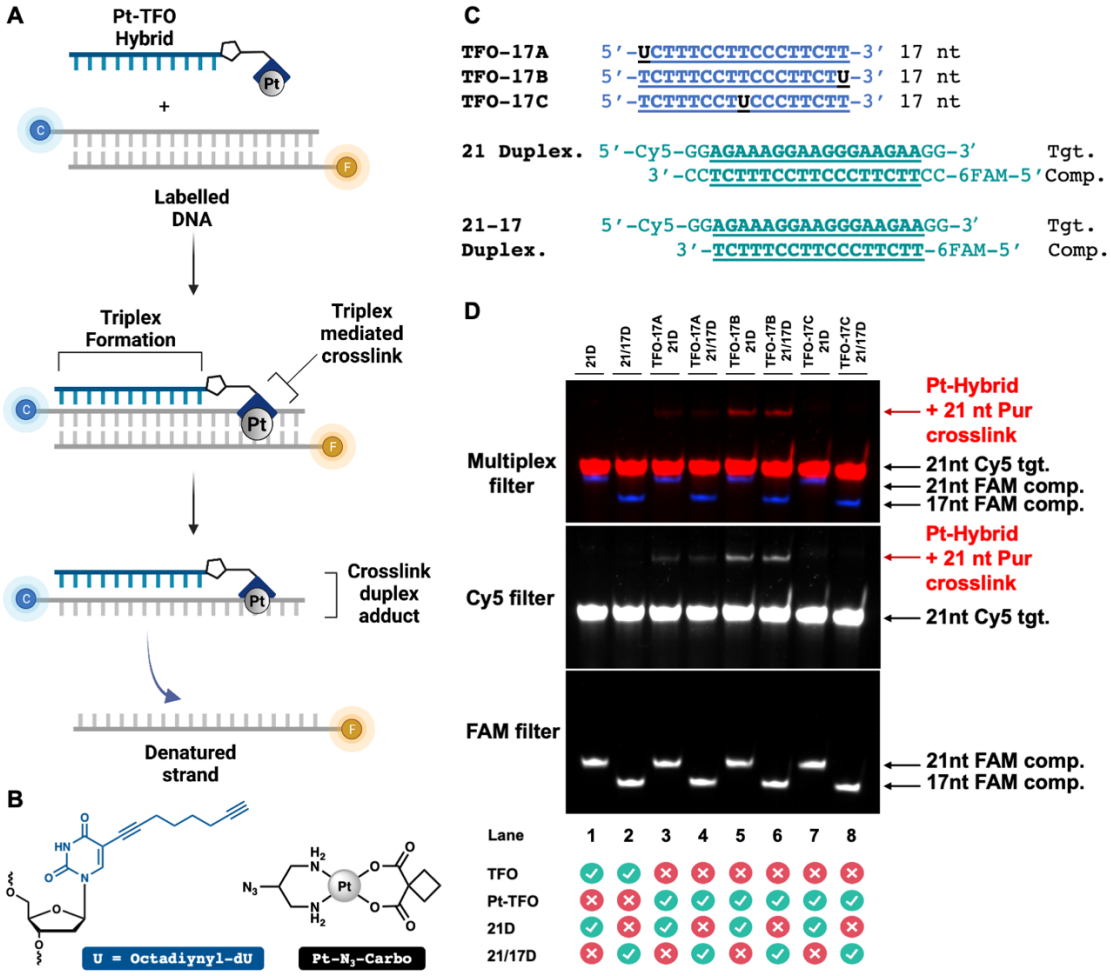

Figure V-12. A. Denaturing PAGE experimental design. **B.** Terminal and internal nucleobase modification octadinyl-dU and azide-functionalised Pt-N_3-Carbo. **C.** Modified TFO sequences and dsDNA targets. **D.** Denaturing PAGE analysis: TFO-hybrids (50 eq.) were incubated at 37 ºC with duplex targets for a minimum of 48 hours prior to electrophoresis. Upper band (Lanes 3-6) under Cy5 filter is indicative of adduct formation with purine strand. No adduct formation observed for TFO-17C (Lanes 7 and 8).

V. 3. Conclusion

This work has demonstrated the development and application of a potential new class of platinum(II)-TFO hybrid. To our knowledge, the use of nucleic acid click chemistry to combine a TFO vector with azide-functionalised *cis*-platinum(II) complexes represents the first example of platinum(II)-TFO hybrids designed in this way. The introduction of an azide moiety into traditional *cis*-platinum(II) analogues did not occlude crosslinking ability and, importantly, provided a suitable handle for click conjugation with alkyne-modified oligonucleotides. In comparison to existing methods used to prepare platinated TFOs, click chemistry affords a modular approach whereby the incorporation of *cis*-platinum(II) at practically any location within the probe strand is possible. This work also overcomes limitations requiring complexation between a platinum(II) reagent, such as a *trans*-platinum(II) complex[21, 22] and the TFO substrate—an approach that hitherto precluded the development of *cis*-platinum(II) type hybrids[18] and the ability to generate 1,2-d(GpG) cisplatin lesions central to their clinical success.

Several platinum(II)-TFO hybrids incorporating Pt-N_3-Cis did not form effective DNA triplexes and this may result from the promiscuity of the cisplatin-type moiety and the plethora of binding opportunities present within the triplex recognition site overriding Hoogsteen interactions derived from the TFO. Of the platinum(II)-TFOs that formed triplexes (i.e. Pt-N_3-Carbo, Pt-N_3-Oxali, and several Pt-N_3-Cis hybrids), all displayed destabilising effects associated with Pt(II) crosslinking. However, no *off*-target effects were observed in the presence of GG/AG rich sequences lacking the triplex recognition site. Importantly, the introduction of thiazole orange (TO) into the TFO probe remediates triplex destabilisation with the inclusion of two TO units pushing triplex stability towards that of the underlying duplex target. The use of PAGE analysis indicates that, for several TFO constructs, numerous platinated triplex adducts can form giving rise to distinctive banding patterns that are reversed upon removal of the crosslink with sodium cyanide. Finally, purine:pyrimidine strand targeting by platinum(II)-TFO hybrids was investigated by denaturing fluorescently labelling duplex sequences with crosslinking evident within the purine strand only. Overall, this work demonstrates a modular approach to the development of *cis*-platinum(II)-

TFO hybrids with recognition and targeting of specific genetic elements possible through triplex-mediated binding. Stability limitations are inherent to triplex motifs and, in these constructs, care must be taken to avoid further destabilisation by the choice and positioning of the *cis*-platinum(II) unit. Crucially, the inclusion of TO intercalators appears to augment triplex stability and remediates the destabilisation effects imposed by the linked platinum(II) complex. A future approach to fully realise the biological potential of these *cis*-platinum(II) hybrids within antigene technology may involve the use of state-of-art modifications such as phosphorothiate backbone linkages, phosphorodiamidate morpholino oligonucleotides, and ribose modifications. These modifications must be combined with a unique targeting strategy whereby mutant genes or oncogenes—particularly those present in recalcitrant cancers such as triple-negative breast cancer or glioblastoma multiforme—are specifically targeted by this technology to achieve selectivity over normal cells.

V. 4. References

1. Lauria, T.; Slator, C.; McKee, V.; Müller, M.; Stazzoni, S.; Crisp, A. L.; Carell, T.; Kellett, A., A Click Chemistry Approach to Developing Molecularly Targeted DNA Scissors. *Chem. Eur. J.* **2020,** *26* (70), 16782-16792.
2. Zuin Fantoni, N.; McGorman, B.; Molphy, Z.; Singleton, D.; Walsh, S.; El-Sagheer, A. H.; McKee, V.; Brown, T.; Kellett, A., Development of Gene-Targeted Polypyridyl Triplex-Forming Oligonucleotide Hybrids. *ChemBioChem* **2020,** *21* (24), 3563-3574.
3. Moghaddam, A. D.; White, J. D.; Cunningham, R. M.; Loes, A. N.; Haley, M. M.; DeRose, V. J., Convenient detection of metal–DNA, metal–RNA, and metal–protein adducts with a click-modified Pt(ii) complex. *Dalton Trans.* **2015,** *44* (8), 3536-3539.
4. Shen, X.; Corey, D. R., Chemistry, mechanism and clinical status of antisense oligonucleotides and duplex RNAs. *Nucleic Acids Res.* **2018,** *46* (4), 1584-1600.
5. Fox, K. R., Targeting DNA with Triplexes. *Curr. Med. Chem.* **2000,** *7*, 17-37.
6. Fox, K. R.; Brown, T.; Rusling, D. A., *DNA-targeting Molecules as Therapeutic Agents*. Royal Society of Chemistry: Royal Society of Chemistry, 2018.
7. Sun, J.-S.; Carestier, T.; Hélène, C., Oligonucleotide directed triple helix formation. *Curr. Opin. Struct. Biol.* **1996,** *6* (3), 327-333.
8. Nielsen, P. E., DNA analogues with nonphosphodiester backbones. *Annu. Rev. Biophys. Biomol. Struct.* **1995,** *24*, 167-83.
9. Takasugi, M.; Guendouz, A.; Chassignol, M.; Decout, J. L.; Lhomme, J.; Thuong, N. T.; Helene, C., Sequence-specific photo-induced cross-linking of the two strands of double-helical DNA by a psoralen covalently linked to a triple helix-forming oligonucleotide. *Proc. Natl. Acad. Sci. U.S.A.* **1991,** *88* (13), 5602-5606.
10. Havre, P. A.; Gunther, E. J.; Gasparro, F. P.; Glazer, P. M., Targeted mutagenesis of DNA using triple helix-forming oligonucleotides linked to psoralen. *Proc. Natl. Acad. Sci. U.S.A.* **1993,** *90* (16), 7879-7883.

11. Oh, D., Triple helix-forming oligonucleotides target psoralen adducts to specific chromosomal sequences in human cells. *Nucleic Acids Res.* **1999,** *27* (24), 4734-4742.
12. Kundu, M.; Nagatsugi, F.; Majumdar, A.; Miller, P. S.; Seidman, M. M., Enhancement and Inhibition by 2'-O-Hydroxyethyl Residues of Gene Targeting Mediated by Triple Helix Forming Oligonucleotides. *Nucleosides Nucleotides Nucleic Acids* **2003,** *22* (10), 1927-1938.
13. Besch, R.; Giovannangeli, C.; Schuh, T.; Kammerbauer, C.; Degitz, K., Characterization and Quantification of Triple Helix Formation in Chromosomal DNA. *J. Mol. Biol.* **2004,** *341* (4), 979-989.
14. Dieter-Wurm, I.; Sabat, M.; Lippert, B., Model for a platinated DNA triplex: Watson-Crick and metal-modified Hoogsteen pairing. *J. Am. Chem. Soc.* **1992,** *114* (1), 357-359.
15. Colombier, C.; Lippert, B.; Leng, M., Interstrand Cross-linking Reaction in Triplexes Containing a Monofunctional Transplatin-Adduct. *Nucleic Acids Res.* **1996,** *24* (22), 4519-4524.
16. Bernal-Méndez, E.; Sun, J.-S.; González-Vílchez, F.; Leng, M., Reactivity of transplatin-modified oligonucleotides in triple-helical DNA complexes. *New. J. Chem.* **1998,** *22* (12), 1479-1483.
17. Gruff, E. S.; Orgel, L. E., An efficient, sequence-specific method for crosslinking complementary oligonucleotides using binuclear platinum complexes. *Nucleic Acids Res.* **1991,** *19* (24), 6849-6854.
18. Sharma, S. K.; McLaughlin, L. W., Cross-Linking of a DNA Conjugate Tethering a cis-Bifunctional Platinated Complex to a Target DNA Duplex. *J. Am. Chem. Soc.* **2002,** *124*, 9658-9659.
19. Sharma, S. K.; McLaughlin, L. W., Triplex mediated delivery of a platinum complex to a specific DNA target site. *J. Inorg. Biochem.* **2004,** *98* (10), 1570-7.
20. Graham, M. K.; Miller, P. S., Inhibition of transcription by platinated triplex-forming oligonucleotides. *J. Biol. Inorg. Chem.* **2012,** *17* (8), 1197-1208.
21. Campbell, M. A.; Mason, T. M.; Miller, P. S., Interactions of platinum(II)-derivatized triplex-forming oligonucleotides with DNA. *Can. J. Chem.* **2007,** *85* (4), 241-248.

22. Campbell, M. A.; Miller, P. S., Cross-linking to an interrupted polypurine sequence with a platinum-modified triplex-forming oligonucleotide. *J. Biol. Inorg. Chem.* **2009,** *14* (6), 873-881.
23. Campbell, M. A.; Miller, P. S., Transplatin-Conjugated Triplex-Forming Oligonucleotides Form Adducts with Both Strands of DNA. *Bioconjug. Chem.* **2009,** *20* (12), 2222-2230.
24. Graham, M. K.; Brown, T. R.; Miller, P. S., Targeting the Human Androgen Receptor Gene with Platinated Triplex-Forming Oligonucleotides. *Biochemistry* **2015,** *54* (13), 2270-2282.
25. Manchanda, R.; Dunham, S. U.; Lippard, S. J., Automated Solid-Phase Synthesis of Site-Specifically Platinated Oligodeoxyribonucleotides. *J. Am. Chem. Soc.* **1996,** *118* (21), 5144-5145.
26. Schmidt, K. S.; Filippov, D. V.; Meeuwenoord, N. J.; van der Marel, G. A.; van Boom, J. H.; Lippert, B.; Reedijk, J., Solid-Phase Synthesis of a Monofunctional *trans*-a2PtII Complex Tethered to a Single-Stranded Oligonucleotide. *Angew. Chem. Int. Ed.* **2000,** *39* (2), 375-377.
27. Cech, D.; Schliepe, J.; Berghoff, U.; Lippert, B., Automated Solid Phase Synthesis of Platinated Oligonucleotides via Nucleoside Phosphonates. *Angew. Chem. Int. Ed.* **1996,** *35* (6), 646-648.
28. Urankar, D.; Košmrlj, J., Preparation of diazenecarboxamide–carboplatin conjugates by click chemistry. *Inorg. Chim. Acta.* **2010,** *363* (14), 3817-3822.
29. Stojanović, N.; Urankar, D.; Brozović, A.; Ambriović-Ristov, A.; Osmak, M.; Košmrlj, J., Design and Evaluation of Biological Activity of Diazenecarboxamide-extended Cisplatin and Carboplatin Analogues. *Acta. Chim. Slov.* **2013,** *60* (2), 368-374.
30. Cunningham, R. M.; DeRose, V. J., Platinum Binds Proteins in the Endoplasmic Reticulum of S. cerevisiae and Induces Endoplasmic Reticulum Stress. *ACS Chem. Biol.* **2017,** *12* (11), 2737-2745.
31. Reshetnikov, V.; Daum, S.; Janko, C.; Karawacka, W.; Tietze, R.; Alexiou, C.; Paryzhak, S.; Dumych, T.; Bilyy, R.; Tripal, P.; Schmid, B.; Palmisano, R.; Mokhir, A., ROS-Responsive N-Alkylaminoferrocenes for Cancer-Cell-Specific Targeting of Mitochondria. *Angew .Chem. Int. Ed.* **2018,** *130* (37), 12119-12122.

32. Kitteringham, E.; Andriollo, E.; Gandin, V.; Montagner, D.; Griffith, D. M., Synthesis, characterisation and in vitro antitumour potential of novel Pt(II) estrogen linked complexes. *Inorg. Chem. Acta.* **2019,** *495*, 118944.
33. Stewart, C. R., Broadening by Acridine Orange of the Thermal Transition of DNA. *Biopolymers* **1968,** *6*, 1737-1743.
34. Escudé, C.; Hélène, C.; Nguen, C. H.; Mergny, J.; Sun, J.-S.; Bisagni, E.; Garestier, T., Selective Stabilisation of DNA Triple Helices by Benzopyridoindole Derivatives. *J. Am. Chem. Soc.* **1995,** *117*, 10212-10219.
35. Guedin, A.; Lacroix, L.; Mergny, J. L., Thermal melting studies of ligand DNA interactions. *Methods Mol. Biol.* **2010,** *613*, 25-35.
36. Mergny, J.; Lacroix, L.; Han, X.; Leroy, J.; Hélène, C., Intramolecular Folding of Pyrimidine Oligodeoxynucleotides into an i-DNA Motif. *J. Am. Chem. Soc.* **1995,** *117* (35), 8887-8898.
37. Mergny, J.; Lacroix, L., Analysis of Thermal Melting Curves. *Oligonucelotides* **2003,** *13* (6), 515-537.
38. Cohen, G.; Bauer, W.; Barton, J.; Lippard, S. J., Binding of *cis- and trans*-Dichlorodiammineplatinum(II) to DNA: Evidence of Unwinding and Shortening of the Double Helix. *Science* **1979,** *203* (4384), 1014-1016.
39. Kelland, L., The resurgence of platinum-based cancer chemotherapy. *Nat. Rev. Cancer.* **2007,** *7* (8), 573-584.
40. Wheate, N. J.; Walker, S.; Craig, G. E.; Oun, R., The status of platinum anticancer drugs in the clinic and in clinical trials. *Dalton Trans.* **2010,** *39* (35), 8113-27.
41. Dasari, S.; Bernard Tchounwou, P., Cisplatin in cancer therapy: Molecular mechanisms of action. *Eur. J. Pharmacol.* **2014,** *740*, 364-378.
42. Thati, B.; Noble, A.; Creaven, B. S.; Walsh, M.; Kavanagh, K.; Egan, D. A., Apoptotic cell death: A possible key event in mediating the in vitro anti-proliferative effect of a novel copper(II) complex, [Cu(4-Mecdoa)(phen)2] (phen=phenanthroline, 4-Mecdoa=4-methylcoumarin-6,7-dioxactetate), in human malignant cancer cells. *Eur. J. Pharmacol.* **2007,** *569* (1-2), 16-28.
43. Zeng, L.; Chen, Y.; Liu, J.; Huang, H.; Guan, R.; Ji, L.; Chao, H., Ruthenium(II) Complexes with 2-Phenylimidazo[4,5-f][1,10]phenanthroline

Derivatives that Strongly Combat Cisplatin-Resistant Tumor Cells. *Sci. Rep.* **2016,** *6* (1), 19449.

44. McFadyen, W. D.; Wakelin, L. P. G.; Roos, I. A. G.; A., L. V., Acitivty of Platinum(II) Intercalating Agents against Murine Leukemia L1210. *J. Med. Chem.* **1985,** *28*, 1113-1116.
45. Johnstone, T. C.; Suntharalingam, K.; Lippard, S. J., The Next Generation of Platinum Drugs: Targeted Pt(II) Agents, Nanoparticle Delivery, and Pt(IV) Prodrugs. *Chem. Rev.* **2016,** *116* (5), 3436-86.
46. Kitteringham, E.; Wu, D.; Cheung, S.; Twamley, B.; O'Shea, D. F.; Griffith, D. M., Development of a novel carboplatin like cytoplasmic trackable near infrared fluorophore conjugate via strain-promoted azide alkyne cycloaddition. *J. Inorg. Biochem.* **2018,** *182*, 150-157.
47. Wirth, R.; White, J. D.; Moghaddam, A. D.; Ginzburg, A. L.; Zakharov, L. N.; Haley, M. M.; DeRose, V. J., Azide vs Alkyne Functionalization in Pt(II) Complexes for Post-treatment Click Modification: Solid-State Structure, Fluorescent Labeling, and Cellular Fate. *J. Am. Chem. Soc.* **2015,** *137* (48), 15169-15175.
48. Walsh, S.; El-Sagheer, A. H.; Brown, T., Fluorogenic thiazole orange TOTFO probes stabilise parallel DNA triplexes at pH 7 and above. *Chem. Sci.* **2018,** *9* (39), 7681-7687.
49. Bijapur, J.; Bergqvist, S.; Brown, T.; Keppler, M. D.; Fox, K. R., 5-(1-propargylamino)-2'-deoxyuridine (UP): A novel thymidine analogue for generating DNA triplexes with increased stability. *Nucleic Acids Res.* **1999,** *27* (8), 1802-1809.
50. Petrov, A.; Tsa, A.; Puglisi, J. D., Analysis of RNA by analytical polyacrylamide gel electrophoresis. *Methods Enzymol.* **2013,** *530*, 301-13.
51. Stellwagen, N. C., Electrophoresis of DNA in agarose gels, polyacrylamide gels and in free solution. *Electrophoresis* **2009,** *30* (S1), S188-S195.
52. Holmes, D. L.; Stellwagen, N. C., Estimation of polyacrylamide gel pore size from Ferguson plots of linear DNA fragements II. Comparison of gels with different crosslinker concentrations, added agarose and added linear polyacrylamide. *Electrophoresis* **1991,** *12* (9), 612-619.
53. Raudaschl-Sieber, G.; Lippert, B., Reaction of cyanide with platinum-nucleobase complexes: preparative, spectroscopic, and structural studies.

Unexpected stability of platinum-thymine and platinum-uracil complexes. *Inorg. Chem.* **1985,** *24* (15), 2426-2432.

54. Lippard, S. J.; Hoeschele, J. D., Binding of cis- and trans-dichlorodiammineplatinum(II) to the nucleosome core. *Proc. Natl. Acad. Sci. U.S.A.* **1979,** *76* (12), 6091-6095.

Chapter VI

Development of Second-generation *cis*-Pt(II)-TFO Hybrids

The work presented in this chapter details the development of *cis*-Pt(II) AA-TOTFO hybrids generated through CuAAC click chemistry. A draft manuscript reporting the results of this work is in preparation. 3-(5-carboxypentyl)-2-((1'-methylquinolin-4'(1H)-ylidene)methyl)benzo-[*d*]-thiazol-3-ium hexafluorophosphate (TO_{B6}) was kindly provided by Sinéad O'Carroll, Kellett Research Group, DCU.

VI. 1. Abstract

The combining of an azide-functionalised *cis*-platinum(II) analogue (Pt-N_3-Carbo) and the AA-TOTFO vectors have yielded *cis*-platinum(II)-modified AA-TOTFO constructs that demonstrate targeted crosslinking capabilities. In this work, we demonstrate the ability to successfully couple both a platinum(II) unit and an intercalating moiety on the same nucleobase with greater crosslinking activity demonstrated. Comparison with standard Pt(II)-TFO hybrids allows for an investigation into the effects that the linked thiazole orange unit exerts upon the crosslinking affinity. The enhanced affinity for triplex formation and crosslinking is herein reported for these second-generation *cis*-platinum(II)-TFO hybrids.

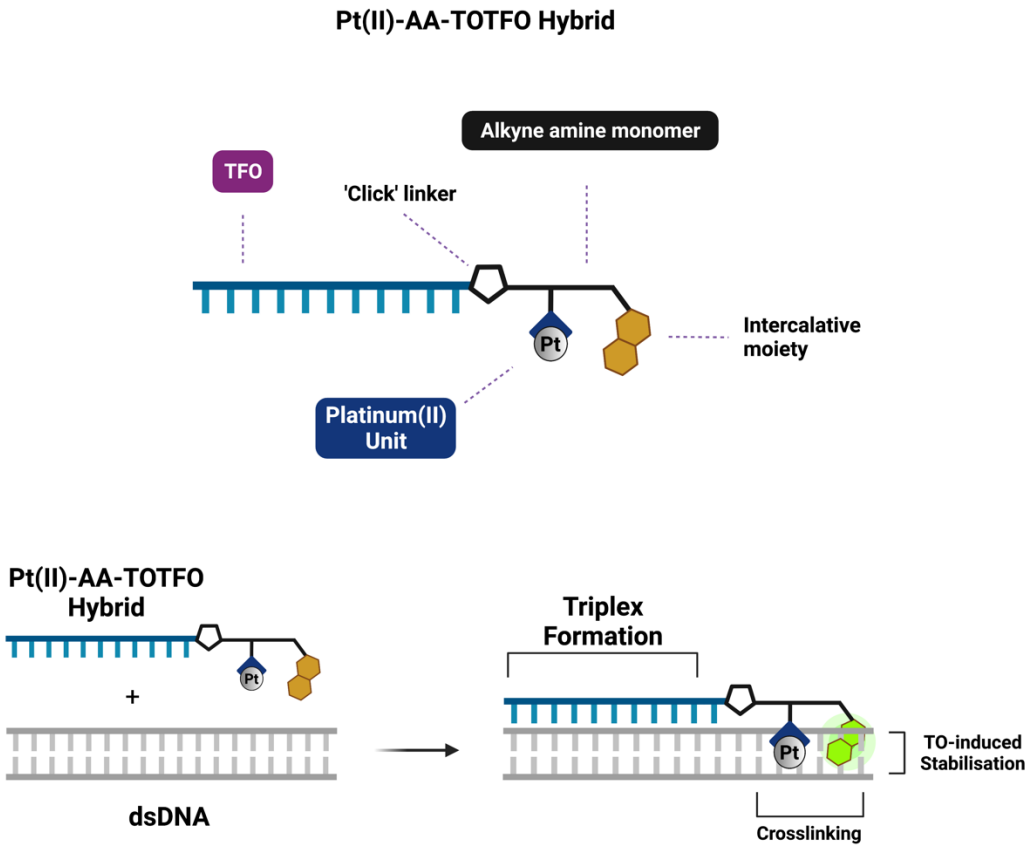

Figure VI-1. Overview of Pt(II)-AA-TOTFO hybrid construction and triplex-mediated crosslinking ability.

VI. 1. 1. Chapter Aims

- To generate a series of AA-TOTFO sequences through solid-phase oligonucleotide phosphoramidite synthesis.

- To generate *cis*-Pt(II) AA-TOTFO constructs using the CuAAC click strategy.

- To identify the enhancement in triplex stability and crosslinking affinity for the *cis*-Pt(II)-AA-TOTFO hybrids.

VI. 1. 2. Rationale

With the successful generation of *cis*-platinum(II)-TFO hybrids and the demonstration of their ability to sequence specifically target and crosslink genes of interest without *off*-target effects, the next step in the realisation of their potential is to minimise the inherent challenges that they present – namely the destabilisation of the triplex system upon crosslink formation. The use of TO modified TFO vectors should provide an enhancement in stability for a new generation of *cis*-Pt(II)-AA-TOTFO hybrids through the intercalating properties of the TO moiety. Additionally, the alkyne-amine monomeric nucleobase may present a novel approach for the conjugation of a *cis*-Pt(II) analogue onto the same base as a TO unit. Investigation into the resultant proximity of these molecules and the role that they play in the stabilisation and targeting abilities should reveal key factors required for the design of future TFO hybrids.

VI. 2. Generation of *cis*-Pt(II)-AA-TOTFOs

VI. 2. 1. General Information

Thiazole orange (TO) TFO:TO labelling

In a total volume of approx. 150 μL DMF, 800 nmol (20 eq.) of TO_{B6} carboxylic acid, 800 nmol (20 eq.) of (2-(1*H*-benzotriazol-1-yl)-1,1,3,3-tetramethyluronium hexafluorophosphate (HBTU) and 2400 nmol (48 μL, 50 mM) (60 eq.) of 4-methylmorpholine was dissolved. This mixture was shaken at 25 ºC for 30 min prior to addition to a solution of AA-TOTFO (40 nmol, 1 eq) in 150 μL of carbonate buffer ($NaHCO_3/Na_2CO_3$, 0.1 M, pH 9.2). The entire solution was incubated for approx. 6 h at 37 ºC. The solution was desalted using NAP-10 gel filtration columns and purified using an Amicon Ultra 0.5 mL centrifugal column.

VI. 2. 2. *cis*-Pt(II)-AA-TOTFO design and development

Cis-Pt(II)-AA-TOTFO constructs were prepared through nucleic acid click chemistry by combing Pt-N_3-Carbo and the series of alkyne-amine (AA)-TOTFOs displayed below (**Table VI-1**).

Table VI-1. AA-TOTFO sequences clicked with Pt-N_3-Carbo.

Oligo Name	Sequence	Modification
AA-TOTFO1-Carbo	5′-XCT TTC CTT CCC TTC TTT CGC TTT CCT C-3′	AP-C3-TO (x1), AP-C3-N_3-Pt(II)-Carbo
AA-TOTFO2-Carbo	5′-XCT TTC CUT CCC TTC TTT CGC TTT CCT C-3′	AP-C3-TO (x1), pdU-TO (x1), AP-C3-N_3-Pt(II)-Carbo
AA-TOTFO3-Carbo	5′-XCT TTC CUT CCC TUC TTT CGC TTT CCT C-3′	AP-C3-TO (x1), pdU-TO (x2), AP-C3-N_3-Pt(II)-Carbo
AA-TOTFO4-Carbo	5′-XCT TTC CUT CCC TUC TTT CGC TTU CCT C-3′	AP-C3-TO (x1), pdU-TO (x3), AP-C3-N_3-Pt(II)-Carbo
AA-TOTFO5-Carbo	5′-XTC CCT CTT TCC GCC TGT CC-3′	AP-C3-TO (x1), AP-C3-N_3-Pt(II)-Carbo
AA-TOTFO6-Carbo	5′-XTC CCU CTT TCC GCC TGT CC-3′	AP-C3-TO (x1), pdU-TO (x1), AP-C3-N_3-Pt(II)-Carbo
AA-TOTFO7-Carbo	5′-XTC CCU CTT UCC GCC TGT CC-3′	AP-C3-TO (x1), pdU-TO (x2), AP-C3-N_3-Pt(II)-Carbo
AA-TOTFO8-Carbo	5′-XTC CCU CTT UCC GCC TGU CC-3′	AP-C3-TO (x1), pdU-TO (x3), AP-C3-N_3-Pt(II)-Carbo

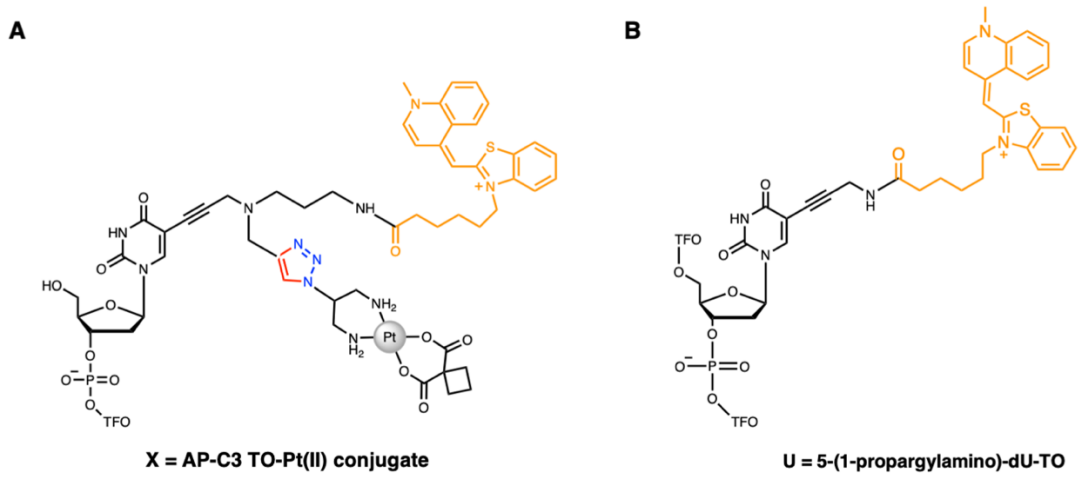

Figure VI-2. Schematic of AA-TOTFO incorporations. **A.** AP-C3 alkyne-amine nucleobase monomer. **B.** 5-(1-propargylamino)-dU modified nucleobase for TO inclusion.

Firstly, the ability of the AA-TOTFOs to form triplexes with target duplex sequences at pH 6 was investigated. AA-TOTFO1-4 were developed based on the design of the standard TFO1, whereby the sequence is shortened by a nucleobase on the 5'- terminus and the octadinyl-dC is replaced by the AP-C3 monomer. Similarly, AA-TOTFO5-8 was developed from the design of TFO4 with the same modifications made. Although TFO4 did not form triplexes at pH6, it was envisaged that the addition of the AP-C3 monomer and TO units would increase the thermal stability of the underlying triplex. However, thermal melting analysis indicated that AA-TOTFO5-8 failed to form quantifiable triplexes and this was further verified by PAGE analysis (**Figure VI-3, B**). As such, investigation of the AA-TOTFO5-8 Carbo series was not performed as part of this study.

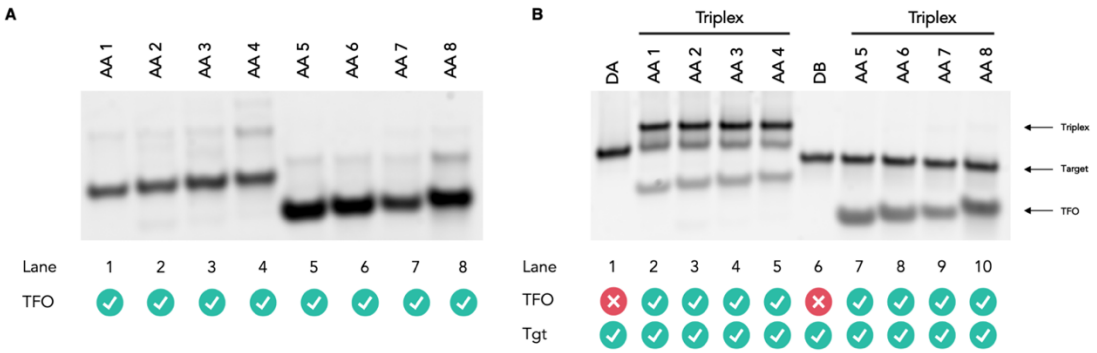

Figure VI-3. A. Preliminary investigation of purity of non-modified AA-TOTFO1-8 sequences. **B**. Triplex formation for AA-TOTFO1-4 with Duplex A (1 pmol, lane 2-5) and AA-TOTFO5-8 with Duplex B (1 pmol, lane 7-10). AA-TOTFO5-8 failed to form triplexes under these conditions. Samples were prepared in 10 mM phosphate buffer, 150 mM NaCl and 2 mM $MgCl_2$ (pH 6) prior to incubation over 24 h at 37 ºC**.** Samples were then loaded onto 20 % PAGE and subjected to electrophoresis for 8 h at 50 V in 50 mM tris-acetate (TA) buffer (pH 6). Gels were post-staiend with SybrGold.

VI. 2. 2. 1. PAGE analysis of AA-TOTFO Carbo Hybrids

Preliminary thermal melting analysis for the AA-TOTFO1-4 Carbo hybrids displayed no quantifiable triplex melting curves when using direct UV thermal melting methods. The profile of the melting curves was indicative of the previous melting trend whereby TO-modified systems pushed the triplex melting stability into the same region as the underlying duplex melt. In comparison to TOTFO1 Carbo, which displayed a significantly increased triplex thermal stability, AA-TOTFO1 Carbo appears to push this further into the duplex region. Thus, the triplex forming ability of the AA-TOTFO1-4 Carbo hybrids was analysed by PAGE at pH 6. All TFOs were treated against target (57 bp) and off-target (40 bp) duplex sequences with no off-target selectivity observed. Triplex formation was successful under the conditions and all appeared to exhibit full triplex formation at approx. 10 eq. of hybrid loading except AA-TOTFO4 Carbo. For AA-TOTFO4 Carbo, incorporating 4 TO units, full formation was observed for loading >10 eq. and may be due to the steric effects that arise from the number of modifications present (**Figure VI-4, B**). This observation has been made previously with regards to the TOTFO3 Carbo whereby the optimal number of thiazole orange units on the sequence was determined to be two.

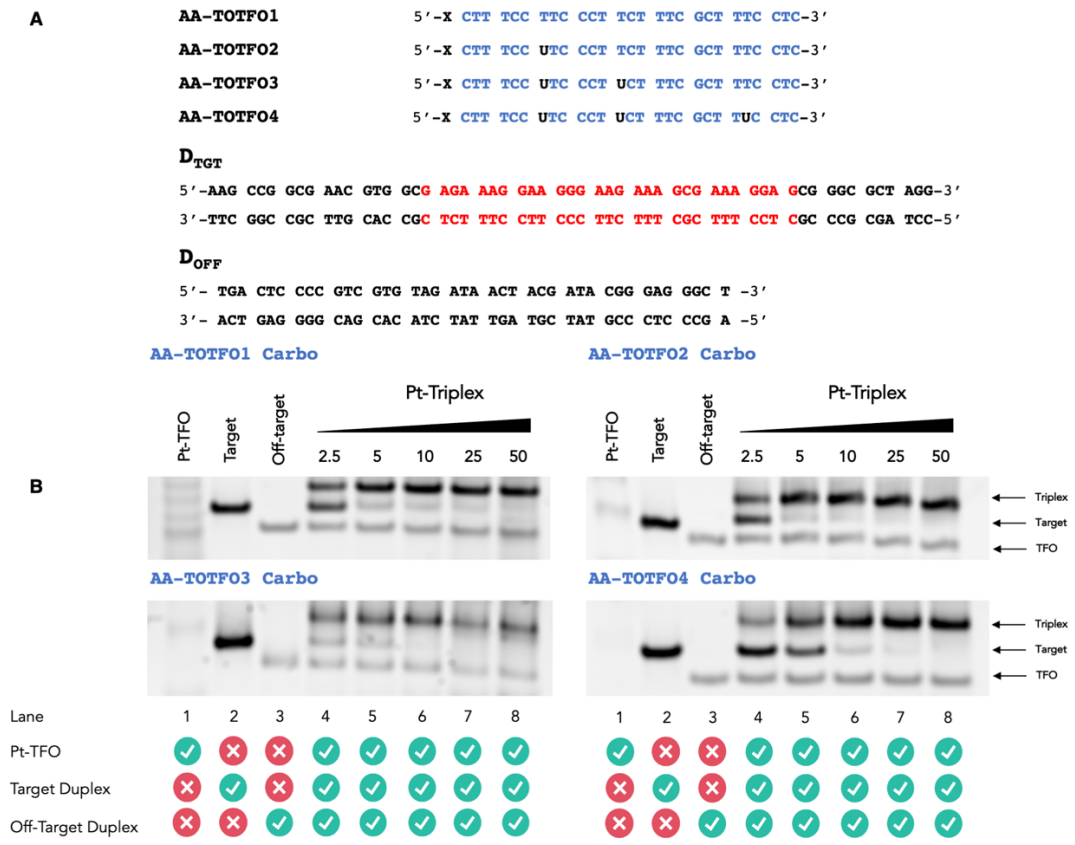

Figure VI-4. A. AA-TOTFO1-4 Carbo sequences with modification sites, where X = AP-C3 alkyne-amine monomer and U = 5-(1-propargylamino)-dU nucleobase modification. 57 bp target and 40 bp off-target are shown. **B.** Triplex formation for AA-TOTFO1-4 Carbo treated against target duplex (57 bp) and off-target duplex (40 bp). No off-target selectivity is observed. AA-TOTFO4 Carbo triplex activity is impeded before >10 eq. (AA-TOTFO4 Carbo, lane 4-8). Samples were prepared in 10 mM phosphate buffer, 150 mM NaCl and 2 mM $MgCl_2$ (pH 6) prior to incubation over 48 h at 37 ºC**.** Samples were then loaded onto 20% PAGE and subjected to electrophoresis for 4h at 70 V in 50 mM tris-acetate (TA) buffer (pH 6). Gels were post-stained with SybrGold.

To investigate the crosslink potential of the AA-TOTFO Carbo hybrids, crosslink reversal experiments using NaCN were performed again to verify the crosslinking nature of the constructs. Duplex 3 (D3,1 pmol, 40 bp) was treated with AA-TOTFO1-4 Carbo (2.5-50 eq.) in the absence of NaCN with crosslinking activity observed. The single banding pattern for N_3-Carbo Pt(II)-TFOs is similarly displayed by the AA-TOTFO Carbo hybrids. Once treated with NaCN (5,000 eq.), almost full reversal of AA-TOTFO-Carbo crosslinking and triplex formation is observed. 5000 eq. of NaCN is the limit at which standard alkyne-modified triplex formation is unhindered and is a key point in investigating the reversal of triplex vs crosslinking formation.

Duplex 3 is a 40 bp target sequence that contains the AA-TOTFO recognition site. The 5'-terminus of the purine strand is labelled with a Cy5 fluorescent tag and a 6-FAM fluorescent tag is adjoined to the 5'-terminus of the complementary pyrimidine strand. All samples were incubated in 10 mM phosphate, 150 mM NaCl and 2 mM $MgCl_2$, pH 6 triplex buffer for 48 h for 37 ºC prior to 20% PAGE electrophoresis for 4 h at 70 V in 50 mM tris-acetate (TA) buffer (pH 6). (**Figure VI-5-8**).

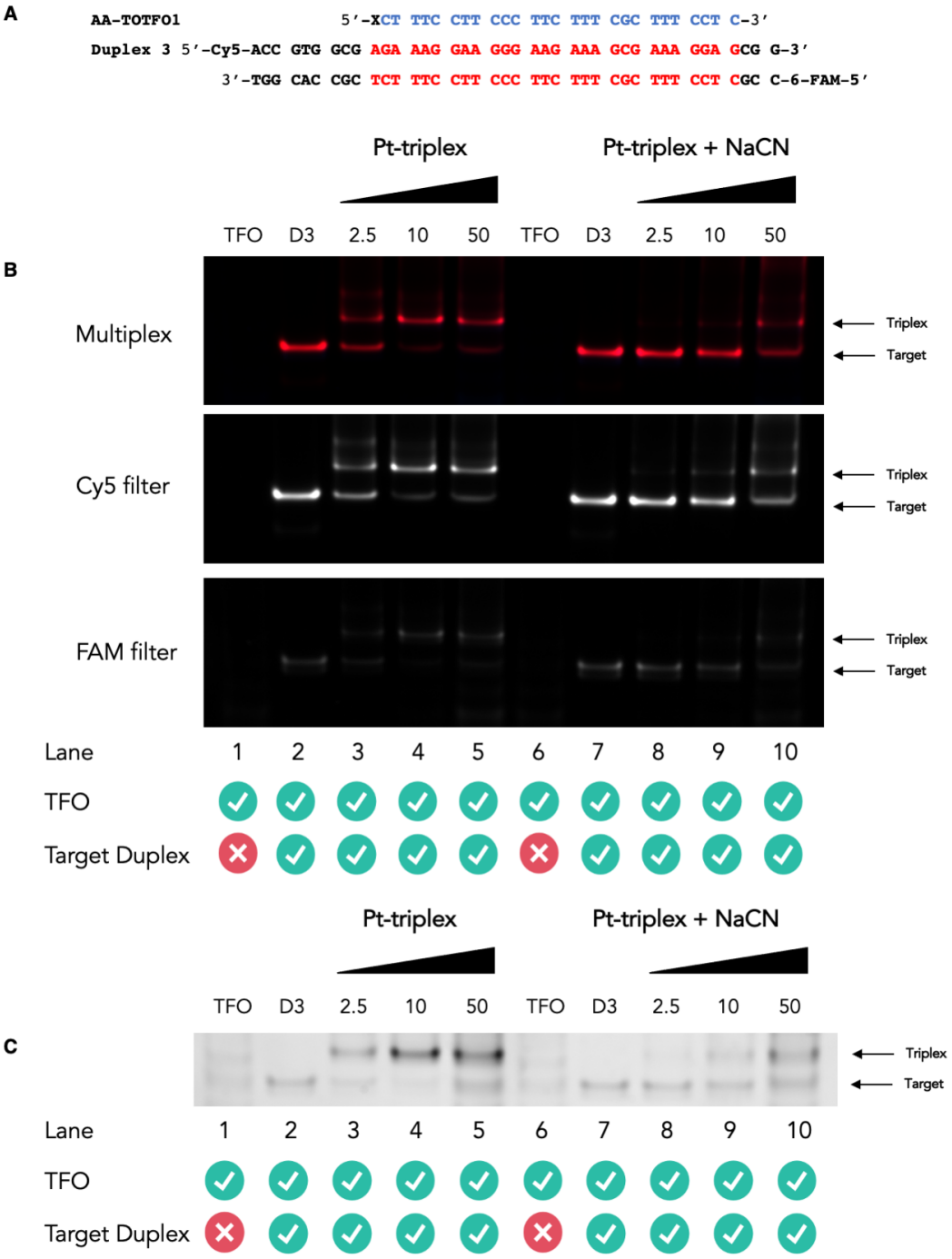

Figure VI-5. A. AA-TOTFO1 Carbo, X = AP-C3 alkyne-amine monomer. Duplex 3 sequence displayed. **B.** Untreated Pt-triplex gradient (lane 3-5) and NaCN (5,000 eq.) treated Pt-triplex gradient (lane 8-9). AA-TOTFO Carbo crosslink reversal is afforded by NaCN treatment. **C.** TO visualisation at 540 nm without staining.

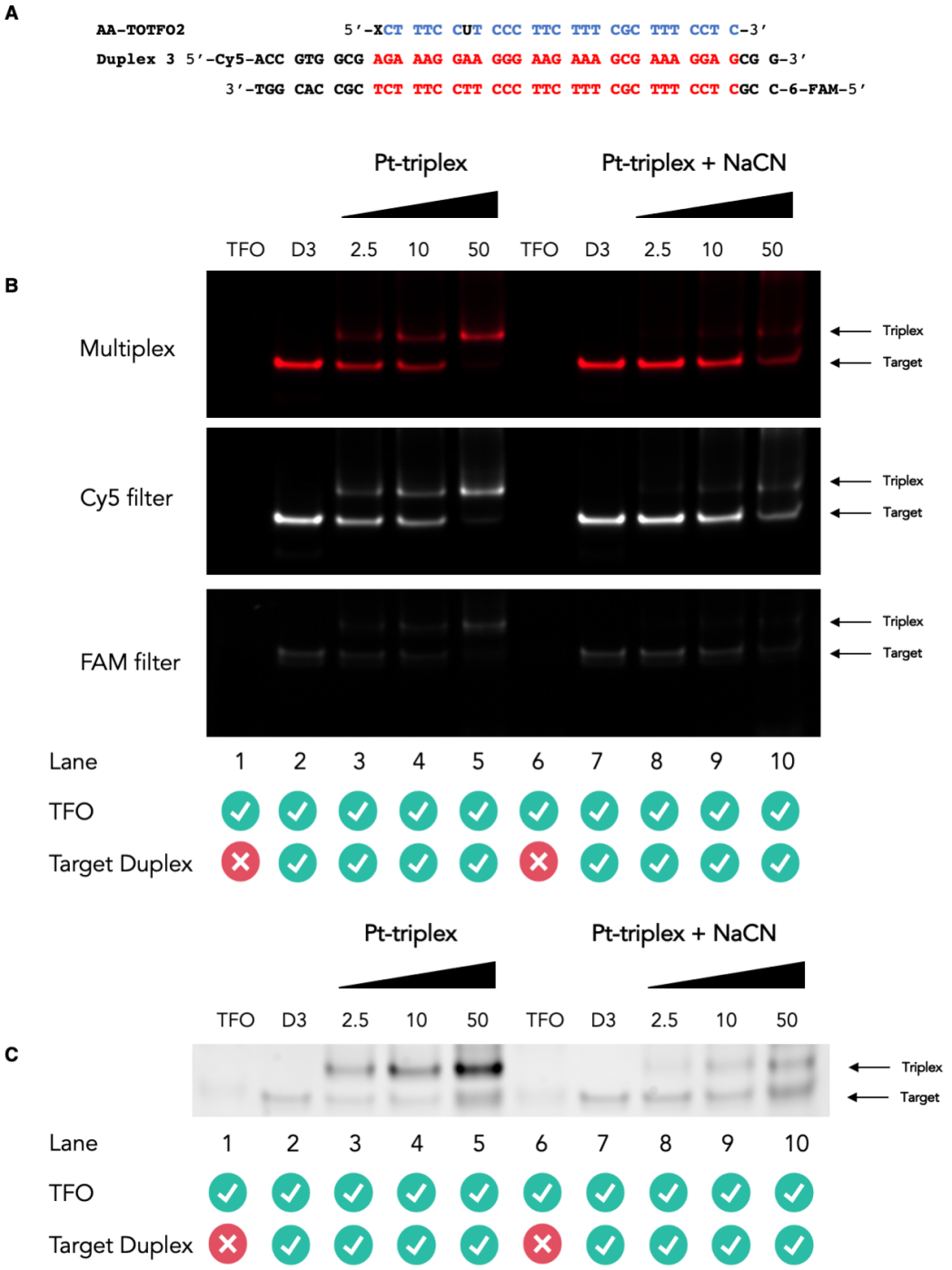

Figure VI-6. A. AA-TOTFO2 Carbo, X = AP-C3 alkyne-amine monomer and U = 5-(1-propargylamino)-dU nucleobase modification. Duplex 3 sequence displayed. **B.** Untreated Pt-triplex gradient (lane 3-5) and NaCN (5,000 eq.) treated Pt-triplex gradient (lane 8-9). AA-TOTFO Carbo crosslink reversal is afforded by NaCN treatment. **C.** TO visualisation at 540 nm without staining.

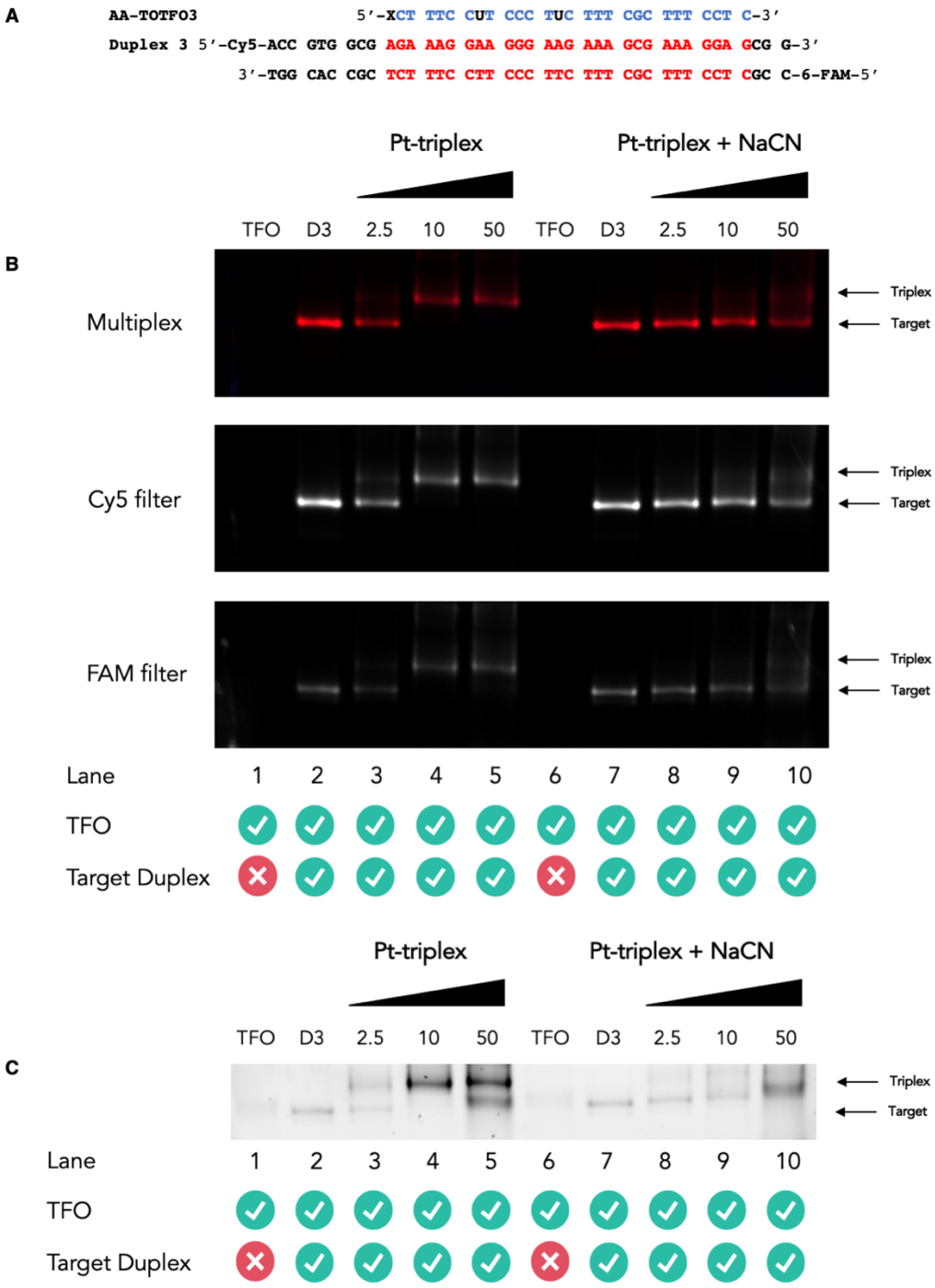

Figure VI-7. A. AA-TOTFO3 Carbo, X = AP-C3 alkyne-amine monomer and U = 5-(1-propargylamino)-dU nucleobase modification. Duplex 3 sequence displayed. **B.** Untreated Pt-triplex gradient (lane 3-5) and NaCN (5,000 eq.) treated Pt-triplex gradient (lane 8-9). AA-TOTFO Carbo crosslink reversal is afforded by NaCN treatment. **C.** TO visualisation at 540 nm without staining.

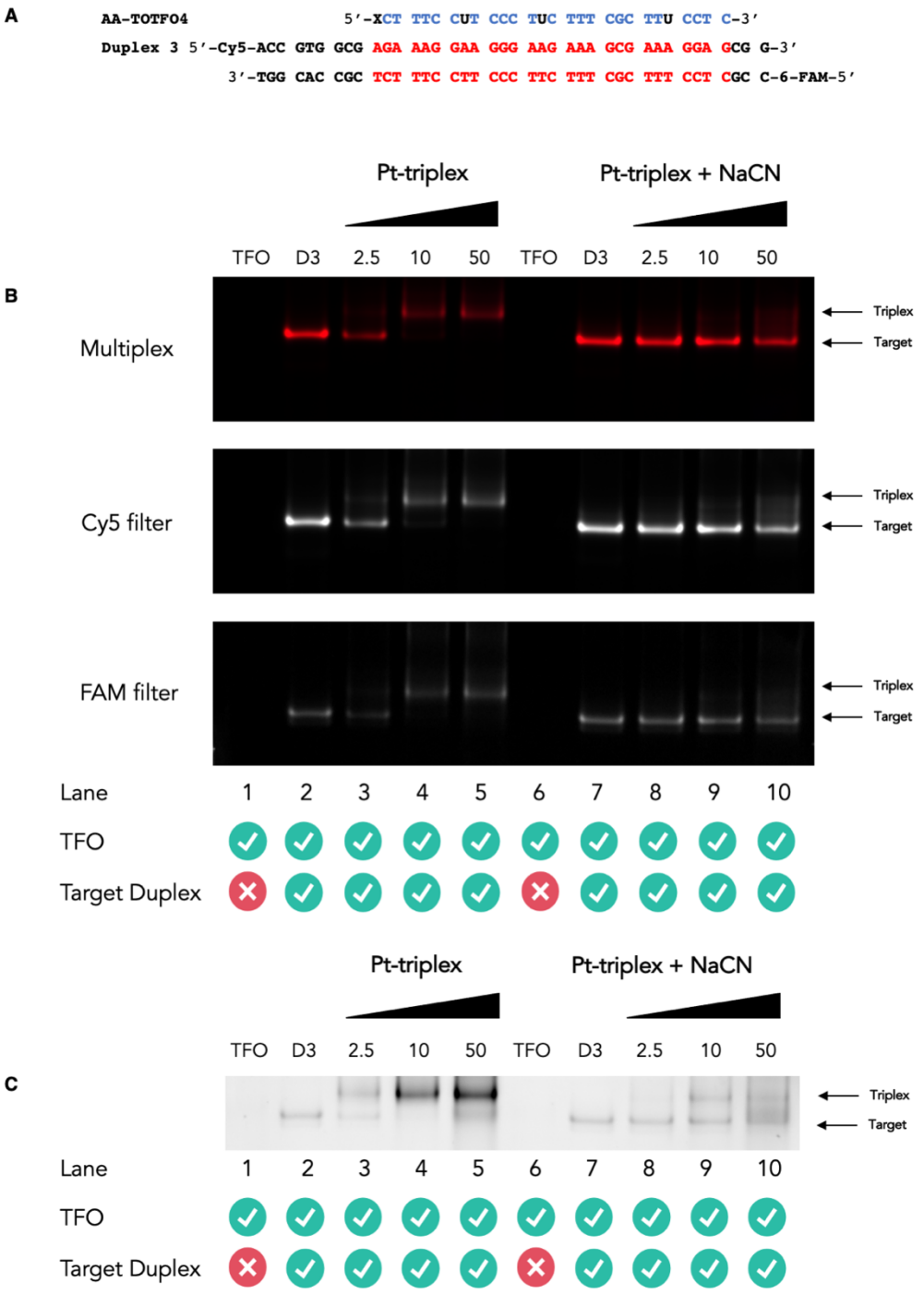

Figure VI-8. A. AA-TOTFO4 Carbo, X = AP-C3 alkyne-amine monomer and U = 5-(1-propargylamino)-dU nucleobase modification. Duplex 3 sequence displayed. **B.** Untreated Pt-triplex gradient (lane 3-5) and NaCN (5,000 eq.) treated Pt-triplex gradient (lane 8-9). AA-TOTFO Carbo crosslink reversal is afforded by NaCN treatment. **C.** TO visualisation at 540 nm without staining.

Finally, a direct comparison between the AA-TOTFO hybrid sequences and standard Pt(II)-TFO hybrids was performed. For this experiment TFO1-Carbo and AA-TOTFO1 Carbo were selected. In order to probe the extent of crosslink formation and whether the TO unit has a greater effect on triplex formation at lower loadings, a lower TFO loading gradient (1-10 eq.) was selected in comparison to the standard triplex formation experiments (**Figure VI-9**).

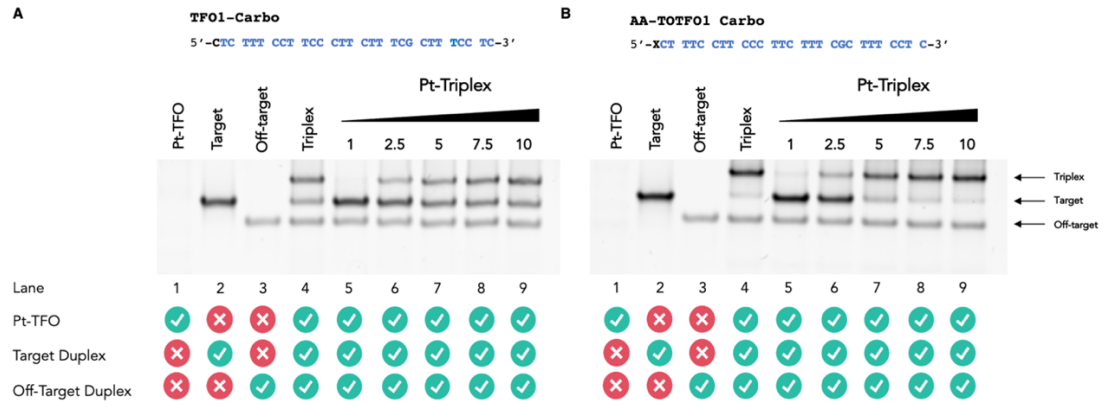

Figure VI-9. Triplex-mediated crosslinking activity for **A.** TFO1-Carbo and **B.** AA-TOTFO1 Carbo. Target (57 bp, 1 pmol, lane 3) and off-target (40 bp, 1 pmol, lane 3) were treated with 1-10 eq. of either TFO1-Carbo or AA-TOTFO1 Carbo. Samples were prepared in 10 mM phosphate buffer, 150 mM NaCl and 2 mM $MgCl_2$ (pH 6) prior to incubation over 48 h at 37 ºC. Samples were then loaded onto 20% PAGE and subjected to electrophoresis for 4h at 70 V in 50 mM tris-acetate (TA) buffer (pH 6). Gels were post-stained with SybrGold.

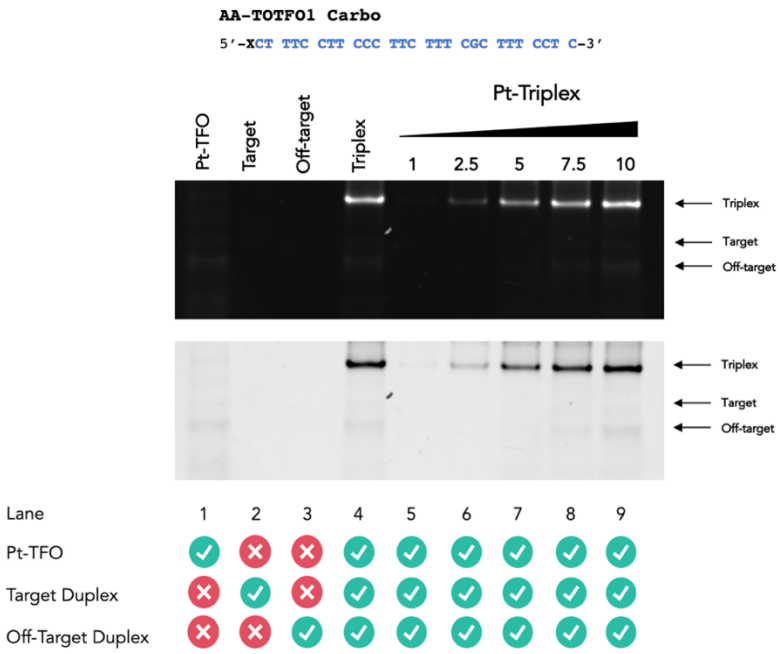

Figure VI-10. TO visualisation of Figure VI-9B at 540 nm with no staining at inverted contrast. TO emission increases with triplex formation. Triplex control is AA-TOTFO1 Carbo at 10 eq. (lane 4).

Crosslinking activity is clearly more pronounced at lower loadings for AA-TOTFO1 Carbo with triplex formation almost complete at approx. 5 eq. (**Figure VI-9, B, lane 7**). TFO1-Carbo on the other hand, fails to attain full triplex/crosslink formation at the highest loading (10 eq.) (**Figure VI-9, A, lane 9**). Thus, it is clear that the TO unit placement on the same nucleobase monomer has a significant effect on triplex formation. Thiazole orange intercalation into the duplex target is verified through the visualisation of the triplex systems without the use of a stain (**Figure VI-10, lane 6-9**). The intensity of TO increases in line with hybrid loading as it fully intercalates the duplex target sequence aiding the formation and stabilisation properties.

VI. 3. Conclusion

Second-generation *cis*-Pt(II)-TFO hybrids have been successfully developed using the Pt-N_3-Carbo analogue and the novel AP-C3 nucleobase monomer. The introduction of thiazole orange onto the same nucleobase as the platinum(II) metal demonstrates greater triplex forming ability than that of standard Pt(II)-TFO hybrids generated previously. Furthermore, crosslinking was demonstrated through the use of NaCN reversal experiments. Although thermal melting analysis proved inconclusive in identifying the triplex thermal stability, PAGE

analysis confirms that indeed crosslinking and triplex formation is occurring. Future work involving the optimisation of thermal melting conditions that prove the melting temperatures of TO-functionalised AA-TFO are equivalent to that of the underlying duplex target would be an important advancement to explore.

Chapter VII

Development of Cu(II)-AMN-TFO Hybrids using the SPAAC Click Chemistry Strategy

The work presented in this chapter details the development of Cu(II)-artificial metallo-nuclease (AMN) TFO hybrids generated through SPAAC click chemistry. A draft manuscript reporting the results of this work is in preparation.

VII. 1. Abstract

Cu(II) artificial metallo-nuclease (AMN) TFO hybrids are of considerable interest as gene-targeted therapeutics and are generated via the conjugation of an AMN with a guide TFO vectors. Recent work has demonstrated the ability to generate these targeted constructs through the use of click chemistry strategies with optimal yields and purities. However, there are still challenges to overcome in the design and optimisation of Cu(II)-AMN-TFO systems, notably the stabilisation characteristics of resultant DNA triplexes. In this work, an alkyne-TFO vector was modified with a terminal strain-promoting cyclooctyne BCN modification. The strain-promoted azide-alkyne (SPAAC) click chemistry protocol was employed to conjugate copper chelating ligand scaffolds in order to afford Cu(II)-AMN-TFO hybrids. These hybrids were investigated for enhanced gene targeting and triplex stabilisation properties through the use of thermal melting and PAGE techniques.

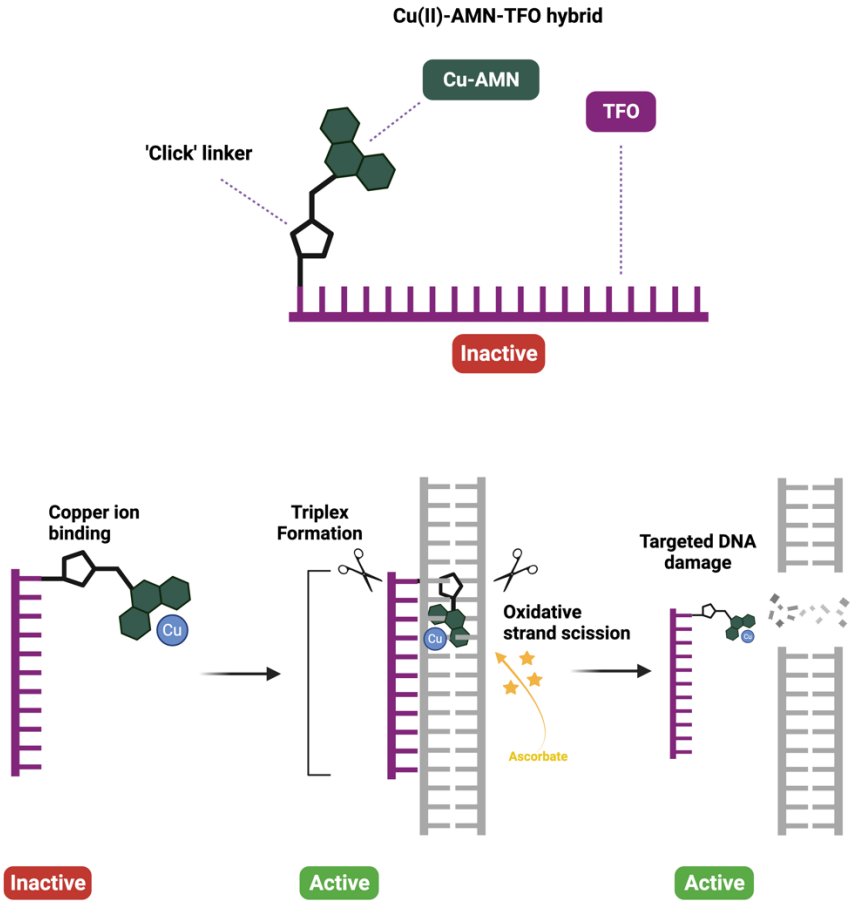

Figure VII-1. Overview of the design of the Cu(II)-AMN-TFO hybrid and potential gene-targeted oxidative DNA damage.

VII. 1. 1. Chapter Aims

- To prepare a library of Cu(II)-phenanthrene analogues for combination with TFO sequences.

- To generate Cu(II)-AMN-TFO hybrids using the SPAAC click strategy.

- To investigate the triplex stabilisation and gene-targeting properties of the Cu(II)-AMN-TFO hybrids.

VII. 1. 2. Rationale

The design of Cu(II)-AMN-TFO hybrids using SPAAC click chemistry strategies is of significant interest due to the biorthogonal application possibilities in gene targeting therapies. As such the aim of this work was to design Cu(II)-AMN-TFO hybrids based on a series of phenazine derivatised ligands and a BCN-modified TFO vector. The hybrids generated here were investigated for their ability to form stable triplex systems combined with sequence specific gene-targeted oxidative DNA damage. A future aim of this work will be to conjugate the pre-eminent ligands with AA-TOTFOs previously generated in order to investigate how targeted DNA damage is affected by introduction of both the AP-C3 monomer and TO intercalating units.

VII. 2. Introduction

Artificial metallo-nucleases (AMNs) are synthetic biomimetics of naturally occurring restriction enzymes and nucleases that possess the ability to discretely cleave single and double stranded DNA substrates. Many biological nucleases contain metal ions such as Ca(II), Zn(II) and Mg(II) which play a key role in the catalytic action they perform.[1] To imitate these natural molecules, AMNs have been designed with the ability to chelate a large variety of redox active metals like Cu, Co, Ru, Fe and Ni to name but a few leading examples. In general, AMNs fall into categories dependent on their mechanism of DNA damage – either by oxidative damage or hydrolytic cleavage along the phosphodiester backbone.[2] Hydrolytic cleavage proceeds through i.) the initial activation of the phosphate toward nucleophilic attack; ii.) the conversion of water to a hydroxyl nucleophile,

and iii.) attack on the phosphate by the hydroxyl nucleophile followed by hydrolysis of the phosphodiester backbone at the 3'-OH end.[3]

Oxidative damage, on the other hand, induces direct strand scission in the presence of exogenous reductant and oxidant. The ability of AMNs to efficiently bind DNA and elicit an oxidative effect is key to their rise in prominence where $[Cu(1,10\text{-phenanthroline})_2]^{2+}$ or Cu-Phen, the first synthetic chemical nuclease, initiated a large surge in the development of this class of molecule. First discovered by Sigman in 1979,[4] Cu-Phen was found to incur direct strand scission along A-T rich tracts in the minor groove. After reduction to the Cu(I) species, Cu-Phen is found to semi-intercalate and abstract the hydrogen of the C1'-position predominantly over the C5'- and C4'- positions of the deoxyribose ring. Greenberg *et al*.[5, 6] critically determined strand breaking occurs by a mechanism proceeding through abstraction at C1' and formation of the peroxyl radical intermediate which in turn expels superoxide and forms the oxidised C1' intermediate. Further β-elimination occurs in the presence of Cu-Phen catalyst with the 3'-furanone product terminally converted to 5-methylfuranone. (**Figure VII-2**)

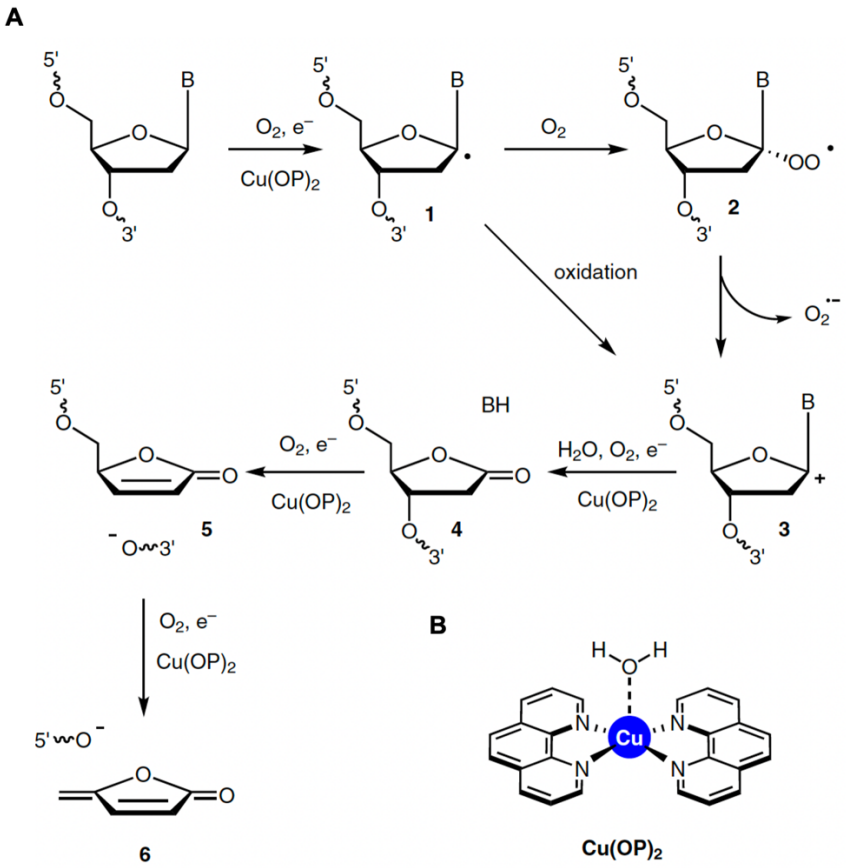

Figure VII-2. A. Radical oxidative cleavage by Cu-Phen resulting in direct strand break formation. **B.** Structure of $[Cu(1,10\text{-phenanthroline})_2(H_2O)]^{2+}$. Figure adapted from ref.[2]

Limitations of Cu-Phen systems include: i.) *off*-target specificity issues; ii.) a high dissociation constant of the secondary ligand; and iii.) a need for exogenous reductant and oxidation.[7] Attempts to enhance the sequence specificity of AMNs have involved covalent attachment with targeting vectors such as peptide nucleic acids (PNAs),[8] proteins,[9] and oligonucleotides.[10] Triplex-forming oligonucleotides (TFOs) represent an emerging class of nucleic acid vector that display affinity for sequence specific binding interactions with target genes of interest. Recently, this group has demonstrated how classes of Cu(II)-AMN can be conjugated through click chemistry strategies to afford Cu(II)-AMN TFO hybrids that possess gene-targeting properties. As such, Cu(II)-AMNs based on a caging *tris*-(2-pyridylmethyl)amine (TPMA) scaffold has been combined with gene-targeting TFO vectors.[11] Additionally, Cu(II)-AMN-TFO hybrids based on traditional phenanthrene-like scaffolds were reported and represent the first known example of a combined triplex stabilising and cleavage system.[12]

VII. 3. Generation of Cu(II)-Phen analogues

VII. 3. 1. Development of synthetic routes

Cu(II)-AMN-TFOs based on phenazine scaffolds have previously demonstrated outstanding ability to positively influence triplex stability and provide sequence selective oxidative DNA damage.

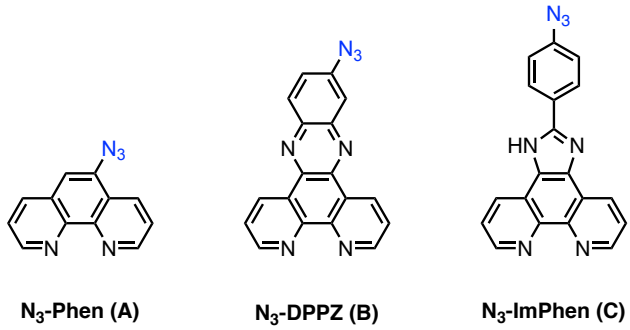

Figure VII-3. Ligand scaffolds for Cu(II)-AMN-TFO hybrid generation.

Azide-functionalised ligand 2-(4-azidophenyl)-1H-imidazo[4,5-f]-1,10-phenanthroline (**19**, N_3-ImPhen, **C**) (**Scheme VII-1**) was selected as a potential scaffold for investigation in developing these hybrids. Additionally, ligands 5-azido-1,10-phenanthroline (**2**, N_3-Phen, **A**) and 11-azidodipyrido[3,2,*a*:2',3'-*c*]phenazine (**7**, N3-DPPZ, **B**) were selected (**Figure VII-3**). These phenanthrene ligands have previously shown exceptional thermal stabilisation properties of >20 ºC within TFO hybrid systems.[12]

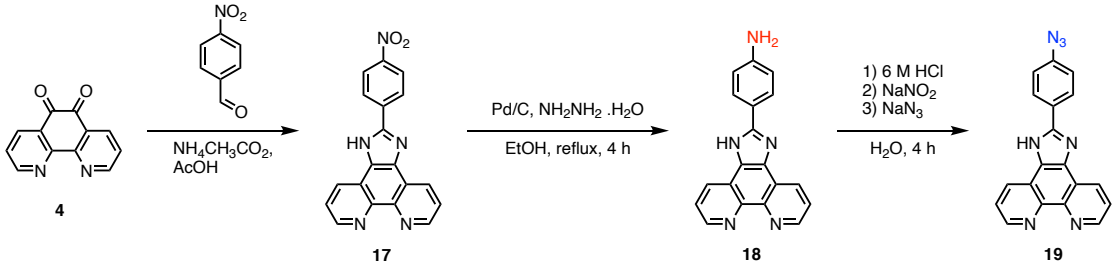

Scheme VII-1. Synthetic routes for the generation of N_3-ImPhen (19).

VII. 3. 2. Materials and Methods

VII. 3. 2. 1. Organic Synthesis

2-(4-nitrophenyl)-1*H*-imidazo[4,5-*f*]-1,10-phenanthroline (17)

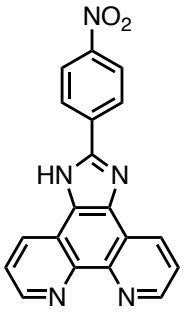

17

Reaction protocol was adapted from the literature method previously reported by Lauria *et al*.[12] Briefly, 1,10-phenanthroline-5,6-dione (0.500 g, 2.37 mmol, 1 eq.) was dissolved in 25 mL of glacial acetic acid. 4-nitobenzaldehyde (0.540 g, 3.57 mmol, 1.5 eq.) was then added, followed by ammonium acetate (5.40 g, 70 mmol, 30 eq.). The mixture was stirred under reflux for 2 h and the pH was neutralized with ammonia solution. The precipitate was isolated by vacuum filtration and washed with 3 x 10 mL of water and 3 x 10 mL of diethyl ether to afford the product as light orange solid. Yield: 0.720 g, 89%.

^{1}H NMR (600 MHz, DMSO) δ 9.00 (dd, *J* = 4.2, 1.8 Hz, 2H), 8.92 (dd, *J* = 8.1, 1.8 Hz, 2H), 8.56 – 8.52 (m, 2H), 8.44 – 8.41 (m, 2H), 7.81 (dd, *J* = 8.0, 4.2 Hz, 2H). ^{13}C NMR (151 MHz, DMSO-d_6): 172.47, 148.70, 148.57, 147.91, 144.41, 136.17, 130.18, 127.37, 124.87, 123.85.

2-(4-aminophenyl)-1*H*-imidazo[4,5-*f*]-1,10-phenanthroline (18)

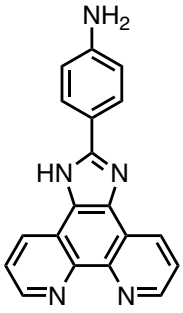

18

Reaction protocol was adapted from the literature method previously reported by Lauria *et al*.[12] Intermediate **17** (500 g, 1.46 mmol, 1 eq.) was dissolved in 110 mL of methanol. Hydrazine hydrate (5 ml) was added dropwise prior to the addition of 10 % Pd/C (0.050 g). The resultant mixture was stirred under reflux for 2 hours, before cooling to room temperature and further stirred for 2 h. The cold mixture was filtered through celite and solvent reduced *in vacuo* until a brown solid precipitated. The precipitate was collected and washed with 3 x 10 mL of water and 3 x 10 mL of diethyl ether, to afford the product as a brown solid. Yield: 0.234 g, 52%.

^{1}H NMR (600 MHz, DMSO) δ 13.30 (s, 1H), 9.00 (dd, *J* = 4.3, 1.8 Hz, 2H), 8.92 – 8.86 (m, 2H), 7.99 – 7.94 (m, 2H), 7.81 (s, 2H), 6.75 – 6.72 (m, 2H), 5.64 (s, 2H). ^{13}C NMR (151 MHz, DMSO-d_6): 152.54, 150.93, 147.96, 147.71, 136.13, 129.98, 129.74, 128.05, 126.13, 124.16, 123.72, 123.51, 119.75, 117.76, 114.11.

2-(4-azidophenyl)-1*H*-imidazo[4,5-*f*]-1,10-phenanthroline (19)

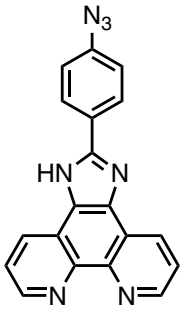

19

Reaction protocol was adapted from the literature method previously reported by Lauria *et al*.[12] Briefly, intermediate **18** (0.200 g, 0.64 mmol, 1 eq.) was stirred in 10 mL of aqueous 6 M hydrochloric acid for 20 min at 0 °C. A solution of sodium nitrite (0.066 g, 0.96 mmol, 1.5 eq.) in 1 mL of water was added dropwise at 0 °C and the mixture was stirred for 30 min, followed by the dropwise addition of sodium azide (0.125 g, 1.92 mmol, 3 eq.) in 1 mL of water. The resultant mixture was further stirred for 2 h at 0 °C and the pH was neutralized with an aqueous ammonia solution. The product was obtained by vacuum filtration and washed with 3 x 10 mL of water and 3 x 10 mL of diethyl ether to afford **19** as an off-yellow solid. Yield: 0.160 g, 74%.

^{1}H NMR (600 MHz, DMSO) δ 13.85 (s, 1H), 9.06 – 8.93 (m, 4H), 8.34 – 8.30 (m, 2H), 7.87 (dt, *J* = 7.8, 3.7 Hz, 2H), 7.39 – 7.34 (m, 2H). ^{13}C NMR (151 MHz, DMSO-d_6): 150.48, 148.12, 143.40, 141.11, 130.55, 128.36, 127.22, 123.99, 120.32, 114.10.

VII. 3. 2. 2. Oligonucleotide Development and General Information

AMN-TFO hybrid generation using click chemistry

For click reactions concerning the 5'-BCN(CEP II)-dC modified TFO2 the following procedure was applied. In a total volume of 500 μL (50:50 H_2O:DMSO) 500 nmol of azide ligand was added to 50 nmol of the alkyne-modified TFO. The click solutions were degassed with argon and stirred at 25 °C for 5 h prior to desalting by elution through a NAP-10 column. AMN-TFO hybrids were purified using Amicon Ultra 0.5 mL centrifugal columns prior to freeze-drying for future use.

Thermal Melting and Triplex Formation Analysis

Thermal melting analysis was performed as previously described in Chapter IV. Triplex formation was analysed by native PAGE. In a total volume of 5 μL triplex buffer (10 mM phosphate, 150 mM NaCl, 2 mM $MgCl_2$ (pH 6)), target (57 bp, 1pmol) and off-target (40 bp, 1 pmol) were treated with increasing concentrations of TFO hybid (2.5-50 eq.). Samples were incubated at 37 ºC for 24h prior to addition of 6X loading dye (Thermo Scientific) and loaded onto a 20% polyacrylamide gel (50 mM Tris acetate, 150 mM NaCl, 2 mM $MgCl_2$, pH 6). Samples contained TO modifications were loaded with 30% glycerol solution. Electrophoresis was performed at 70 V for 240 mins in triplex running buffer (50 mM Tris acetate, pH 6) unless otherwise stated. Polyacrylamide gels were post-stained with SybrGold and visualised and imaged on a Syngene G:Box Mini 9 gel documentation system.

Chemical Nuclease Activity

In a total volume of 6 μL triplex buffer, TFO-hybrid (10 pmol) was treated with $CuSO_4$ (10 pmol) for 30 min at 37 ºC prior to addition to a solution of target (1 pmol), off-target (1 pmol) in the presence or absence of Na-L-ascorbate (10-250 nmol). Samples were incubated at 37 ºC for 24 h prior to addition of 6X loading dye (Thermo Scientific) and loaded onto a 20% polyacrylamide gel (50 mM Tris acetate, 150 mM NaCl, 2 mM $MgCl_2$, pH 6). Samples contained TO modifications were loaded with 30% glycerol solution. Electrophoresis was performed at 70 V

for 240 mins in triplex running buffer (50 mM Tris acetate, pH 6) unless otherwise stated. Polyacrylamide gels were post-stained with SybrGold and visualised and imaged on a Syngene G:Box Mini 9 gel documentation system. Band densitometry analysis was performed using SynGene-GeneTools software (v. 4.3.14.0). Raw peak heights were determined and normalised against raw peak heights of control lanes (Target, Off-target, Triplex). Depletion and cleavage was analysed and graphed using GraphPad Prism 8 software.

VII. 3. 3. Thermal melting analysis of TFO2-AMN hybrids

In order to develop a series of targeted TFO-AMNs, the three ligands described above were selected and combined with TFO2, a 29 nt polypyrimidine TFO with a terminal 5'-BCN(CEP II)-dC nucleobase modification (**Appendix B**). The hybrids were obtained using SPAAC click chemistry in moderate to high yields (TFO2A, **61%**; TFO2B, **51%**; TFO2C, **43%**). Unlike for previous platinum(II)-TFO hybrids, the SPAAC click chemistry methodology is the preferred pathway for Cu-AMN TFO hybrid generation. The ligand scaffolds have significant chelating ability for copper ions and therefore standard CuAAC protocols can prove challenging during the synthesis of the hybrids. SPAAC allows for the addition of the ligands without the need for post-clicking EDTA workups or precise purification methods to remove the EDTA-Cu by-product.

Ligand selection was based on examining the binding affinity of the aromatic system upon triplex formation. N_3-Phen (**A**) is a known DNA semi-intercalator and is an ideal candidate as a chelating scaffold. N_3-DPPZ (**B**) is a similar compound wherein the aromatic system is extended in the attempt to further increase the stabilisation characteristics via intercalation, and N_3-ImPhen (**C**) is quite similar to **B** in size, however the introduction of a rotational centre about the azide-phenyl and imidazole-phen moieties may provide flexibility for binding to a specific target gene.

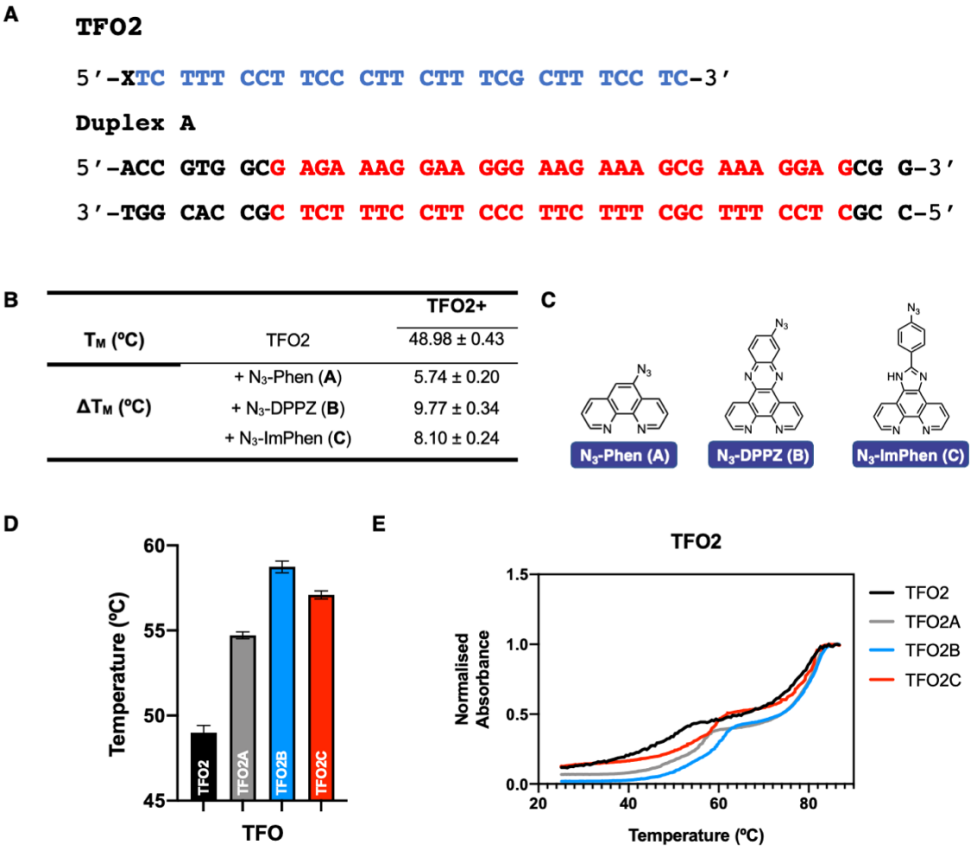

Figure VII-4. A. TFO2 and duplex target A, where X = 5'-BCN(CEP II)-dC. **B.** Thermal melting analysis of TFO2A-C in comparison to TFO2. **C.** Ligands A-C. **D.** ΔT_M for TFO2 hybrids. **E.** Melting curves for TFO2 hybrids.

Duplex A was treated against TFO2 and TFO2A-C hybrids in 10 mM phosphate, 150 mM NaCl and 2 mM $MgCl_2$ pH 6 for 24 h at 37 ºC prior to melting analysis. Each hybrid displayed significant thermal stabilisation over the TFO2 control. The extended aromatic systems (N_3-DPPZ and N_3-ImPhen) produced greater stability (**Figure VII-4, B**) over the smaller N_3-Phen system, where increased thermal stability followed the pattern **B** > **C** > **A**. This effect is most likely due to the reduced flexibility and size of the more rigid phenanthroline scaffold. Notably, the N_3-DPPZ produces the greatest thermal stabilisation – the larger aromatic system conveying greater stability and affinity. Similarly the N_3-ImPhen produces thermal stability in the same range whereby the rotational freedom appears to enhance the DNA triplex. Finally, hybrids of TFO2A-C were analysed for thermal stability in the presence of free copper ions ($CuSO_4$) in solution to identify their effect on triplex formation. Melting temperature differences were observed to be negligible in the presence of free Cu(II) ions and confirmed that triplex formation is thus unhindered by their presence.

VII. 3. 4. PAGE Analysis and Chemical Nuclease Activity of TFO2 Hybrids

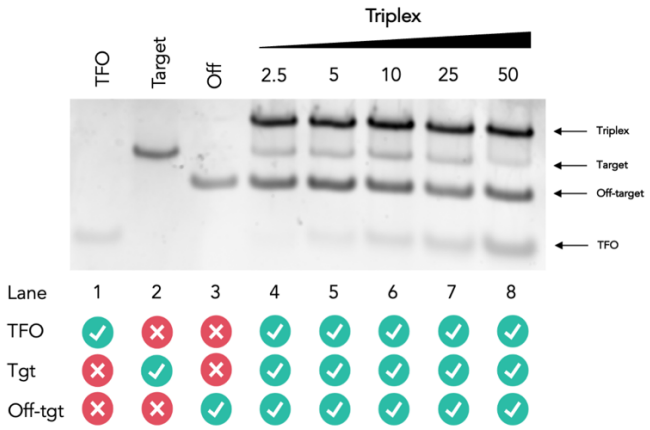

Figure VII-5. Alkyne-modified TFO2 triplex control.

Next, hybrid systems were investigated for their triplex forming ability and sequence-selectivity against *on*- and *off*-target duplex sequences (**Figure VII-6, A**) using PAGE analysis. TFO2 hybrid triplex formation was measured over an increasing concentration of 2.5-50 eq. and compared to the unmodified TFO2 control (**Figure VII-5**). TFO2B was observed to generate full triplex formation at 2.5 eq. (**Figure VII-6, C, lane 5**) and is comparable to TFO2 itself. TFO2C only presents complete triplex formation as higher equivalents are added i.e. >10 eq. (**Figure VII-6, D, lane 8**) whereas TFO2A presents the poorest triplex forming ability with > 25 eq. TFO-hybrid required to generate full triplex systems. Triplex formation for the TFO2 hybrids follows the pattern demonstrated above whereby triplex forming affinity is found to be : **B** > **C** > **A**. Although enhanced thermal stability appears to correlate with triplex formation this does not account for the equivalent formation that both the TFO2 control and TFO2B hybrids present, where TFO2 has the lowest triplex thermal stability among the oligonucleotides. Therefore, the ligand scaffold is clearly playing a part in the binding kinetics of the TFO2 hybrids.

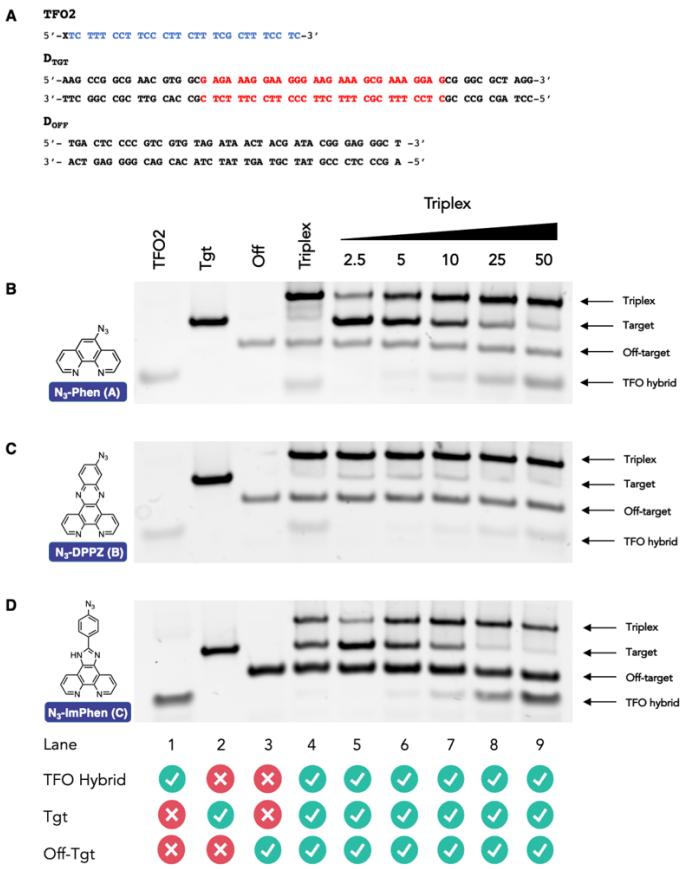

Figure VII-6. A. TFO2 and D_{ON} (57 bp) and D_{OFF} (40 bp) sequences where X = 5'-BCN(CEP II)-dC. Triplex formation for **B**. TFO2A. **C**. TFO2B and **D**. TFO2C. Target (57 bp, 1 pmol, lane 2) and off-target (40 bp, 1 pmol, lane 3) were treated with 2.5-50 eq. of TFO2 hybrid. Samples were prepared in 10 mM phosphate buffer, 150 mM NaCl and 2 mM $MgCl_2$ (pH 6) prior to incubation over 24 h at 37 ºC**.** Samples were then loaded onto 20% PAGE and subjected to electrophoresis for 4h at 70 V in 50 mM tris-acetate (TA) buffer (pH 6). Gels were post-stained with SybrGold.

With thermal stability and triplex formation identified for the TFO2-hybrids, the chemical nuclease activity of the hybrids was next investigated. In these experiments triplex formation was investigated against *on*- and *off*-target sequences in the presence of Cu(II) ions and Na-*L*-ascorbate. Initially, TFO2A was selected for the preliminary experiments to identify the ascorbate loading required to trigger targeted cleavage. TFO2A (10 pmol, 10 eq.) was incubated with $CuSO_4$ (10 pmol, 10 eq.) for 30 min at 37 ºC prior to addition to a solution of target duplex (57 bp, 1 pmol, 1 eq.). The addition of ascorbate (10-250 nmol, 10-250 eq.) was required to initiate the cleavage reaction. Samples were incubated for 24 h at 37 ºC prior to loading onto 20% PAGE. At lower ascorbate loadings, triplex formation proceeds unhindered as observed below (**Figure VII-7, A**),

however as the loading of reductant increases controlled triplex depletion is demonstrated alongside target depletion (**Figure VII-7, B**).

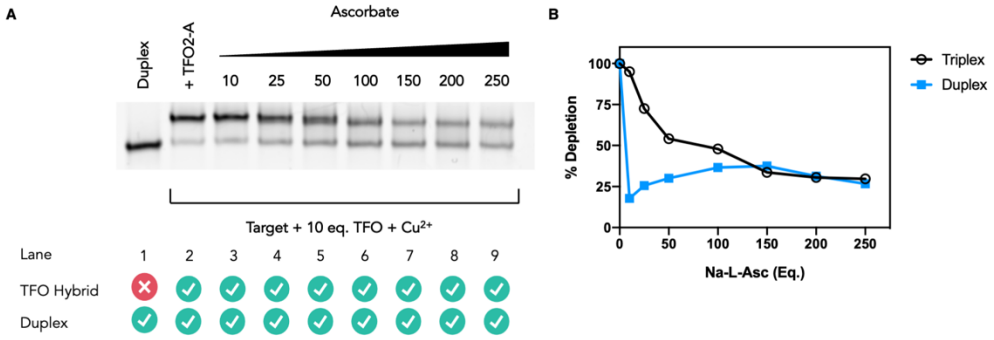

Figure VII-7. A. TFO2A cleavage optimisation with increasing ascorbate loading. **B**. Band densitometry analysis of the cleavage reaction. Band intensities were normalised to lane 1 (duplex target) and lane 2 (triplex formation without ascorbate). Samples were prepared in 10 mM phosphate buffer, 150 mM NaCl and 2 mM $MgCl_2$ (pH 6) prior to incubation over 24 h at 37 ºC**.** Samples were then loaded onto 20% PAGE and subjected to electrophoresis for 4h at 70 V in 50 mM tris-acetate (TA) buffer (pH 6). Gels were post-stained with SybrGold.

With the cleavage range determined, next the TFO2 hybrids were compared for their sequence specific cleavage activity across an increasing ascorbate loading gradient (**Figure VII-8**). TFO2 hybrid loadings were kept as before (10 pmol) as was the quantity of *on*-target duplex (D_{ON}, 57 bp, 1 pmol). However, for these experiments, an *off*-target (D_{OFF}, 40 bp, 1 pmol) was also added to explore the possibility of indiscriminate cleavage damage by the hybrid. As before, TFO2 hybrids were incubated with $CuSO_4$ prior to addition to a solution containing the target and off-target sequences. Cleavage was initiated by the addition of ascorbate. The system follows the protocol D:TFO:Cu:Asc = 1:10:10:X, where X = 10-250 eq. of TFO2 hybrid. Samples were incubated in triplex buffer for 24 h at 37 ºC prior to analysis on 20% PAGE. Band densitometry analysis was performed to examine the extent of triplex and target duplex depletion. All TFO2 hybrids demonstrated cleavage activity. Similar to the thermal stability and triplex formation, TFO2B presents the greatest cleavage activity with up to 91% triplex depletion observed and 63% D_{ON} depletion (**Figure VII-8, B** and **D**). TFO2A demonstrates similar activity with 80% triplex and 65 % D_{ON} depletion observed (**Figure VII-8, A** and **D**). Although TFO2C displayed significant depletion of triplex and D_{ON}, the activity was not as pronounced as the former hybrids (**Figure VII-8, C** and **D**). The pattern of cleavage activity follows:

B > A > C (**Figure VII-8, E**). In comparison to D_{ON} cleavage, damage to the D_{OFF} was relatively insignificant although it is not negligible. TFO2A presented the greatest amount of indiscriminate duplex target with approx. 45% depletion of the D_{OFF} target.

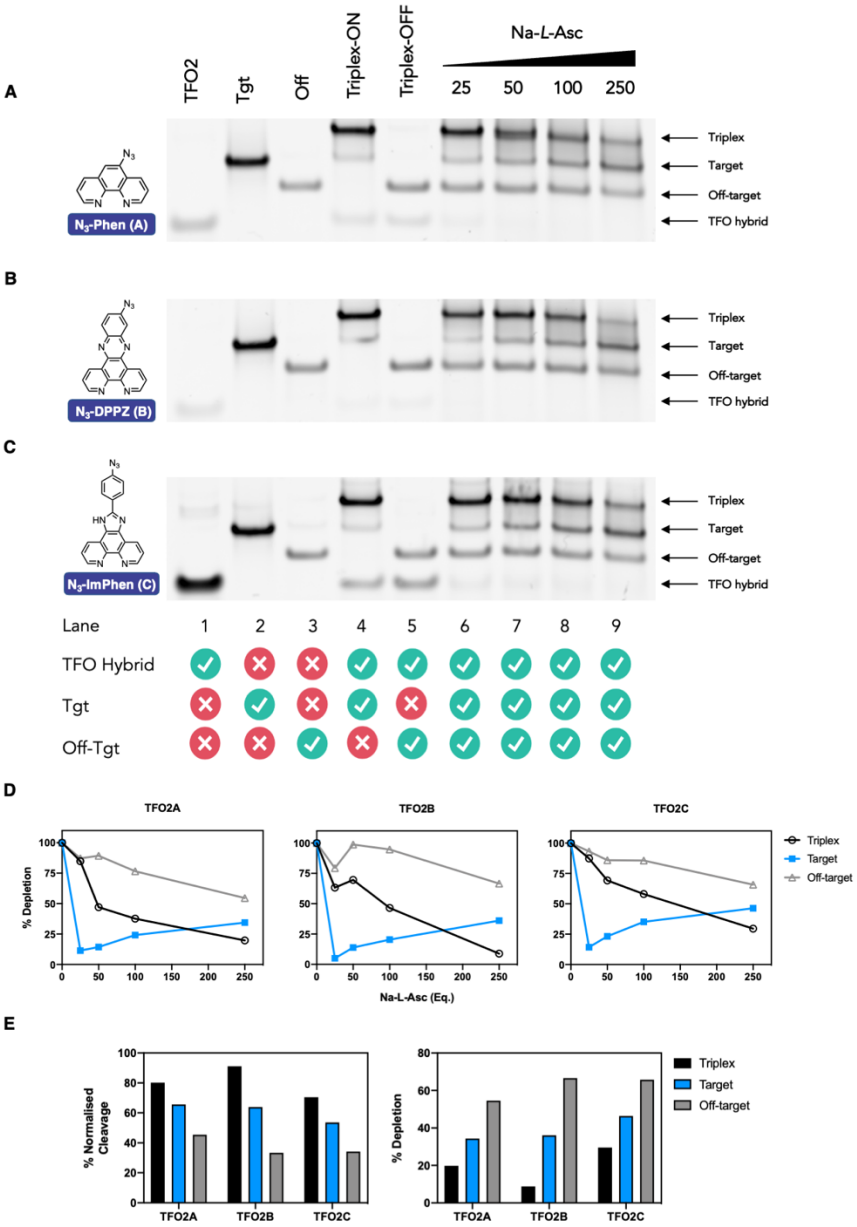

Figure VII-8. TFO2 hybrid cleavage activity. Cleavage for **A**. TFO2A. **B**. TFO2B and **C**. TFO2C. Target (57 bp, 1 pmol, lane 2) and off-target (40 bp, 1 pmol, lane 3) were treated with 10 eq. of TFO2 hybrid and 10 eq. of $CuSO_4$. Increasing concentrations of ascorbate were added to initiate cleavage reaction. **D**. Band densitometry analysis of the cleavage reaction. Band intensities were normalised to lane 2 (duplex target), lane 3 (off-target duplex) and lane 4 (triplex formation without Cu(II)/Na-L-asc). **E**. % Normalised cleavage and % depletion of sample bands. Samples were prepared in 10 mM phosphate buffer, 150 mM NaCl and 2 mM $MgCl_2$ (pH 6) prior to incubation over 24 h at 37 ºC**.** Samples were then loaded onto 20% PAGE and subjected to electrophoresis for 4h at 70 V in 50 mM tris-acetate (TA) buffer (pH 6). Gels were post-stained with SybrGold.

VII. 3. 4. 1. Summary

Hybrids of TFO2 have demonstrated significant potential as Cu(II)-AMN-TFO hybrid targeted cleavage agents with high nuclease activity observed. The absence of complete disintegration of the D_{ON} and D_{OFF} structures may imply that single-stranded DNA damage is implicated as the form of cleavage. Targeted GFP gene cleavage was achieved without the need for high levels of hybrid or Cu(II) loading to initiate damage. However, even though target specificity is quite good, the *off*-target cleavage cannot be ignored and thus future work may need to focus on minimising these negative effects. The development of Cu(II)-AMN-AA-TOTFOs is a plausible pathway to follow for the development of future hybrids. The incorporation of TO units, specifically onto the same nucleobase, may alleviate the indiscriminatory side-effects through increased specificity and binding affinity for the D_{ON} sequence. Finally, mechanistic studies are planned to investigate the free radical generation which is responsible for the cleavage activity. Coinciding with this, sequencing experiments are planned to precisely investigate the site at which single strand breaks are mediated.

VII. 3. 4. 2. Future Work

As the hybrid design produced significant triplex stability and nuclease activity, a future aim is to expand the library of ligand scaffolds to identify optimal ligand parameters such as size, rigidity and linker applicability. 4-azido-N-(dipyrido[3,2-a:2',3'-c]phenazine-11-yl)butanamide (**21**, N_3-But-DPPZ) is a fitting candidate for investigation with both standard alkyne modified TFOs and also AA-TOTFOs – the extended aromatic system paired with the ability to freely rotate has demonstrated significant thermal stability in previous work performed by the Kellett group.[12] The ligand has not yet been combined through SPAAC methodologies however and thus is an ideal compound for future work (**Scheme VII-2**).

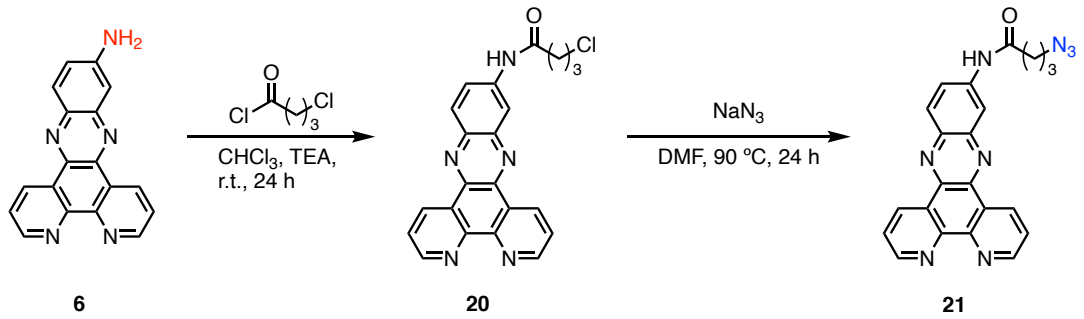

6 **20** **21**

Scheme VII-2. Synthetic routes for the generation of N_3-But-DPPZ.

Additionally, a class of azide-modified ascididemin derivatives are proposed as an alternative scaffold. Natural marine alkaloids have long been studied for their anticancer properties. In particular, the marine alkaloids based off pyrido-acridine scaffolds have been intensely studied with Ascididemin the preeminent compound of the family.[13] Acididemin has demonstrated the ability to elicit reductive DNA cleavage mediated by reactive oxygen species even in the absence of redox metals.[14] Therefore the choice of ascididemin-derived cleavage agents presents the ability to generate analogues that can chelate copper and undergo typical redox metal mediated ROS generation but also allows for the design of a series of self-activating ascididemin-AMN-TFO hybrids that display novel DNA binding and cleavage properties. A proposed synthetic route for the development of ascididemin derivatives based on a pyrido-phenanthrolin-7-one scaffold[15] (**Scheme VII-3**) that contain an azide click handle can be found below.

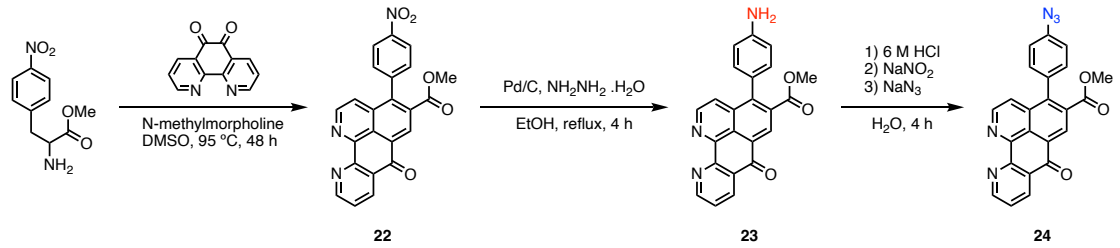

22 23 24

Scheme VII-3. Synthetic routes for the generation of Methyl 4-(4-azidophenyl)-7-oxo-7H-pyrido[4,3,2-de][1,10]phenanthroline-5-carboxylate.

Studies performed by Kiss *et al.*[16] have shown that some synthetic ascididemin analogues display greater anticancer activity than the natural parent alkaloid. As such, these analogues have provided the inspiration for another azide-modified derivative[17] (**Scheme VII-4)** that can generate hybrids with TFO substrates.

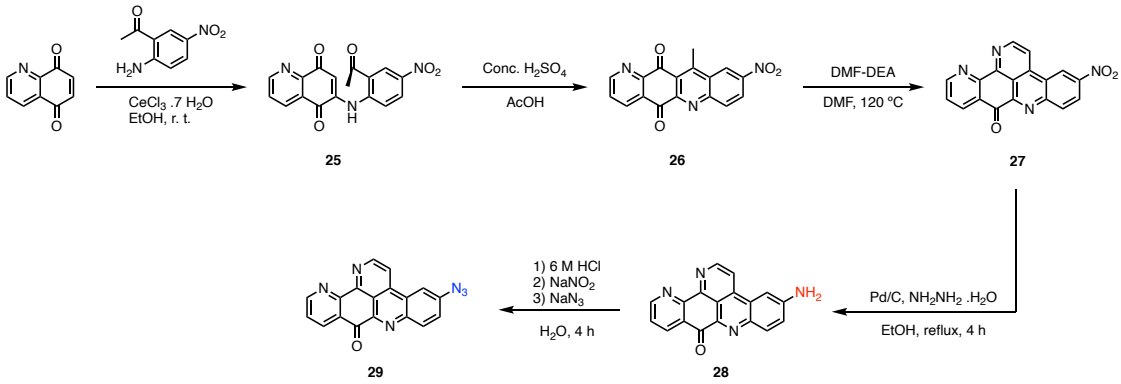

25 26 27 28 29

Scheme VII-4. Synthetic routes for the generation of 5-azidoascididemin.

VII. 4. Conclusion

A new class of Cu(II)-AMN scaffold was prepared using SPAAC click chemistry methodology. These hybrids display significant thermal stability, triplex formation, and targeted cleavage activity. The constructs represent a new class of Cu(II)-AMN-TFO hybrids with specific gene targeting and damaging properties. The use of SPAAC click chemistry ideally allows for future endeavours to be aimed at interesting biorthogonal applications where CuAAC pathways may prove undesirable. Future work aims to incorporate AA-TOTFOs into the pool of possible TFO vectors for Cu(II)-AMN-TFO hybrid generation whereby the advent of the TO unit and bifunctional AP-C3 nucleobase afford possible increases in triplex stability and target specificity whilst enhancing targeted DNA damage.

VII. 5. References

1. Mancin, F.; Scrimin, P.; Tecilla, P.; Tonellato, U., Artificial metallonucleases. *ChemComm* **2005,** (20), 2540.
2. Kellett, A.; Fantoni, N.; Lauria, T., Genome Engineering with Synthetic Copper Nucleases. *Synlett* **2015,** *26* (19), 2623-2626.
3. Bashkin, J. K.; Jenkins, L. A., The Role of Metals in the Hydrolytic Cleavage of DNA and RNA. *Comments Inorg. Chem.* **2006,** *16* (1-2), 77-93.
4. Sigman, D. S.; Mazumder, A.; Perrin, D. M., Chemical Nucleases. *Chem. Rev.* **1993,** *93*, 2295-2316.
5. Chen, T.; Greenberg, M. M., Model Studies Indicate That Copper Phenanthroline Induces Direct Strand Breaks via B-Elimination of the 2'-Deoxyribonolactone Intermediate Observed in Enediyne Mediated DNA Damage. *J. Am. Chem. Soc.* **1998,** *120*, 3815-3816.
6. Bales, B. C.; Pitié, M.; Meunier, B.; Greenberg, M. M., A Minor Groove Binding Copper-Phenanthroline Conjugate Produces Direct Strand Breaks via β-Elimination of 2-Deoxyribonolactone. *J. Am. Chem. Soc.* **2002,** *124* (31), 9062-9063.
7. Kellett, A.; Molphy, Z.; Slator, C.; McKee, V.; Farrell, N. P., Molecular methods for assessment of non-covalent metallodrug–DNA interactions. *Chem. Soc. Rev.* **2019,** *48* (4), 971-988.
8. Yamamoto, Y.; Mori, M.; Aiba, Y.; Tomita, T.; Chen, W.; Zhou, J.-M.; Uehara, A.; Ren, Y.; Kitamura, Y.; Komiyama, M., Chemical modification of Ce(IV)/EDTA-based artificial restriction DNA cutter for versatile manipulation of double-stranded DNA. *Nucleic Acids Res.* **2007,** *35* (7), e53.
9. Gallagher, J.; Chen, C.-H. B.; Pan, C. Q.; Perrin, D. M.; Cho, Y.-M.; Sigman, D. S., Optimizing the Targeted Chemical Nuclease Activity of 1,10-Phenanthroline−Copper by Ligand Modification. *Bioconjug. Chem.* **1996,** *7* (4), 413-420.
10. Dreyer, G. B.; Dervan, P. B., Sequence-specific cleavage of single-stranded DNA: oligodeoxynucleotide-EDTA X Fe(II). *Proc. Natl. Acad. Sci.* **1985,** *82* (4), 968-972.

11. Zuin Fantoni, N.; McGorman, B.; Molphy, Z.; Singleton, D.; Walsh, S.; El-Sagheer, A. H.; McKee, V.; Brown, T.; Kellett, A., Development of Gene-Targeted Polypyridyl Triplex-Forming Oligonucleotide Hybrids. *ChemBioChem* **2020,** *21* (24), 3563-3574.
12. Lauria, T.; Slator, C.; McKee, V.; Müller, M.; Stazzoni, S.; Crisp, A. L.; Carell, T.; Kellett, A., A Click Chemistry Approach to Developing Molecularly Targeted DNA Scissors. *Chem. Eur. J.* **2020,** *26* (70), 16782-16792.
13. Molinski, T. F., Marine Pyridoacridine Alkaloids: Structure, Synthesis, and Biological Chemistry. *Chem. Rev.* **1993,** *93*, 1825-1838.
14. Matsumoto, S. S.; Sidford, M. H.; Holden, J. A.; Barrows, L. R.; Copp, B. R., Mechanism of action studies of cytotoxic marine alkaloids: ascididemin exhibits thiol-dependent oxidative DNA cleavage. *Tetrahedron Lett.* **2000,** *41* (10), 1667-1670.
15. Ahmed, M.; Rooney, D.; McCann, M.; Casey, J.; O'Shea, K.; Twamley, B., Tuning the reaction pathways of phenanthroline-Schiff bases: routes to novel phenanthroline ligands. *Dalton Trans.* **2019,** *48* (40), 15283-15289.
16. Delfourne, E.; Darro, F.; Portefaix, P.; Galaup, C.; Bayssade, S.; Bouteillé, A.; Le Corre, L.; Bastide, J.; Collignon, F.; Lesur, B.; Frydman, A.; Kiss, R., Synthesis and In Vitro Antitumor Activity of Novel Ring D Analogues of the Marine Pyridoacridine Ascididemin: Structure−Activity Relationship. *J. Med. Chem.* **2002,** *45* (17), 3765-3771.
17. Gellerman, G.; Rudi, A.; Kashman, Y., Biomimetic Synthesis of Ascididemin and Derivatives. *Synthesis* **1993,** *03*, 239-241.

Thesis Conclusions and Future Work

This work focused on the design and synthesis of a series of azide-functionalised *cis*-platinum(II) based on molecular phenazine scaffolds and traditional *cis*-platinum(II) analogues. Solid-phase oligonucleotide synthesis was employed to generate a library of alkyne-TFO nucleic acid vectors and, through the use of click chemistry strategies, a novel class of targeted *cis*-platinum(II)-TFO hybrids was realised. Initially envisioned to provide enhanced stability through the intercalant, the *cis*-platinum(II) phenazine analogues, **Pt-N_3-Phen** and **Pt-N_3-DPPZ**, presented solubility issues and participation in biological studies was not possible. The *cis*-platinum(II) complexes derived from the traditional analogues (**Pt-N_3-Cis**, **Pt-N_3-Carbo** and **Pt-N_3-Oxali**) demonstrated the azide moiety did not affect their ability to interact with GFP dsDNA targets, and upon interaction, notable destabilisation was observed for all targets with Pt-N_3-Cis exerting the greatest activity. However, their antiproliferative activity against various breast cancer cell lines (MCF-7, MDA-MB-231, MDA-MB-468, T47D and MCF-10a) was significantly curtailed and demonstrated that the azide functionality has a detrimental effect on the antineoplastic character of the complexes. Independently, the complexes may not serve as suitable anticancer agents in their native form although the azide handle can provide opportunities to modulate the properties of the drug through conjugation of various biomolecules that can affect transportation, localisation, and activation properties.

CuAAC and SPAAC click strategies were, for the first time, reported to generate a new class of *cis*-platinum(II)-TFO hybrid that combined the triplex recognition affinity of the TFO nucleic acid vector and retained the crosslinking properties of the platinum(II) metal ion for specific gene targeting. Notably, not all hybrids were able to form triplex motifs and for those that did, destabilisation of the triplex system was observed. Significantly, the *cis*-platinum(II)-TFO hybrids were capable of discriminating between target and purine-rich *off*-target sequences. Introduction of thiazole orange (TO) intercalating units through the bio-orthogonal SPAAC method provided augmented triplex stability for *cis*-Pt(II)-

TFO hybrid systems. Specific sequence crosslink targeting was identified for the hybrids. Next, through the introduction of an innovative AP-C3 nucleobase, a series of novel AA-TOTFO sequences were generated and combined with *cis*-platinum(II) complexes using click chemistry that demonstrated gene-targeting properties with enhanced crosslinking. Employment of these TFOs and **Pt-N_3-Carbo** afforded a novel class of *cis*-Pt(II)-TFO hybrids that possessed significant thermal stability.

SPAAC click chemistry protocols were used in conjunction with Cu(II)-AMN ligands to generate a novel class of Cu(II)-AMN-TFO hybrids that demonstrated significant thermal stabilisation capabilities and sequence-specific gene targeting properties. These constructs demonstrated the ability to enact targeted oxidative DNA damage without significant indiscriminate *off*-target degradation. The future introduction of the AA-TOTFO probes into this avenue of work presents an excellent opportunity to further improve on the work presented.

As a continuation of this work, options can be considered to optimise the solubility characteristics of the platinum(II) phenazine derivatives such as the introduction of additional functional groups onto the azide scaffold. The generation of bifunctional scaffolds that can chelate multiple platinum(II) units is also an avenue to investigate. To combat the poor triplex stability issues inherent to the *cis*-platinum(II)-TFO hybrids, the use of modified backbones or alternatives should be considered. PS and PMO oligonucleotide modifications are alternatives that have displayed considerable stabilisation properties and could find use in combination with the *cis*-platinum(II) TFO and Cu(II)-AMN-TFO constructs. The use of peptide nucleic acid (PNA) oligos is an option that would enable the adoption and implementation of these hybrids at neutral pHs and further their application *in vivo*.

Chapter VIII

Appendices

Appendix A NMR, IR and ESI-MS analysis of prepared ligand precursors and N_3-Platinum(II) complexes (Chapter III).

Appendix B ESI-MS analysis of alkyne-modified TFOs, duplex targets and *cis*-platinum(II)-TFO hybrids (Chapter IV).

Appendix C Thermal melting analysis of N_3-Platinum(II) complexes, alkyne-TFO controls and *cis*-platinum(II)-TFO hybrids (Chapter IV and V).

Appendix D Cell line characteristics and cell viability experimental parameters (Chapter V).

Appendix E Supplementary PAGE analysis (Chapter V).

Appendix F NMR analysis of phenanthrene-like ligand scaffolds (Chapter VII).
HPLC and ESI-MS for TFO2 hybrids (Chapter VII).

VIII. 1. Appendix A

VIII. 1. 1. NMR, IR and ESI-MS analysis

(1) 1,10-phenanthroline-5,6-epoxide spectra:

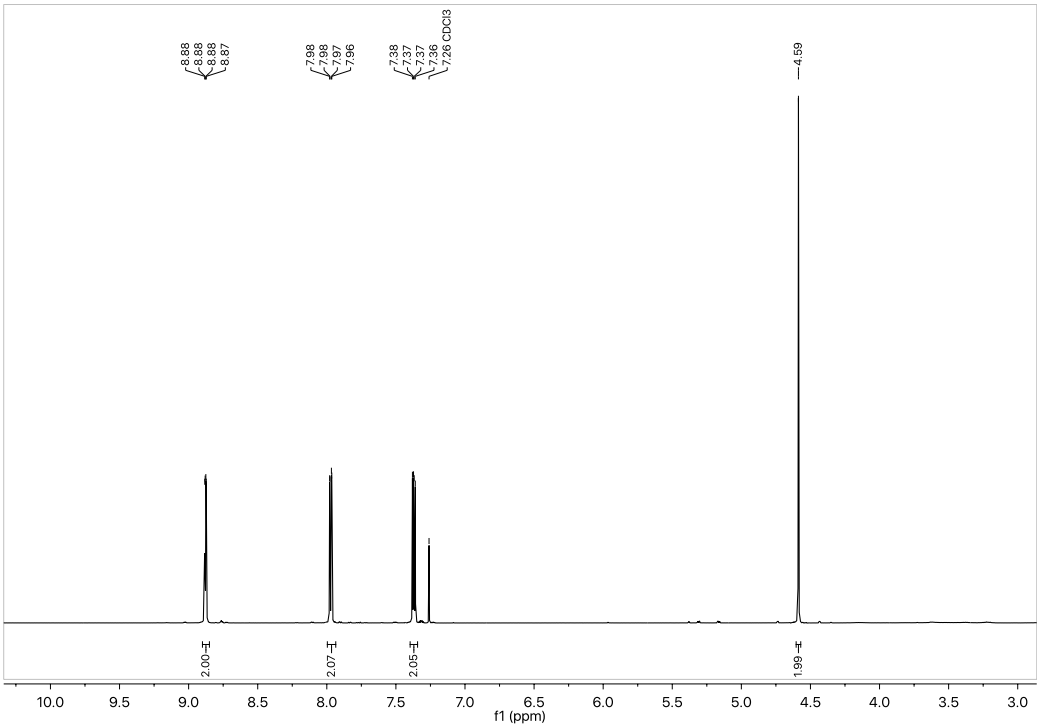

Figure VIII-1. ^{1}H NMR spectra for 1,10-phenanthroline-5,6-epoxide (**1**).

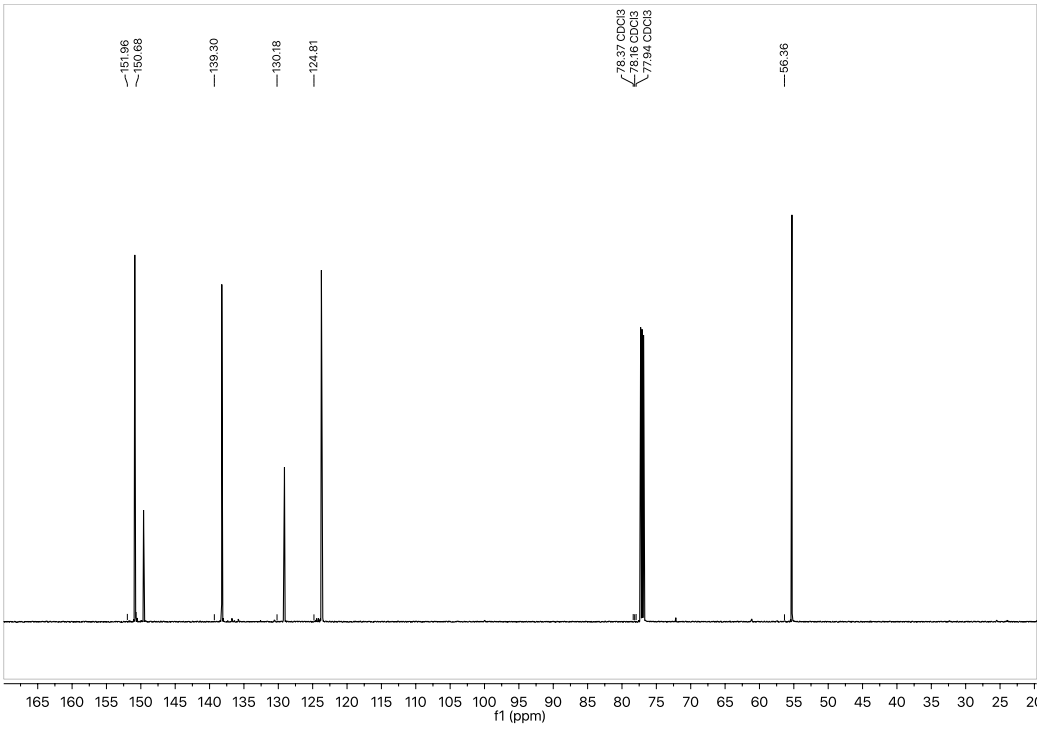

Figure VIII-2. ^{13}C NMR spectra for 1,10-phenanthroline-5,6-epoxide (**1**).

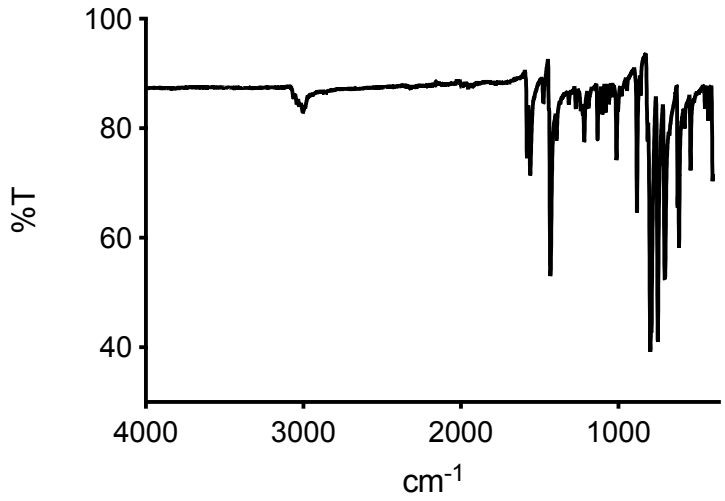

Figure VIII-3. IR spectrum for 1,10-phenanthroline-5,6-epoxide (**1**).

(2) 5-azido-1,10-phenanthroline spectra:

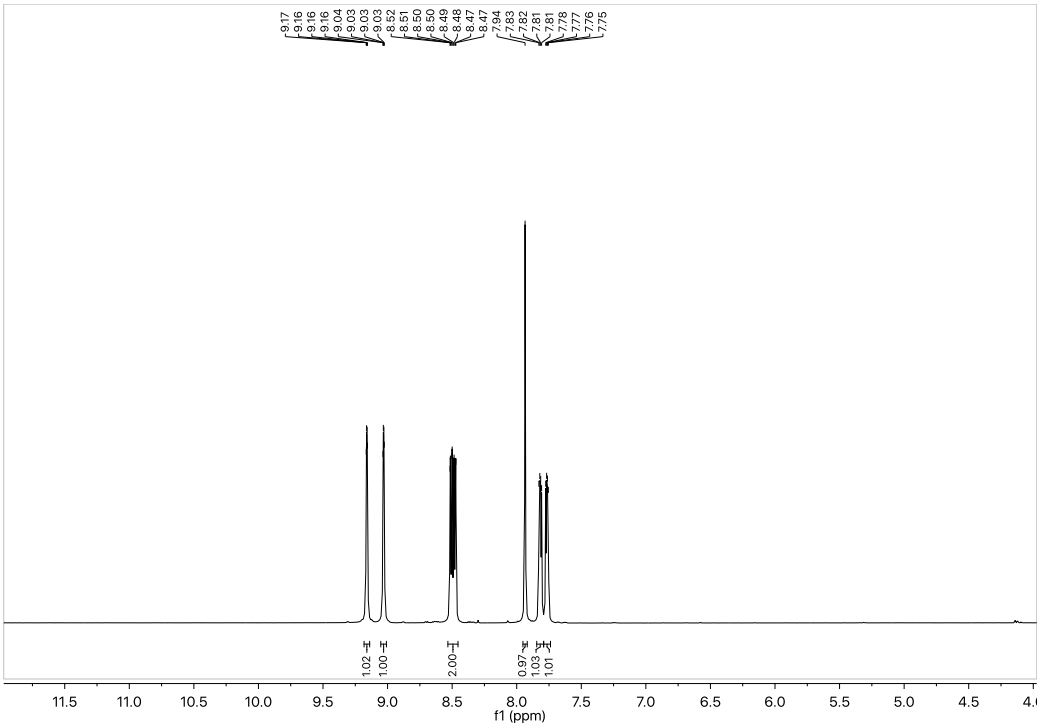

Figure VIII-4. ^{1}H NMR spectra for 5-azido-1,10-phenanthroline (**2**).

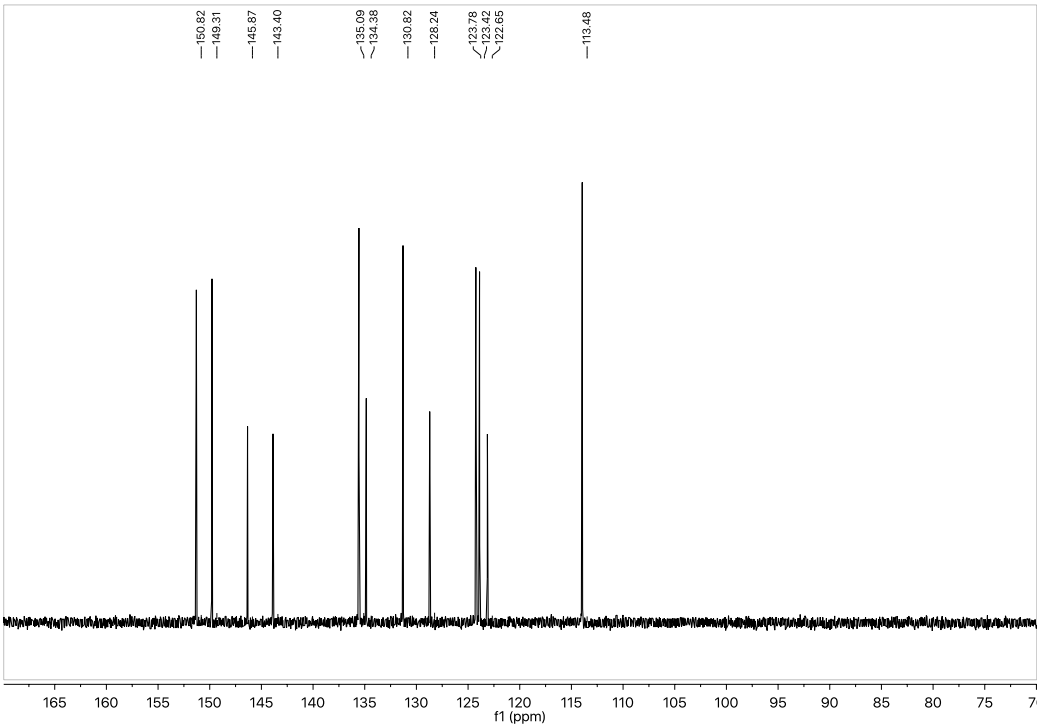

Figure VIII-5. ^{13}C NMR spectra for 5-azido-1,10-phenanthroline (**2**).

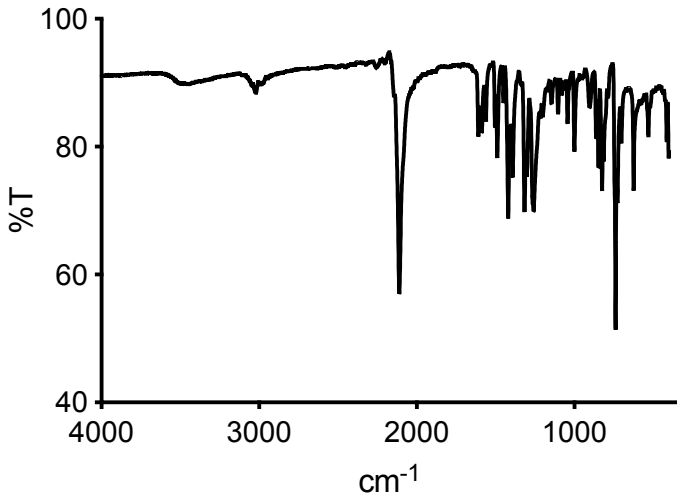

Figure VIII-6. IR spectrum for 5-azido-1,10-phenanthroline (**2**).

(3) [Pt(5-azido-1,10-phenanthroline)Cl_2] spectra:

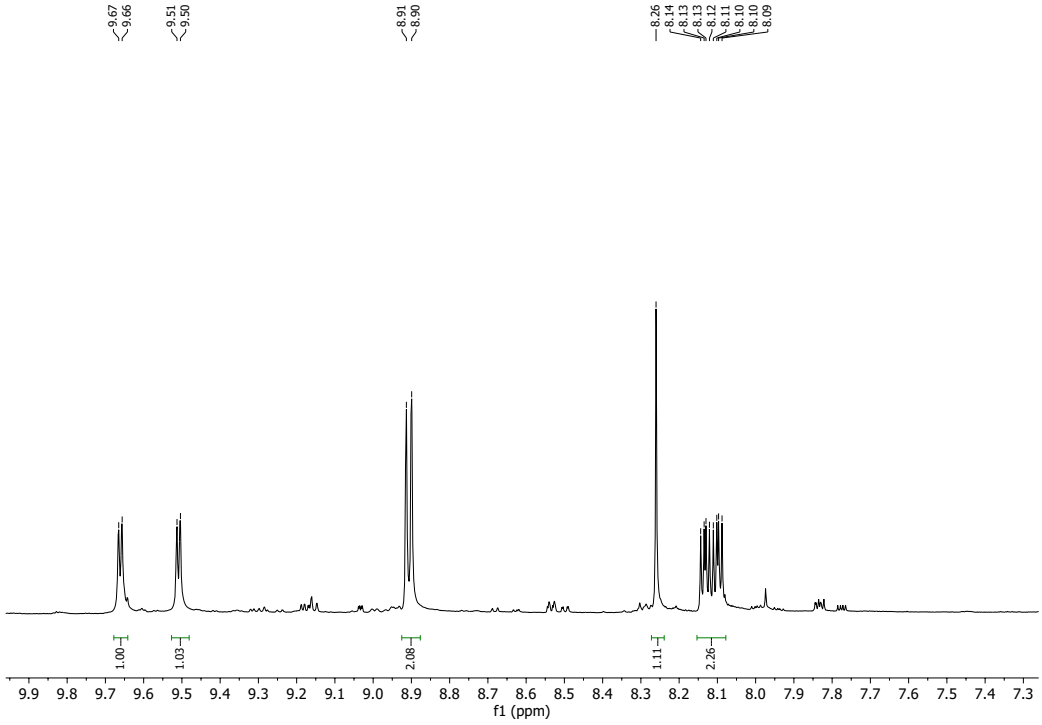

Figure VIII-7. ^{1}H NMR spectra for [Pt(5-azido-1,10-phenanthroline)Cl_2] (**3**).

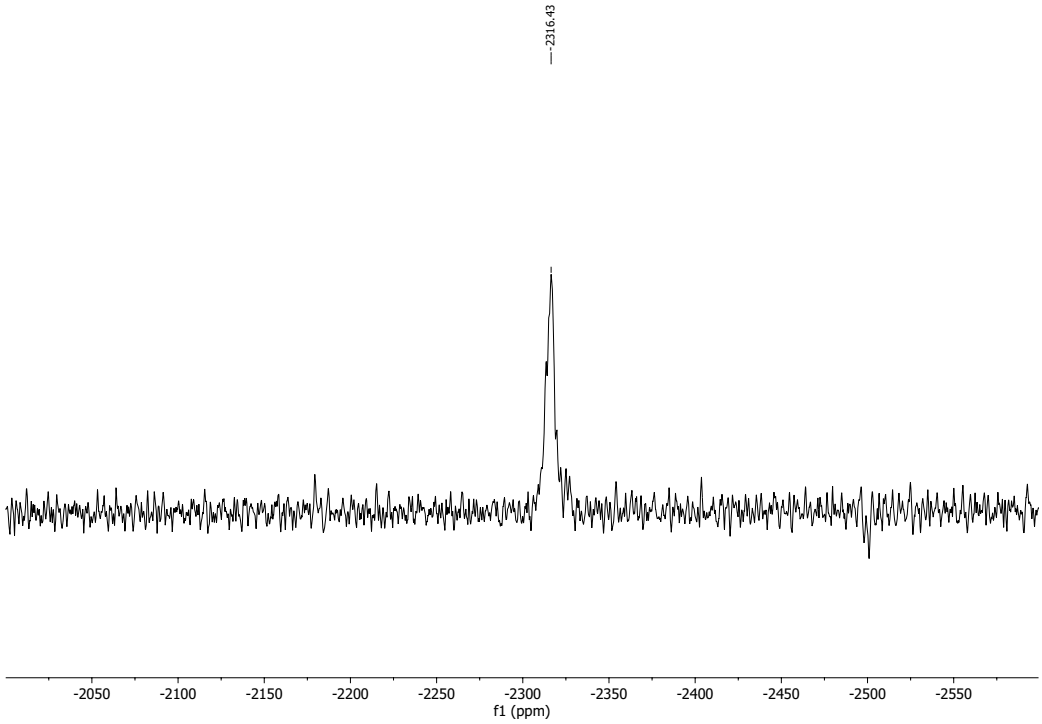

Figure VIII-8. ^{195}Pt NMR spectra for [Pt(5-azido-1,10-phenanthroline)Cl_2] (**3**).

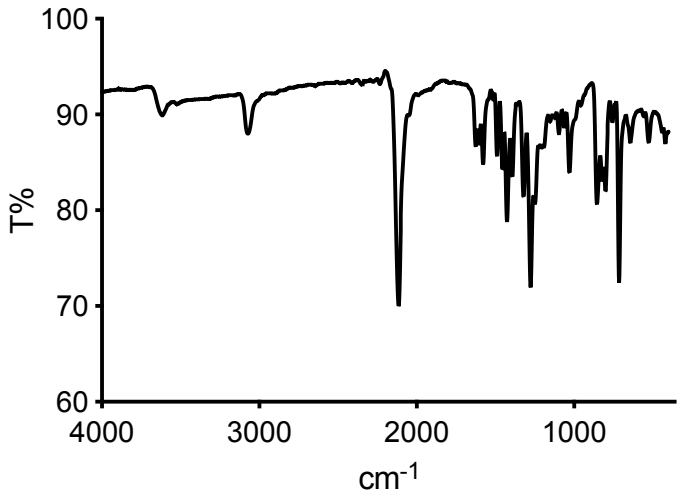

Figure VIII-9. IR spectrum for [Pt(5-azido-1,10-phenanthroline)Cl_2] (**3**).

(4) 1,10-phenanthroline-5,6-dione

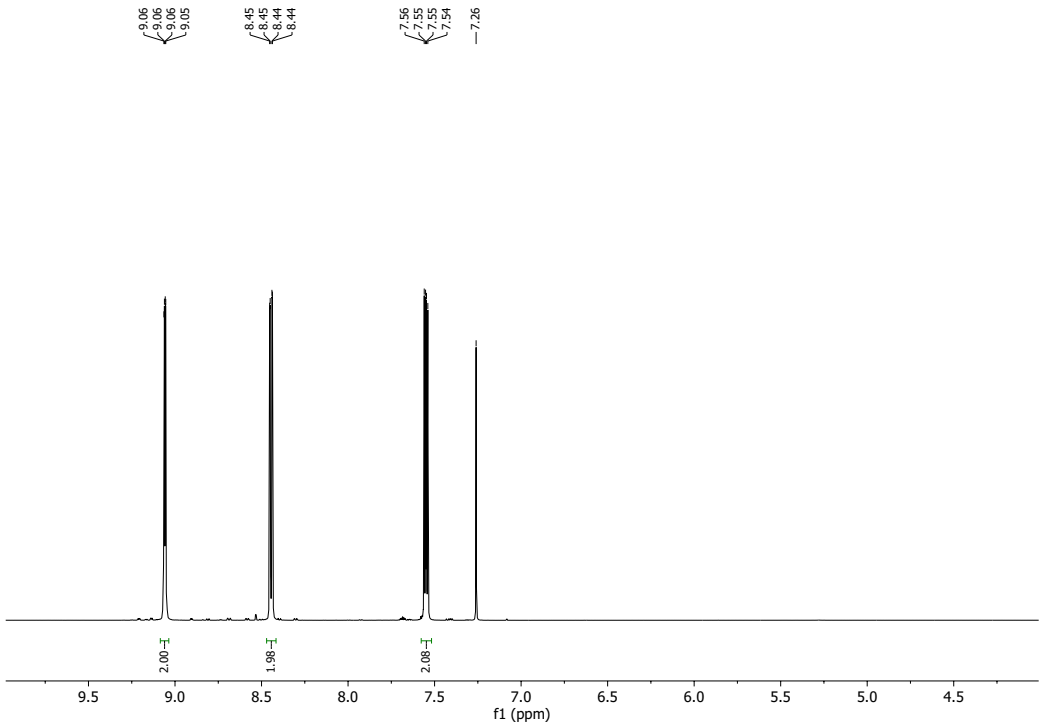

Figure VIII-10. ^{1}H NMR spectra for 1,10-phenanthroline-5,6-dione (**4**).

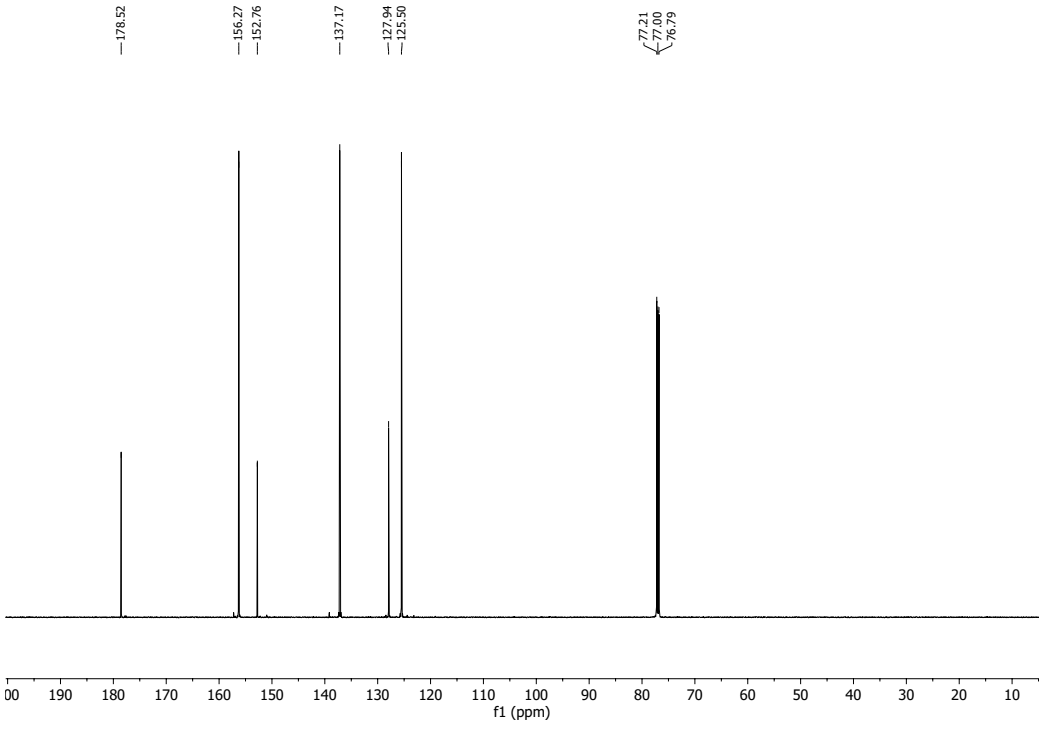

Figure VIII-11. ^{13}C NMR spectra for 1,10-phenanthroline-5,6-dione (**4**).

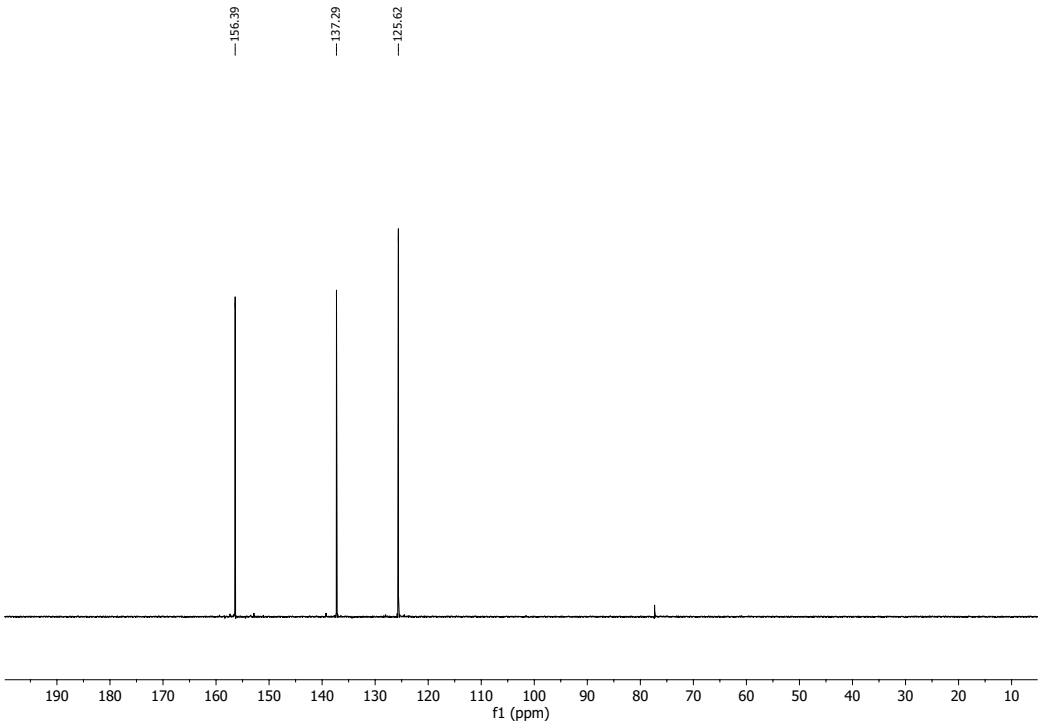

Figure VIII-12. ^{13}C DEPT NMR spectra for 1,10-phenanthroline-5,6-dione (**4**).

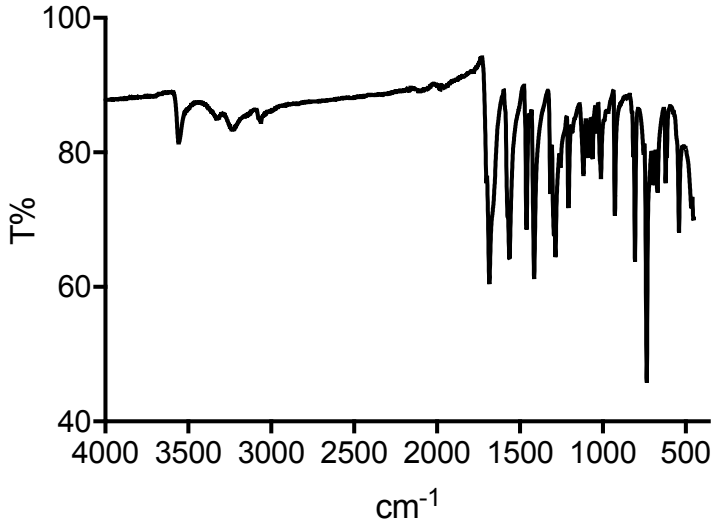

Figure VIII-13. IR spectrum for 1,10-phenanthroline-5,6-dione (**4**).

(5) 11-nitro dipyrido[3,2-*a*:2',3'-*c*]phenazine spectra:

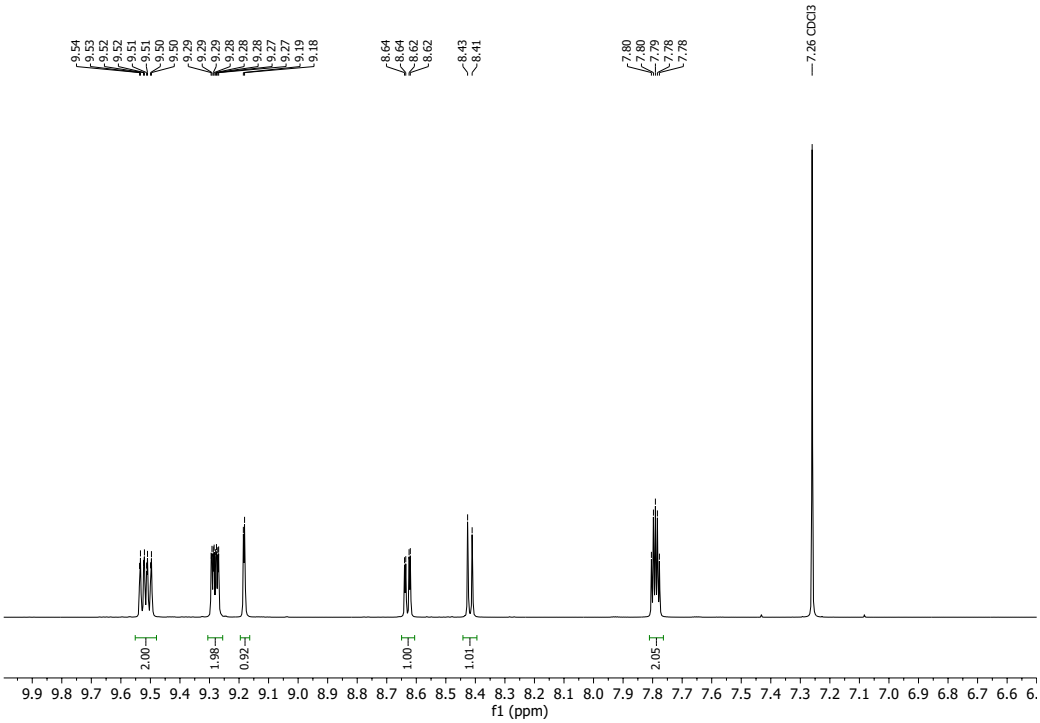

Figure VIII-14. ^{1}H NMR spectra for 11-nitrodipyrido[3,2-a:2',3'-c]phenazine (**5**).

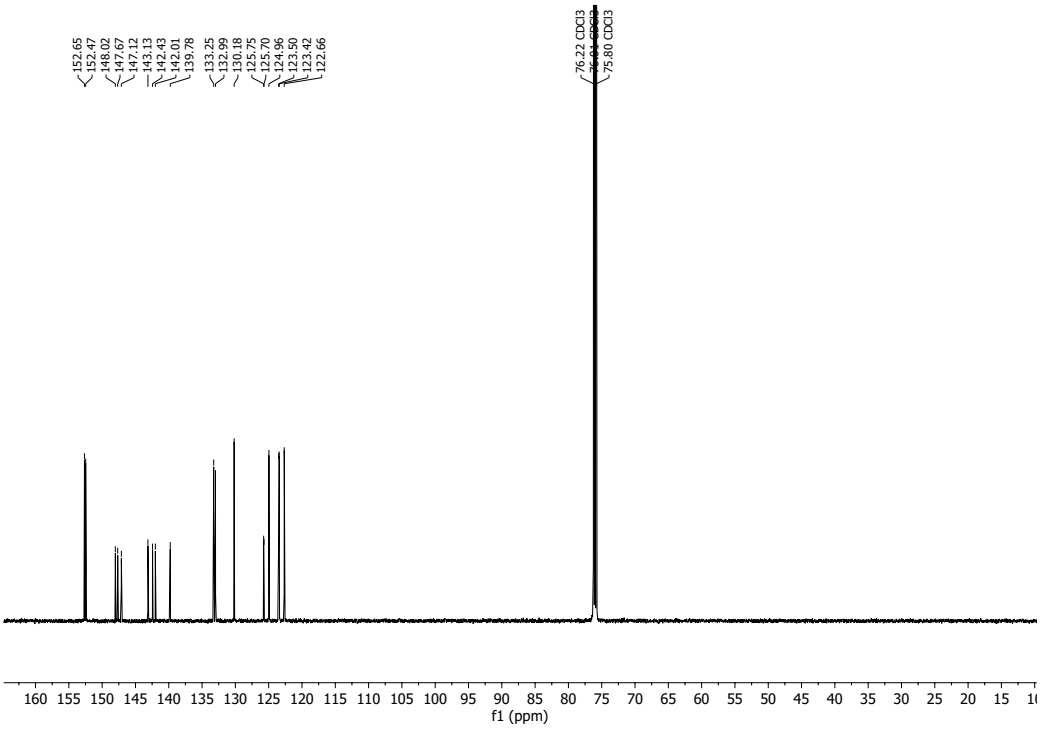

Figure VIII-15. ^{13}C NMR spectra for 11-nitrodipyrido[3,2-a:2',3'-c]phenazine (**5**).

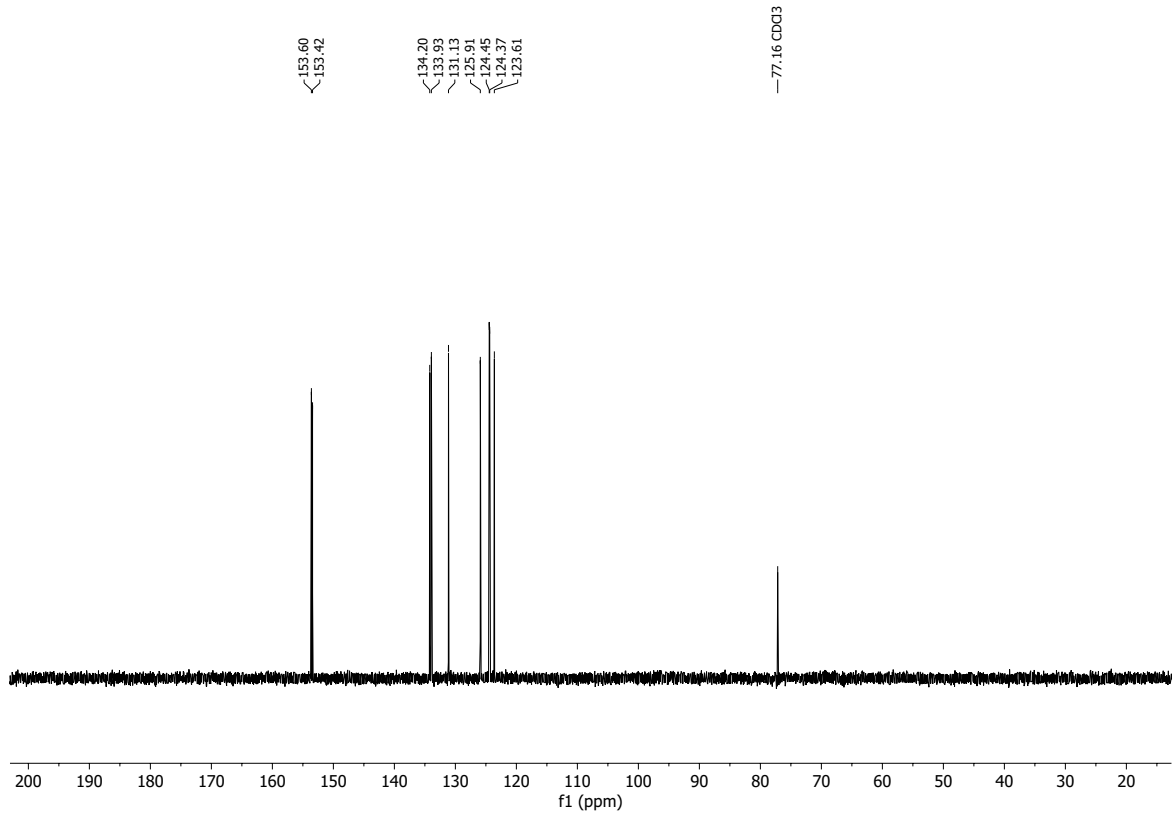

Figure VIII-16. ^{13}C DEPT NMR spectra for 11-nitrodipyrido[3,2-a:2',3'-c]phenazine (**5**).

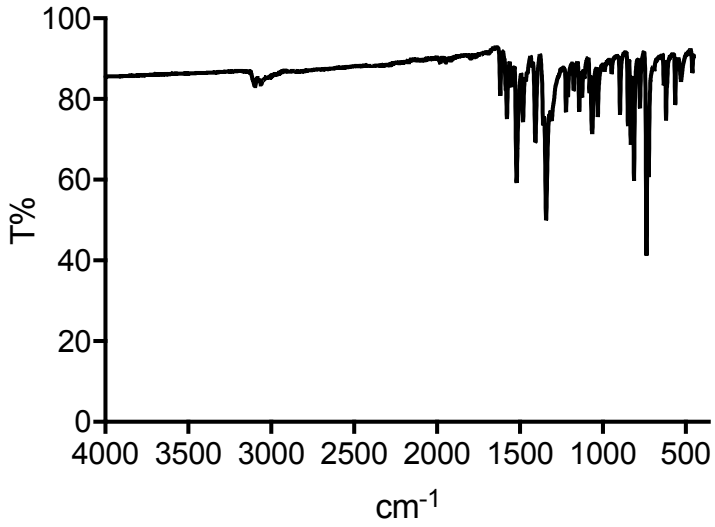

Figure VIII-17. IR spectrum for 11-nitrodipyrido[3,2-a:2',3'-c]phenazine (**5**).

(6) 11-amino dipyrido[3,2-*a*:2',3'-*c*]phenazine spectra:

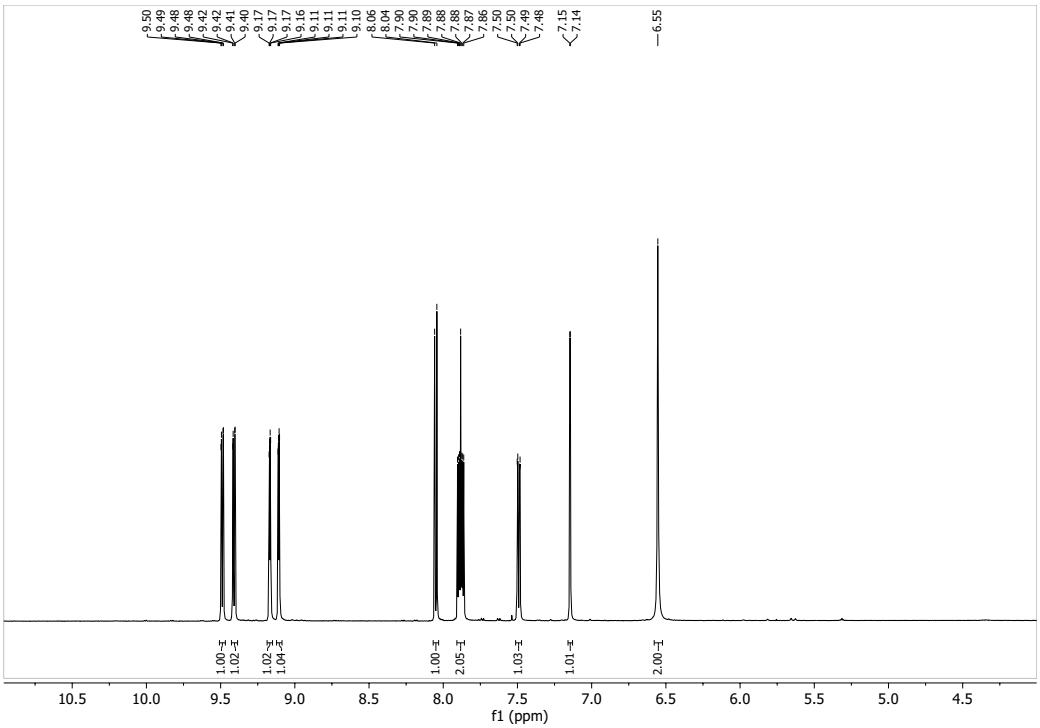

Figure VIII-18. ^{1}H NMR spectra for 11-aminodipyrido[3,2-a:2',3'-c]phenazine (**6**).

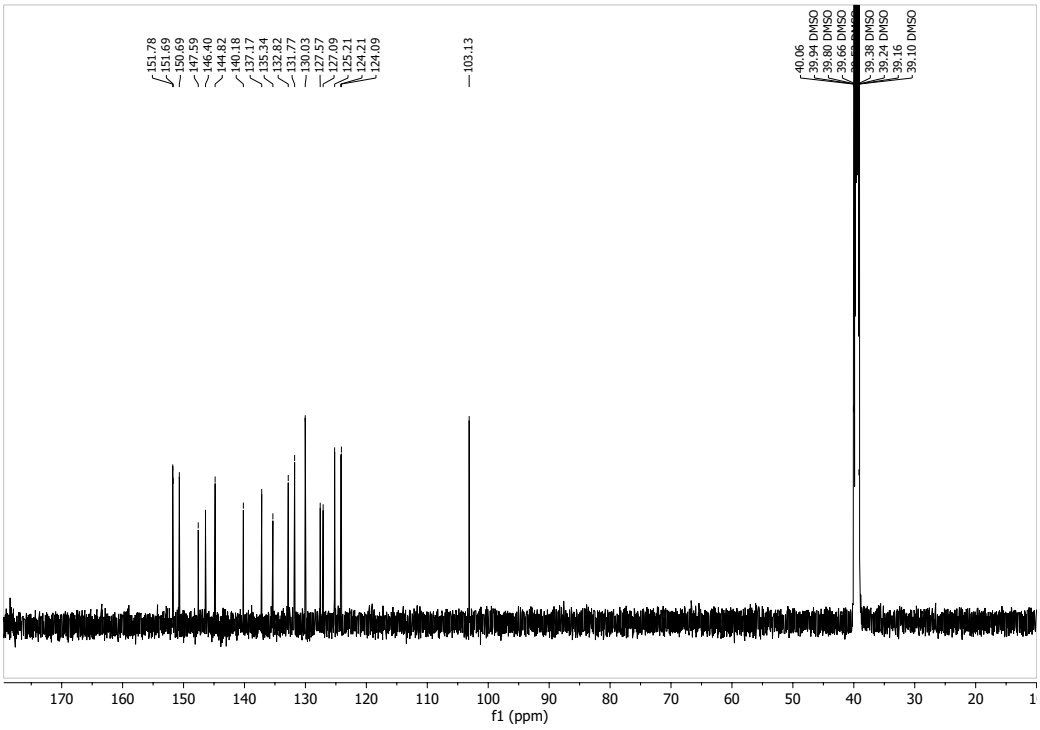

Figure VIII-19. ^{13}C NMR spectra for 11-aminodipyrido[3,2-a:2',3'-c]phenazine (**6**).

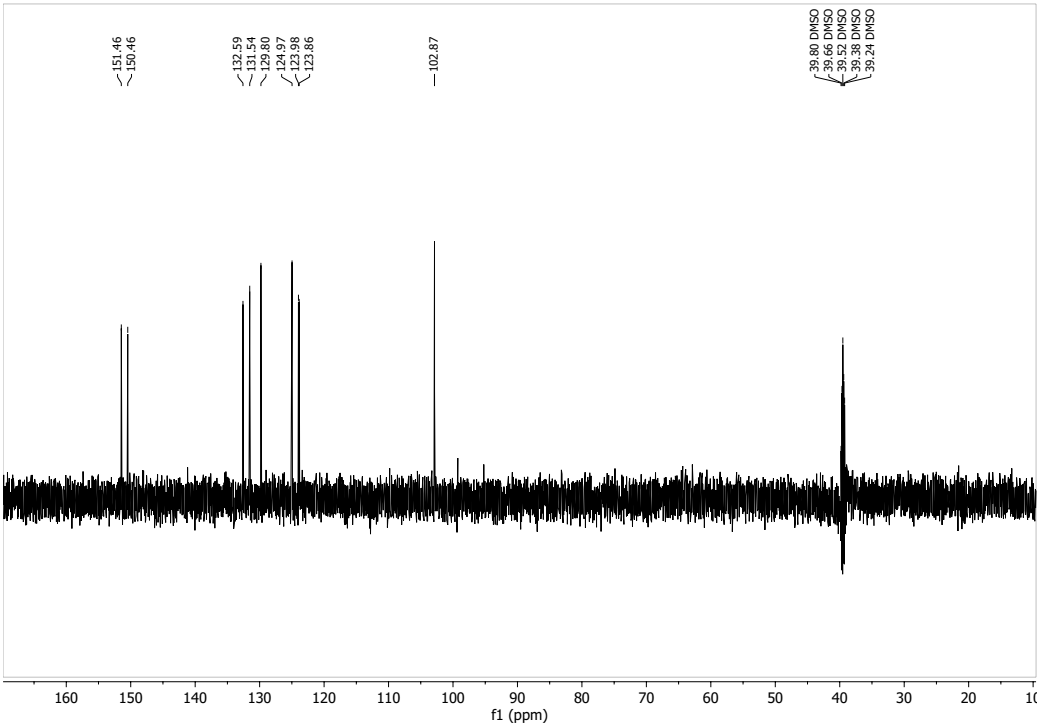

Figure VIII-20. ^{13}C DEPT NMR spectra for 11-aminodipyrido[3,2-a:2',3'-c]phenazine (**6**).

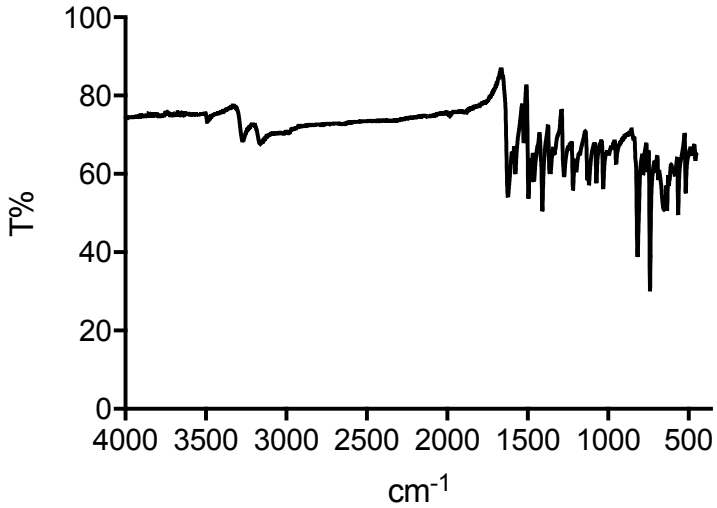

Figure VIII-21. IR spectrum for 11-aminodipyrido[3,2-a:2',3'-c]phenazine (**6**).

(7) 11-azidodipyrido[3,2-*a*:2',3'-*c*]phenazine spectra:

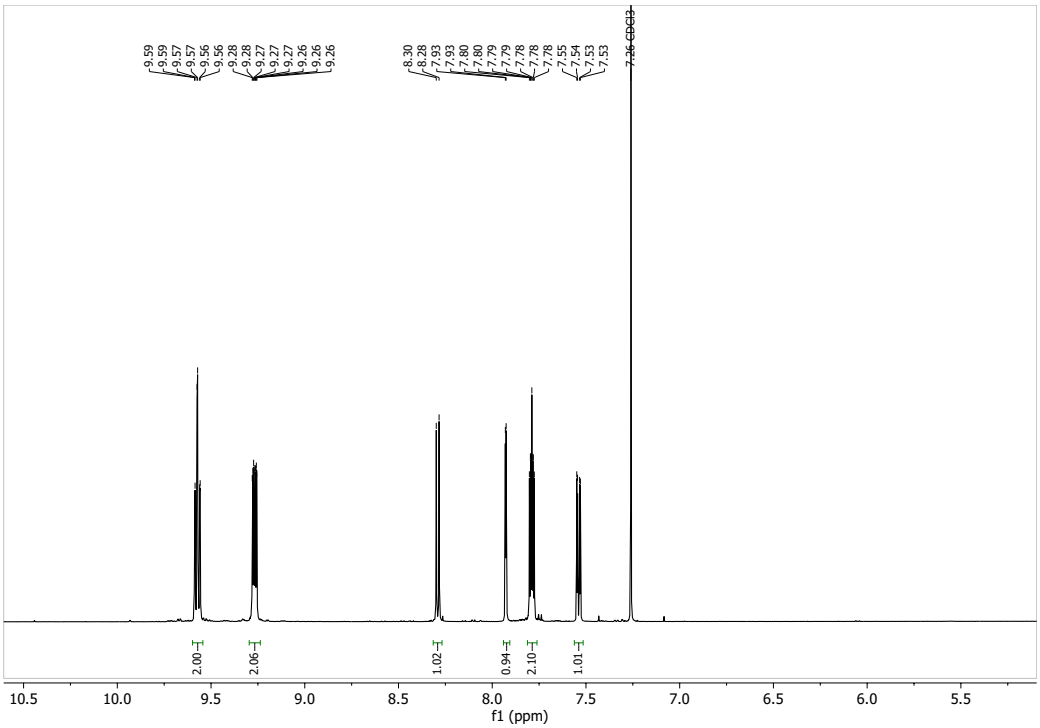

Figure VIII-22. ^{1}H NMR spectra for 11-azidodipyrido[3,2-a:2',3'-c]phenazine (**7**).

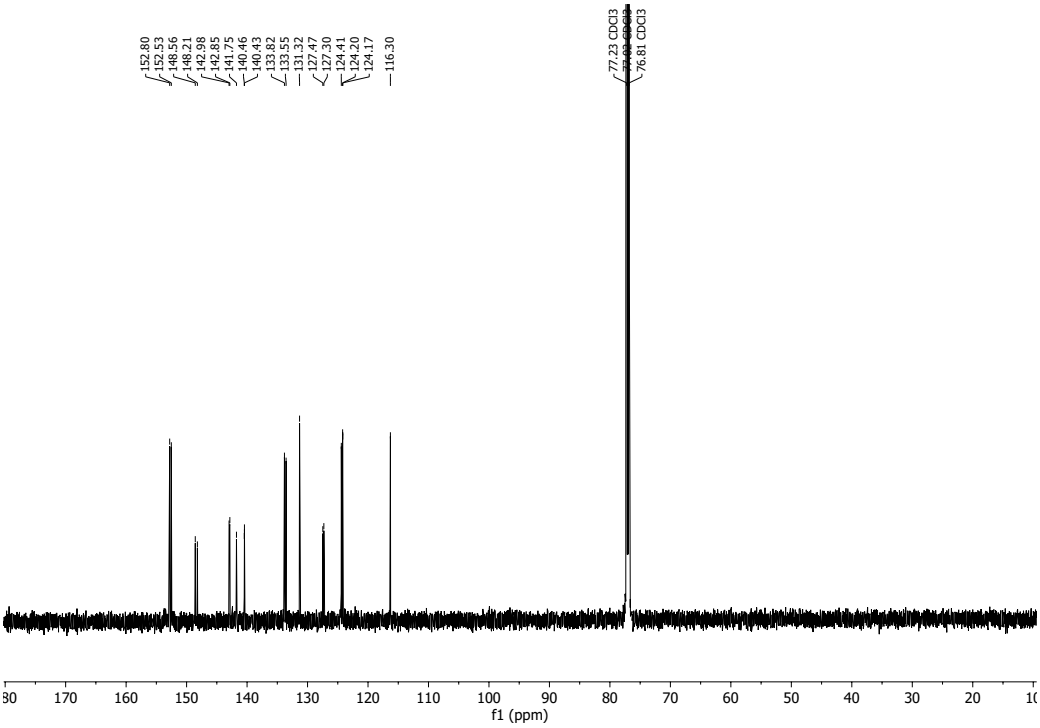

Figure VIII-23. ^{13}C NMR spectra for 11-azidodipyrido[3,2-a:2',3'-c]phenazine (**7**).

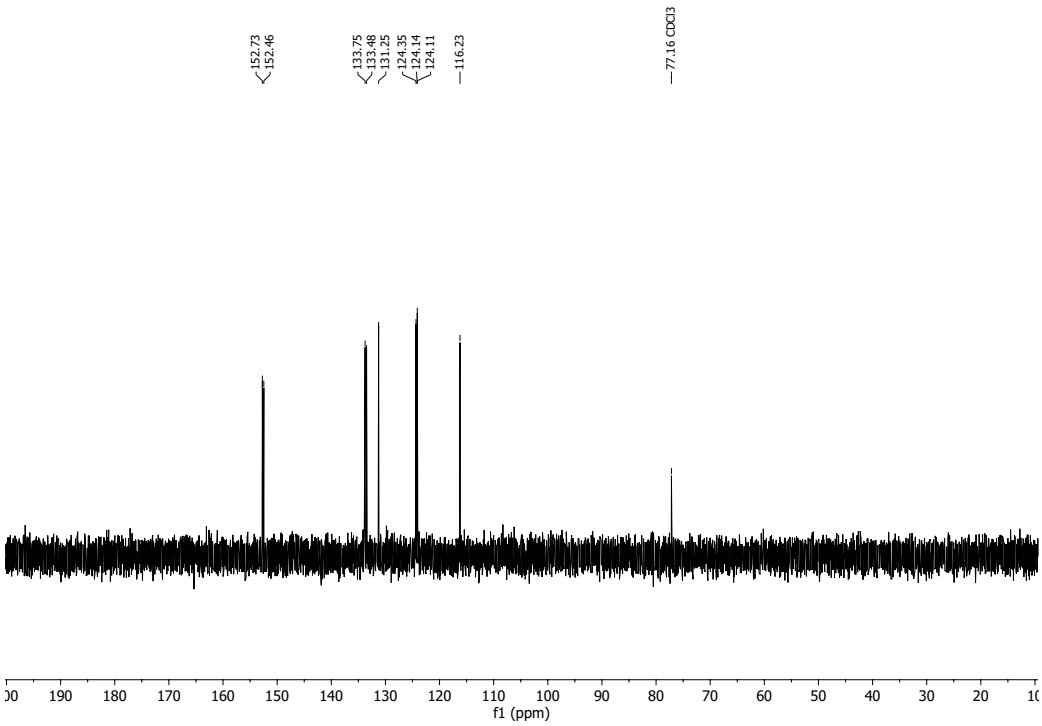

Figure VIII-24. ^{13}C DEPT NMR spectra for 11-azidodipyrido[3,2-a:2',3'-c]phenazine (**7**).

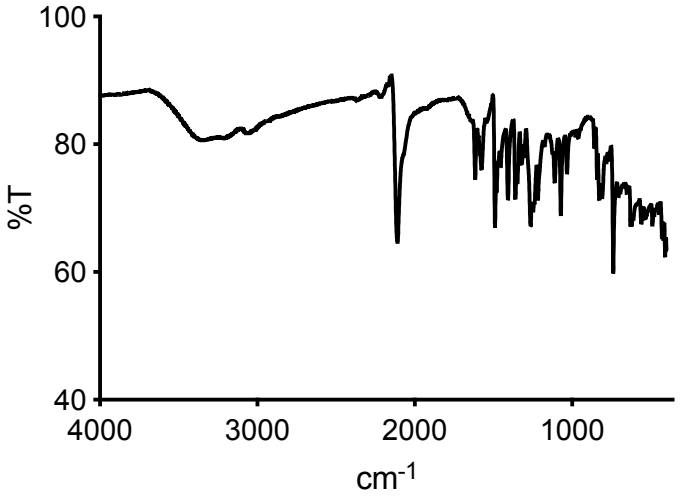

Figure VIII-25. IR spectrum for 11-azidodipyrido[3,2-a:2',3'-c]phenazine (**7**).

(8) [Pt(11-azidodipyrido[3,2-*a*:2',3'-*c*]phenazine)Cl_2] spectra:

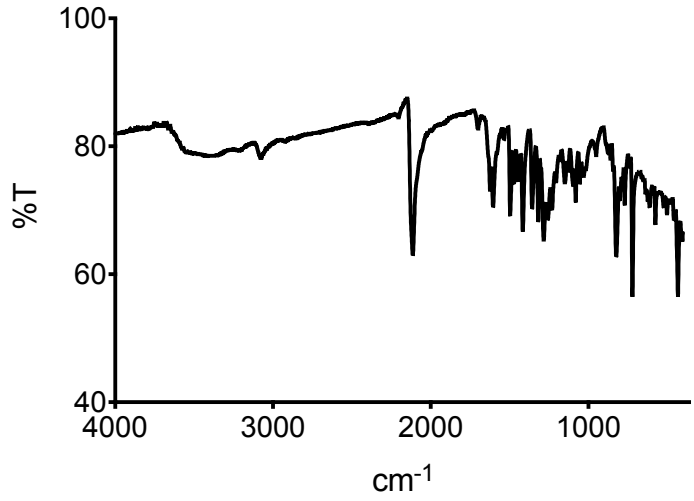

Figure VIII-26. IR spectrum for [Pt(11-azidodipyrido[3,2-a:2',3'-c]phenazine)Cl_2] (**8**).

(9) Di-*tert*-boc-2-hydroxy-1,3-diaminopropane spectra:

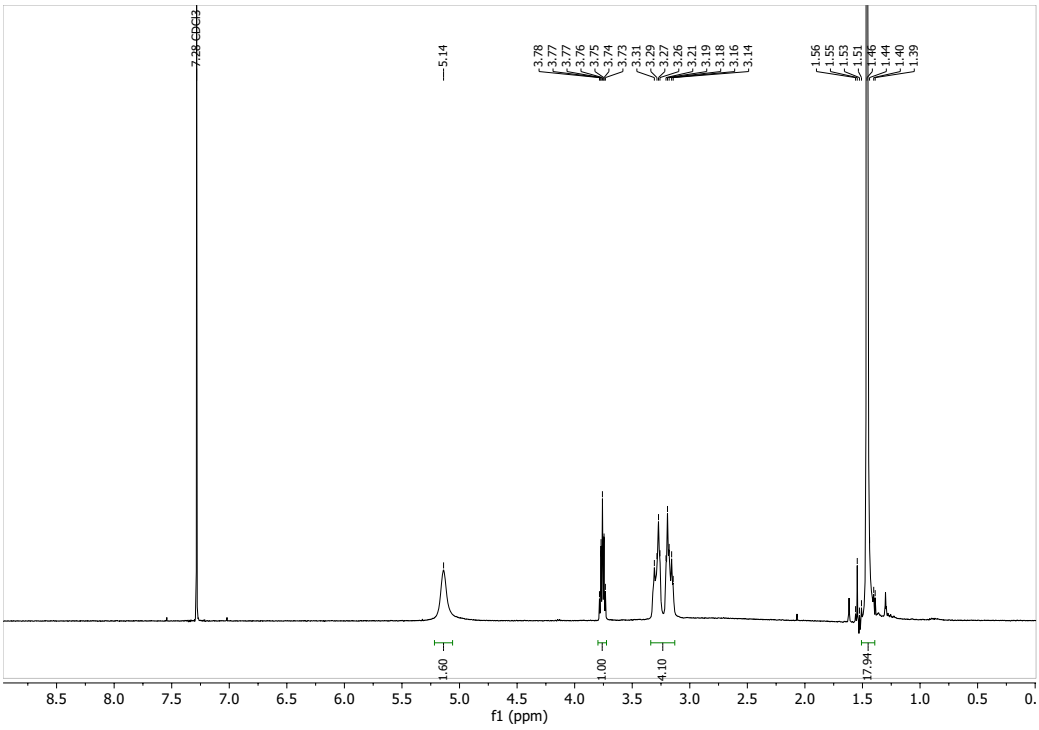

Figure VIII-27. ^{1}H NMR spectra for Di-tert-boc-2-hydroxy-1,3-diaminopropane (**9**).

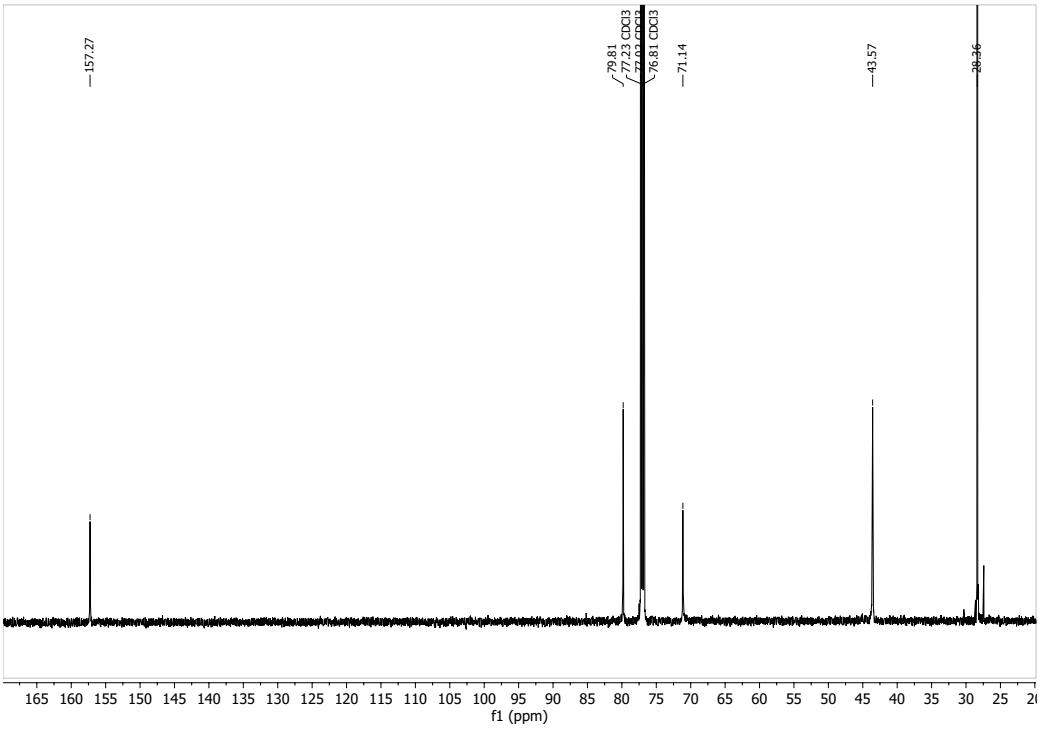

Figure VIII-28. ^{13}C NMR spectra for Di-tert-boc-2-hydroxy-1,3-diaminopropane (**9**).

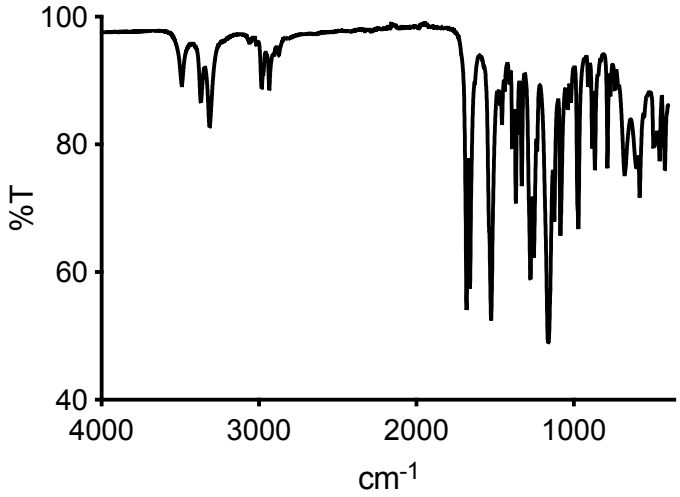

Figure VIII-29. IR spectrum for Di-tert-boc-2-hydroxy-1,3-diaminopropane (**9**).

(10) Di-*tert*-boc-2-methanesulfonyl-1,3-diaminopropane spectra:

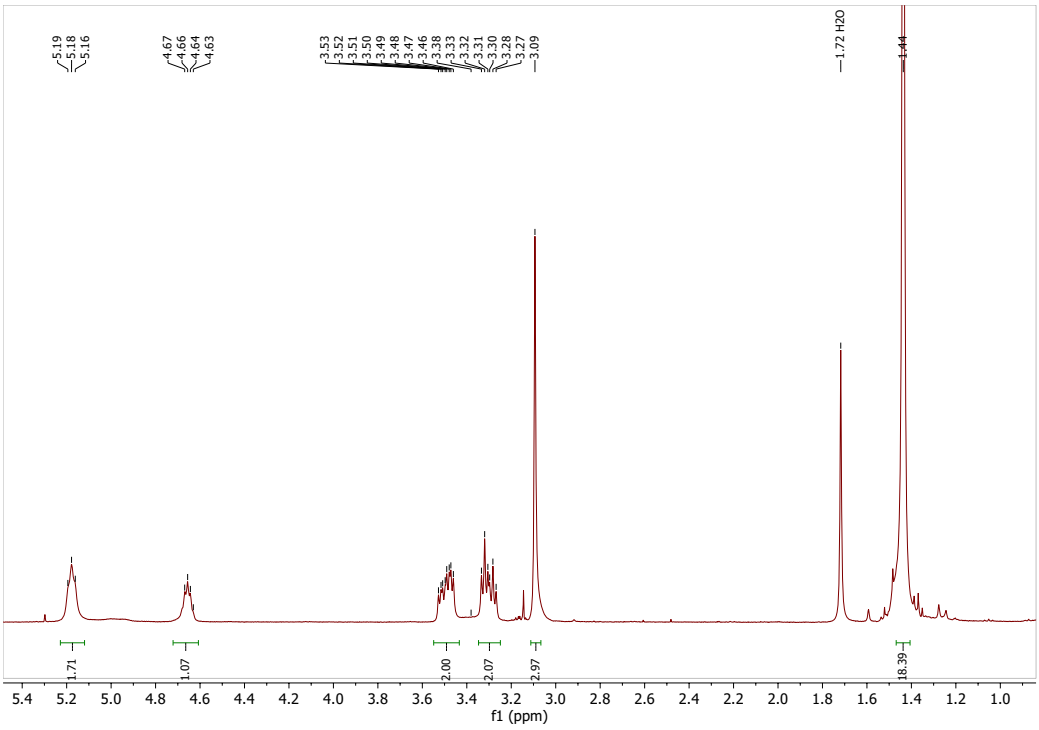

Figure VIII-30. ^{1}H NMR spectra for Di-tert-boc-2-methanesulfonyl-1,3-diaminopropane (**10**).

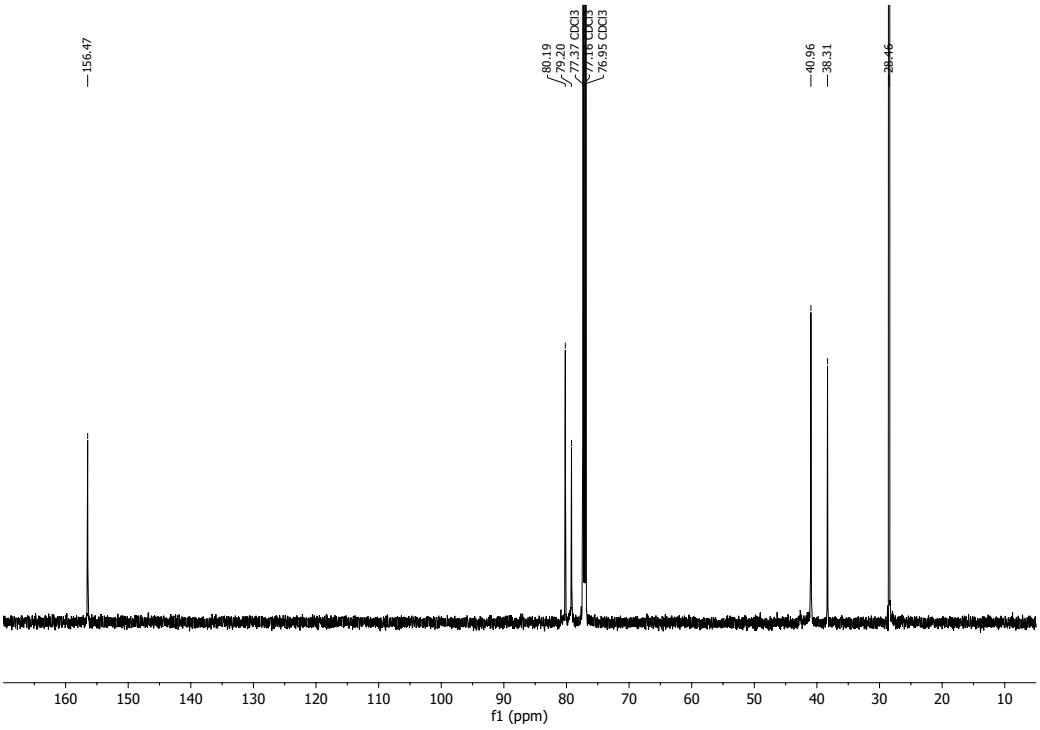

Figure VIII-31. ^{13}C NMR spectra for Di-tert-boc-2-methanesulfonyl-1,3-diaminopropane (**10**).

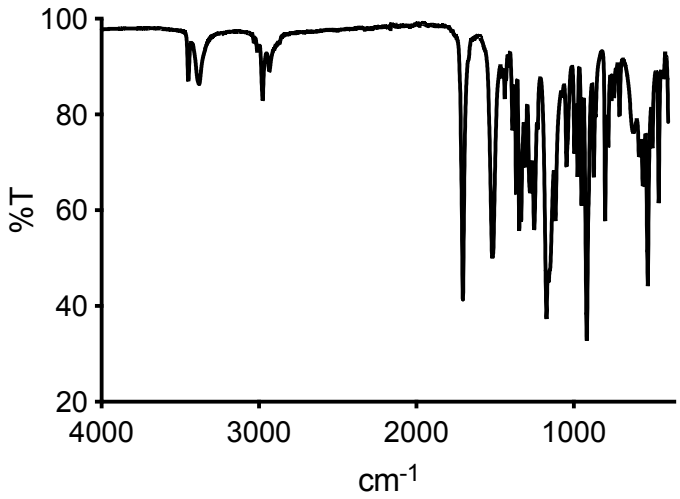

Figure VIII-32. ^{13}C NMR spectra for Di-tert-boc-2-methanesulfonyl-1,3-diaminopropane (**10**).

(11) Di-*tert*-boc-2-azido-1,3-diaminopropane spectra:

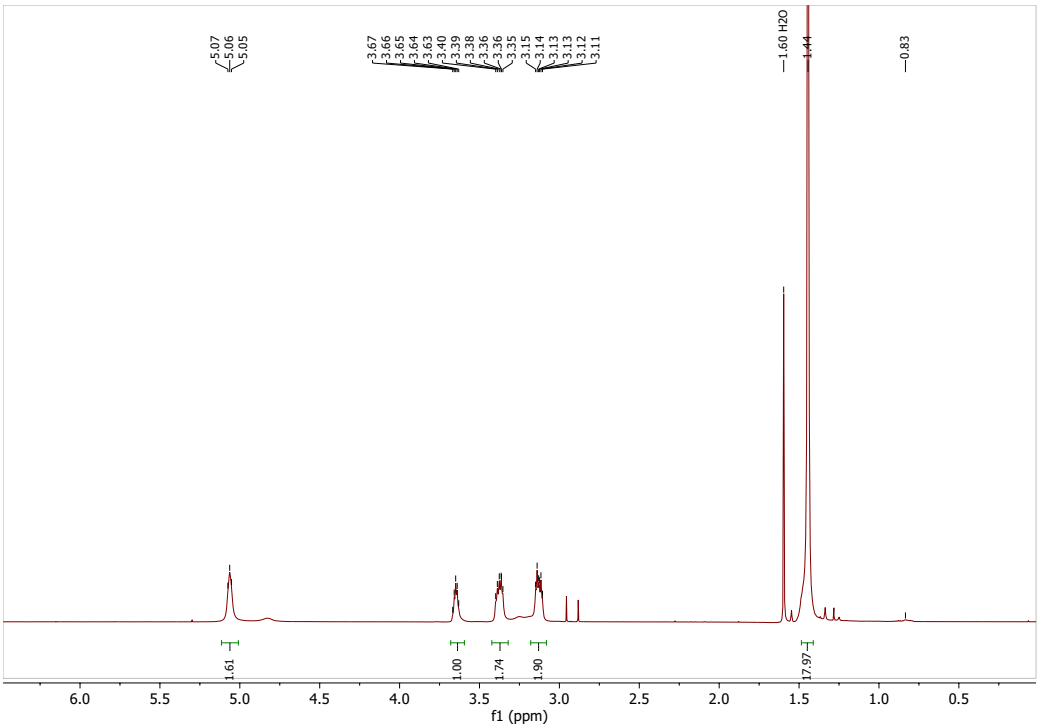

Figure VIII-33. ^{1}H NMR spectra for Di-tert-boc-2-azido-1,3-diaminopropane (**11**).

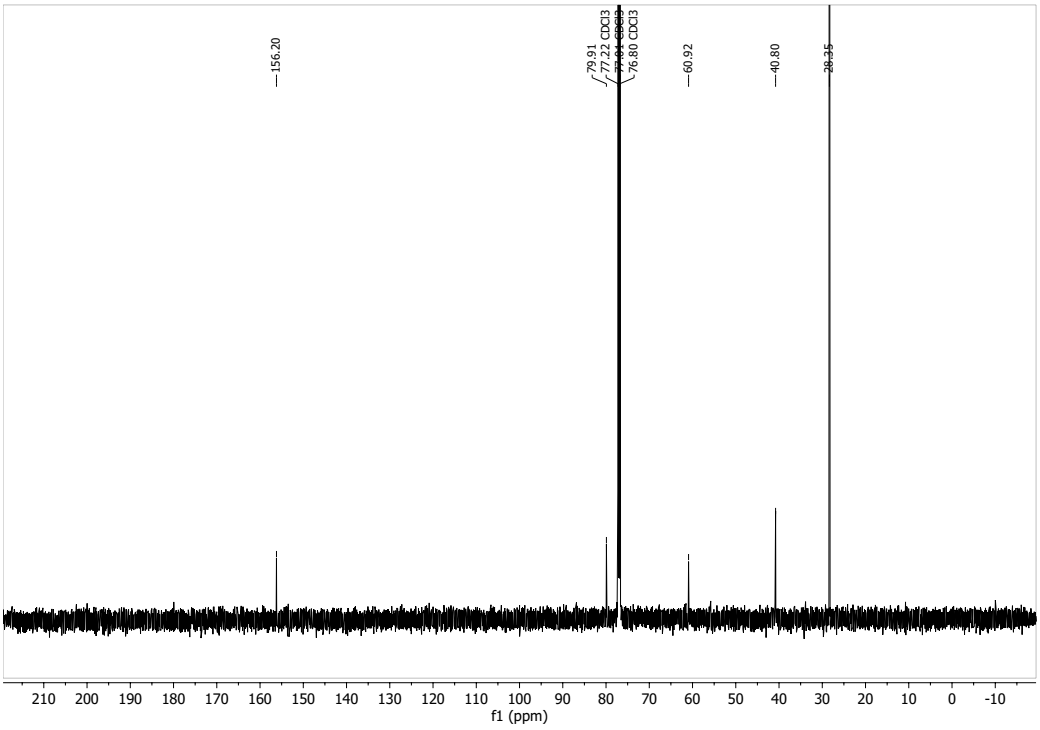

Figure VIII-34. ^{13}C NMR spectra for Di-tert-boc-2-azido-1,3-diaminopropane (**11**).

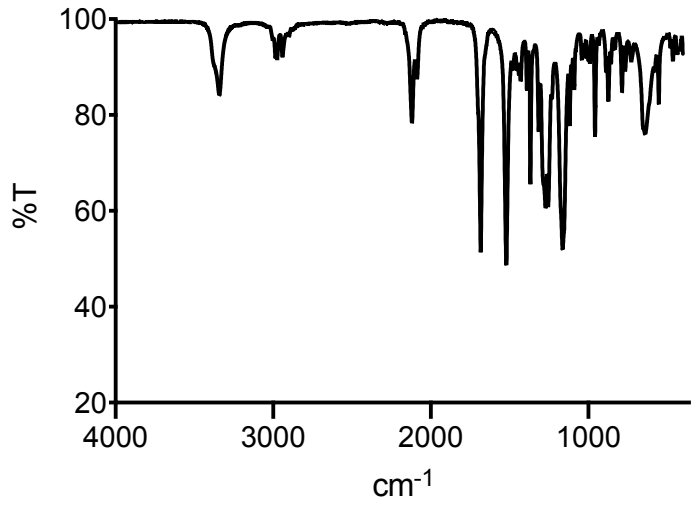

Figure VIII-35. IR spectrum for Di-tert-boc-2-azido-1,3-diaminopropane (**11**).

(12) 2-azidopropane-1,3-diamine dihydrochloride spectra:

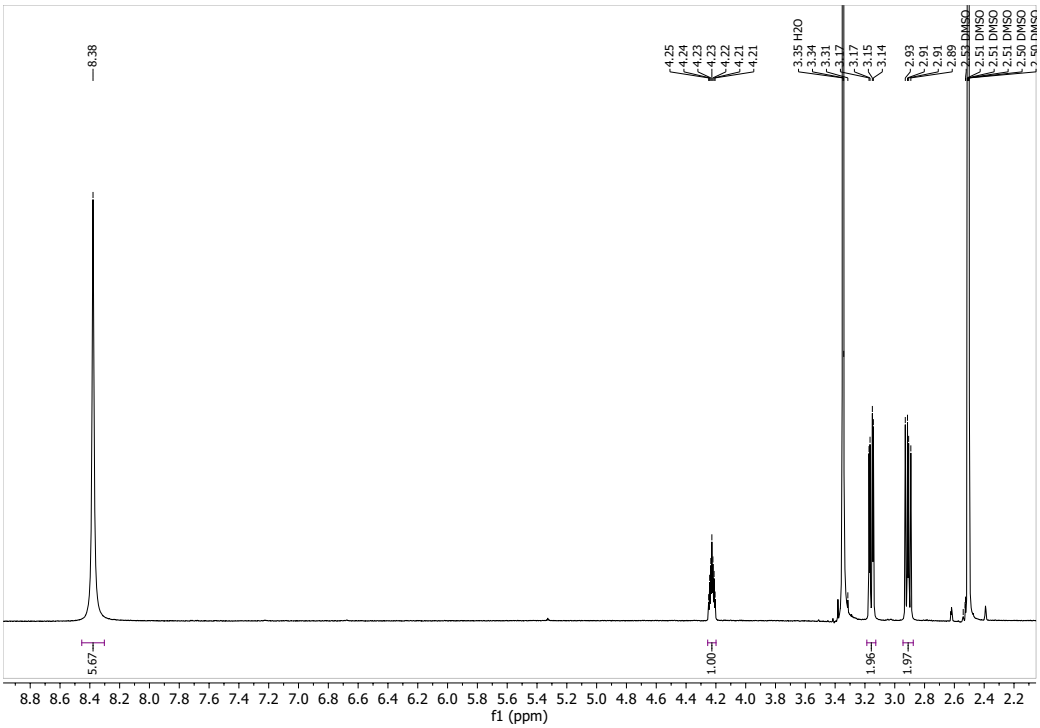

Figure VIII-36. ^{1}H NMR spectra for 2-azidopropane-1,3-diamine dihydrochloride (**12**).

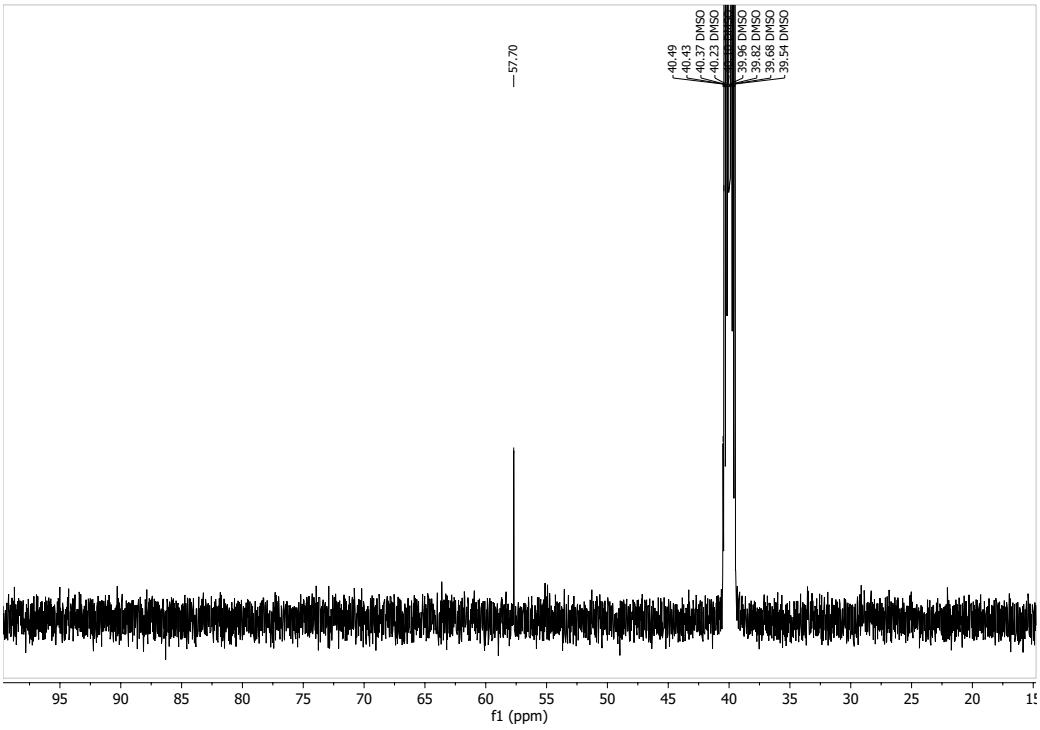

Figure VIII-37. ^{13}C NMR spectra for 2-azidopropane-1,3-diamine dihydrochloride (**12**).

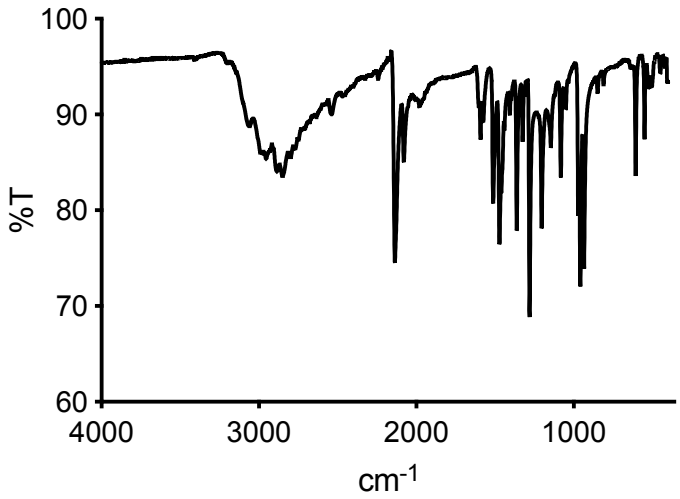

Figure VIII-38. IR spectrum for 2-azidopropane-1,3-diamine dihydrochloride (**12**).

(13) *cis*-[Pt(2-azidopropane-1,3-diamine)Cl_2] spectra:

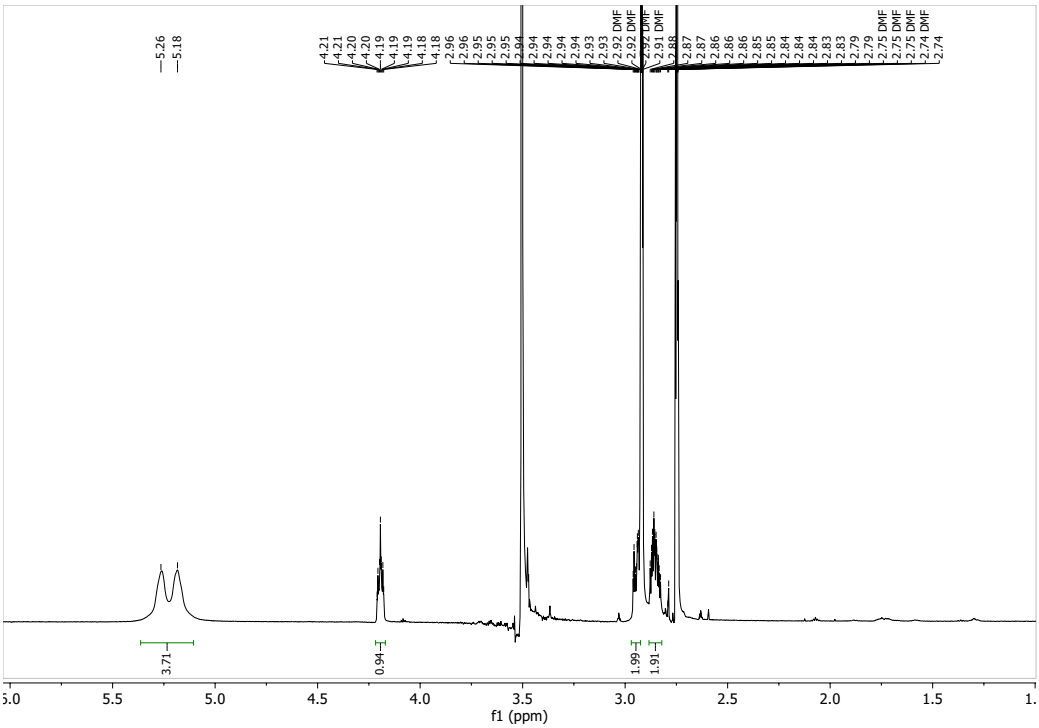

Figure VIII-39. ^{1}H NMR spectra for *cis*-[Pt(2-azidopropane-1,3-diamine)Cl_2] (**13**).

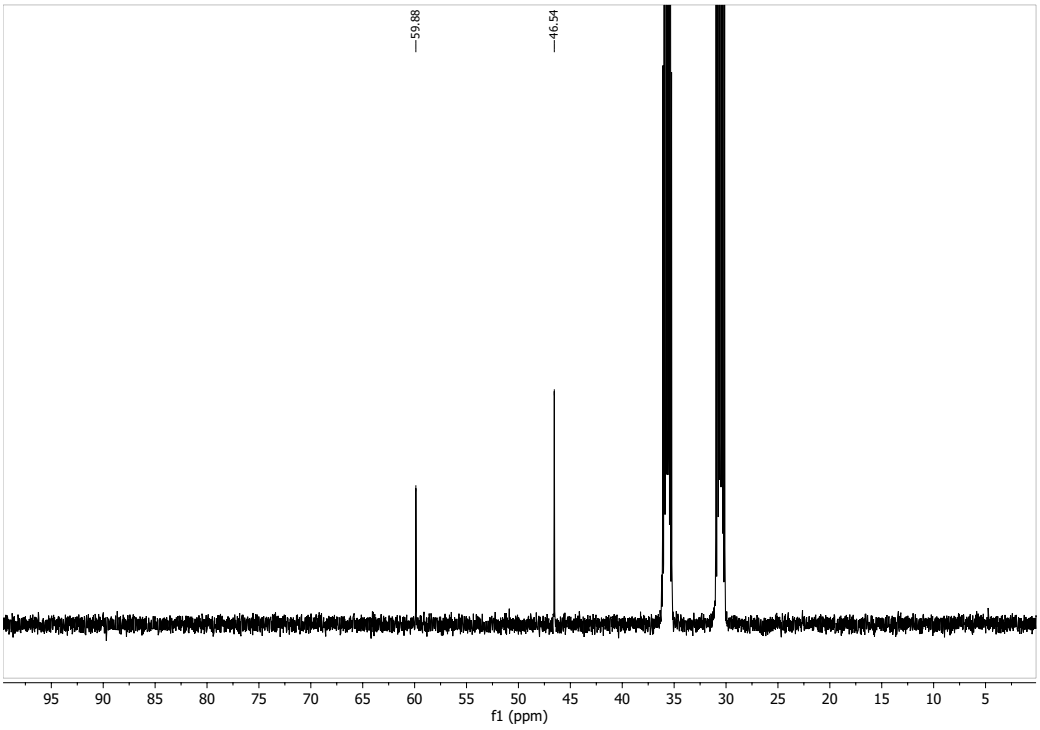

Figure VIII-40. ^{13}C NMR spectra for *cis*-[Pt(2-azidopropane-1,3-diamine)Cl_2] (**13**).

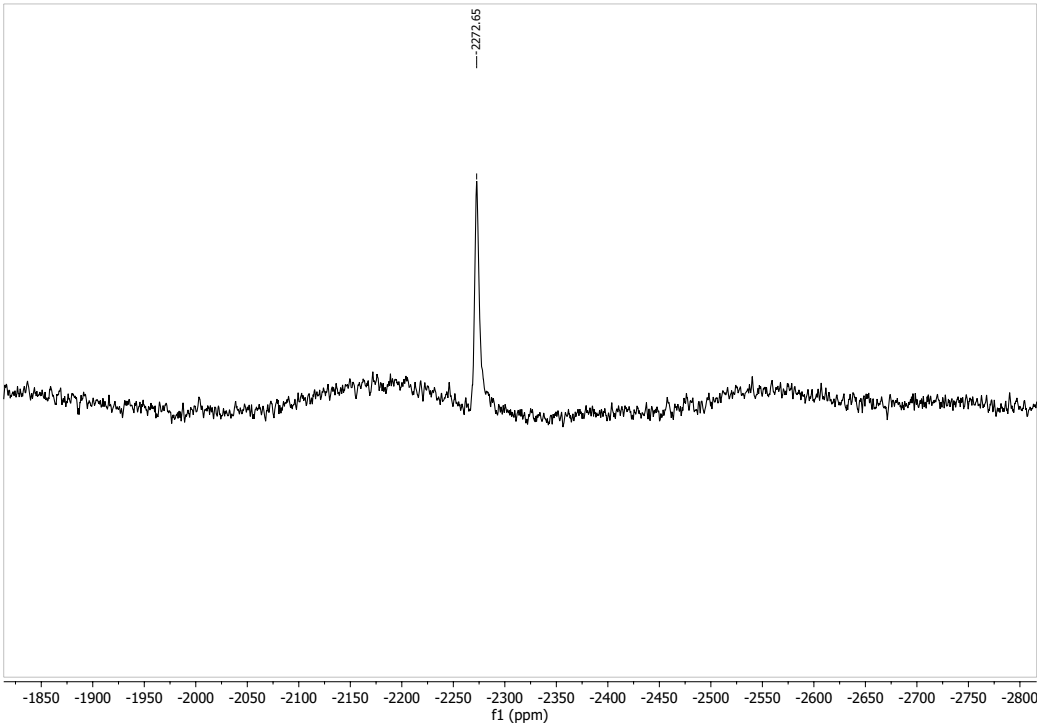

Figure VIII-41. ^{195}Pt NMR spectra for *cis*-[Pt(2-azidopropane-1,3-diamine)Cl_2] (**13**).

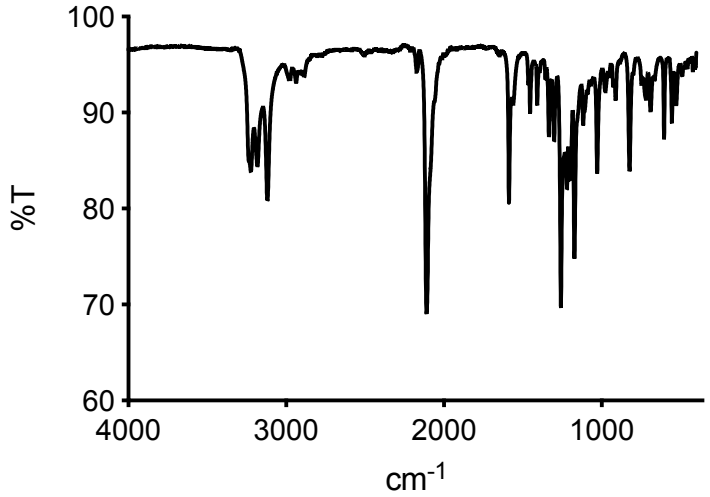

Figure VIII-42. IR spectrum for *cis*-[Pt(2-azidopropane-1,3-diamine)Cl_2] (**13**).

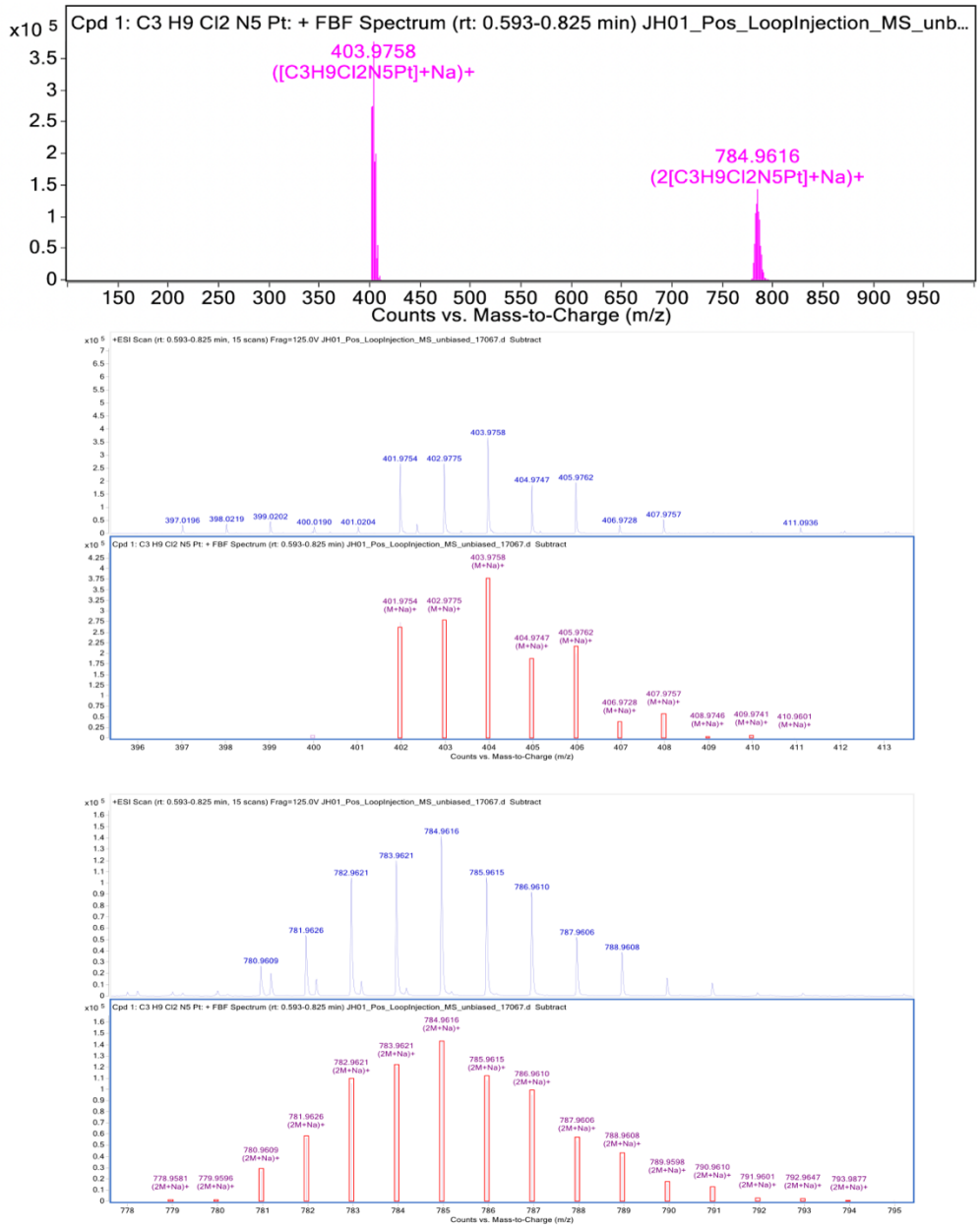

Figure VIII-43. ESI-MS for *cis*-[Pt(2-azidopropane-1,3-diamine)Cl_2] (**13**).

(15) *cis*-[Pt(2-azidopropane-1,3-diamine)CBDCA] spectra:

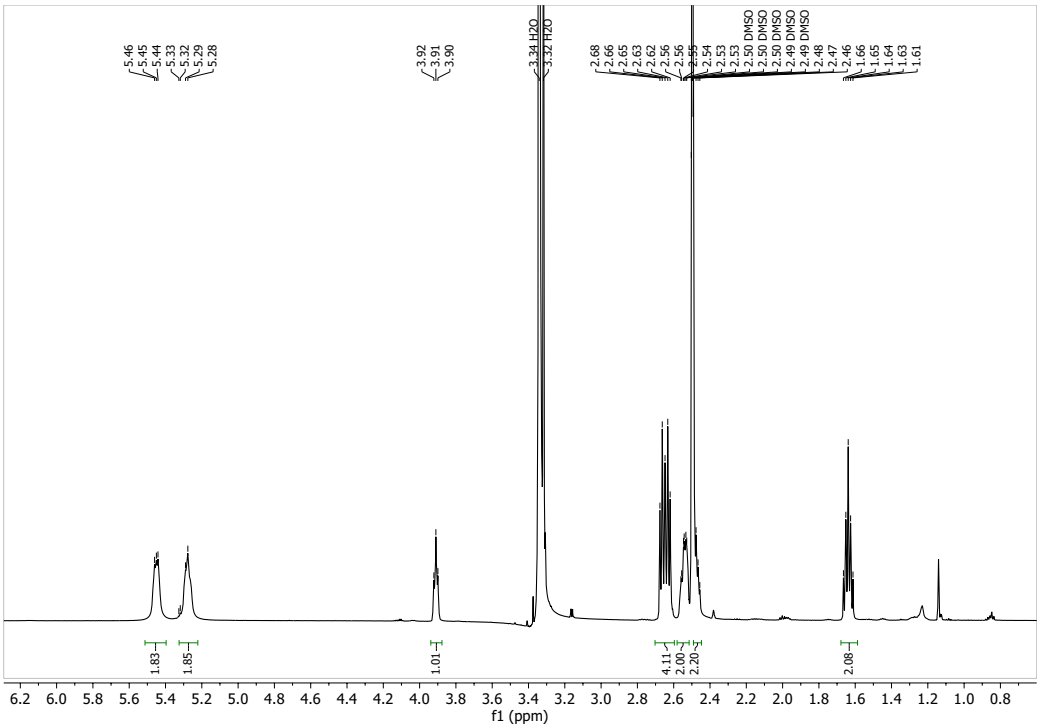

Figure VIII-44. ^{1}H NMR spectra for *cis*-[Pt(2-azidopropane-1,3-diamine)CBDCA] (**15**).

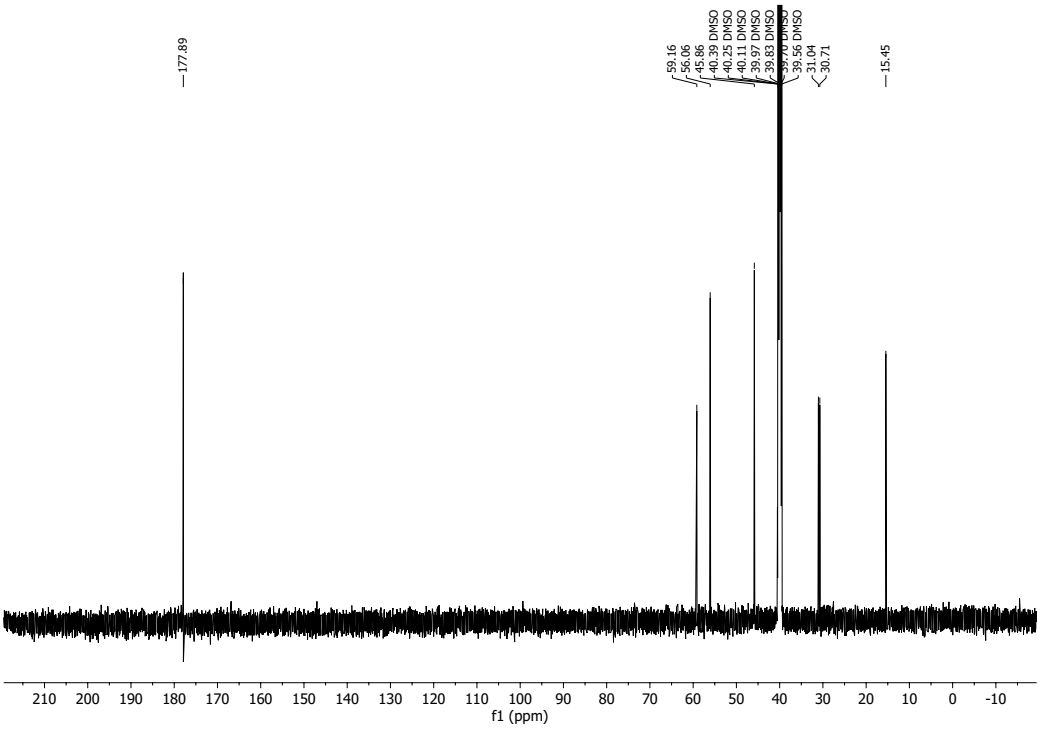

Figure VIII-45. ^{13}C NMR spectra for *cis*-[Pt(2-azidopropane-1,3-diamine)CBDCA] (**15**).

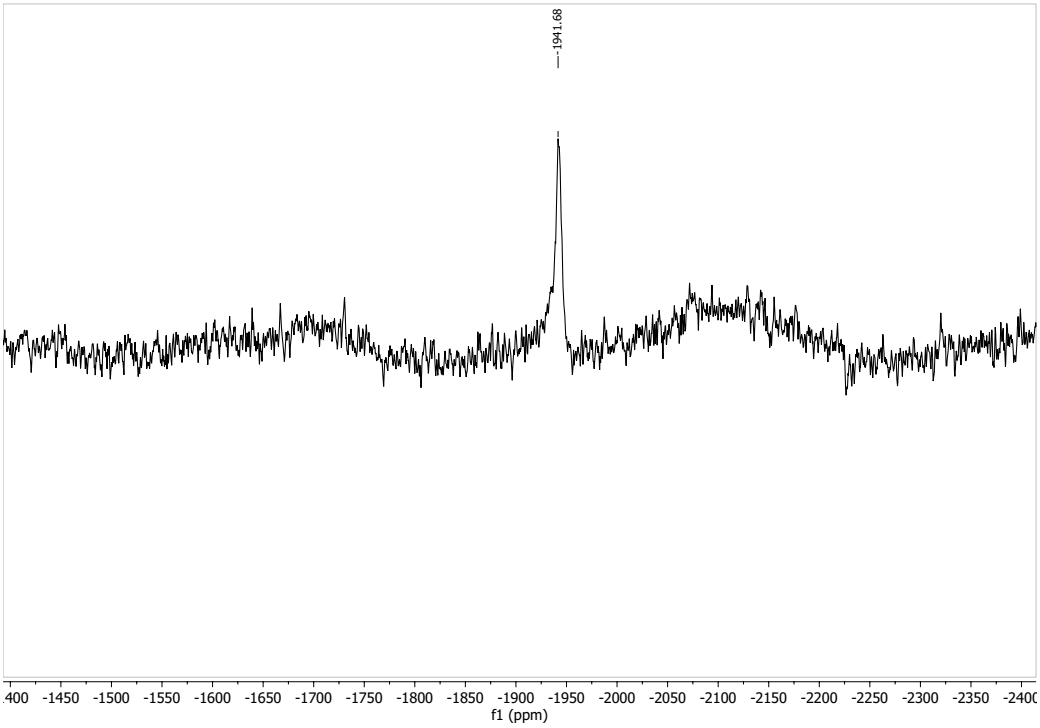

Figure VIII-46. ^{195}Pt NMR spectra for *cis*-[Pt(2-azidopropane-1,3-diamine)CBDCA] (**15**).

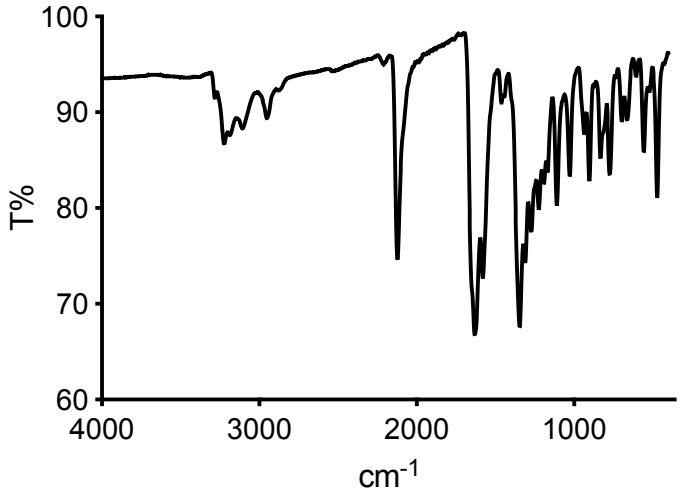

Figure VIII-47. IR spectrum for *cis*-[Pt(2-azidopropane-1,3-diamine)CBDCA] (**15**).

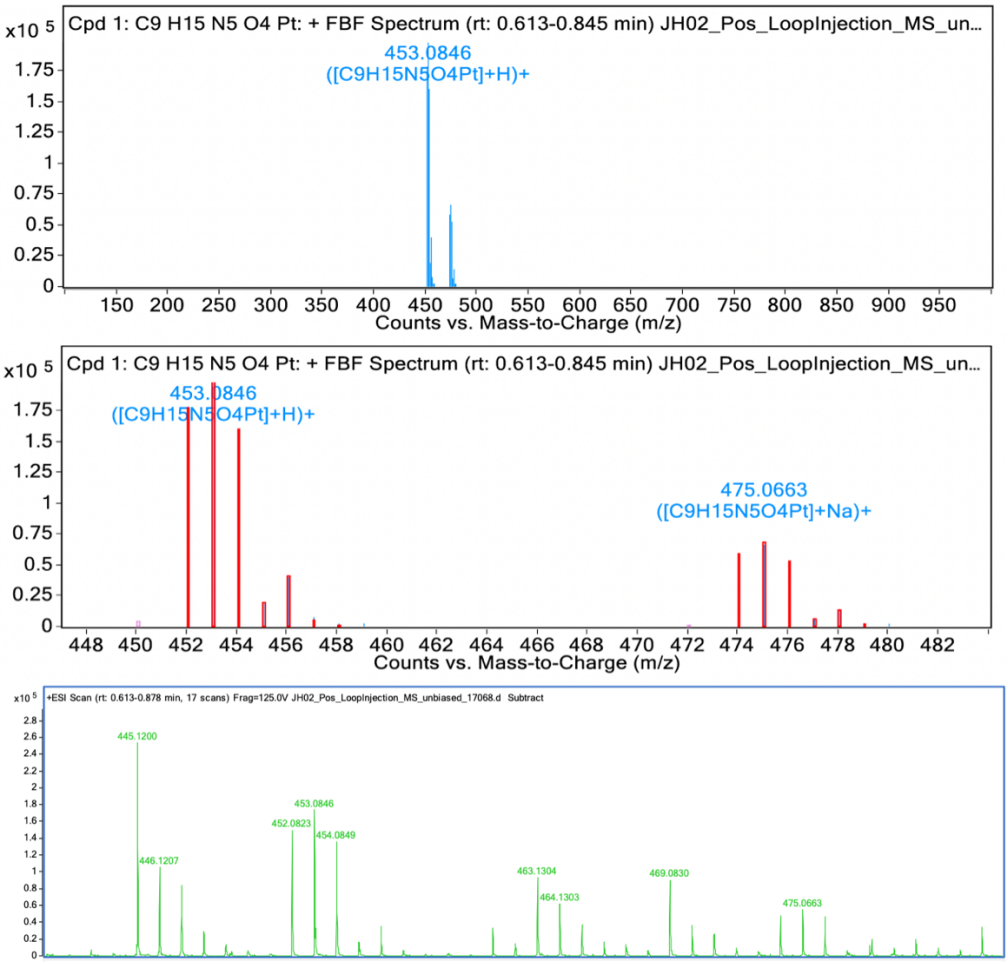

Figure VIII-48. ESI-MS for *cis*-[Pt(2-azidopropane-1,3-diamine)CBDCA] (**15**).

(16) *cis*-[Pt(2-azidopropane-1,3-diamine)Oxalate] spectra:

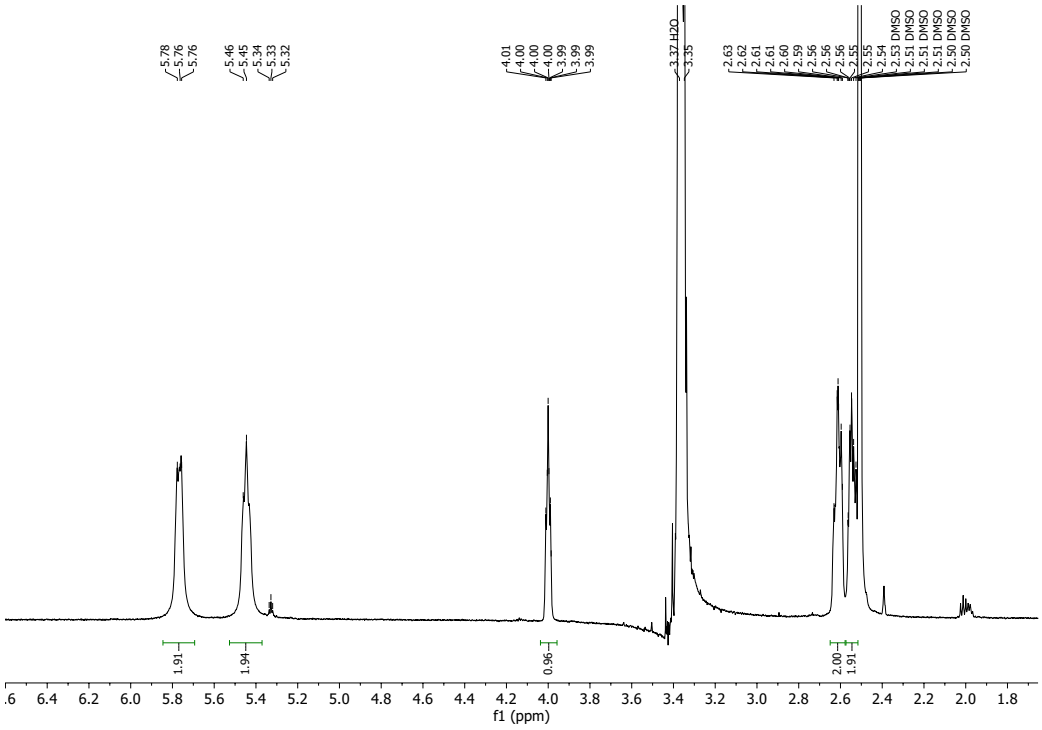

Figure VIII-49. ^{1}H NMR spectra for *cis*-[Pt(2-azidopropane-1,3-diamine)Oxalate] (**16**).

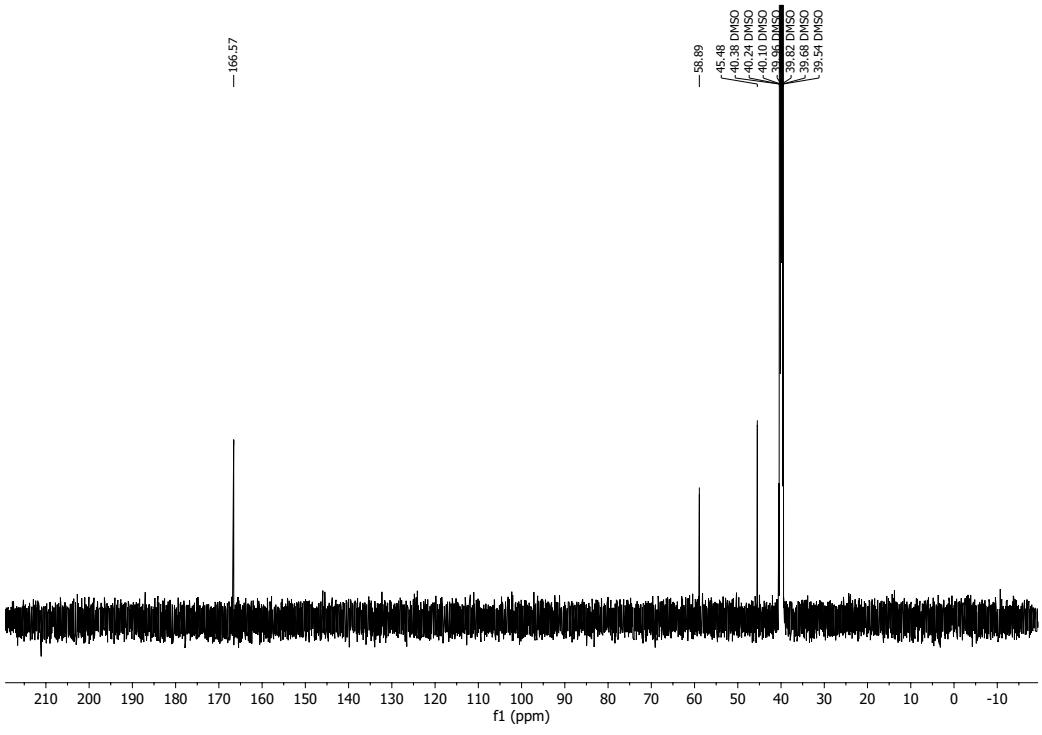

Figure VIII-50. ^{13}C NMR spectra for *cis*-[Pt(2-azidopropane-1,3-diamine)Oxalate] (**16**).

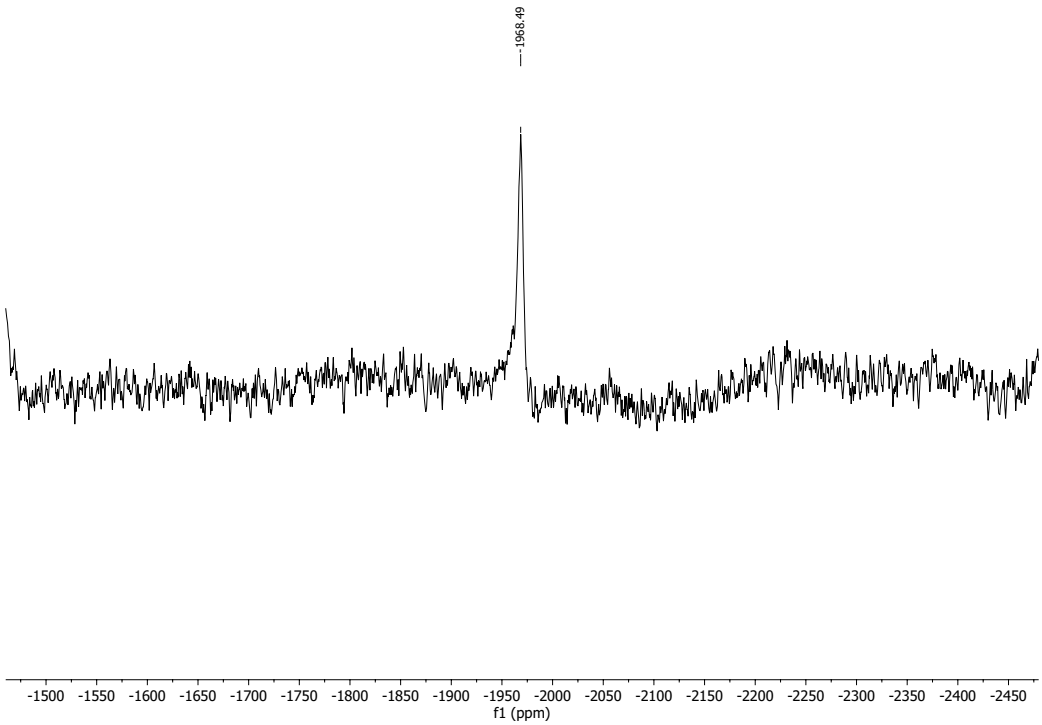

Figure VIII-51. ^{195}Pt NMR spectra for *cis*-[Pt(2-azidopropane-1,3-diamine)Oxalate] (**16**).

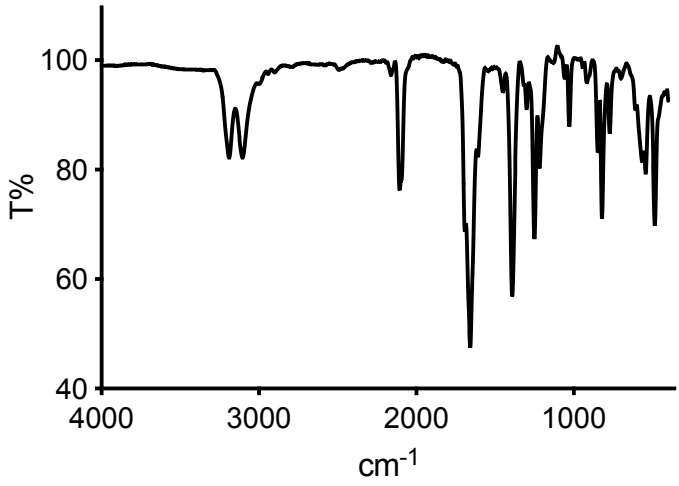

Figure VIII-52. IR spectrum for *cis*-[Pt(2-azidopropane-1,3-diamine)Oxalate] (**16**).

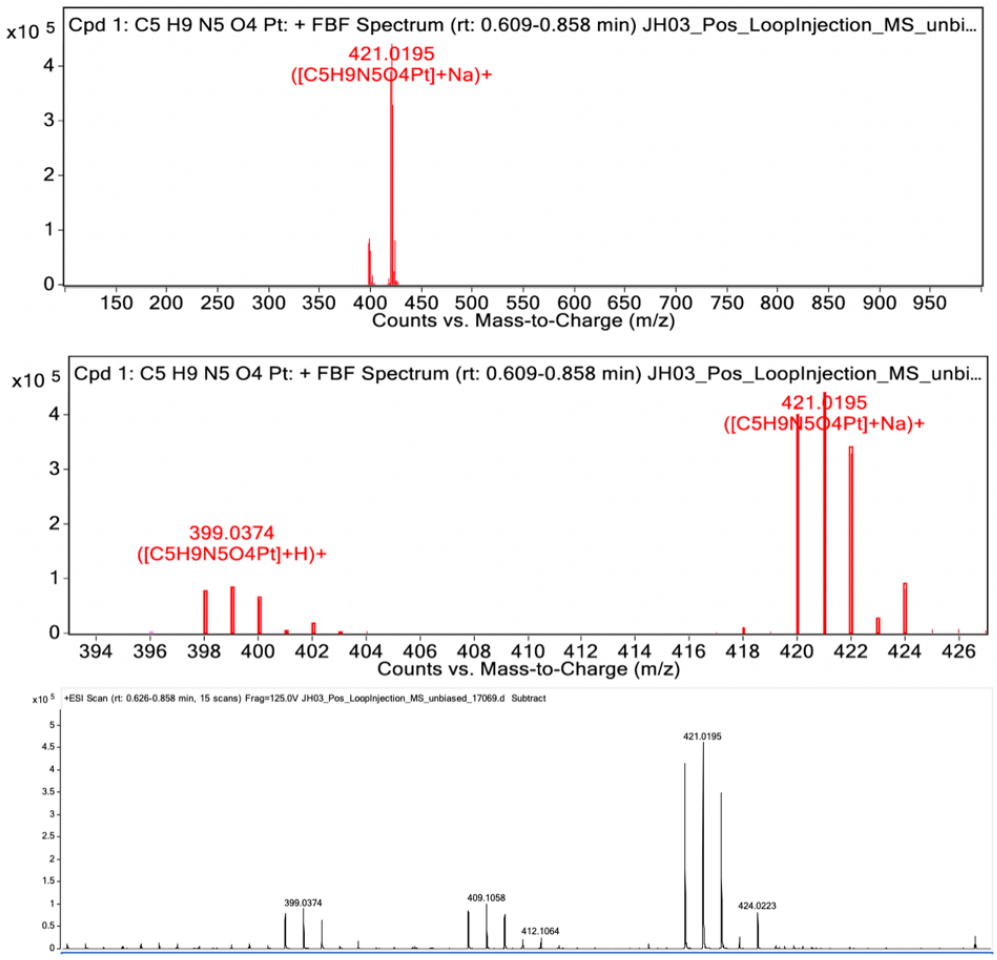

Figure VIII-53. ESI-MS for *cis*-[Pt(2-azidopropane-1,3-diamine)Oxalate] (**16**).

VIII. 2. Appendix B

VIII. 2. 1. Alkyne-Modified TFOs, Pt(II)-TFO Hybrids and Cu(II)-AMN-TFOs

Table VIII-1. Oligonucleotide, Pt(II)-TFO hybrid oligonucleotide sequences and modifications. Calculated and observed m/z: (a) = -71 m/z caused by loss of the chloride ligands during ionisation process; (b) = -88 m/z caused by loss of oxalate ligand during ionisation process; (c) = ESI-MS displayed additional peak with +56 m/z, corresponding to Fe^{3+} ion. **5'-dC** = 5'-(5)octadinyl-deoxycytidine; **int-dU** = internal-octadinyl-deoxyuridine; **5'-BCN-dC** = 5'-BCN(CEP II)-deoxycytidine; **N_3-Pt(II)-Cis** = *cis*-[Pt(2-azidopropane-1,3-diamine)Cl_2]; **N_3-Pt(II)-Carbo** = *cis*-[Pt(2-azidopropane-1,3-diamine)(CBDCA)]; **N_3-Pt(II)-Oxali** = *cis*-[Pt(2-azidopropane-1,3-diamine)(Oxalate)]; **DA tgt.** = Duplex A polypurine target strand; **DA comp.** = Duplex A polypyrimidine complementary strand. Duplex A is the target sequence for oligos TFO1-TFO3. **DB** and **DC** = Duplex B and Duplex C. Duplex B is the target sequence for oligos TFO4-TFO5. Duplex C is the target sequence for TFO6. The 57 bp target is a target sequence for TFO1-3 used in PAGE analysis.

Oligo	Sequence	Modification (X)(C)(U)	Calc. Mass	Obs. Mass
TFO1	**5'-** CTC TTT CCT TCC CTT CTT TCG CTT TCC TC **-3'**	5'-dC	8694.1	8694.3
TFO1-Cis	**5'-** CTC TTT CCT TCC CTT CTT TCG CTT TCC TC **-3'**	5'-dC-N_3-Pt(II)-Cis	9075	9001.7[a]
TFO1-Carbo	**5'-** CTC TTT CCT TCC CTT CTT TCG CTT TCC TC **-3'**	5'-dC-N_3-Pt(II)-Carbo	9146	9146
TFO1-Oxali	**5'-** CTC TTT CCT TCC CTT CTT TCG CTT TCC TC **-3'**	5'-dC-N_3-Pt(II)-Oxali	9091.2	9002[b]
TFO2	**5'-** XTC TTT CCT TCC CTT CTT TCG CTT TCC TC **-3'**	5'-BCN-dC	8932	8933.6
TFO2-Cis	**5'-** XTC TTT CCT TCC CTT CTT TCG CTT TCC TC **-3'**	5'-BCN-dC-N_3-Pt(II)-Cis	9313	9240[a]
TFO2-Carbo	**5'-** XTC TTT CCT TCC CTT CTT TCG CTT TCC TC **-3'**	5'-BCN-dC-N_3-Pt(II)-Carbo	9384	9384.9
TFO2-Oxali	**5'-** XTC TTT CCT TCC CTT CTT TCG CTT TCC TC **-3'**	5'-BCN-dC-N_3-Pt(II)-Oxali	9330	9240.8[b]
TFO3	**5'-** CTC TTT CCT TCC CTT CTT TCG CTT UCC TC **-3'**	Int-dU	8680	8680.5
TFO3-Cis	**5'-** CTC TTT CCT TCC CTT CTT TCG CTT UCC TC **-3'**	Int-dU-N_3-Pt(II)-Cis	9061	8987.8[a]
TFO3-Carbo	**5'-** CTC TTT CCT TCC CTT CTT TCG CTT UCC TC **-3'**	Int-dU-N_3-Pt(II)-Carbo	9132	9132
TFO3-Oxali	**5'-** CTC TTT CCT TCC CTT CTT TCG CTT UCC TC **-3'**	Int-dU-N_3-Pt(II)-Oxali	9078	8987.8[b]
DA tgt.	**5'-** ACC GTG GCG AGA AAG GAA GGG AAG AAA GCG AAA GGA GCG G **-3'**	-	12625	12625.4

DA comp.	**3′-** TGG CAC CGC TCT TTC CTT CCC TTC TTT CGC TTT CCT CGC C **-5′**	-	11970	11970.1
TFO4	**5′-** CTT CCC TCT TTC CGC CTG TCC **-3′**	5′-dC	6315	6315.7
TFO4-Cis	**5′-** CTT CCC TCT TTC CGC CTG TCC **-3′**	5′-dC-N_3-Pt(II)-Cis	6696	6623[a]
TFO4-Carbo	**5′-** CTT CCC TCT TTC CGC CTG TCC **-3′**	5′-dC-N_3-Pt(II)-Carbo	6767	6767
TFO4-Oxali	**5′-** CTT CCC TCT TTC CGC CTG TCC **-3′**	5′-dC-N_3-Pt(II)-Oxali	6713	6623.2[b]
TFO5	**5′-** CTT CCC TCT TUC CGC CTG TCC **-3′**	Int-dU	6301	6301.7
TFO5-Cis	**5′-** CTT CCC TCT TUC CGC CTG TCC **-3′**	Int-dU-N_3-Pt(II)-Cis	6682	6608.9[a]
TFO5-Carbo	**5′-** CTT CCC TCT TUC CGC CTG TCC **-3′**	Int-dU-N_3-Pt(II)-Carbo	6753	6753
TFO5-Oxali	**5′-** CTT CCC TCT TUC CGC CTG TCC **-3′**	Int-dU-N_3-Pt(II)-Oxali	6699	6608.9[b]
DB tgt.	**5′-** CGC TTC CCG AAG GGA GAA AGG CGG ACA GGT AT **-3′**	-	9948	9948.6
DB comp.	**3′-** GCG AAG GGC TTC CCT CTT TCC GCC TGT CCA TA **-5′**	-	9703	9703.7
TFO6	**5′-** UAA GGG AAA GAA GGG AAG GAA AGA **-3′**	5′-dU	7696	7696.7
DC tgt.	**5′-**CCG TGG CGA GAA AGG AAG GGA AGA AAG CGA AAG GA**-3′**	-	11035	11035.4
DC comp.	**3′-**GGC ACC GCT CTT TCC TTC CCT TCT TTC GCT TTC CT**-5′**	-	10469	10469.2
57 bp tgt.	**5′-** AAG CCG GCG AAC GTG GCG AGA AAG GAA GGG AAG AAA GCG AAA GGA GCG GGC GCT AGG **-3′**	-	17972.5	17972.8
57 bp comp.	**3′-** TTC GGC CGC TTG CAC CGC TCT TTC CTT CCC TTC TTT CGC TTT CCT CGC CCG CGA TCC **-5′**	-	17129.9	17129.7
40 bp off tgt.	**5′-** TGA CTC CCC GTC GTG TAG ATA ACT ACG ATA CGG GAG GGC T **-3′**	-	12336.9	-
40 bp off comp.	**3′-** ACT GAG GGG CAG CAC ATC TAT TGA TGC TAT GCC CTC CCG A **-5′**	-	12256.9	-
TFO-17A	**5′-** UCT TTC CTT CCC TTC TT **-3′**	5′-dU	5094.4	5094.9
TFO-17B	**5′-** TCT TTC CTT CCC TTC TU **-3′**	3′-dU	5094.4	5094.9
TFO-17C	**5′-** TCT TTC CTU CCC TTC TT **-3′**	Int-dU	5094.4	5094.3
21 D tgt.	**5′-** Cy5- GGA GAA AGG AAG GGA AGA AGG **-3′**	5′-Cyanine 5 label	7224	7224.8

21 D comp.	**3'**- CCT CTT TCC TTC CCT TCT TCC -6FAM -**5'**	5'-6-FAM label	6698.5	6697.3
17 D comp.	**3'**-TCT TTC CTT CCC TTC TT -6FAM -**5'**	5'-6-FAM label	5541.7	5541.1
TFO2A	**5'**- **X**TC TTT CCT TCC CTT CTT TCG CTT TCC TC -**3'**	5'-BCN-dC 5'-BCN-dC-N_3-Phen	9153.2	9154.3[c]
TFO2B	**5'**- **X**TC TTT CCT TCC CTT CTT TCG CTT TCC TC -**3'**	5'-BCN-dC 5'-BCN-dC-N_3-DPPZ	9256.3	9256.3[c]
TFO2C	**5'**- **X**TC TTT CCT TCC CTT CTT TCG CTT TCC TC -**3'**	5'-BCN-dC 5'-BCN-dC-N_3-ImPhen	9270.4	-

VIII. 2. 2. Pt(II)-TOTFO sequences and Hybrids

Table VIII-2. Oligonucleotide, Pt(II)-TOTFO and Pt(II)-AA-TOTFO hybrid oligonucleotide sequences and modifications. Calculated and observed m/z: **5'-dC** = 5'-(5)octadinyl-deoxycytidine; **AP-C3** = alkyne-amine monomer nucleobase; **pdU** = 5-(1-propargylamino)-deoxyuridine; **pdU-TO** = pdU with TO (thiazole orange) coupled**; N_3-Pt(II)-Carbo** = *cis*-[Pt(2-azidopropane-1,3-diamine)(CBDCA)]. *** =** ESI-MS data for TOTFO6-Carbo was not obtained.

Oligo	Sequence	Modification (X)(C)(U)	Calc. Mass	Obs. Mass
TOTFO1	5'-CTC TTT CCU TCC CTT CTT TCG CTT TCC TC-3'	5'-dC, pdU-TO	9120.0	9119.7
TOTFO1-Carbo	5'-CTC TTT CCU TCC CTT CTT TCG CTT TCC TC-3'	5'-dC-N_3-Pt(II)-Carbo, pdU-TO	9572.3	9571.9
TOTFO2	5'-CTC TTT CCU TCC CTU CTT TCG CTT TCC TC-3'	5'-dC, pdU-TO (x2)	9546.0	9545
TOTFO2-Carbo	5'-CTC TTT CCU TCC CTU CTT TCG CTT TCC TC-3'	5'-dC-N_3-Pt(II)-Carbo, pdU-TO (x2)	9998.2	9997.2
TOTFO3	5'-CTC TTT CCU TCC CTU CTT TCG CTT UCC TC-3'	5'-dC, pdU-TO (x3)	9971.9	9970.4
TOTFO3-Carbo	5'-CTC TTT CCU TCC CTU CTT TCG CTT UCC TC-3'	5'-dC-N_3-Pt(II)-Carbo, pdU-TO (x3)	10424.3	10422.8
TOTFO4	**5'-**CTT CCC UCT TTC CGC CTG TCC**-3'**	5'-dC, pdU-TO	6740.7	6741.2
TOTFO4-Carbo	**5'-**CTT CCC UCT TTC CGC CTG TCC**-3'**	5'-dC-N_3-Pt(II)-Carbo, pdU-TO	7193.0	7193.1
TOTFO5	**5'-**CTT CCC UCT TUC CGC CTG TCC**-3'**	5'-dC, pdU-TO (x2)	7167.2	7166.7
TOTFO5-Carbo	**5'-**CTT CCC UCT TUC CGC CTG TCC**-3'**	5'-dC-N_3-Pt(II)-Carbo, pdU-TO (x2)	7619.0	7618.7
TOTFO6	**5'-**CTT CCC UCT TUC CGC CTG UCC**-3'**	5'-dC, pdU-TO (x3)	7592.8	7592.1
TOTFO6-Carbo	**5'-**CTT CCC UCT TUC CGC CTG UCC**-3'**	5'-dC-N_3-Pt(II)-Carbo, pdU-TO (x3)	8045.1	-*
AA-TOTFO1	**5'-**XCT TTC CTT CCC TTC TTT CGC TTT CCT C**-3'**	AP-C3-TO (x1)	8821.7	8821.4
AA-TOTFO1-Carbo	**5'-**XCT TTC CTT CCC TTC TTT CGC TTT CCT C**-3'**	AP-C3-TO (x1), AP-C3-N_3-Pt(II)-Carbo	9274.0	9273.9
AA-TOTFO2	**5'-**XCT TTC CUT CCC TTC TTT CGC TTT CCT C**-3'**	AP-C3-TO (x1), pdU-TO (x1)	9247.7	9246.9
AA-TOTFO2-Carbo	**5'-**XCT TTC CUT CCC TTC TTT CGC TTT CCT C**-3'**	AP-C3-TO (x1), pdU-TO (x1), AP-C3-N_3-Pt(II)-Carbo	9700.2	9699.1
AA-TOTFO3	**5'-**XCT TTC CUT CCC TUC TTT CGC TTT CCT C**-3'**	AP-C3-TO (x1), pdU-TO (x2)	9673.5	9672.5
AA-TOTFO3-Carbo	**5'-**XCT TTC CUT CCC TUC TTT CGC TTT CCT C**-3'**	AP-C3-TO (x1), pdU-TO (x2), AP-C3-N_3-Pt(II)-Carbo	10126.0	10124.6
AA-TOTFO4	**5'-**XCT TTC CUT CCC TUC TTT CGC TTU CCT C**-3'**	AP-C3-TO (x1), pdU-TO (x3)	10100.3	10098.3

AA-TOTFO4-Carbo	**5'-XCT TTC CUT CCC TUC TTT CGC TTU CCT C-3'**	AP-C3-TO (x1), pdU-TO (x3), AP-C3-N_3-Pt(II)-Carbo	10552.1	10550.1
AA-TOTOFO5	**5'-XTC CCT CTT TCC GCC TGT CC-3'**	AP-C3-TO (x1)	6442.6	6442.8
AA-TOTFO5-Carbo	**5'-XTC CCT CTT TCC GCC TGT CC-3'**	AP-C3-TO (x1), AP-C3-N_3-Pt(II)-Carbo	6895.0	6895.0
AA-TOTFO6	**5'-XTC CCU CTT TCC GCC TGT CC-3'**	AP-C3-TO (x1), pdU-TO (x1)	6868.6	6868.3
AA-TOTFO6-Carbo	**5'-XTC CCU CTT TCC GCC TGT CC-3'**	AP-C3-TO (x1), pdU-TO (x1), AP-C3-N_3-Pt(II)-Carbo	7321.0	7320.5
AA-TOTFO7	**5'-XTC CCU CTT UCC GCC TGT CC-3'**	AP-C3-TO (x1), pdU-TO (x2)	7294.5	7298.3
AA-TOTFO7-Carbo	**5'-XTC CCU CTT UCC GCC TGT CC-3'**	AP-C3-TO (x1), pdU-TO (x2), AP-C3-N_3-Pt(II)-Carbo	7747.1	7746.2
AA-TOTOFO8	**5'-XTC CCU CTT UCC GCC TGU CC-3'**	AP-C3-TO (x1), pdU-TO (x3)	7720.7	7719.0
AA-TOTFO8-Carbo	**5'-XTC CCU CTT UCC GCC TGU CC-3'**	AP-C3-TO (x1), pdU-TO (x3), AP-C3-N_3-Pt(II)-Carbo	8173.0	8171.6

VIII. 2. 3. ESI-MS and HPLC of Oligonucleotides

VIII. 2. 3. 1. Alkyne-TFOs

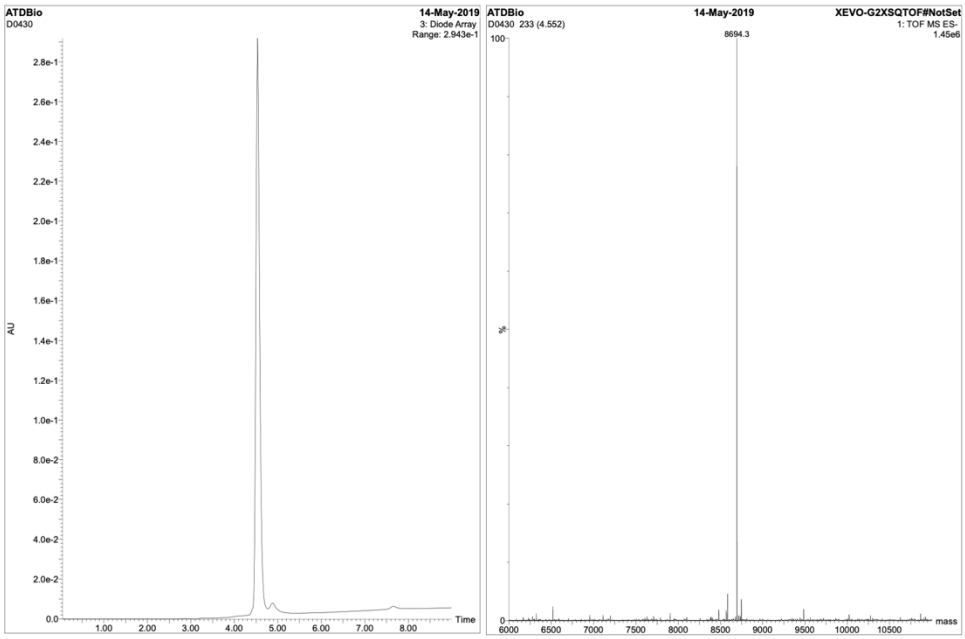

Figure VIII-54. HPLC and ESI-MS spectra for alkyne-TFO1.

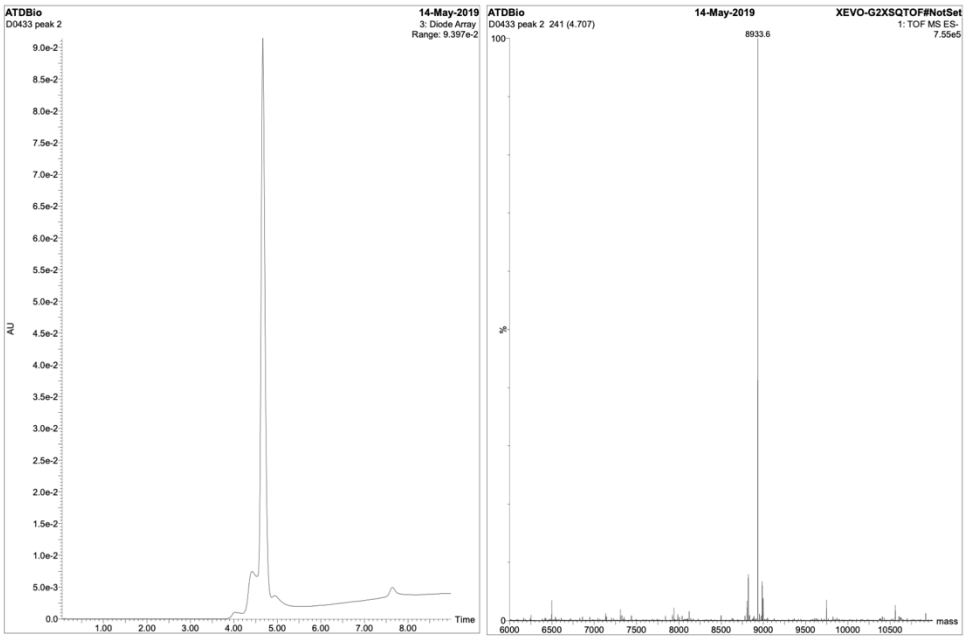

Figure VIII-55. HPLC and ESI-MS spectra for alkyne-TFO2.

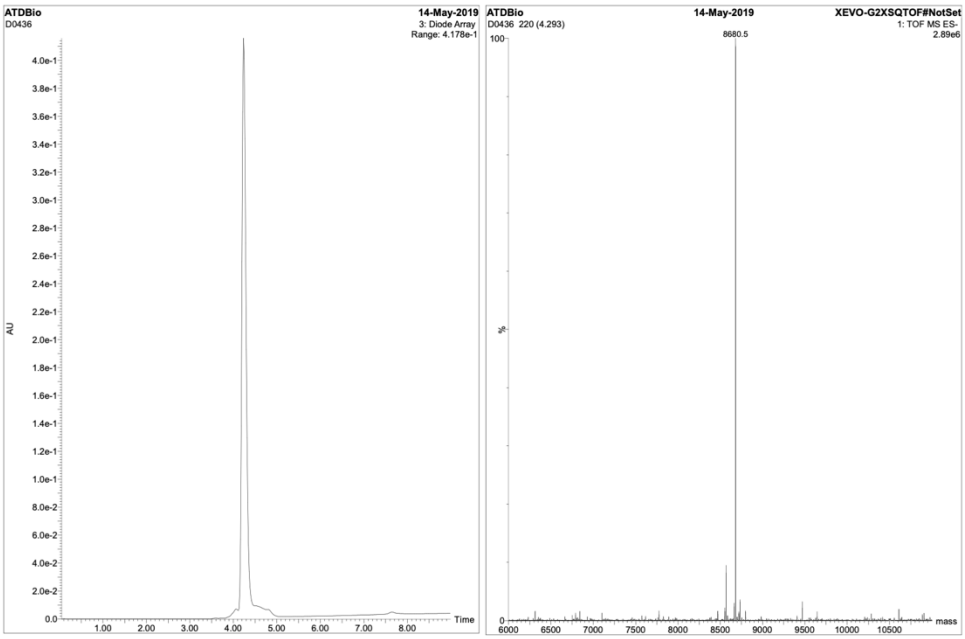

Figure VIII-56. HPLC and ESI-MS spectra for alkyne-TFO3.

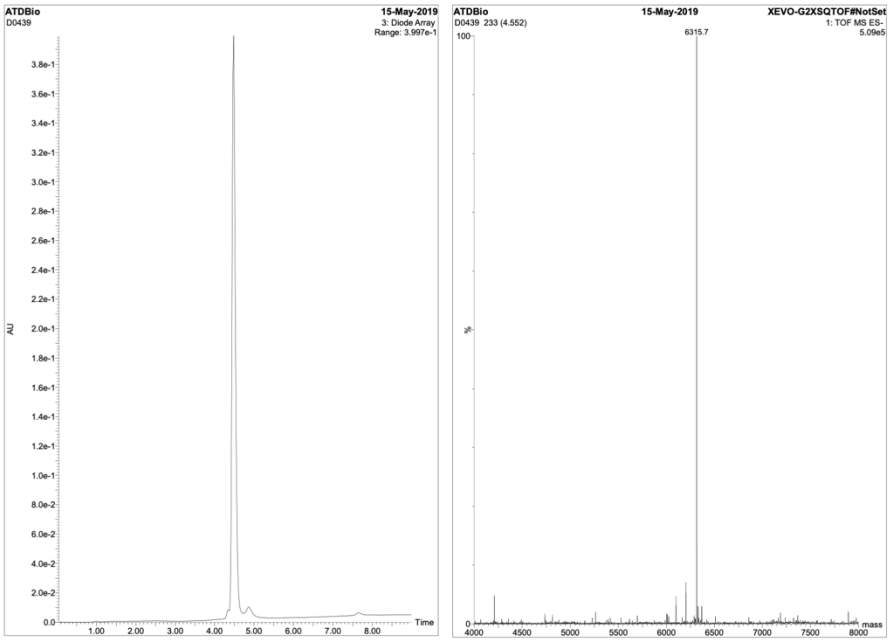

Figure VIII-57. HPLC and ESI-MS spectra for alkyne-TFO4.

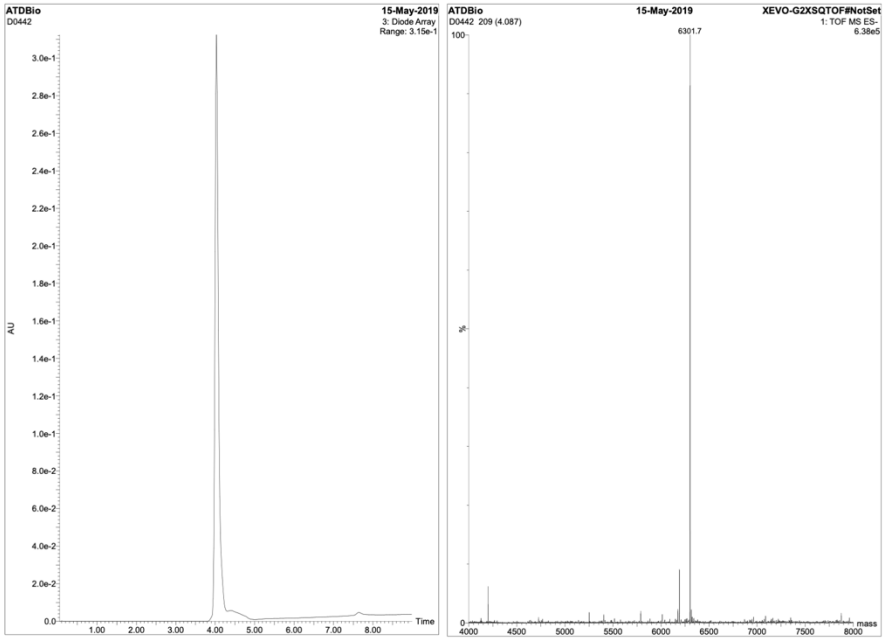

Figure VIII-58. HPLC and ESI-MS spectra for alkyne-TFO5.

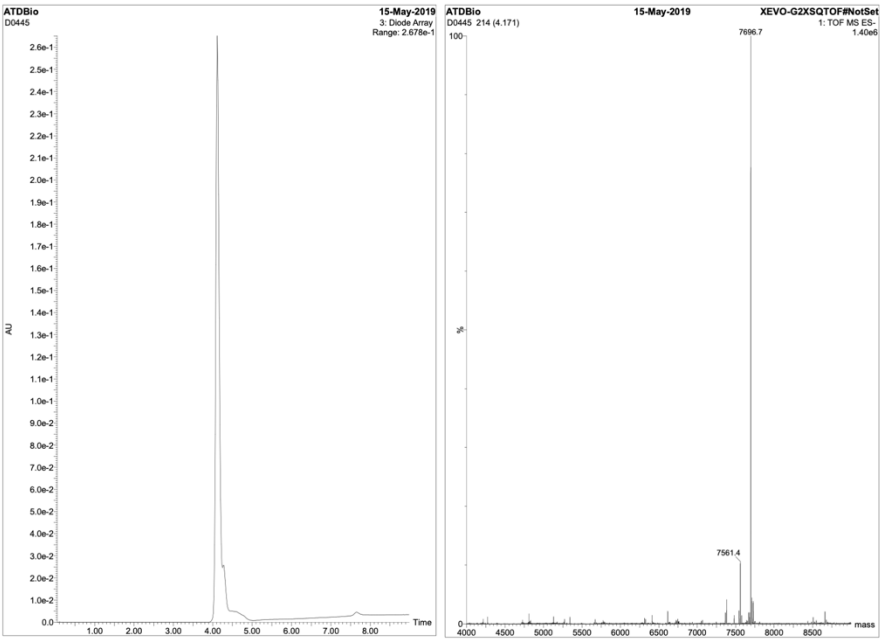

Figure VIII-59. HPLC and ESI-MS spectra for alkyne-TFO6.

VIII. 2. 3. 2. Pt(II)-TFO Hybrids

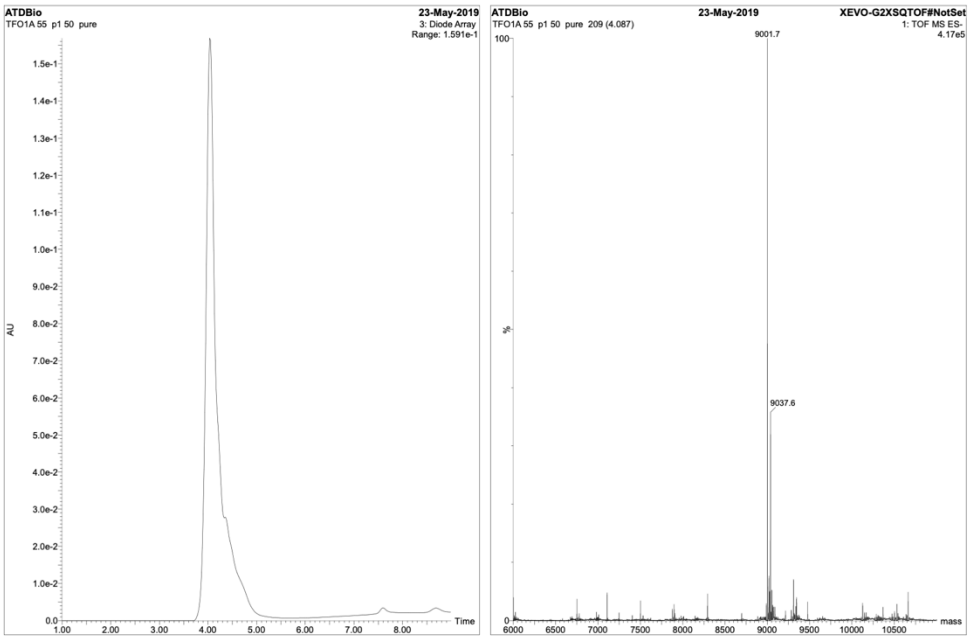

Figure VIII-60. HPLC and ESI-MS spectra for TFO1-Cis.

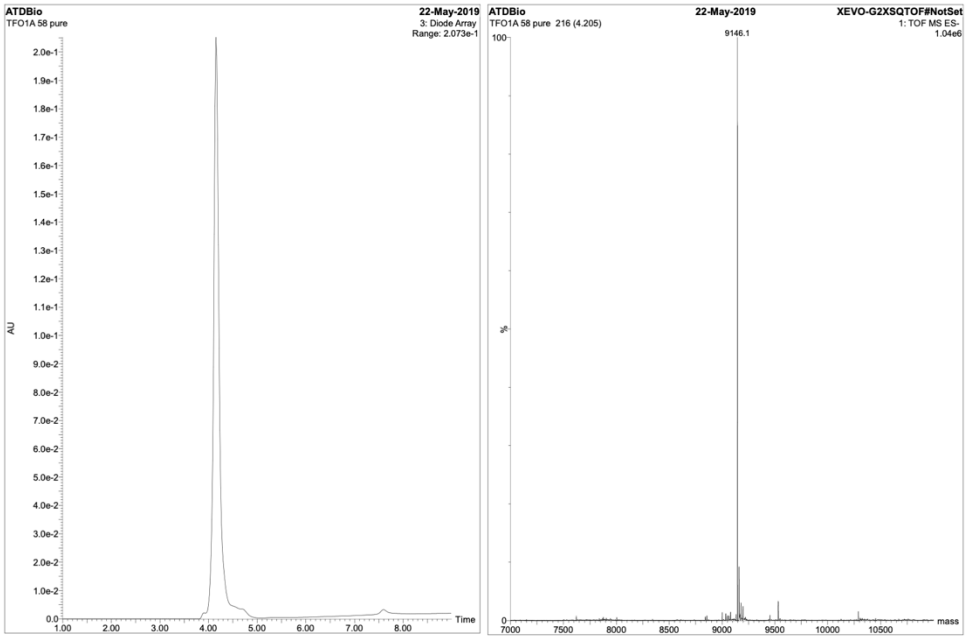

Figure VIII-61. HPLC and ESI-MS spectra for TFO1-Carbo.

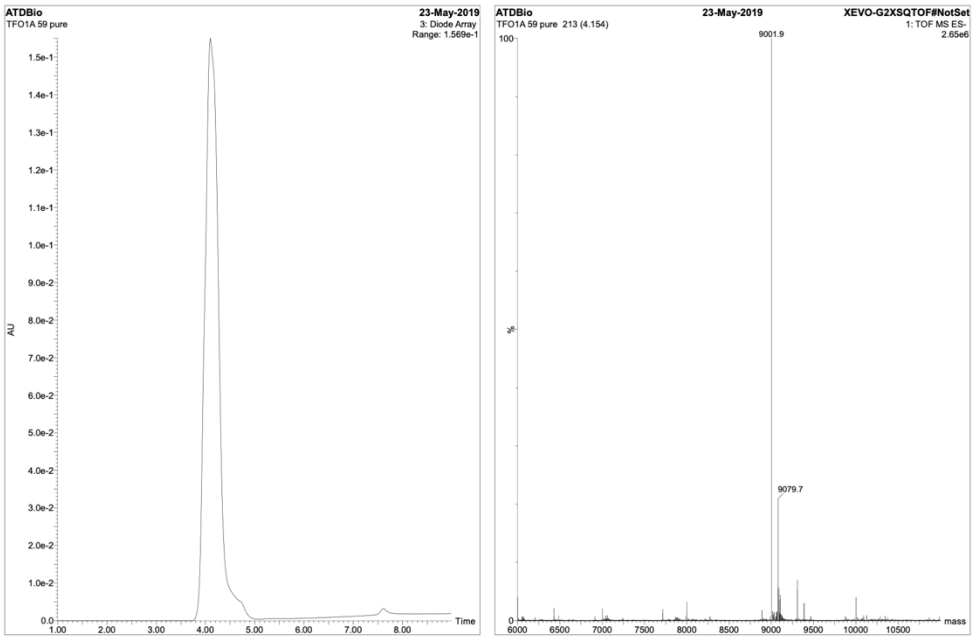

Figure VIII-62. HPLC and ESI-MS spectra for TFO1-Oxali.

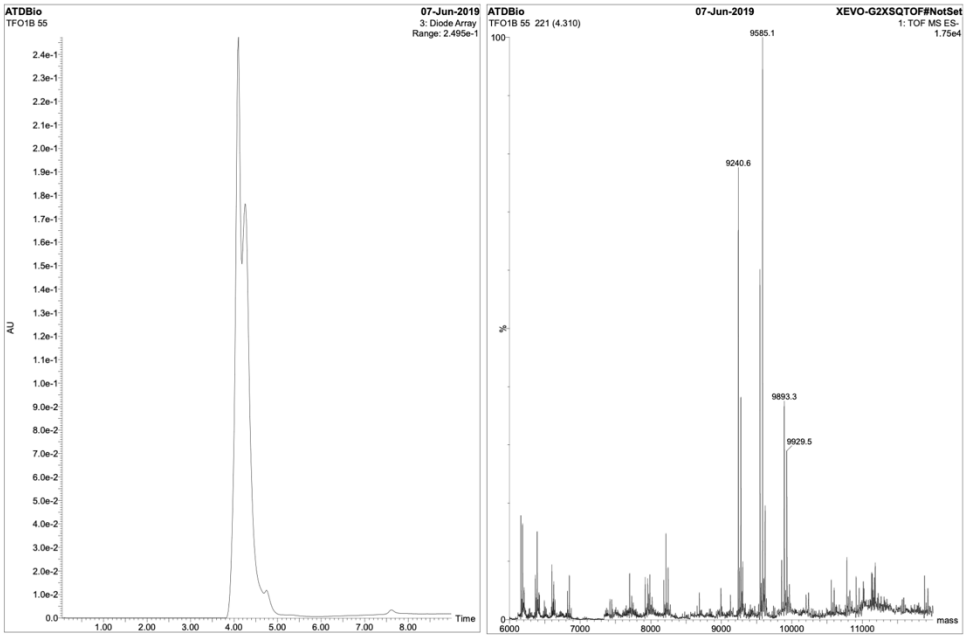

Figure VIII-63. HPLC and ESI-MS spectra for TFO2-Cis.

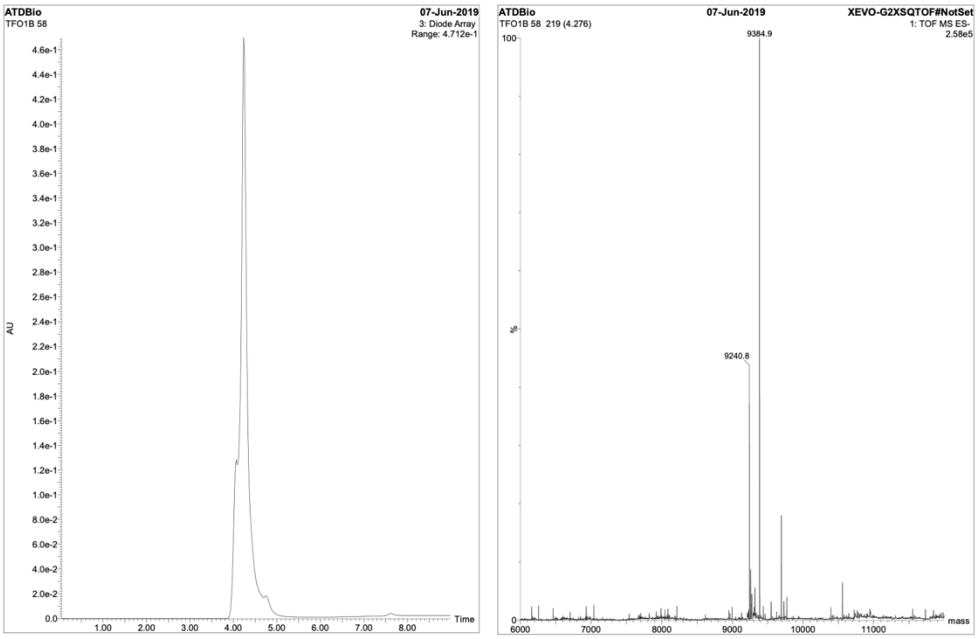

Figure VIII-64. HPLC and ESI-MS spectra for TFO2-Carbo.

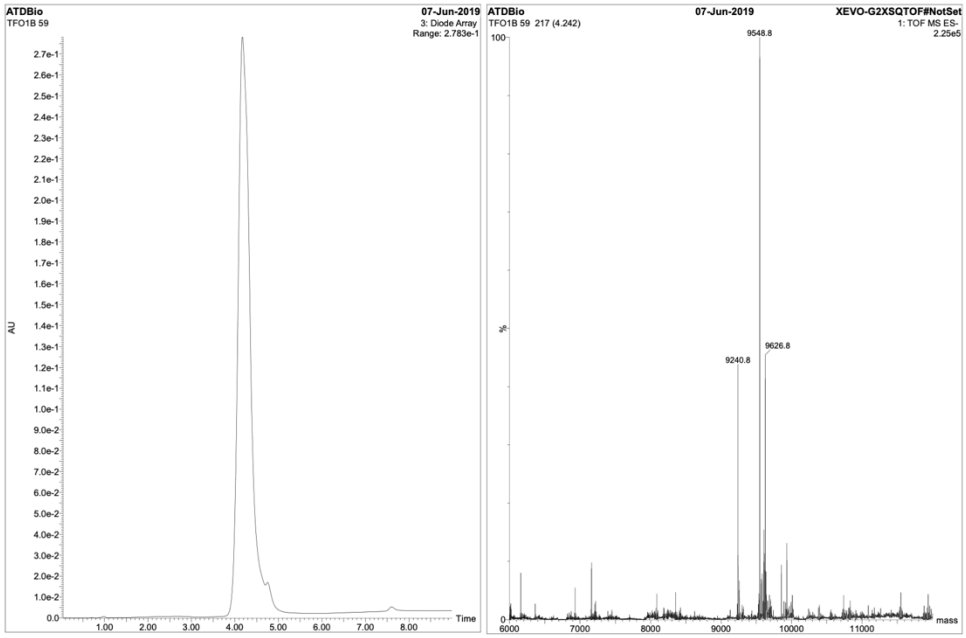

Figure VIII-65. HPLC and ESI-MS spectra for TFO2-Oxali

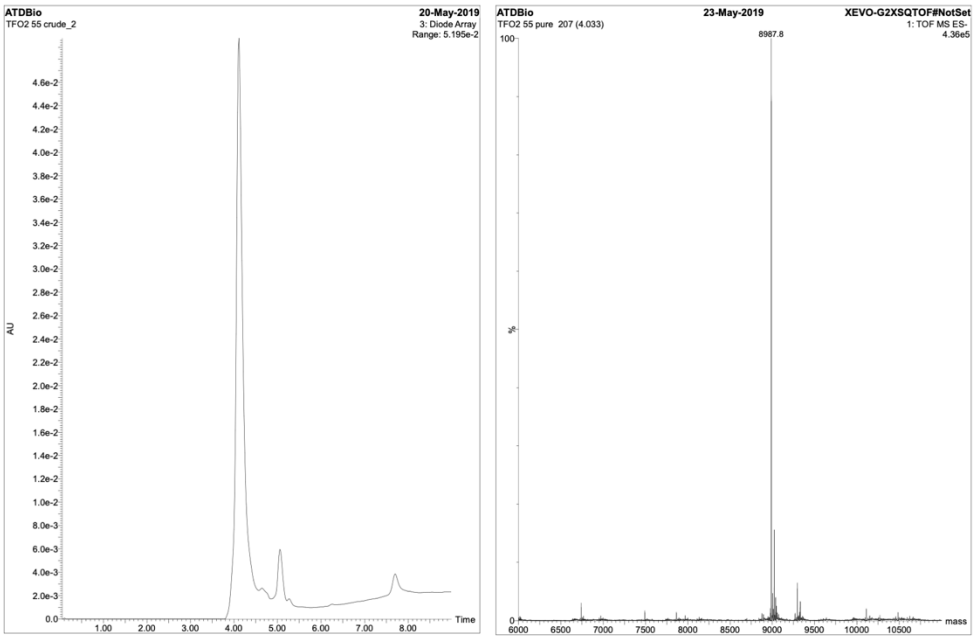

Figure VIII-66. HPLC and ESI-MS spectra for TFO3-Cis.

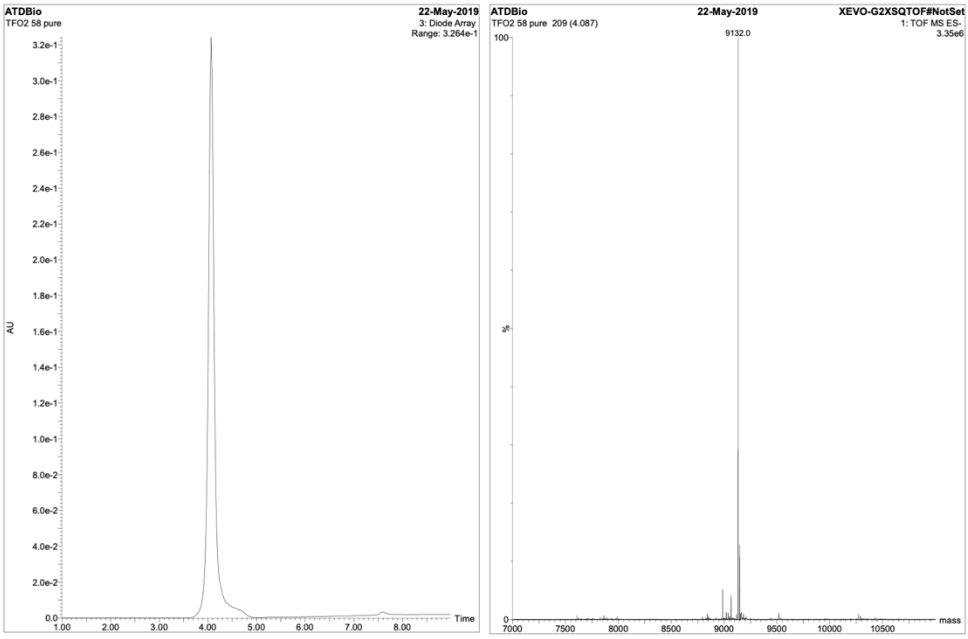

Figure VIII-67. HPLC and ESI-MS spectra for TFO3-Carbo.

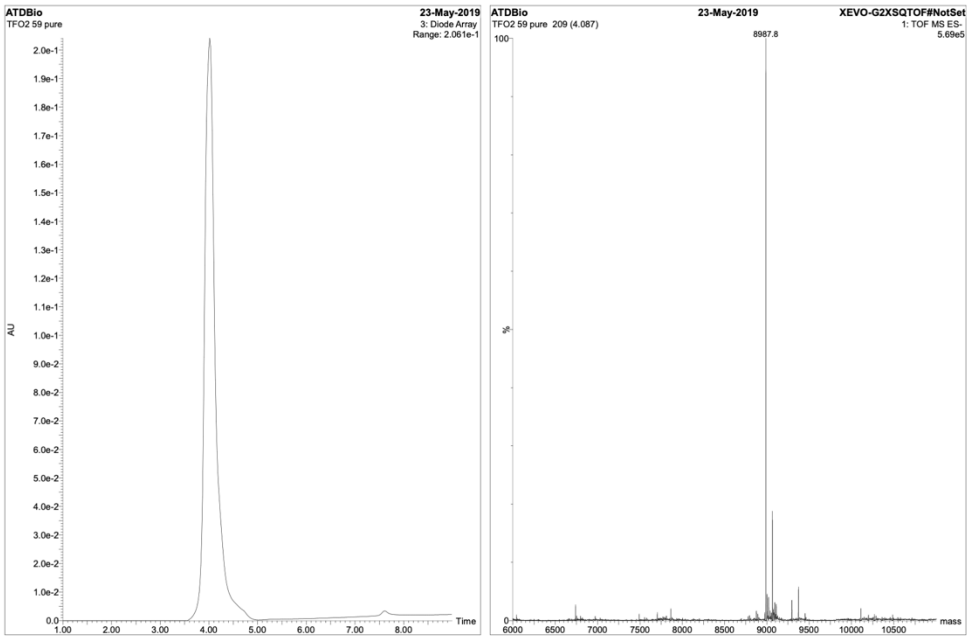

Figure VIII-68. HPLC and ESI-MS spectra for TFO3-Oxali.

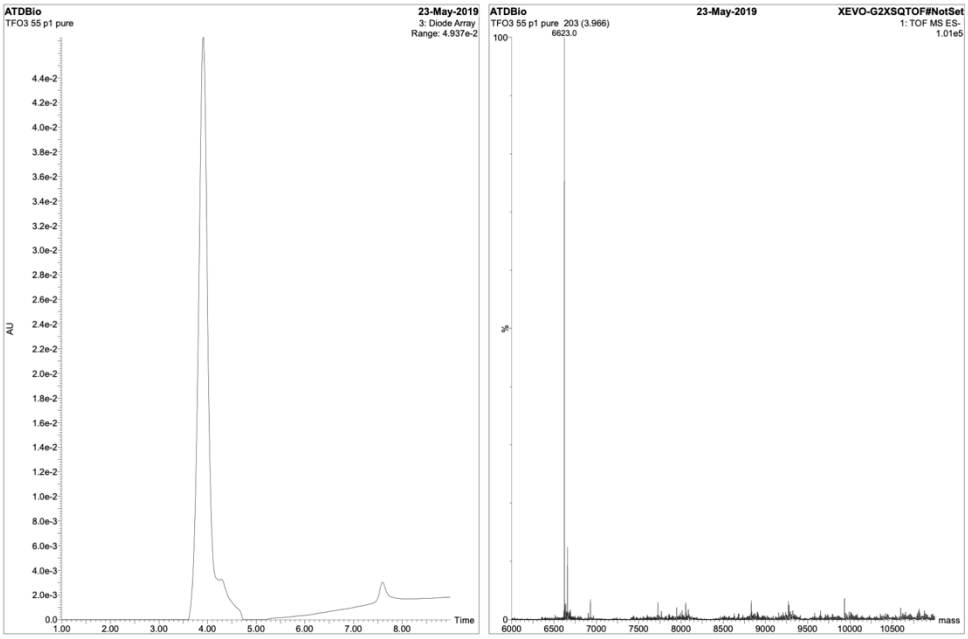

Figure VIII-69. HPLC and ESI-MS spectra for TFO4-Cis.

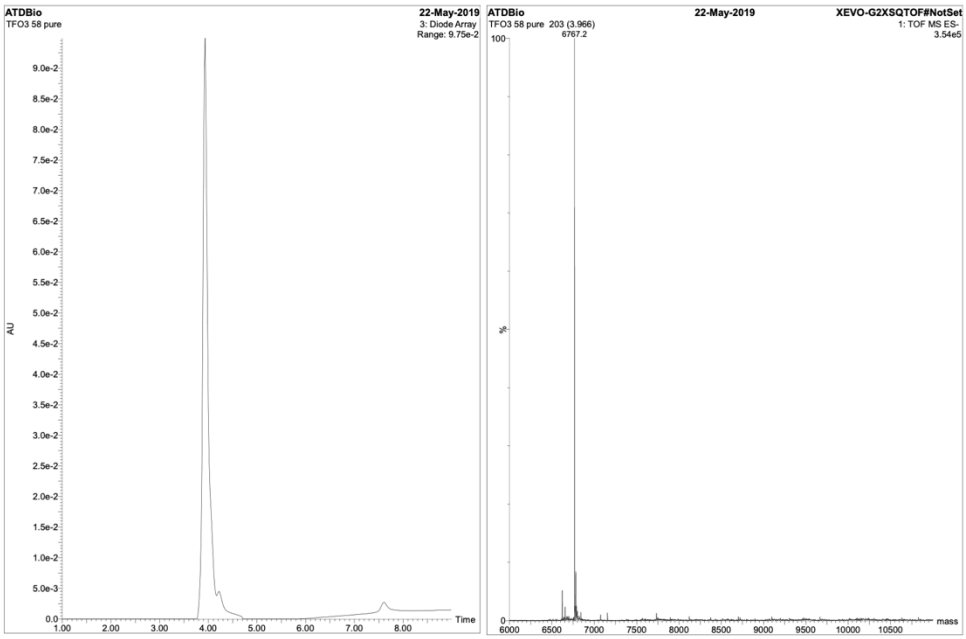

Figure VIII-70. HPLC and ESI-MS spectra for TFO4-Carbo.

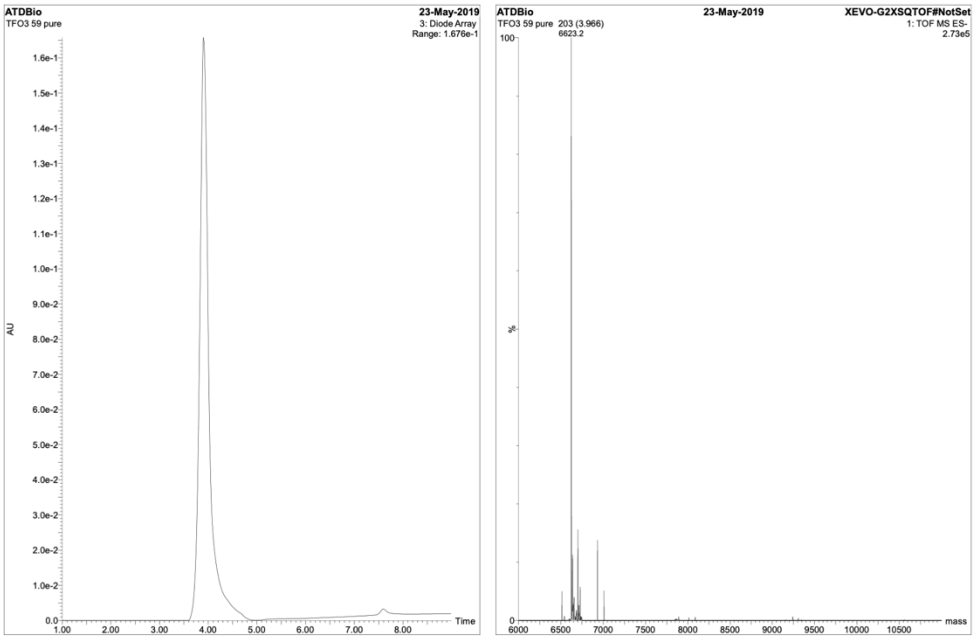

Figure VIII-71. HPLC and ESI-MS spectra for TFO4-Oxali.

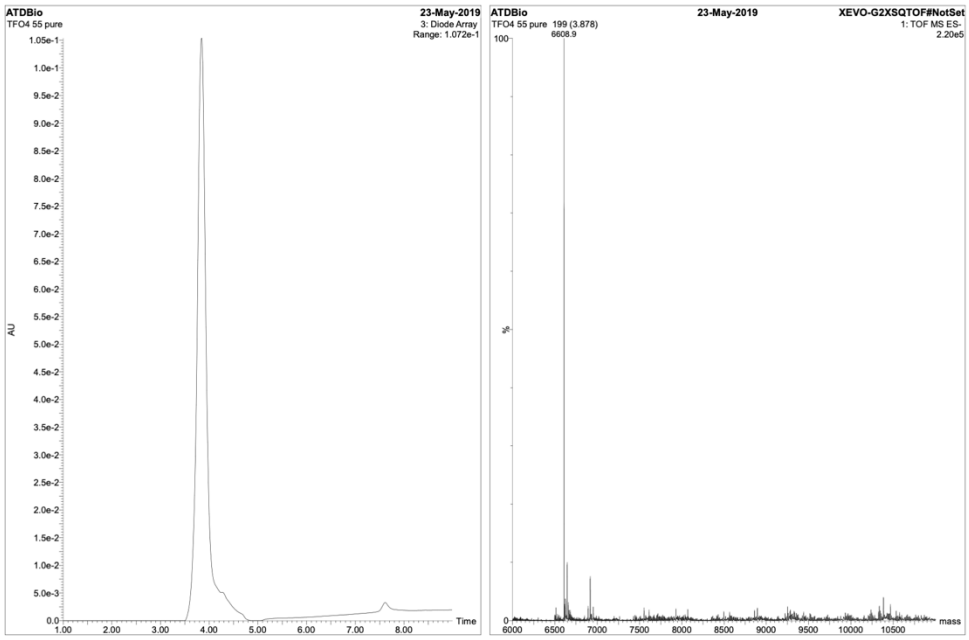

Figure VIII-72. HPLC and ESI-MS spectra for TFO5-Cis.

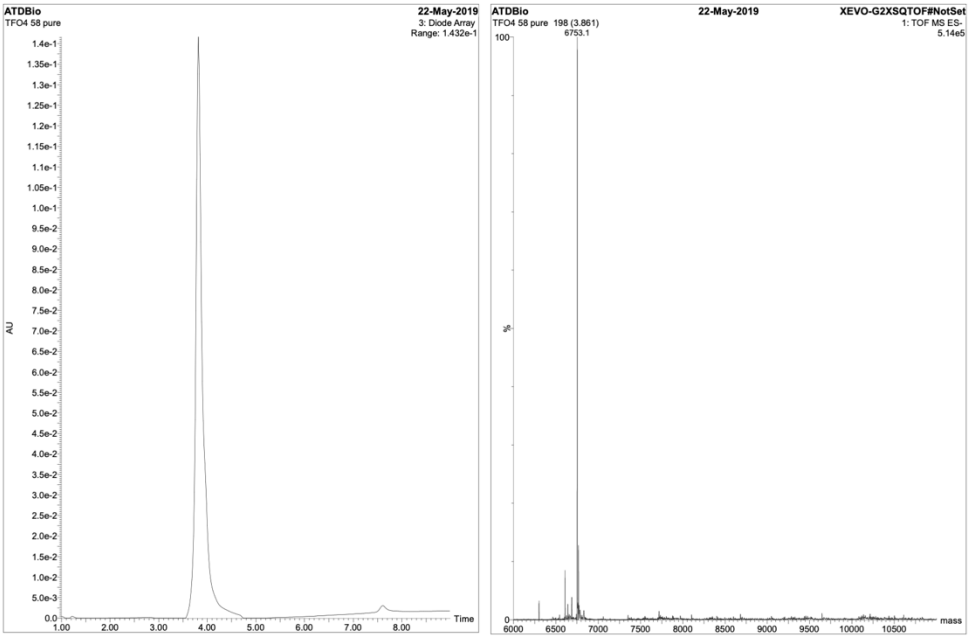

Figure VIII-73. HPLC and ESI-MS spectra for TFO5-Carbo.

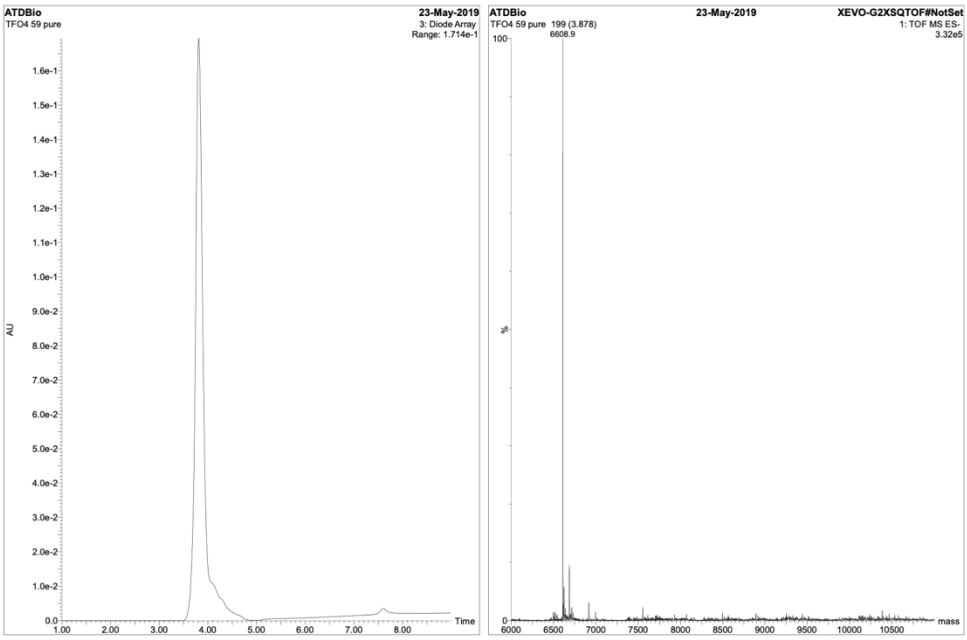

Figure VIII-74. HPLC and ESI-MS spectra for TFO5-Oxali.

VIII. 2. 3. 3. TOTFOs and Pt(II)-TOTFOs

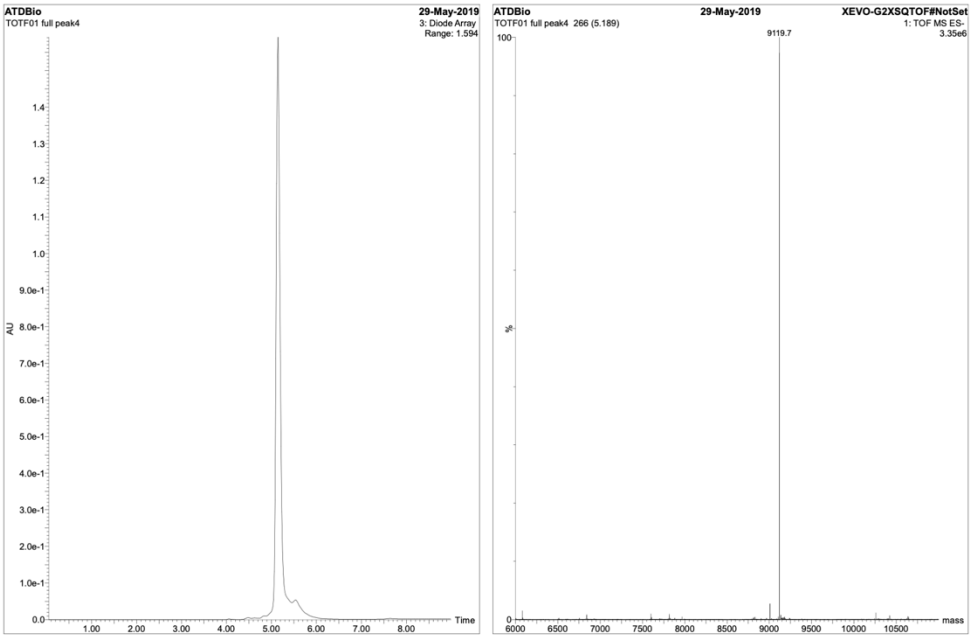

Figure VIII-75. HPLC and ESI-MS spectra for TOTFO1.

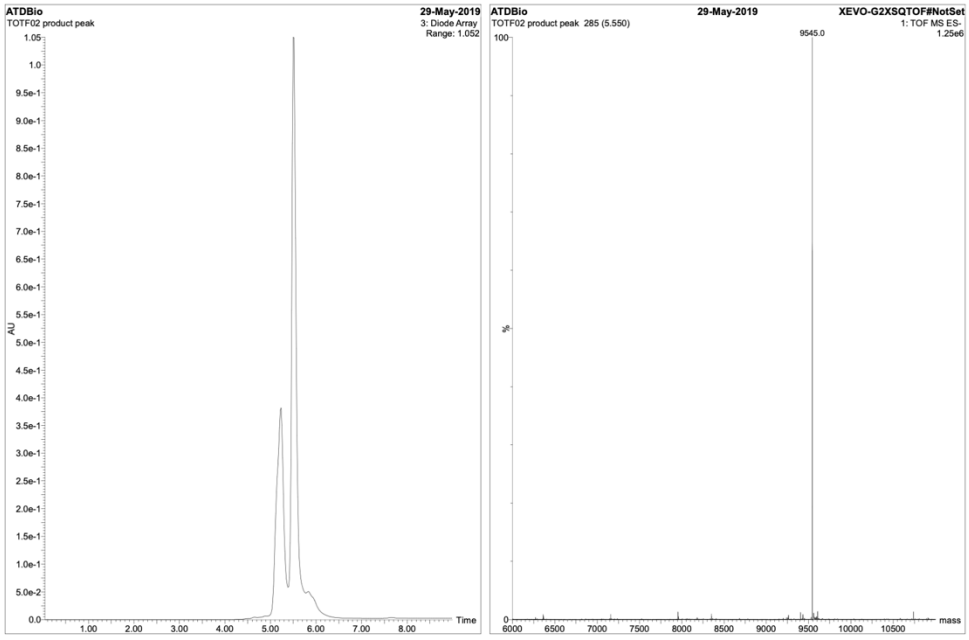

Figure VIII-76. HPLC and ESI-MS spectra for TOTFO2.

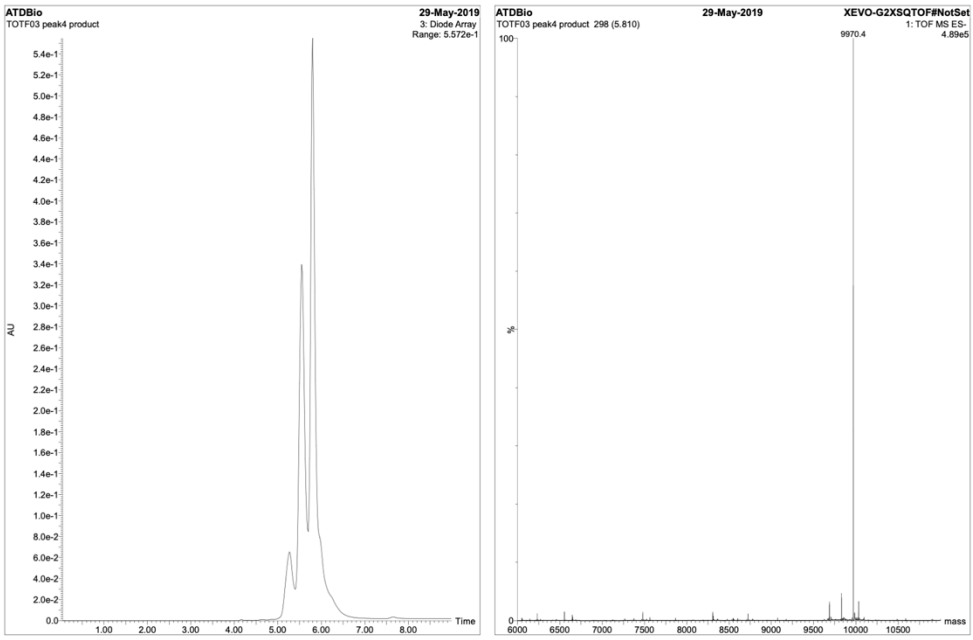

Figure VIII-77. HPLC and ESI-MS spectra for TOTFO3.

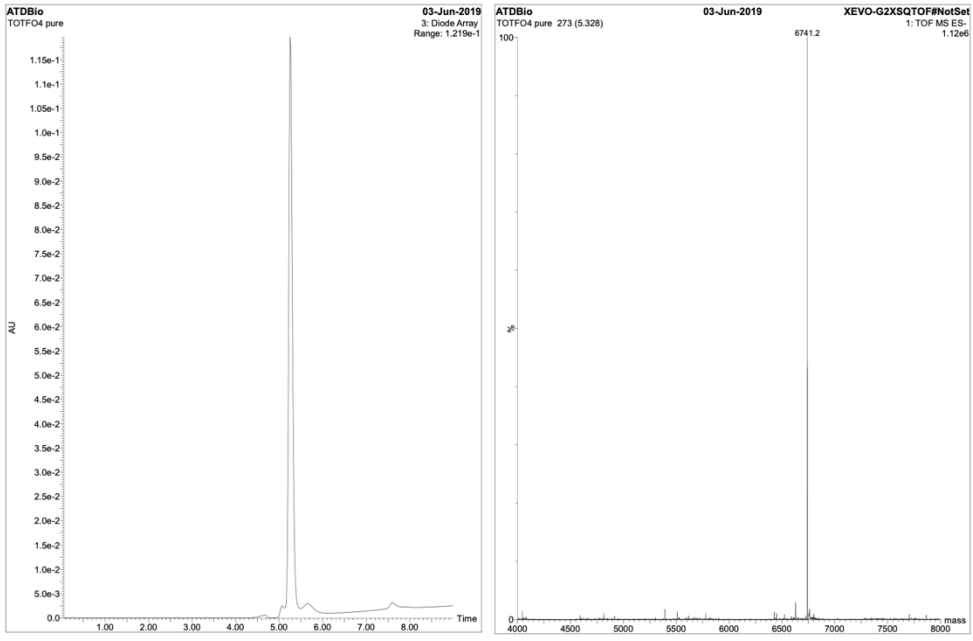

Figure VIII-78. HPLC and ESI-MS spectra for TOTFO4.

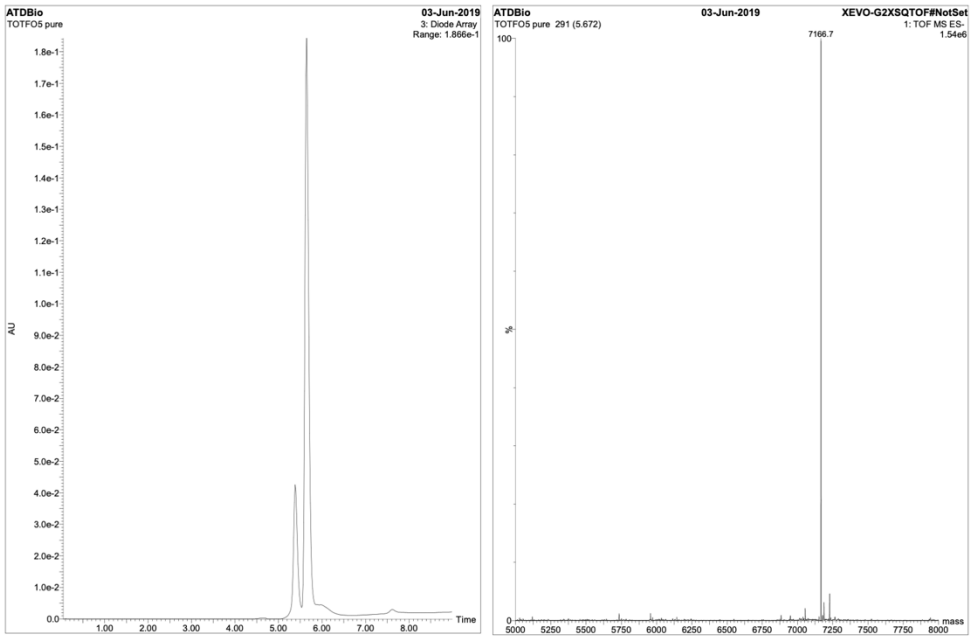

Figure VIII-79. HPLC and ESI-MS spectra for TOTFO5.

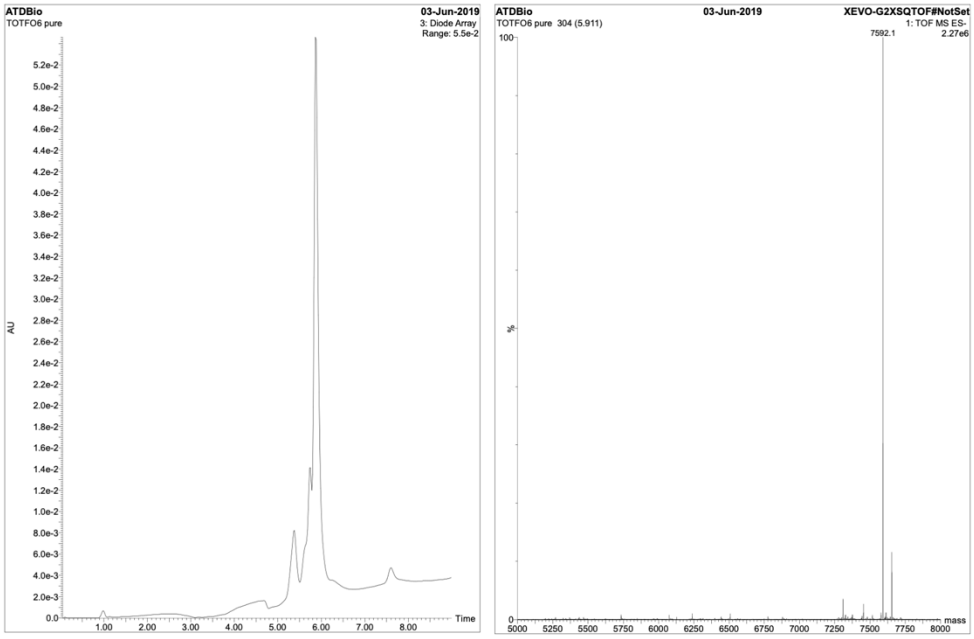

Figure VIII-80. HPLC and ESI-MS spectra for TOTFO6.

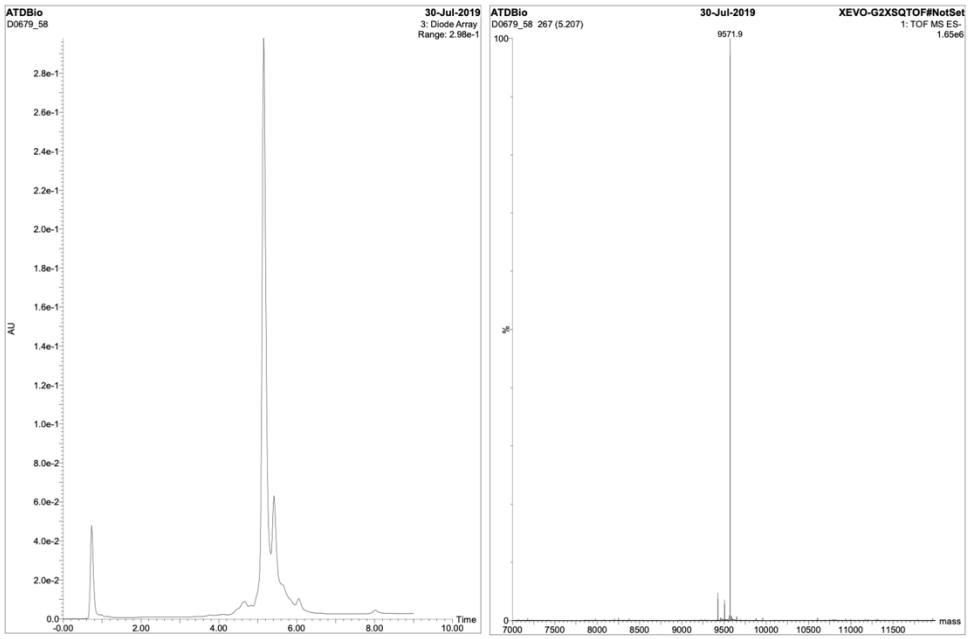

Figure VIII-81. HPLC and ESI-MS spectra for TOTFO1-Carbo.

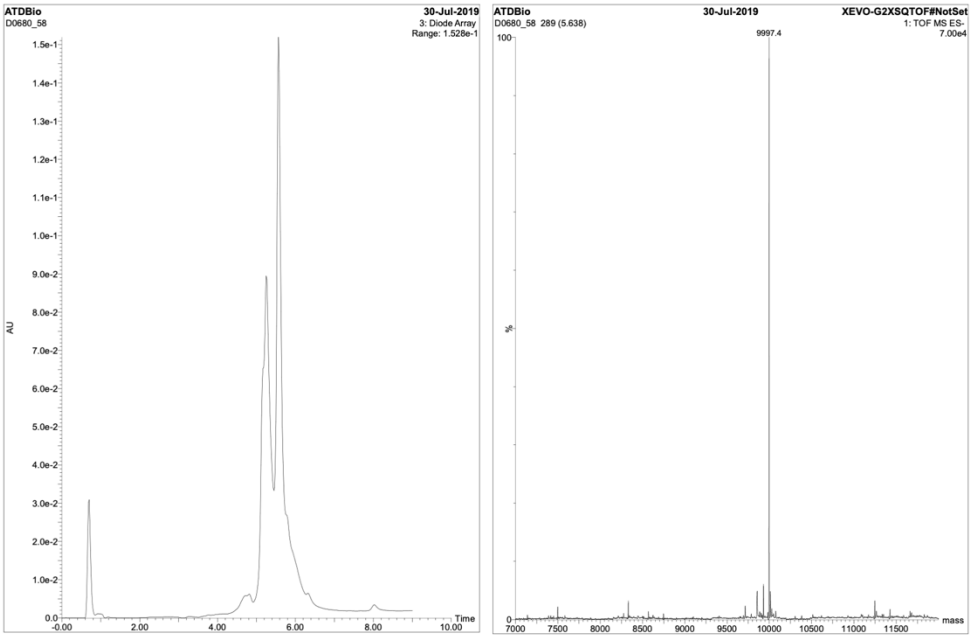

Figure VIII-82. HPLC and ESI-MS spectra for TOTFO2-Carbo.

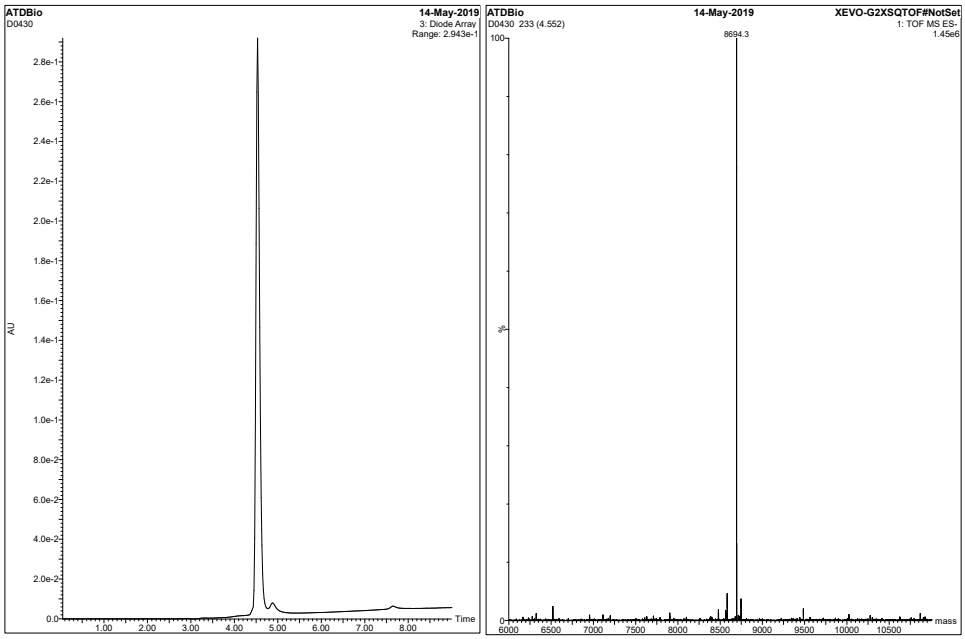

Figure VIII-83. HPLC and ESI-MS spectra for TOTFO3-Carbo.

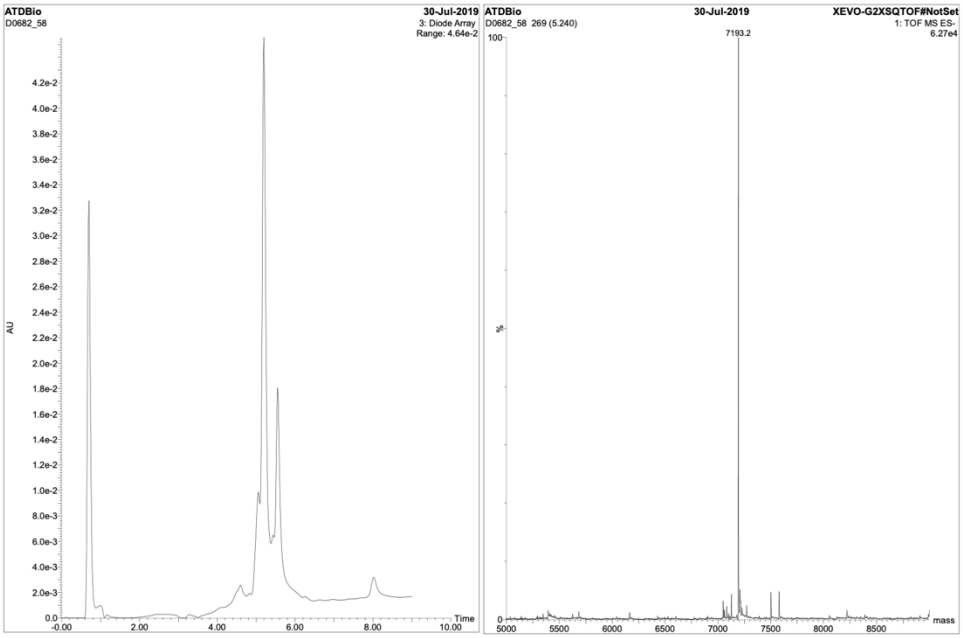

Figure VIII-84. HPLC and ESI-MS spectra for TOTFO4-Carbo.

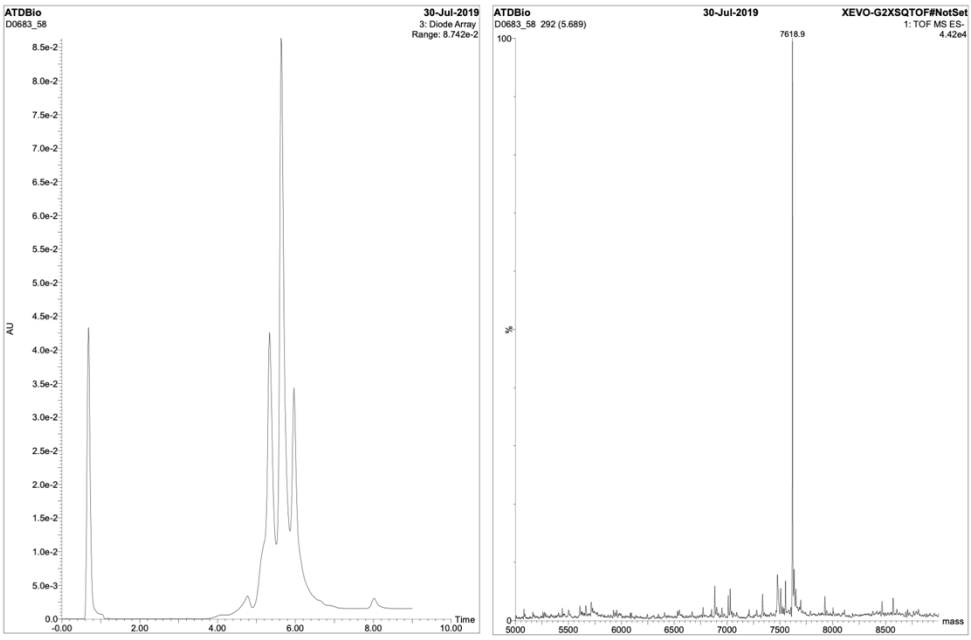

Figure VIII-85. HPLC and ESI-MS spectra for TOTFO5-Carbo.

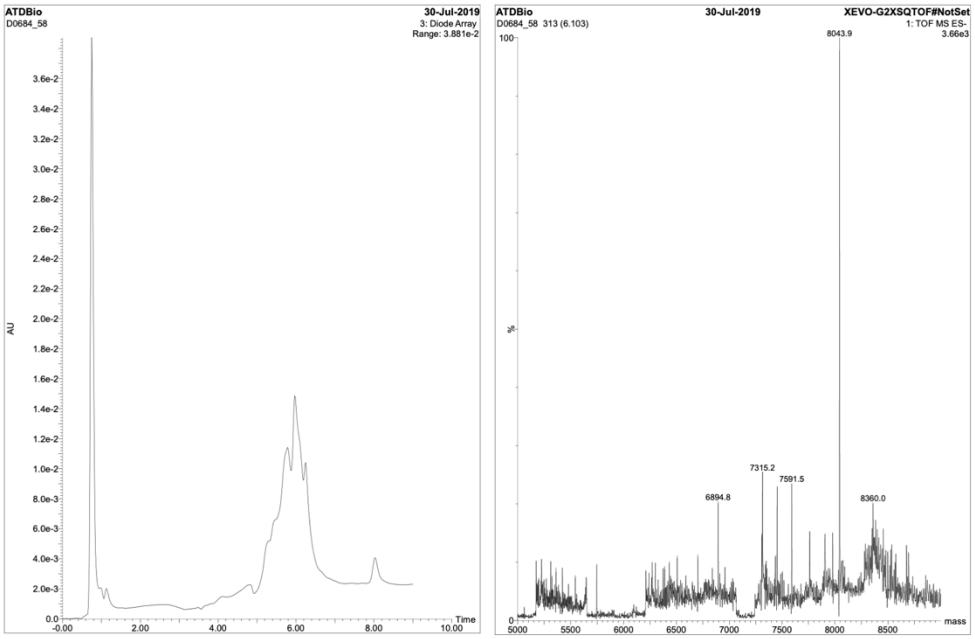

Figure VIII-86. HPLC and ESI-MS spectra for TOTFO6-Carbo.

VIII. 2. 3. 4. AA-TOTFOs and Pt(II)-AA-TOTFOs

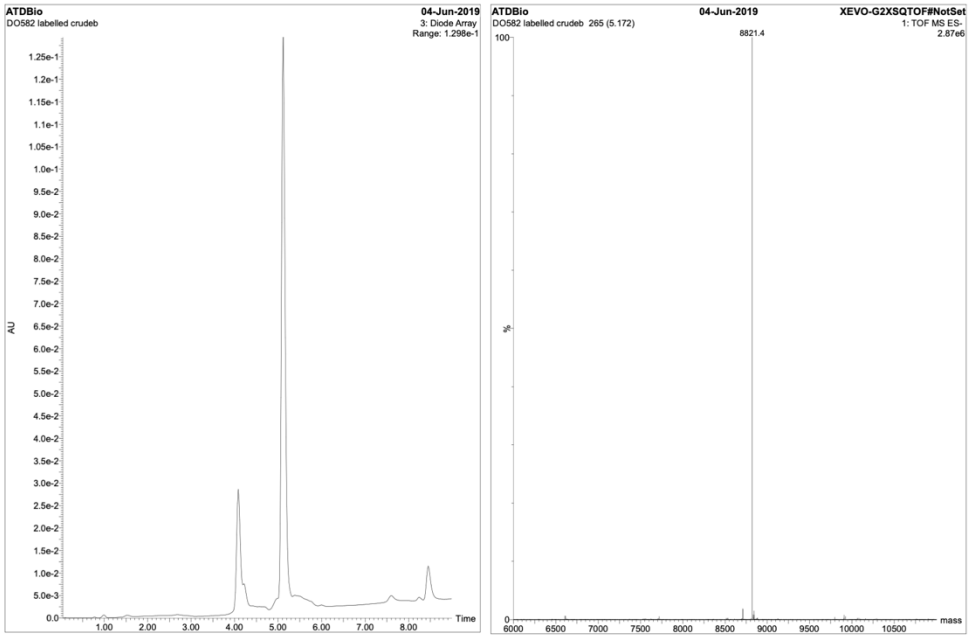

Figure VIII-87. HPLC and ESI-MS spectra for AA-TOTFO1.

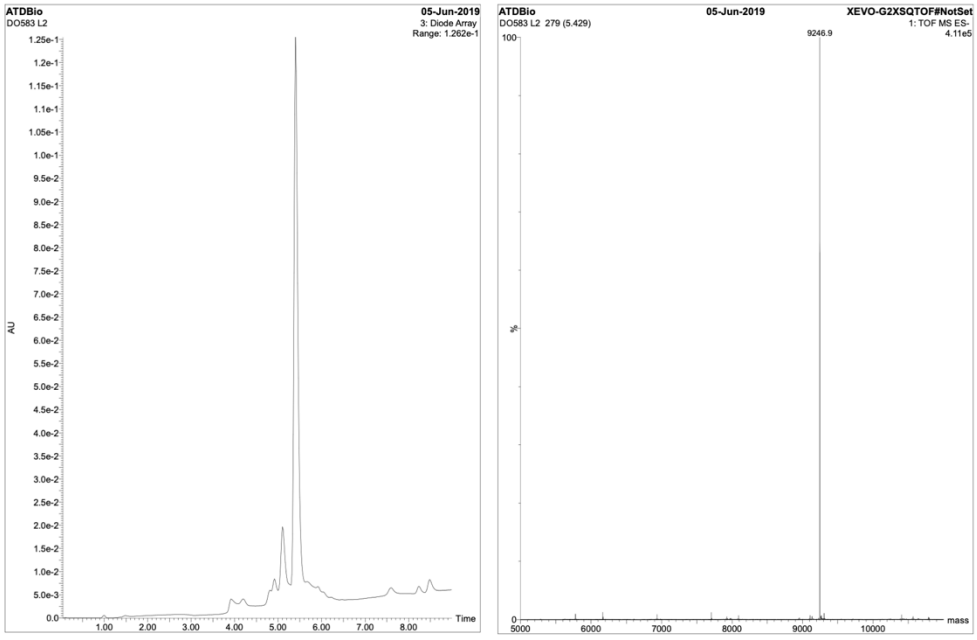

Figure VIII-88. HPLC and ESI-MS spectra for AA-TOTFO2.

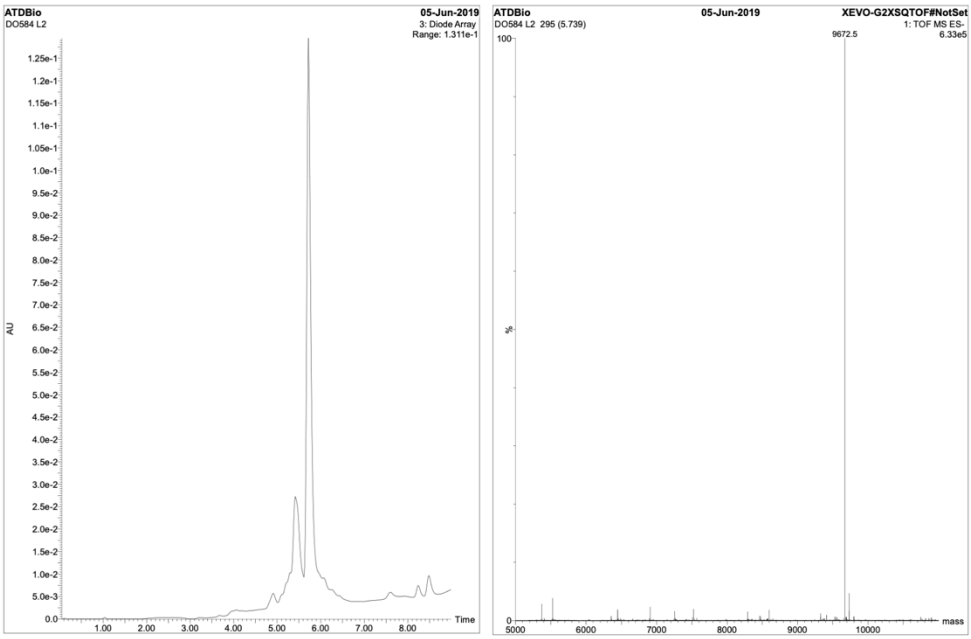

Figure VIII-89. HPLC and ESI-MS spectra for AA-TOTFO3.

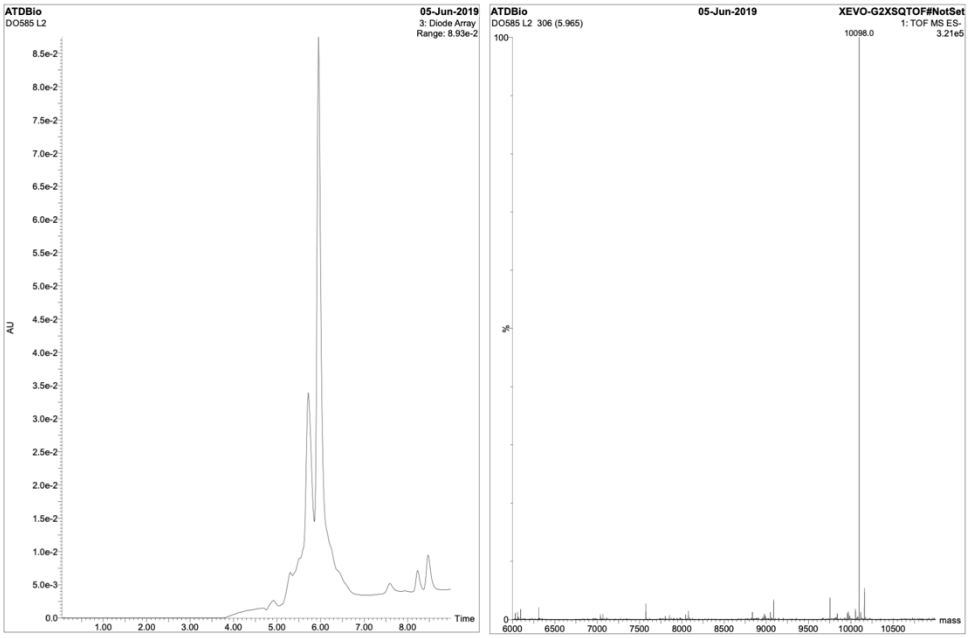

Figure VIII-90. HPLC and ESI-MS spectra for AA-TOTFO4.

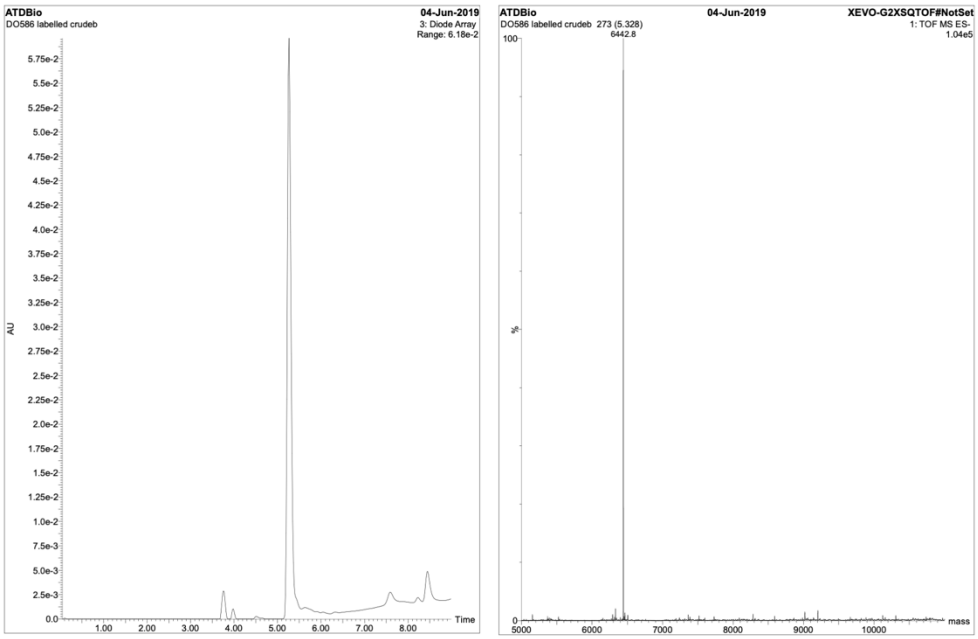

Figure VIII-91. HPLC and ESI-MS spectra for AA-TOTFO5.

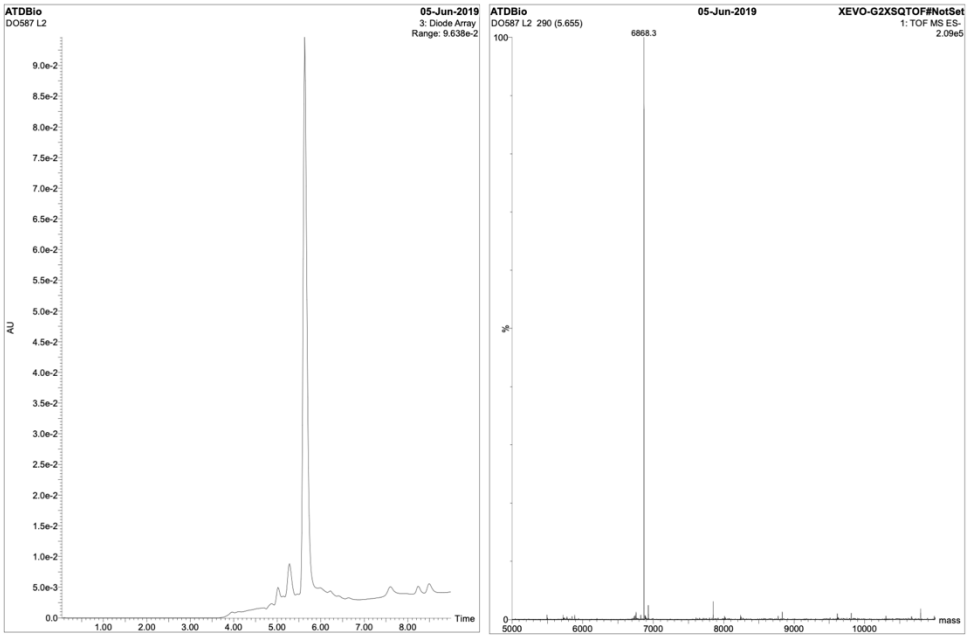

Figure VIII-92. HPLC and ESI-MS spectra for AA-TOTFO6.

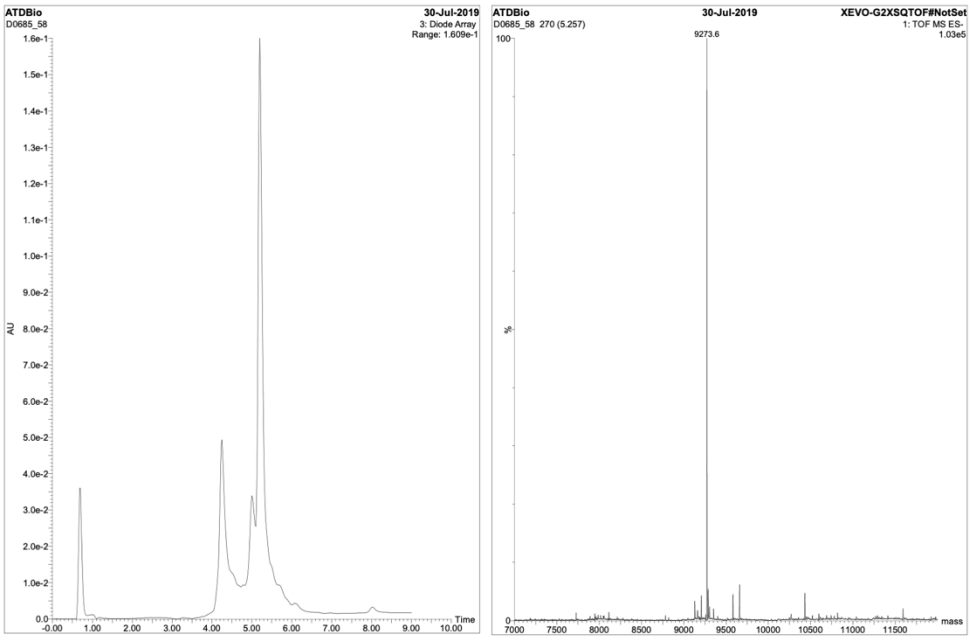

Figure VIII-93. HPLC and ESI-MS spectra for AA-TOTFO1-Carbo.

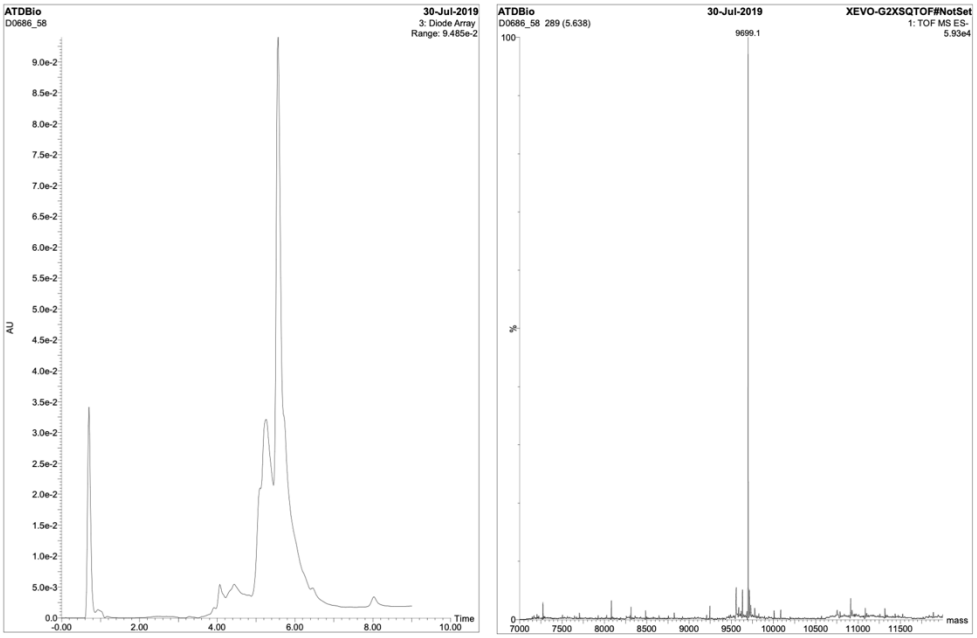

Figure VIII-94. HPLC and ESI-MS spectra for AA-TOTFO2-Carbo.

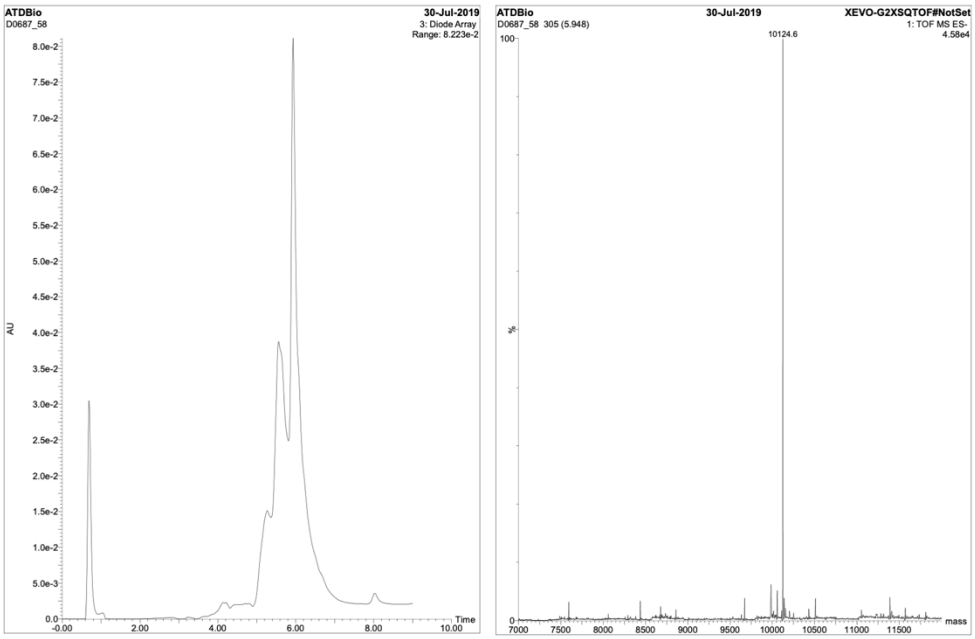

Figure VIII-95. HPLC and ESI-MS spectra for AA-TOTFO3-Carbo.

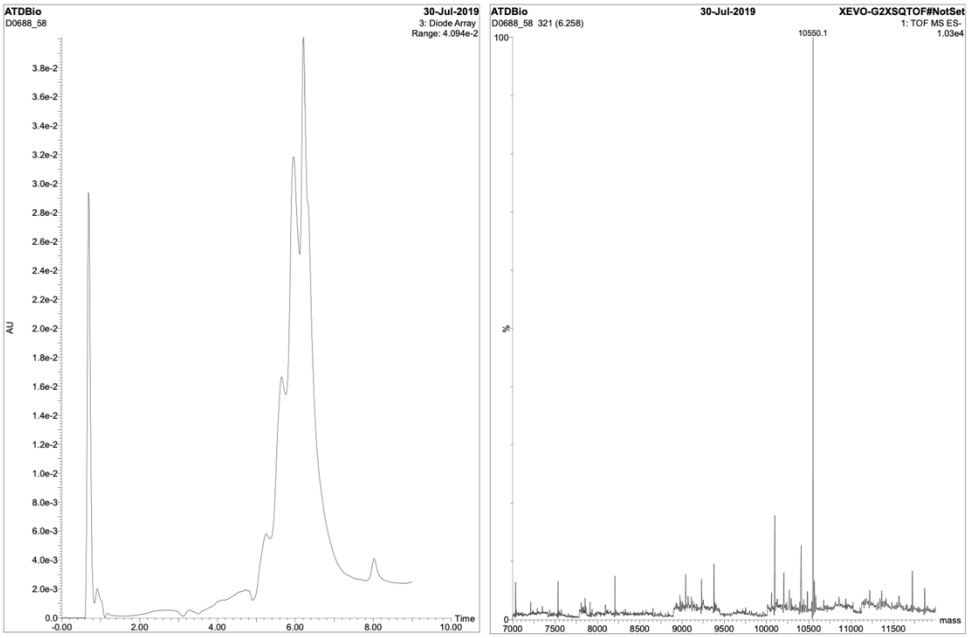

Figure VIII-96. HPLC and ESI-MS spectra for AA-TOTFO4-Carbo.

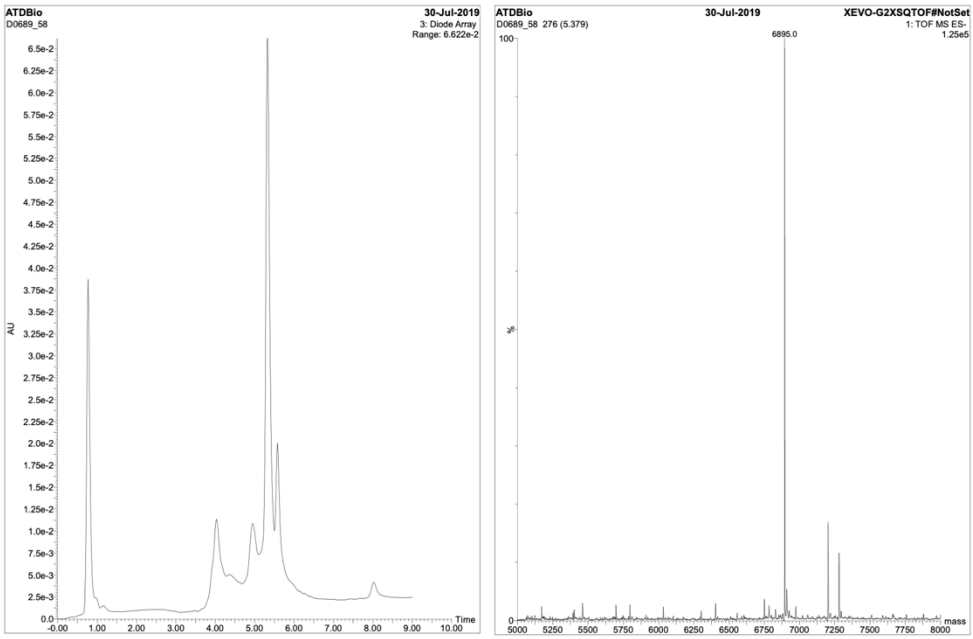

Figure VIII-97. HPLC and ESI-MS spectra for AA-TOTFO5-Carbo.

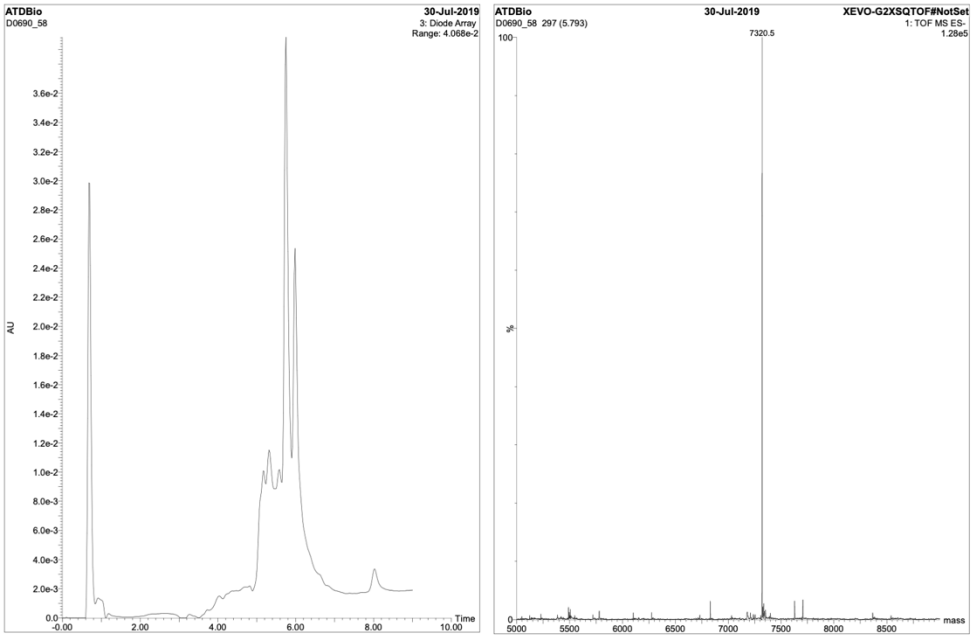

Figure VIII-98. HPLC and ESI-MS spectra for AA-TOTFO6-Carbo.

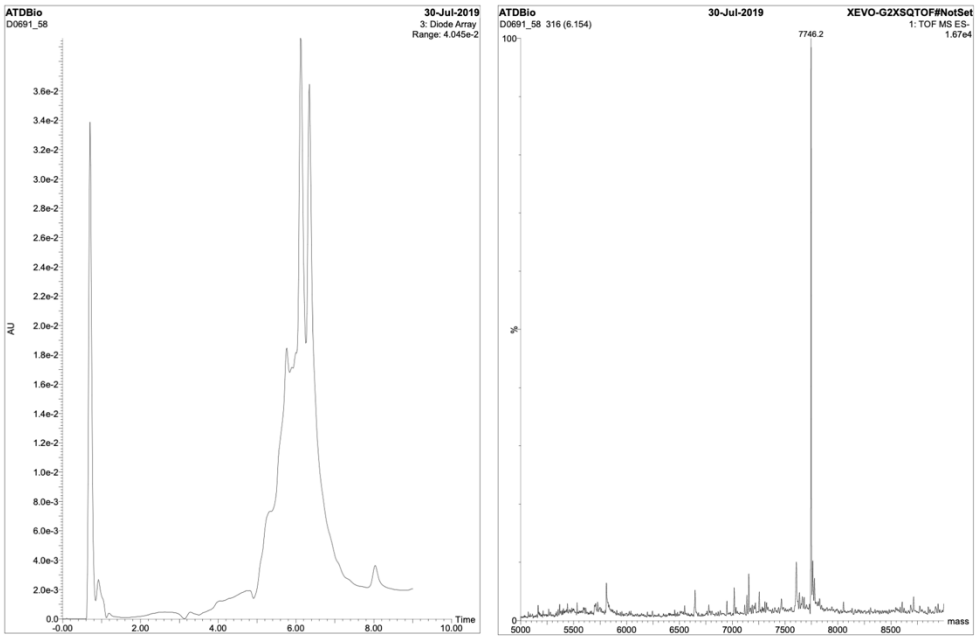

Figure VIII-99. HPLC and ESI-MS spectra for AA-TOTFO7-Carbo.

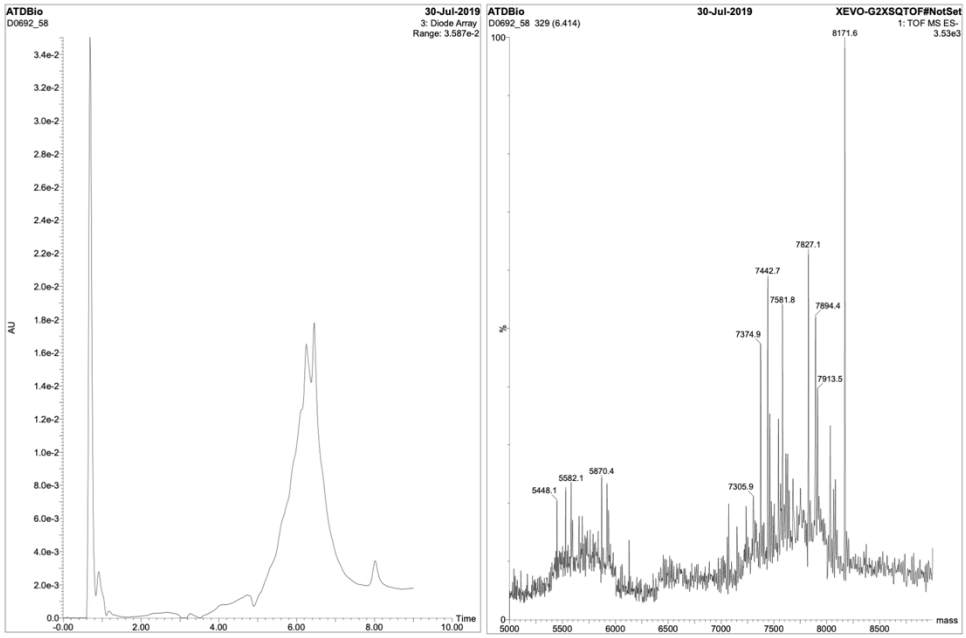

Figure VIII-100. HPLC and ESI-MS spectra for AA-TOTFO8-Carbo.

VIII. 3. Appendix C

VIII. 3. 1. Thermal Melting Analysis for N_3-Platinum(II) Complexes

Table VIII-3. Fluorescent thermal melting analysis for Duplex A-C after incubation with cisplatin at 37 ºC.

Oligo	T_M (ºC)	T_M (ºC) - + Cis 24h	ΔT_M (ºC) - + Cis 24h	T_M (ºC) - + Cis 48h	ΔT_M (ºC) -+ Cis 48h
Duplex A	82.46 ± 0.01	82.50 ± 0.03	+0.04	56.40 ± 2.34	-26.06
Duplex B	79.97 ± 0.03	80.41 ± 0.06	+0.44	69.19 ± 1.10	-10.78.
Duplex C	79.80 ± 0.06	79.62 ± 0.16	-0.18	75.07 ± 0.19	-4.73

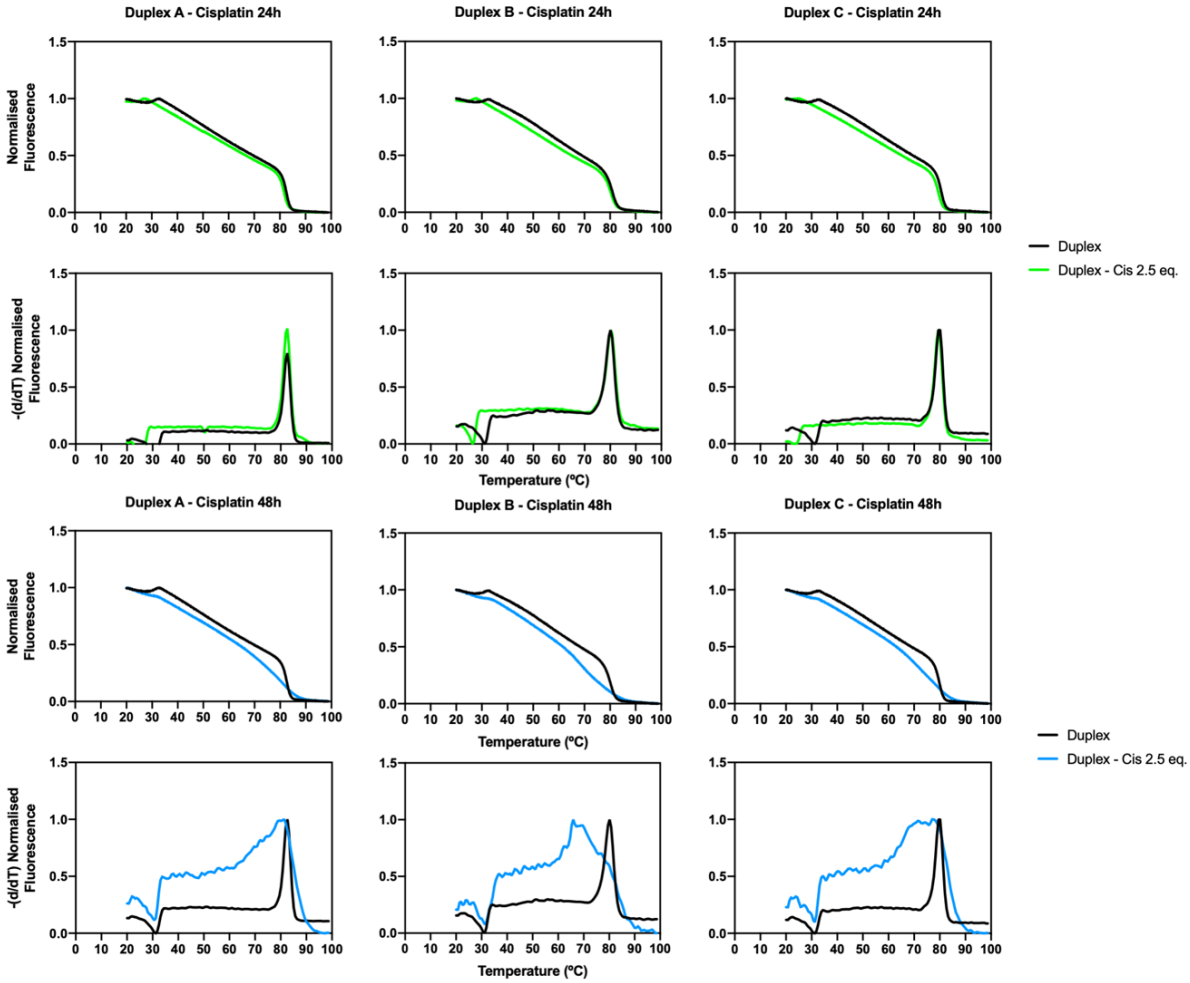

Figure VIII-101. High resolution fluorescent melting of Duplex A-C controls with and without cisplatin treatment. Melting curves are normalised with control melts (black) plotted in comparison to duplex melts after 24 h (green) and 48 h (blue) cisplatin incubation. First negative derivative of normalised fluorescence of duplex curves displayed in rows 2 and 4.

Table VIII-4. Thermal melting analysis for Duplex A-C after incubation with N_3-Pt-Cis at 37 ºC.

Oligo	Sequence	Complex	T_M (ºC) - 24 h	ΔT_M – 24 h	T_M (ºC) - 48 h	ΔT_M – 48 h
Duplex A	**5'**– ACC GTG GCG AGA AAG GAA GGG AAG AAA GCG AAA GGA GCG G – **3'** **3'**– TGG CAC CGC TCT TTC CTT CCC TTC TTT CGC TTT CCT CGC C – **5'**	N_3-Pt-Cis	80.0 ± 0.3	-6.3 ± 0.9	79.4 ± 0.4	-6.1 ± 0.9
Duplex B	**5'**– CGC TTC CCG AAG GGA GAA AGG CGG ACA GGT AT **–3'** **3'**– GCG AAG GGC TTC CCT CTT TCC GCC TGT CCA TA **–5'**	N_3-Pt-Cis	79.0 ± 0.2	-7.6 ± 0.6	79.0 ± 0.2	-8.3 ± 1.1
Duplex C	**5'**–CCG TGG CGA GAA AGG AAG GGA AGA AAG CGA AAG GA–**3'** **3'**–GGC ACC GCT CTT TCC TTC CCT TCT TTC GCT TTC CT–**5'**	N_3-Pt-Cis	78.4 ± 0.2	-6.4 ± 0.6	78.1 ± 0.1	-7.2 ± 1.1

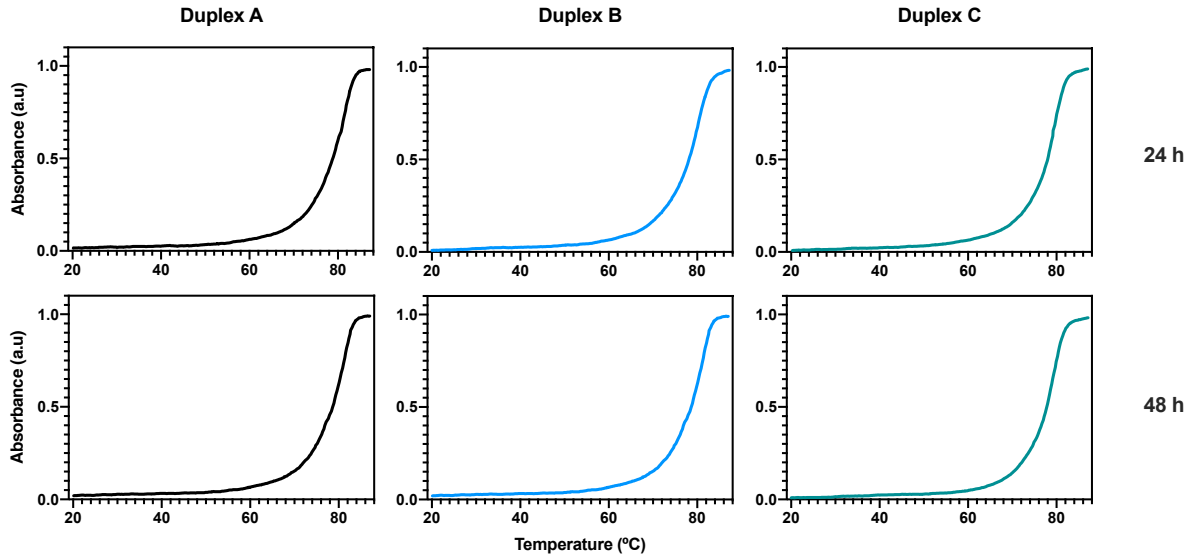

Figure VIII-102. UV melting curves for Duplex A-C over 24-48 h recorded as a function of temperature.

Table VIII-5. Thermal melting analysis for Duplex A-C after incubation with N_3-Pt-Carbo at 37 ºC.

Oligo	Sequence	Complex	T_M (ºC) - 24 h	ΔT_M – 24 h	T_M (ºC) - 48 h	ΔT_M – 48 h
Duplex A	**5'**– ACC GTG GCG AGA AAG GAA GGG AAG AAA GCG AAA GGA GCG G – **3'** **3'**– TGG CAC CGC TCT TTC CTT CCC TTC TTT CGC TTT CCT CGC C – **5'**	N_3-Pt-Carbo	80.0 ± 0.3	-3.4 ± 0.2	79.4 ± 0.4	-2.6 ± 0.4
Duplex B	**5'**– CGC TTC CCG AAG GGA GAA AGG CGG ACA GGT AT –**3'** **3'**– GCG AAG GGC TTC CCT CTT TCC GCC TGT CCA TA –**5'**	N_3-Pt-Carbo	79.0 ± 0.2	-3.8 ± 0.1	79.0 ± 0.2	-3.3 ± 0.2
Duplex C	**5'**–CCG TGG CGA GAA AGG AAG GGA AGA AAG CGA AAG GA–**3'** **3'**–GGC ACC GCT CTT TCC TTC CCT TCT TTC GCT TTC CT–**5'**	N_3-Pt-Carbo	78.4 ± 0.2	-3.5 ± 0.1	78.1 ± 0.1	-3.0 ± 0.1

Table VIII-6. Thermal melting analysis for Duplex A-C after incubation with N_3-Pt-Oxali at 37 ºC.

Oligo	Sequence	Complex	T_M (ºC) - 24 h	ΔT_M – 24 h	T_M (ºC) - 48 h	ΔT_M – 48 h
Duplex A	**5'**– ACC GTG GCG AGA AAG GAA GGG AAG AAA GCG AAA GGA GCG G – **3'** **3'**– TGG CAC CGC TCT TTC CTT CCC TTC TTT CGC TTT CCT CGC C – **5'**	N_3-Pt-Oxali	80.0 ± 0.3	-3.8 ± 0.4	79.4 ± 0.4	-2.3 ± 0.2
Duplex B	**5'**– CGC TTC CCG AAG GGA GAA AGG CGG ACA GGT AT –**3'** **3'**– GCG AAG GGC TTC CCT CTT TCC GCC TGT CCA TA –**5'**	N_3-Pt-Oxali	79.0 ± 0.2	-2.8 ± 0.2	79.0 ± 0.2	-3.7 ± 0.2
Duplex C	**5'**–CCG TGG CGA GAA AGG AAG GGA AGA AAG CGA AAG GA–**3'** **3'**–GGC ACC GCT CTT TCC TTC CCT TCT TTC GCT TTC CT–**5'**	N_3-Pt-Oxali	78.4 ± 0.2	-2.7 ± 0.2	78.1 ± 0.1	-3.3 ± 0.2

VIII. 3. 2. UV Thermal Melting Analysis *cis*-Pt(II)-TFO Hybrids

Table VIII-7. T_M values were recorded in 10 mM phosphate (PO_4^{3-}), 150 mM NaCl, 2 mM $MgCl_2$, pH 6 buffer. Samples were incubated for 24-48 h prior to melting analysis. T_M temperatures were calculated by the first derivative of a non-linear sigmoidal regression curve using GraphPad Prism 8.0. Final T_M values are an average of 3 melting cycles. ΔT_M values for Pt(II)-TFOs are relative to the unclicked alkyne TFO precursor (e.g. TFO1 and TFO1-Carbo). **5'-dC** = 5'-(5)octadinyl-deoxycytidine; **int-dU** = internal-octadinyl-deoxyuridine; **5'-BCN-dC** = 5'-BCN(CEP II)-deoxycytidine; **pdU** = 5-(1-propargylamino)-deoxyuridine; **pdU-TO** = pdU with TO (thiazole orange) coupled; **N_3-Pt(II)-Cis** = *cis*-[Pt(2-azidopropane-1,3-diamine)Cl_2]; **N_3-Pt(II)-Carbo** = *cis*-[Pt(2-azidopropane-1,3-diamine)(CBDCA)]; **N_3-Pt(II)-Oxali** = *cis*-[Pt(2-azidopropane-1,3-diamine)(Oxalate)]; **n.t.o.** = no triplex observed; **n.d.** = not determined due to T_M < 12 ºC.

Oligo	Modification	T_M (ºC) - 24 h	ΔT_M – 24 h	T_M (ºC) - 48 h	ΔT_M – 48 h
TFO1	5'-dC	45.6 ± 0.2	-	49.6 ± 0.3	-
TFO1-Cis	5'-dC-N_3-Pt(II)-Cis	n.t.o.	-	n.t.o.	-
TFO1-Carbo	5'-dC-N_3-Pt(II)-Carbo	49.2 ± 1.3	3.7	49.2 ± 0.7	-0.4
TFO1-Oxali	5'-dC-N_3-Pt(II)-Oxali	45.9 ± 0.3	0.3	43.5 ± 0.9	-6.1
TOTFO1-Carbo	5'-dC-N_3-Pt(II)-Carbo pdU-TO (x1)	55.6 ± 0.3	10.0	57.2 ± 0.7	11.6
TOTFO2-Carbo	5'-dC-N_3-Pt(II)-Carbo pdU-TO (x2)	> 65.0	-	> 65.0	-
TOTFO3-Carbo	5'-dC-N_3-Pt(II)-Carbo pdU-TO (x3)	> 65.0	-	> 65.0	-
TFO2	5'-BCN-dC	48.3 ± 0.2	-	51.4 ± 0.5	-
TFO2-Cis	5'-BCN-dC-N_3-Pt(II)-Cis	n.t.o.	-	n.t.o.	-
TFO2-Carbo	5'-BCN-dC-N_3-Pt(II)-Carbo	47.2 ± 0.7	-1.1	46.8 ± 0.1	-4.6
TFO2-Oxali	5'-BCN-dC-N_3-Pt(II)-Oxali	44.7 ± 0.5	-3.5	n.t.o	-
TFO3	Int-dU	48.6 ± 0.2	-	52.0 ± 0.1	-
TFO3-Cis	Int-dU-N_3-Pt(II)-Cis	42.7 ± 1.4	-5.9	42.6 ± 0.5	-9.4
TFO3-Carbo	Int-dU-N_3-Pt(II)-Carbo	46.3 ± 0.3	-2.3	45.5 ± 0.1	-6.6
TFO3-Oxali	Int-dU-N_3-Pt(II)-Oxali	44.0 ± 0.4	-4.6	44.1 ± 0.6	-7.9
TFO4	5'-dC	n.d.	-	n.d.	-
TFO4-Cis	5'-dC-N_3-Pt(II)-Cis	n.t.o.	-	n.t.o.	-
TFO4-Carbo	5'-dC-N_3-Pt(II)-Carbo	n.t.o.	-	n.t.o.	-
TFO4-Oxali	5'-dC-N_3-Pt(II)-Oxali	n.t.o.		n.t.o.	-
TFO5	Int-dU	19.8 ± 0.2	-	22.9 ± 0.2	-
TFO5-Cis	Int-dU-N_3-Pt(II)-Cis	n.d.	-	n.d.	-
TFO5-Carbo	Int-dU-N_3-Pt(II)-Carbo	23.0 ± 0.2	3.2	22.1 ± 0.3	-0.9
TFO5-Oxali	Int-dU-N_3-Pt(II)-Oxali	n.d.	-	20.7 ± 1.0	-2.2

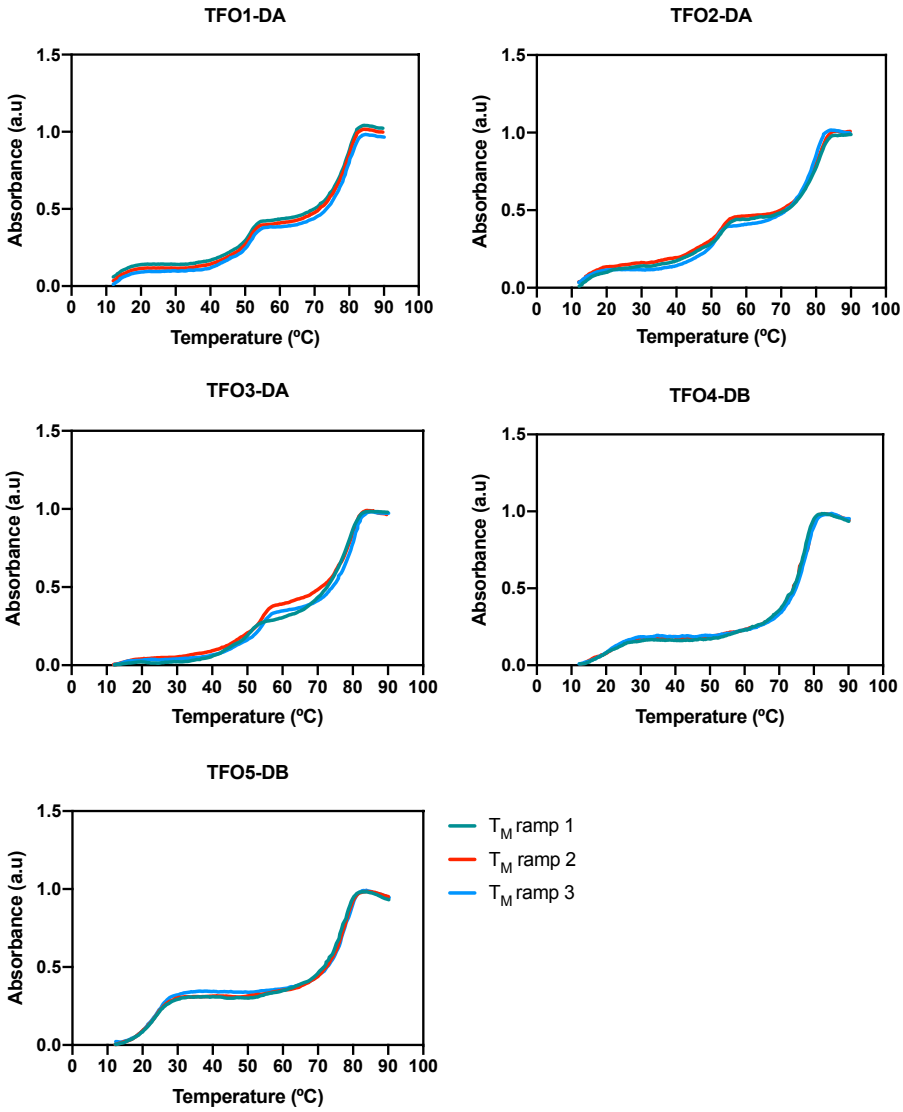

Figure VIII-103. Thermal melting analysis of alkyne-TFO1-5 recorded as a function of temperature (12–90 ºC).

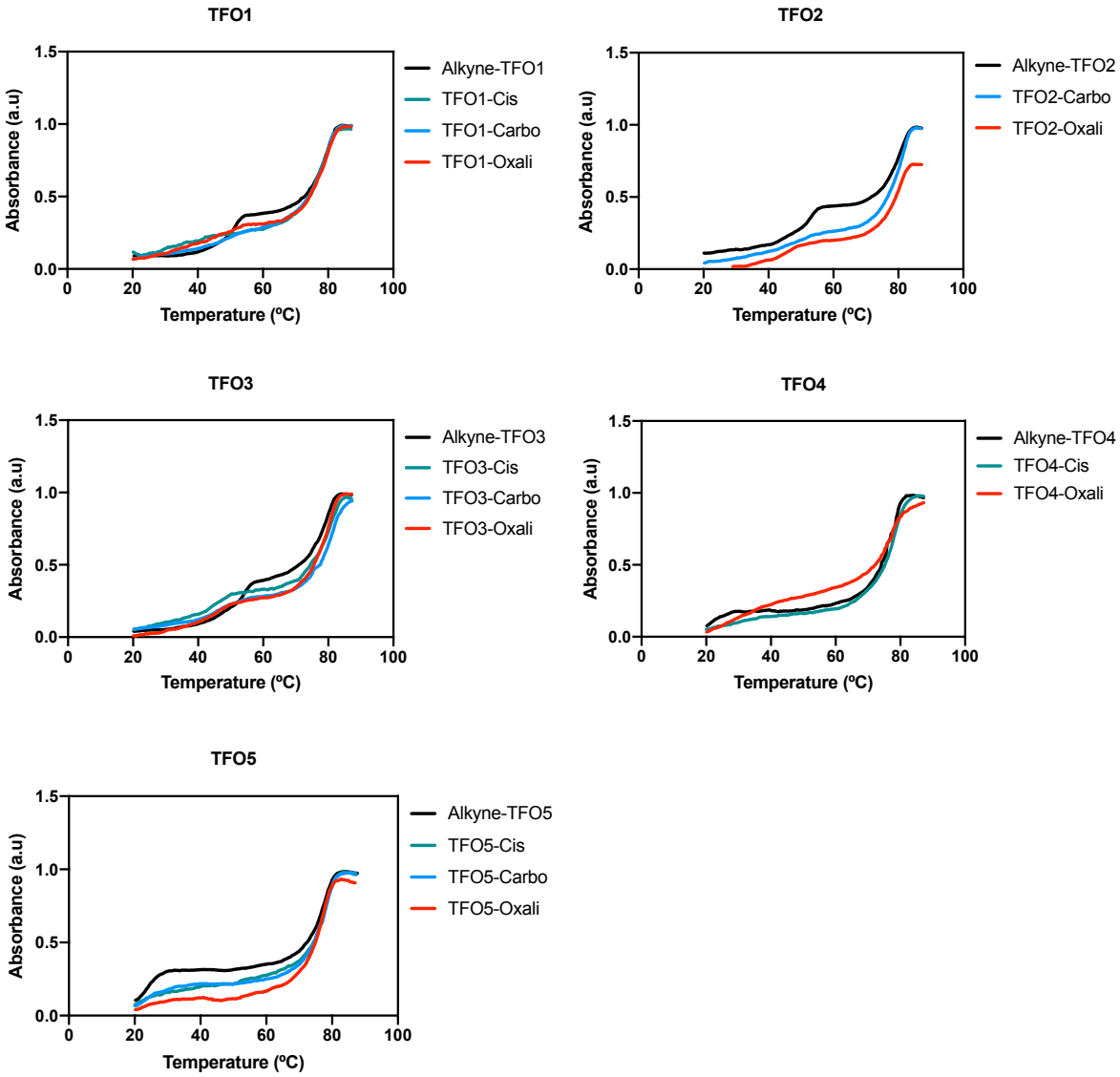

Figure VIII-104. Thermal melting analysis of *cis*-Pt(II)-TFO hybrids with alkyne-TFO as reference. UV melting curves recorded as a function of temperature, normalised and smoothed. Curves displayed from 20-87 ºC.

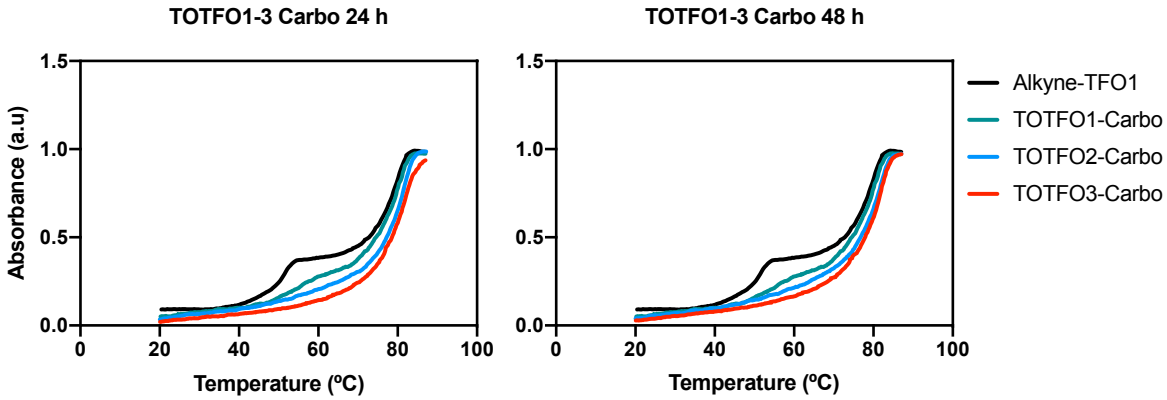

Figure VIII-105. Thermal melting analysis of *cis*-Pt(II)-TOTFO constructs after 24-48 h incubation with alkyne-TFO1 as reference. Curves displayed from 20-87 ºC.

VIII. 4. Appendix D

VIII. 4. 1. Cell Line Characteristics and Cell Viability Experimental Parameters

Table VIII-8. Cell line characteristics utilised in cell viability studies. Four breast cancer cell lines were selected: MCF-7, T-47D, MDA-MB-231 and MDA-MB-468. MCF-10a is an immortalised non-tumorigenic breast cancer cell line. Results obtained for the treatment of MCF-10a cells are preliminary, 3 biological replicates need to be performed to produce reliable results.

Cell lines	ER	PR	HER 2	Mutation status	Sub-type	Other mutations	Seeding density (cells/well)	Resazurin incubation (h)	Biological replicate (n)
MCF-7	+	+	−		Luminal A	CDKN2A, PIK3CA	5000	4	3
T-47D	+	−	−		Luminal A	TP53, PIK3CA	7500	6	3
MDA-MB-231	−	−	−	TNB	Mesenchymal	TP53, CDKN2A, BRAF, KRAS,NF2	5000	6	3
MDA-MB-468	−	−	−	TNA	Basal-like 1	TP53, PTEN, RB1, SMAD4	5000	6	3
MCF-10a	−	−	+				5000	6	2*

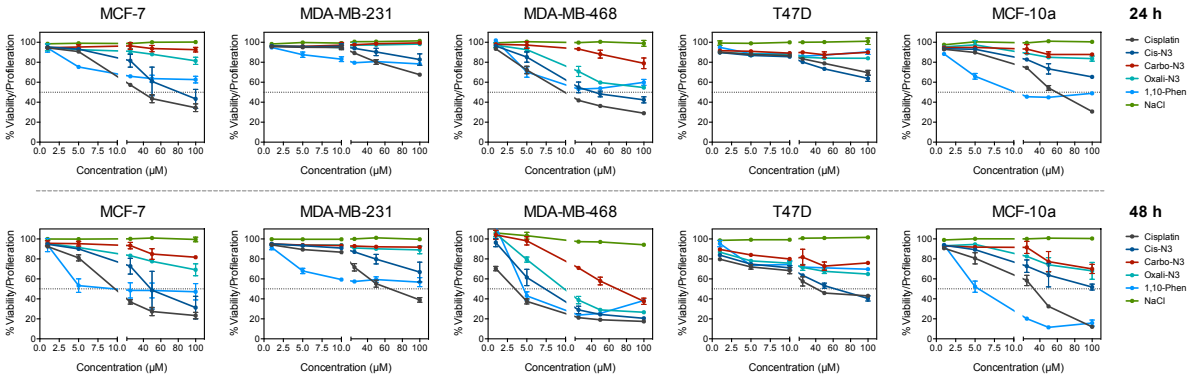

Figure VIII-106. Cell viability expressed as normalized percent of viable cells relative to controls of cisplatin, NaCl and 1,10-phenanthroline. Cell lines treated with platinum complexes and control compounds over 24 h and 48 h incubations.

VIII. 5. Appendix E

VIII. 5. 1. Supplementary PAGE analysis

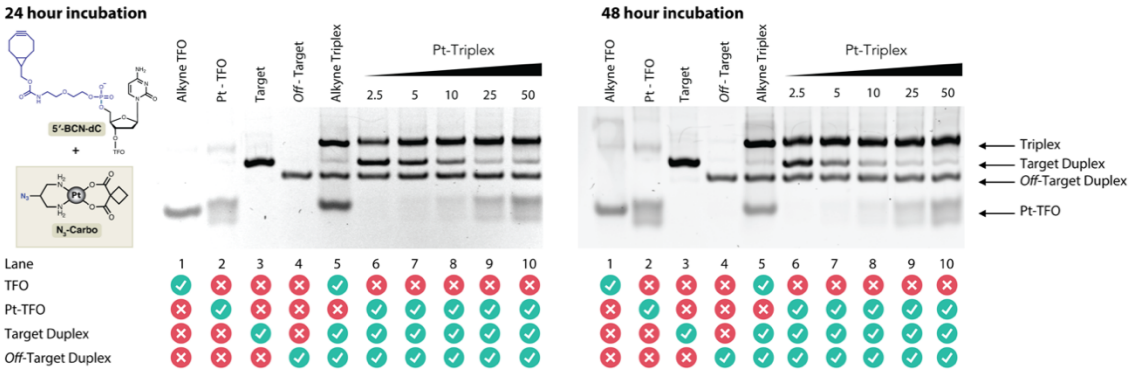

Figure VIII-107. Triple formation and cross-linking for TFO2-Carbo. **24 h**. Triplex formation after 24 hour incubation of duplex target (1 pmol, Lane 6-10) with increasing equivalents of TFO2-Carbo hybrid (2.5-50 eq., Lane 6-10). Triplex formation increases with larger loading while no off-target triplex formation or cross-linking is observed (Off-target duplex, Lane 6-10). **48 h.** Triplex formation after 48 hour incubation. Formation occurs at lower loading of TFO2-Carbo (10-25 eq., Lane 8-9) compared to 24 hour incubation. Samples were prepared in 10 mM phosphate buffer with 150 mM NaCl and 2 mM $MgCl_2$) (pH 6.0) in a volume of 5 μL + 1 μL 6x loading dye. Samples were incubated for either 24 h (left) or 48 h (right) at 37 °C, loaded onto 20% PAGE and subjected to electrophoresis for 4 h at 70 V in 50 mM TA triplex buffer (pH 6.0).

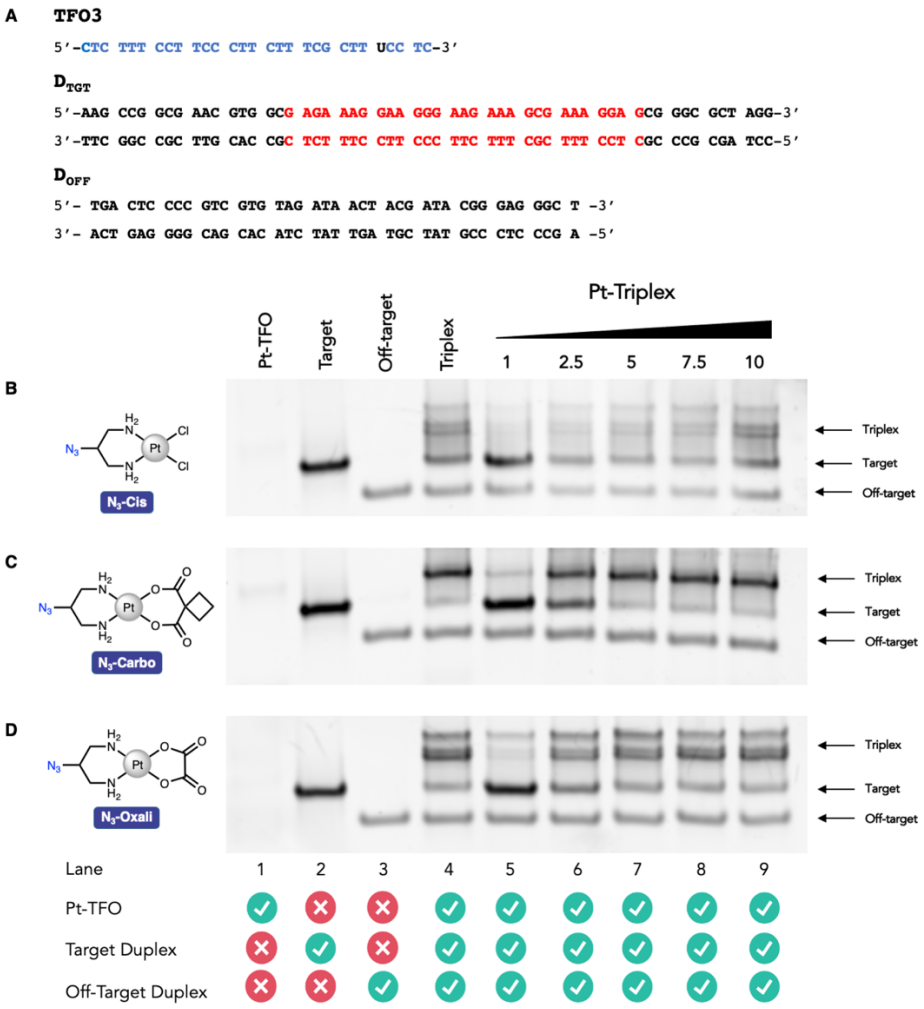

Figure VIII-108. A. Alkyne-modified TFO3 and D_{ON} and D_{OFF} target sequences. Triplex-mediated crosslinking for **B.** TFO3-Cis. **C.** TFO3-Carbo and **D.** TFO3-Oxali. Target (57 bp, 1 pmol, lane 3) and off-target (40 bp, 1 pmol, lane 3) were treated with 1-10 eq. of TFO3 hybrid. Samples were prepared in 10 mM phosphate buffer, 150 mM NaCl and 2 mM $MgCl_2$ (pH 6) prior to incubation over 48 h at 37 ºC**.** Samples were then loaded onto 20% PAGE and subjected to electrophoresis for 4h at 70 V in 50 mM tris-acetate (TA) buffer (pH 6). Gels were post-stained with SybrGold.

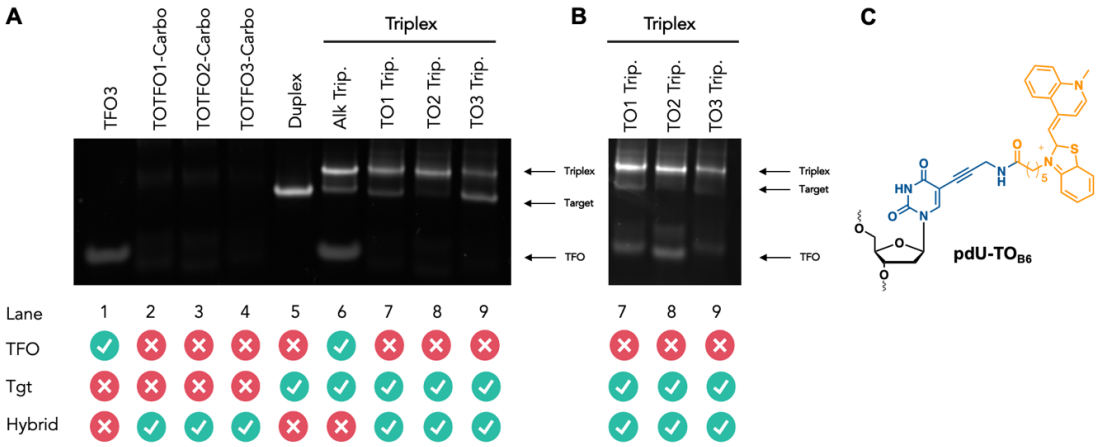

Figure VIII-109. A. Triplex formation for TOTFO1-3 Carbo (50 eq., Lanes 7-9). TOTFO2 displays enhanced triplex formation compared with TOTFO1-Carbo and TOTFO3-Carbo. Gel is post-stained with SYBRGold stain. **B.** Non-stained visualisation of the same gel. TOTFO2-Carbo displays enhanced fluorescent emission. PAGE analysis was performed in TA triplex buffer (10 mM phosphate 150 mM NaCl 2 mM $MgCl_2$, pH 6.0) at 70 V for 240 mins. **C.** Propargylamino-dU nucleobase modification with coupled TO_{B6}.

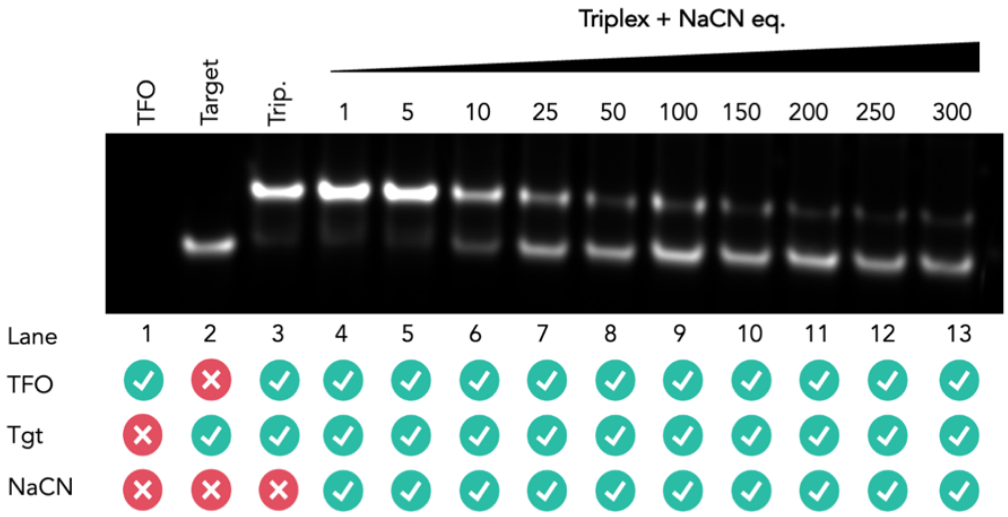

Figure VIII-110. Optimisation of triplex reversal with sodium cyanide. Triplex formation for TFO3 (50 eq.) with fluorescently labelled Duplex 3 (1 eq., 1 pmol) (Lane 3). Introduction of increasing concentrations of NaCN solution (1000-300000 pmol, Lanes 4-13). PAGE performed in TA triplex buffer (10 mM phosphate 150 mM NaCl 2 mM $MgCl_2$, pH 6.0) at 70 V for 240 mins. Gel visualised and imaged using Cy5 filter.

Table VIII-9. Raw PAGE analysis images for Chapter V Figure V-10 and Figure V-11. Images were visualised using a Syngene G:Box Mini 9 gel documentation system. Raw PAGE images for: **A.** Figure V-10B. **B.** Figure V-10C. **C.** Figure V-10D. **D.** Figure V-11C (Cy5). **E.** Figure V-11C (FAM). **F.** Figure V-11C (Multiplex).

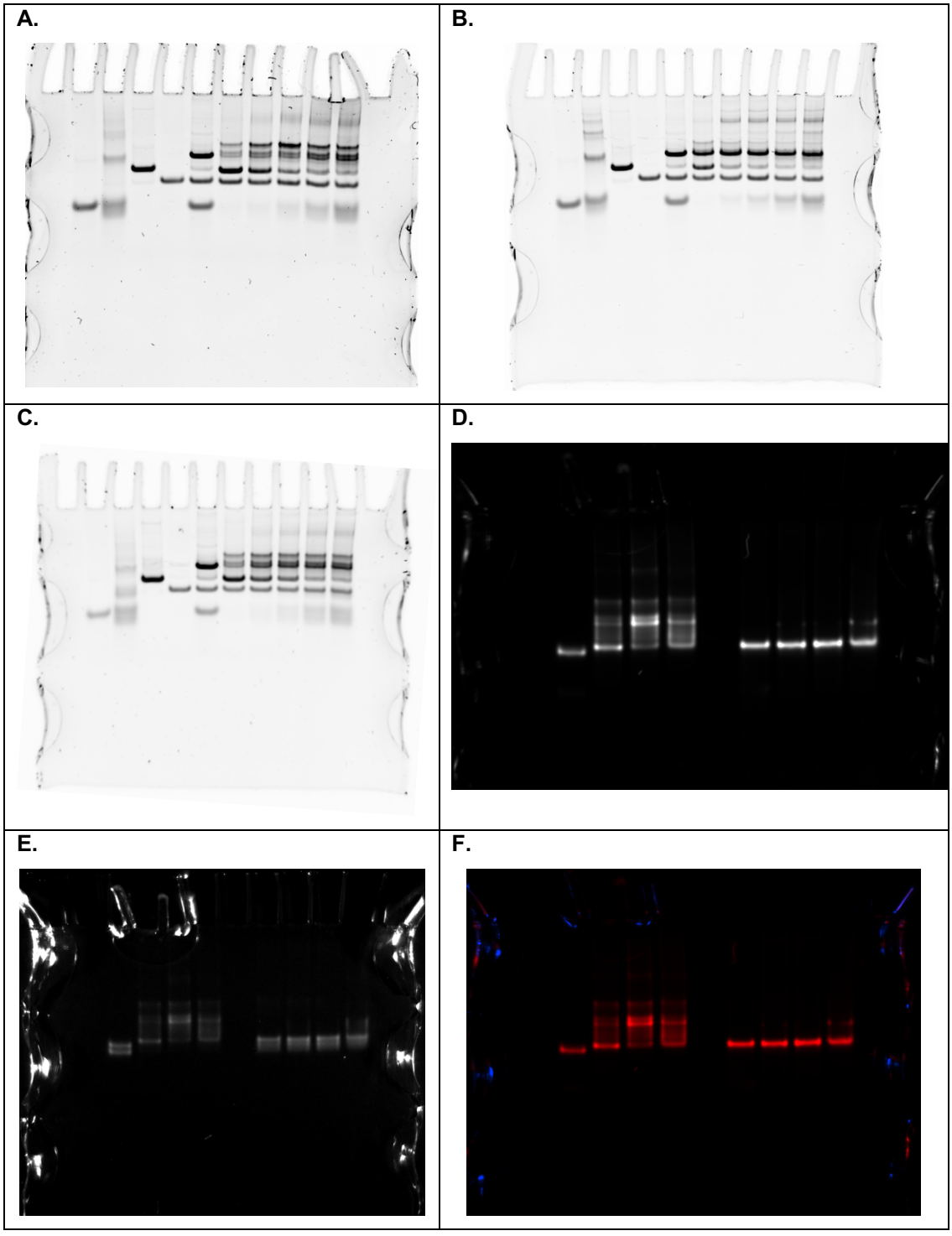

Table VIII-10. Raw PAGE analysis images for Chapter V Figure V-12D. Images were visualised on a Syngene G:Box Mini 9 gel documentation system. Raw PAGE images for: **A.** Figure V-12D (Multiplex). **B.** Figure V-12D (Cy5). **C.** Figure V-12D (FAM).

A.

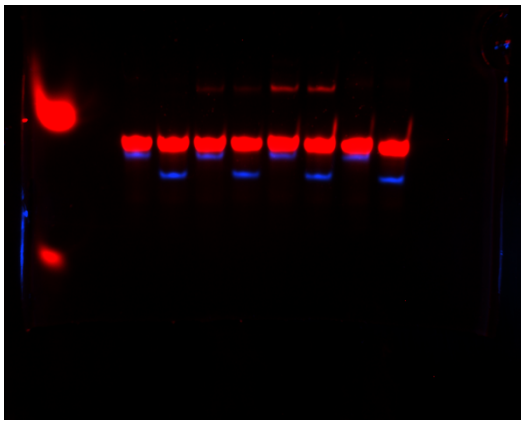

B.

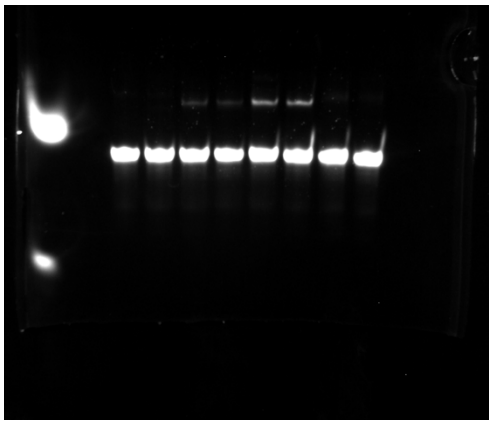

C.

VIII. 6. Appendix F

VIII. 6. 1. NMR analysis

(17) 2-(4-nitrophenyl)-1*H*-imidazo[4,5-*f*]-1,10-phenanthroline spectra:

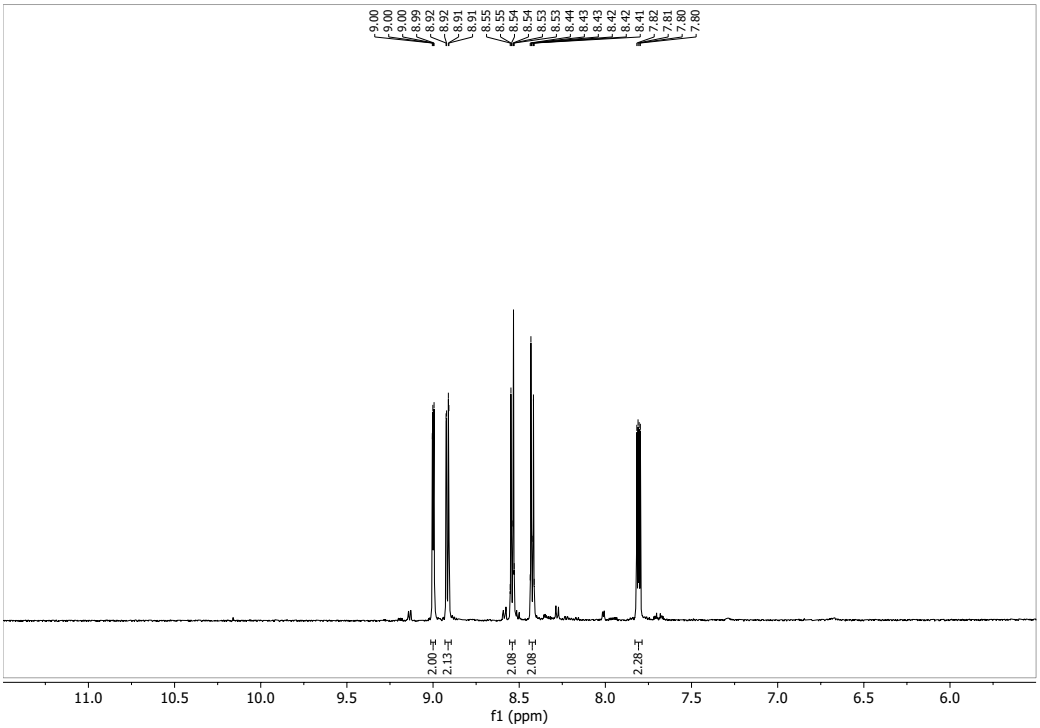

Figure VIII-111. ^{1}H NMR spectra for 2-(4-nitrophenyl)-1H-imidazo[4,5-f]-1,10-phenanthroline.

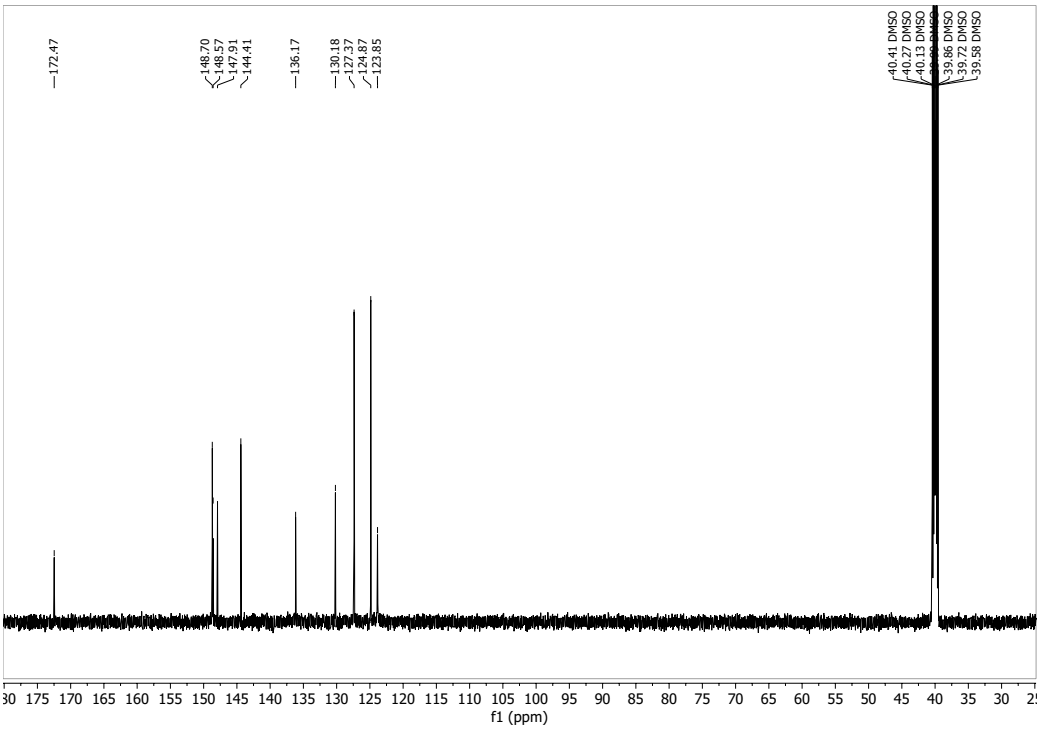

Figure VIII-112. ^{13}C NMR spectra for 2-(4-nitrophenyl)-1H-imidazo[4,5-f]-1,10-phenanthroline.

(18) 2-(4-aminophenyl)-1*H*-imidazo[4,5-*f*]-1,10-phenanthroline spectra:

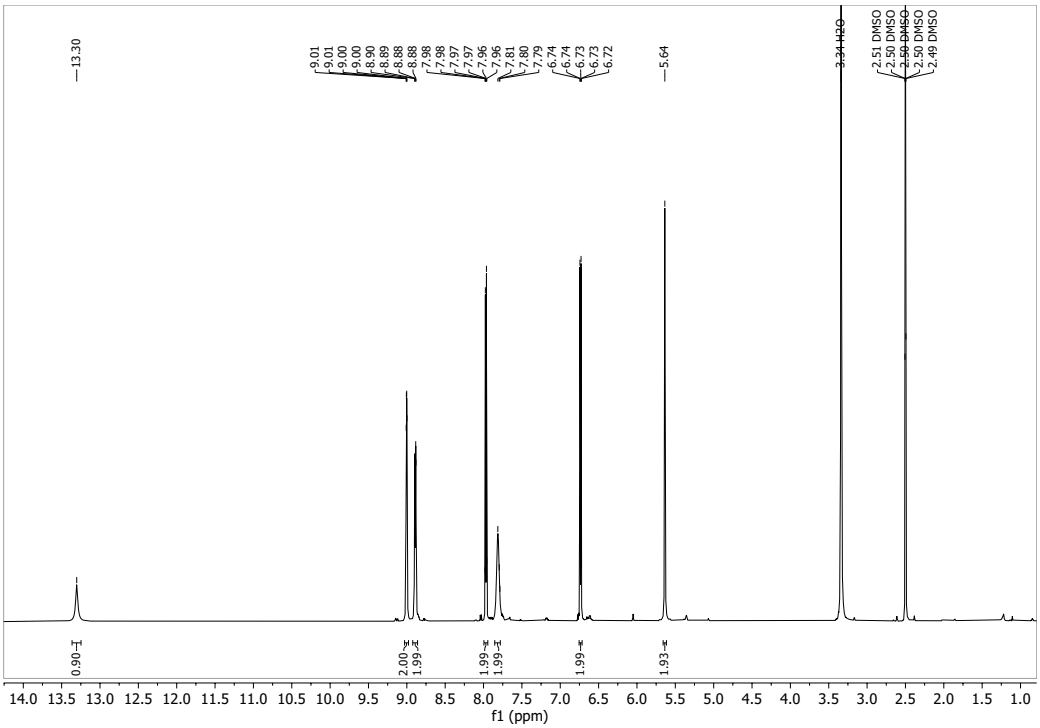

Figure VIII-113. [1]H NMR spectra for 2-(4-aminophenyl)-1H-imidazo[4,5-f]-1,10-phenanthroline.

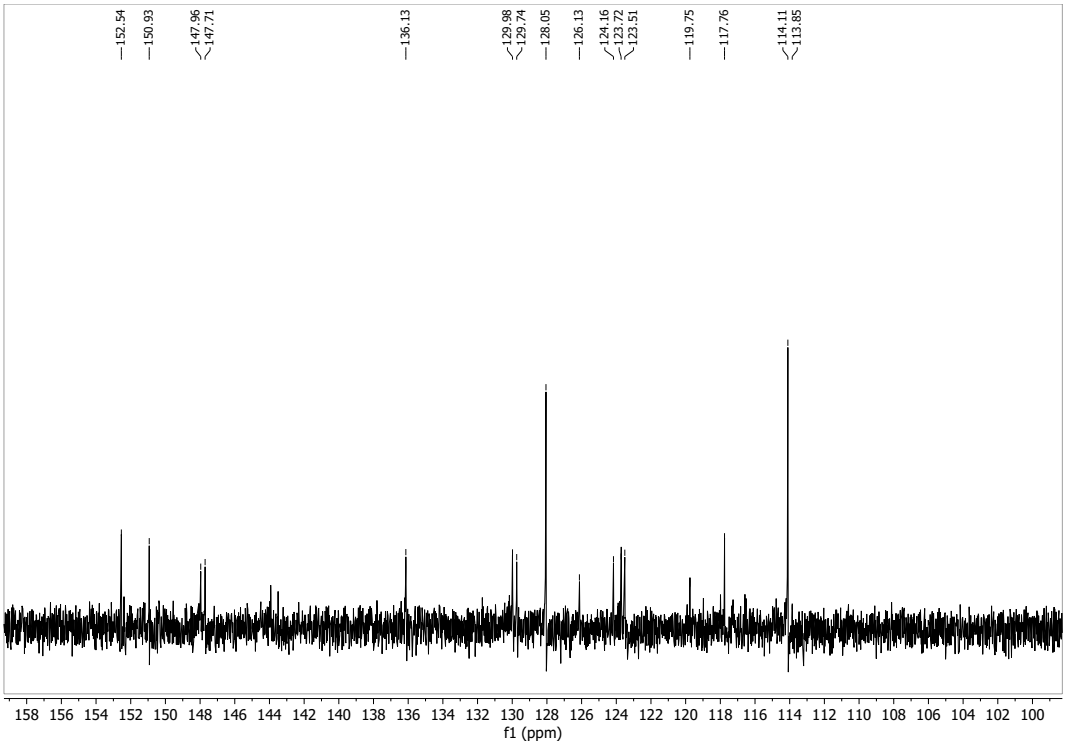

Figure VIII-114. [13]C NMR spectra for 2-(4-aminophenyl)-1H-imidazo[4,5-f]-1,10-phenanthroline.

(19) 2-(4-azidophenyl)-1*H*-imidazo[4,5-*f*]-1,10-phenanthroline spectra:

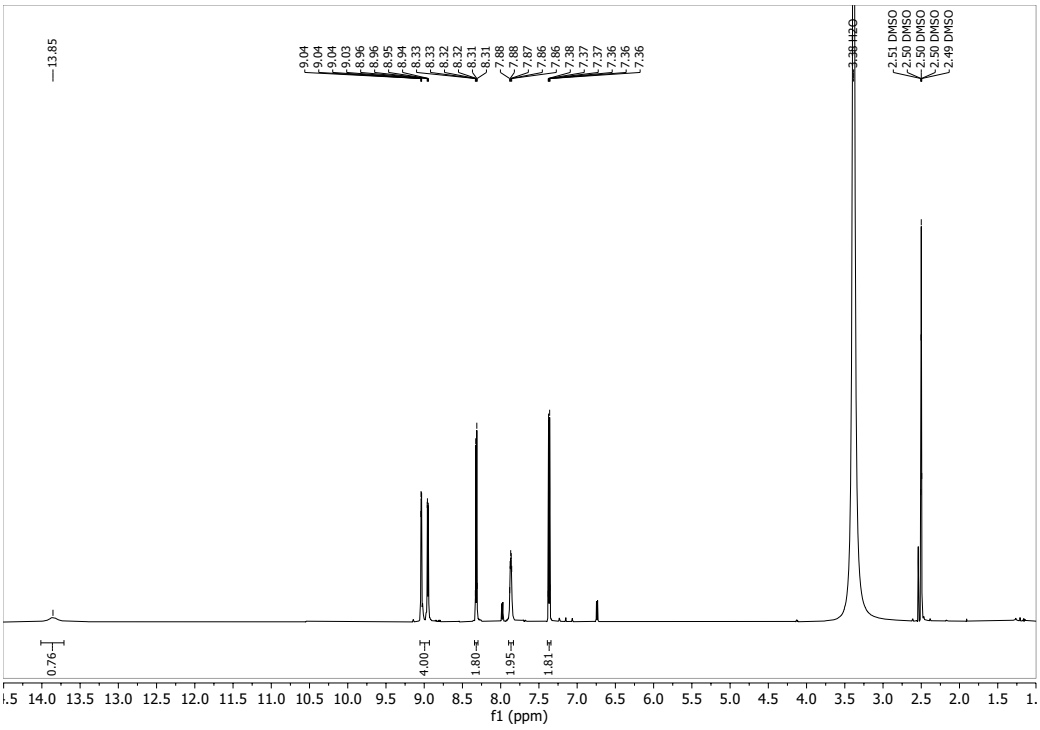

Figure VIII-115. ^{1}H NMR spectra for 2-(4-azidophenyl)-1H-imidazo[4,5-f]-1,10-phenanthroline.

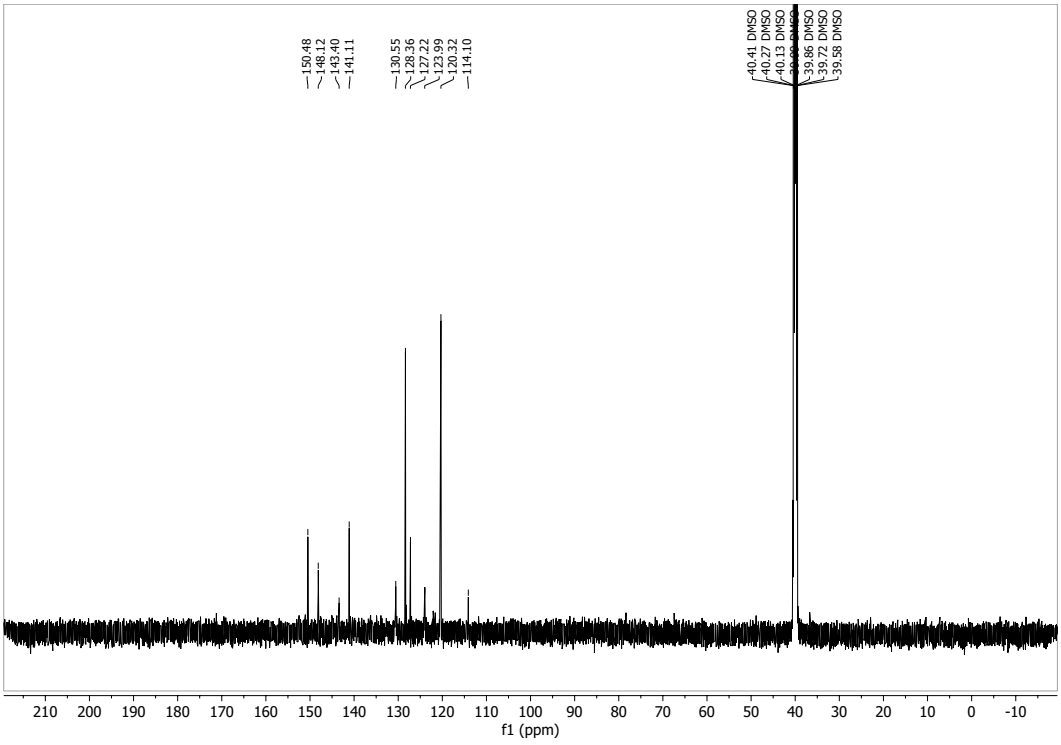

Figure VIII-116. ^{13}C NMR spectra for 2-(4-azidophenyl)-1H-imidazo[4,5-f]-1,10-phenanthroline.

VIII. 6. 2. ESI-MS and HPLC for TFO2 Hybrids

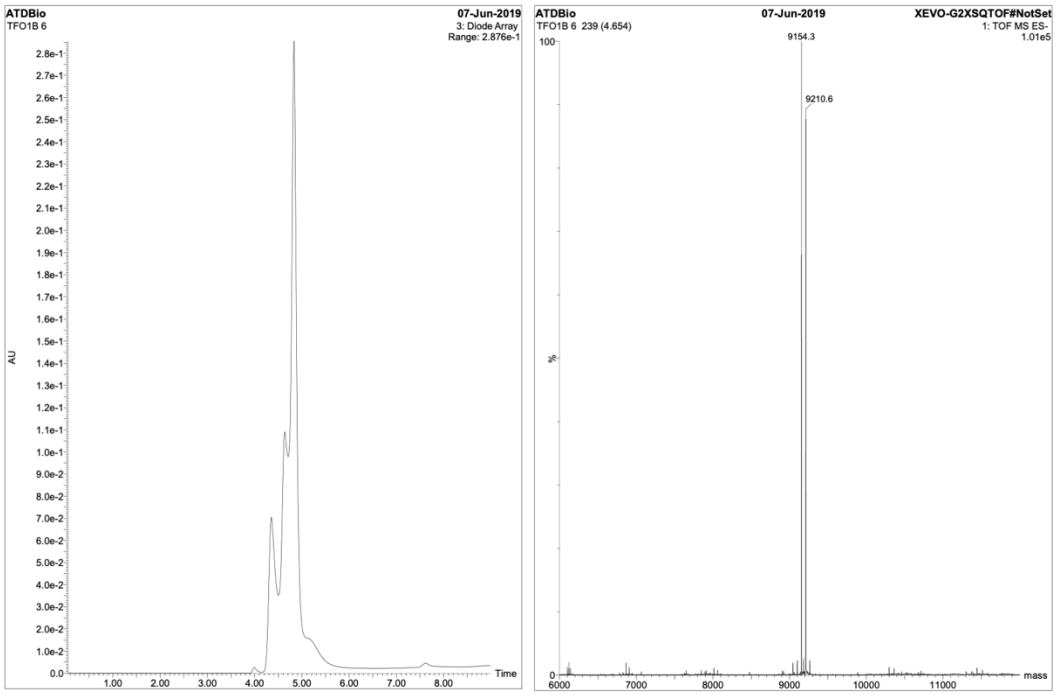

Figure VIII-117. HPLC and ESI-MS spectra for TFO2A.

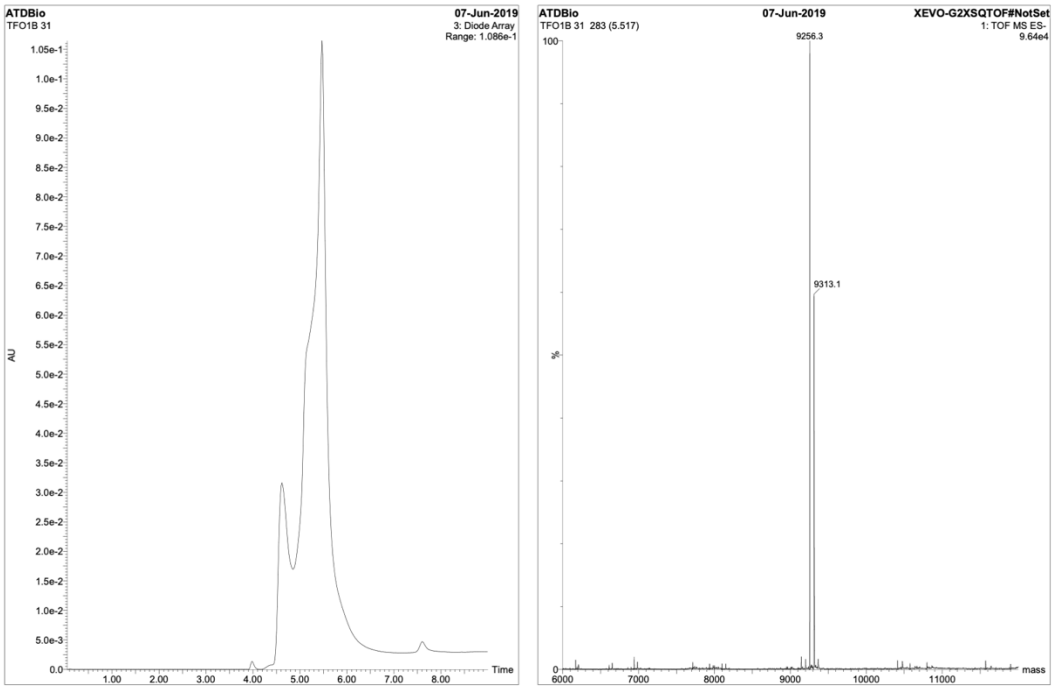

Figure VIII-118. HPLC and ESI-MS spectra for TFO2B.